Introduction

- RR Lyrae stars are short-period pulsating variable stars
- Population II objects
- in Milky Way they are found in galactic halo, thick disk, bulge and in globular clusters
- old evolved stars occupying horizontal branch in the CMD of globular cluster

Observational properties

- spectral types from A2 to F6
- periods from 0.2 to 0.9 d
- ranges of V-light variations from 0.3 to 2 mag

Classification of RR Lyrae stars

- period, range of variability, light curve shape
- RRab, RRc, RRd, Blazhko effect

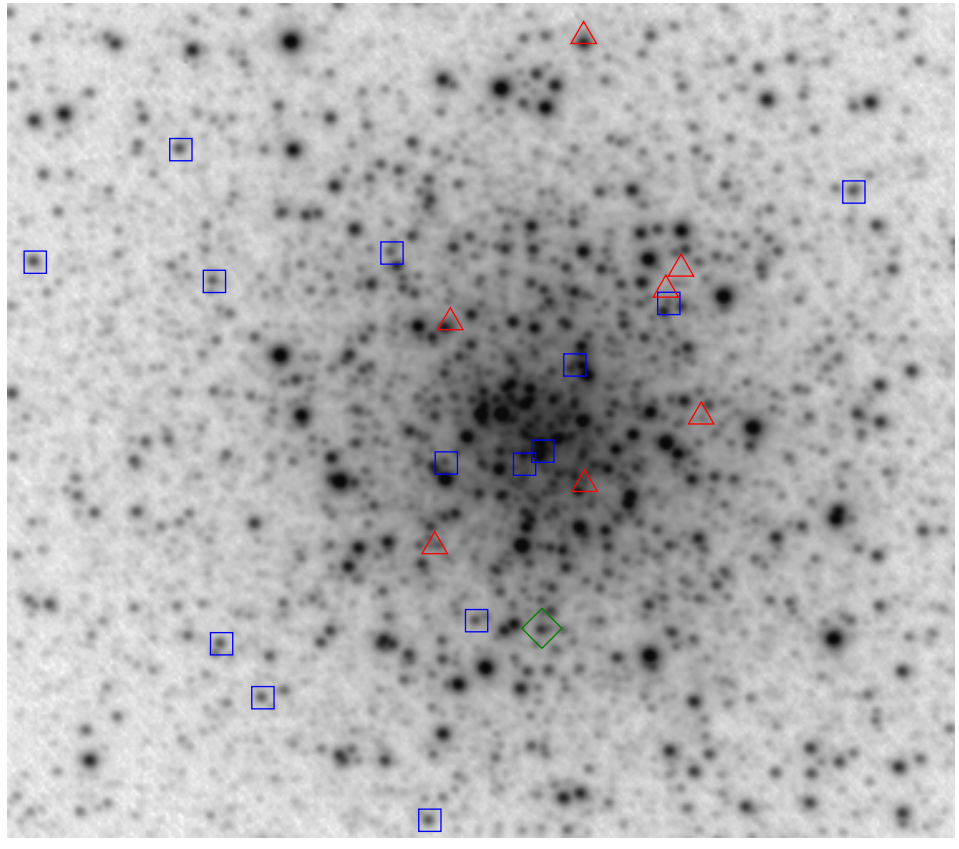

The 3.9×3.5 arcmin^2 field in the core of M 92. RR Lyrae stars are indicated with squares, Population II Cepheid, with a diamond, and SX Phoenicis stars, with triangles.

RR Lyrae subtype ab (RRab)

- periods from 0.4 to 0.9 d
- asymetric light curve: fast increase of brightness

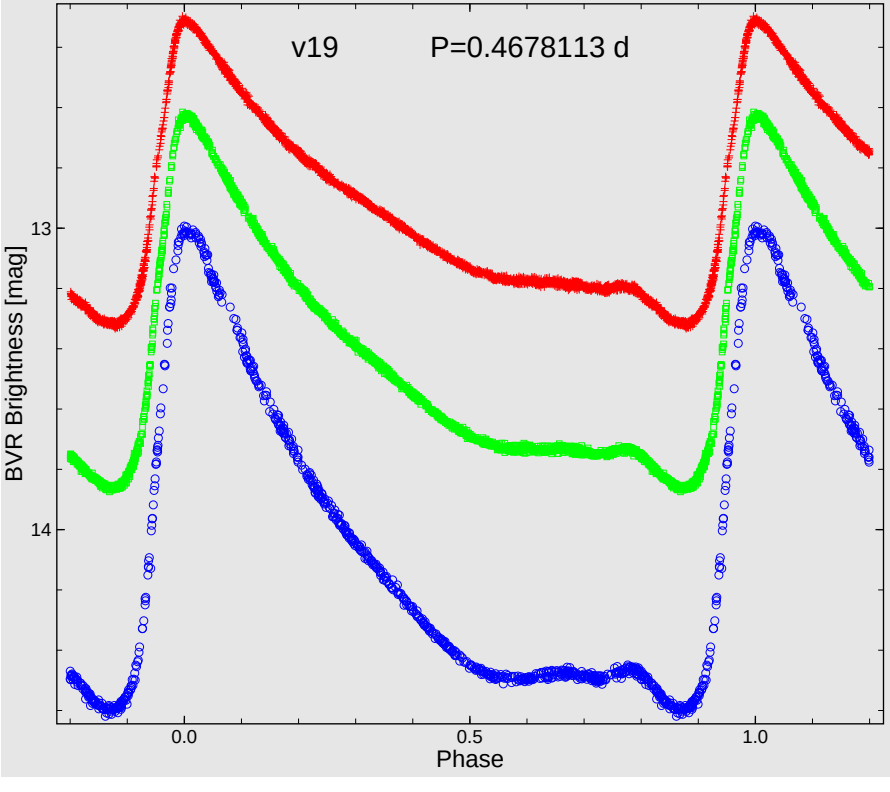

BVR light curves of the RRab star from M 4

RR Lyrae subtype c (RRc)

- periods from 0.2 to 0.5 d
- symetric light curve: almost sinusoidal

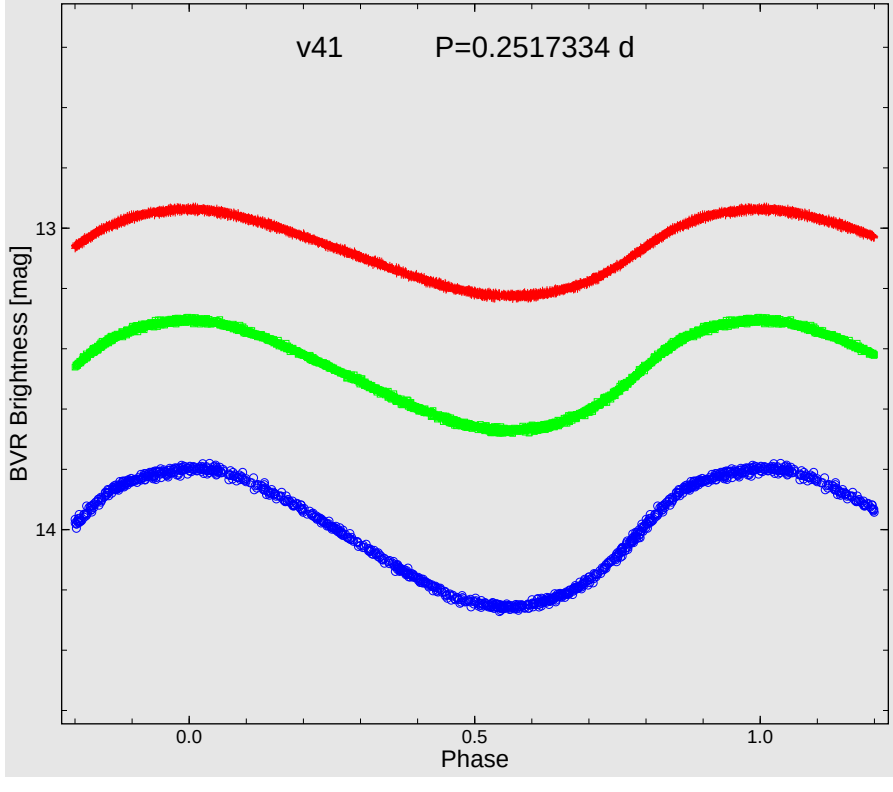

BVR light curves of the RRc star from M 4

Radial pulsations

- spherical symmetry throughout the oscillation cycle
- number of nodes along radius (radial order n)
  - $n = 0$ represents fundamental mode,
  - $n = 1$ – first overtone,
  - $n = 2$ – second overtone, etc.

Mode identification

- RRab – fundamental mode
- RRc – first overtone

Pulsation cycle

- brightness $\rightarrow$ changes of luminosity L
- colour $\rightarrow$ changes of effective temperature $T_{\rm eff}$
- radial velocity $\rightarrow$ changes of radius R
- light maximum corresponds to highest temperature and smallest radius

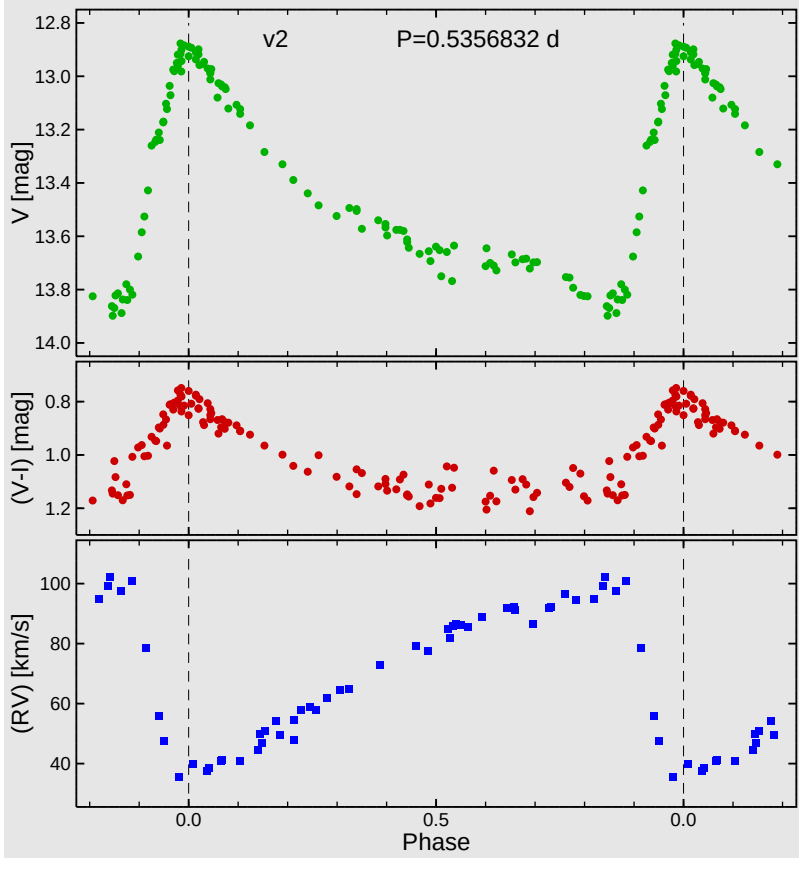

V light, $(V - I)$ colour, and radial velocity curves for RRab star from M 4 (Clementini et al. 1994, Liu and Janes 1990).

Driving mechanism for pulsations in RR Lyrae stars

- modulation of the energy flux inside star through a 'valve'
- dependence of opacity κ on temperature T
  - normally κ decreases as T increases $\Rightarrow$ ***damping zones***
  - in the H and He partial ionization zones κ increases with $T \Rightarrow$ ***driving zones***
- partial ionization zone (PIZ) is the region where 50 % of a given ion or element is ionized
- H + He II IZs in RR Lyrae stars

How does this engine work?

- gas in the PIZ is compressed by the infalling layers
- PIZ heats up and becomes more opaque because radiation energy goes for ionization of the gaz
- heat builds up in PIZ until it stores more energy than necessary to balance preassure from upper layers
- extra restoring force causes PIZ to expand
- κ and T decrease
- release of energy through recombination
- PIZ absorbs not enough energy to balance the weight of the upper layers
- upper layers fall on the PIZ (this is start of a new cycle)
- ***κ-mechanism***

RR Lyrae subtype d (RRd)

- two radial modes excited: fundamental ($P_{\rm F}$) and first overtone ($P_{\rm FO}$)
- usually first-overtone is a dominant mode
- $P_{\rm FO}/P_{\rm F} \approx 0.745$

Petersen diagram

- period ratio vs. period of fundamental mode
- position of an RRd star is almost independent of its luminosity and temperature
- radial pulsations are mainly governed by gravity
  - $P_{\rm FO} = f_1(M,R) + P_{\rm FO} = f_2(M,R) \Rightarrow M$
- pulsational (0.65 $M_\odot$) and evolutionary (0.8 $M_\odot$) mass discrepancy
  - resolved by new opacities

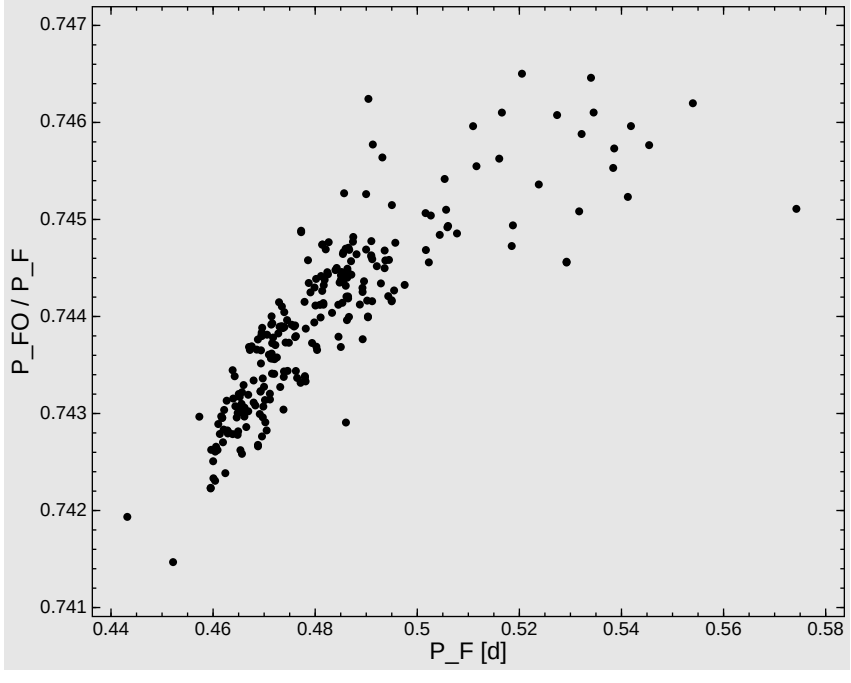

Petersen diagram for RRd stars from LMC (Soszyński et al. 2003)

- metallicity and/or mass spread in LMC
- the width of the band may be explained by mass spread at given metallicity

RR Lyrae subtype e (RRe)

- RR Lyrae stars pulsating in second overtone

Observations

- secondary peak in the period distribution of RRc stars in LMC
  - $\langle P \rangle_{\mathrm{RRe}} \approx 0.28$ d $\quad \langle P \rangle_{\mathrm{RRc}} \approx 0.34$ d
- RRc stars in GGCs having very short periods
- RR12 stars in LMC (MACHO) and Galactic Bulge (OGLE)
  - $P_{\mathrm{SO}}/P_{\mathrm{FO}} \approx 0.804$

Theoretical predictions

- RRc stars with shortest periods should have smaller amplitudes
- RRe stars should have more asymmetric light curves then RRc stars
- difficult to discriminate between RRc and RRe

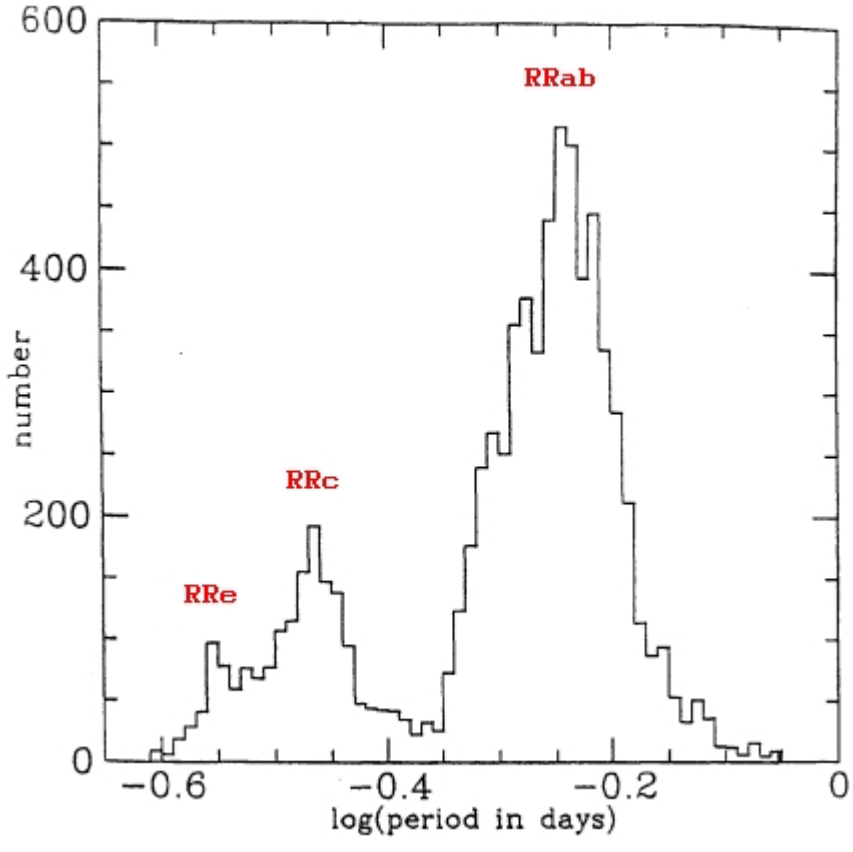

Histogram of periods of RR Lyrae stars from LMC. Three peaks can be clearly seen: at 0.59 d (RRab), at 0.34 d (RRc) and at 0.28 d (RRe) (Alcock etal. 1996).

Blazhko effect

- phase and/or amplitude modulation
- periodic change of light-curve shape
- before Olech et al. (1999) this effect was observed only in field RRab stars
- light curve of a Blazhko RRab star can be described as a set of equidistant frequency triplets centered on the fundamental frequency and its harmonics
  - Borkowski (1980)
  - combination frequencies

f_1	$f_1 + \Delta f = f_2$	$f_1 - \Delta f = 2f_1 - f_2$
$2f_1$	$2f_1 + \Delta f = f1 + f_2$	$2f_1 - \Delta f = 3f_1 - f_2$
$3f_1$	$3f_1 + \Delta f = 2f1 + f_2$	$3f_1 - \Delta f = 4f_1 - f_2$
.....	..... = ...	..... = ...

- the greatest amplitude of a Blazhko star equals to an amplitude of regular star with the same period

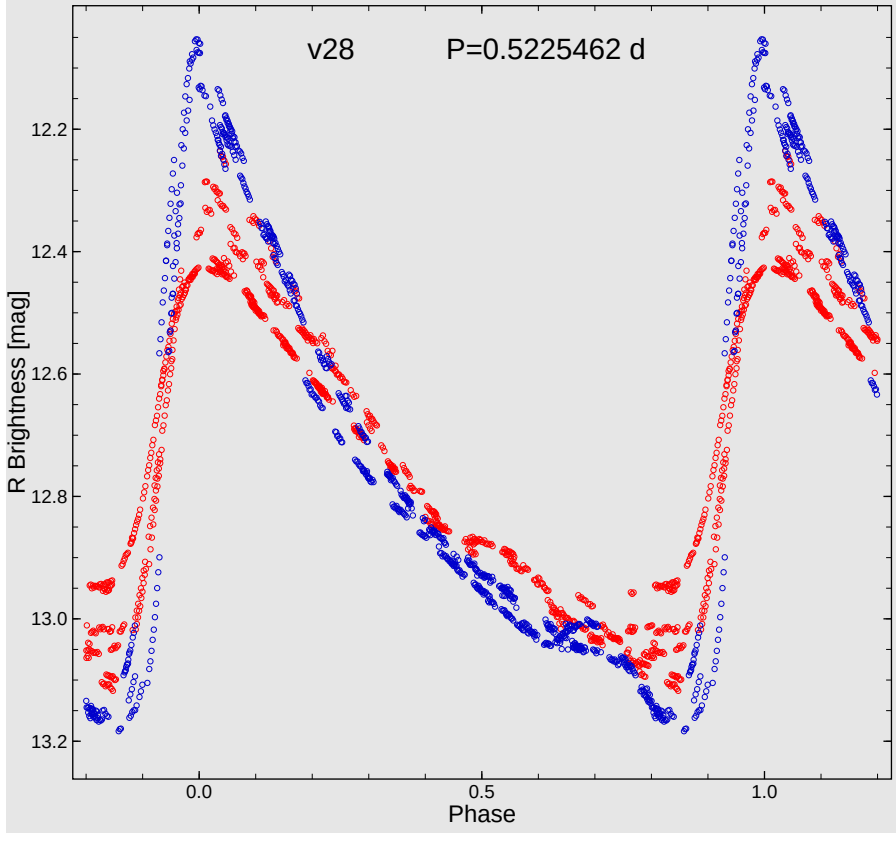

R light curve of an Blazhko RRab star from M 4. The time span of observations is 76 d. The data were divided into two groups to show changes in amplitude of variability.

Globular clusters

- single event of star formation
- stellar systems with the same
  - age,
  - distance,
  - metallicity (spread, CNO overabundance)
- halo, disc and bulge objects
- Population II objects
- the oldest components of Galaxy ($12 - 13$ Gyr)

Variable stars in globular clusters

- Type II Cepheids (BL Her, W Vir, RV Tau)
- RR Lyrae stars
- SX Phoenicis stars
- variable red giants
- eclipsing binaries

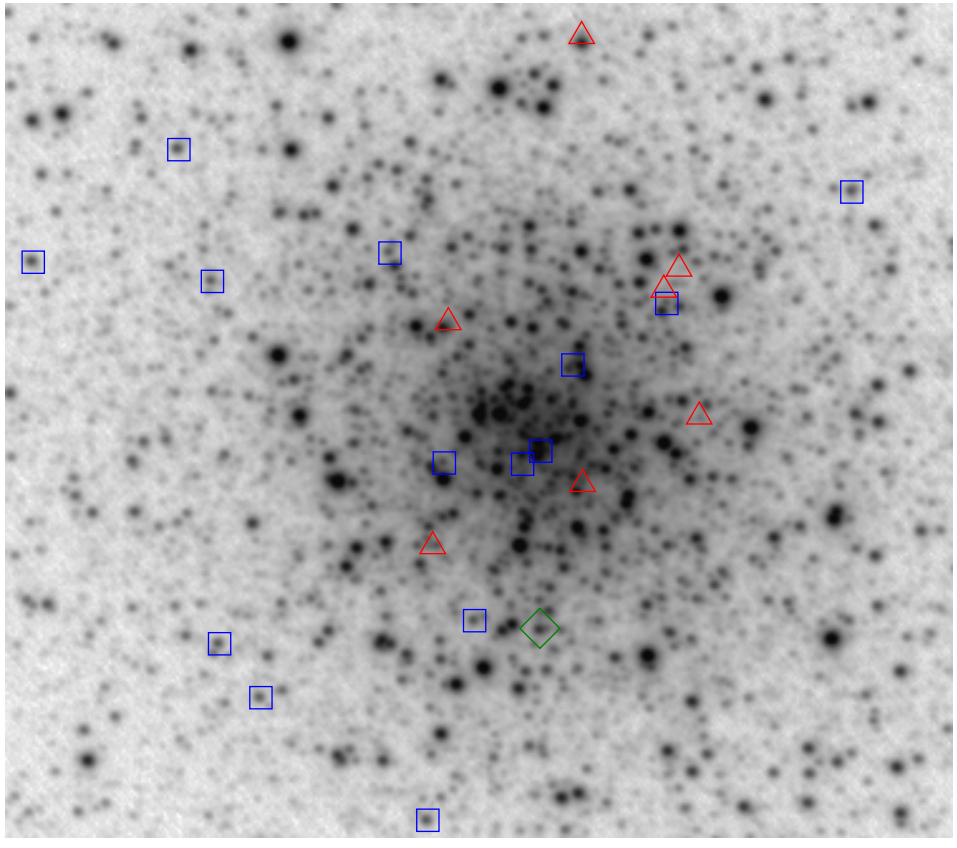

The 3.9×3.5 arcmin^2 field in the core of M 92. RR Lyrae stars are indicated with squares, Population II Cepheid, with diamonds, and SX Phoenicis stars, with triangles.

Image Subtraction Method

- resampling all frames to common astrometric system
- creating reference frame from best-seeing frames
- blurring the reference frame to the seeing of a given frame
    - matching seeing, flux scale and background difference
- subtraction of the blurred reference frame from a given frame
- time series of difference frames

Search for variable stars in globular clusters at Białków Observarory

- CCD observations of the 6×4 arcsec^2 field centered on the cluster core
- M 13 : 9 RR Lyr (3 new), 4 SX Phe (2 new)
- M 53 : 37 RR Lyr (4 new)
- M 56 : 2 RR Lyr (0 new)
- M 92 : 17 RR Lyr (4 new), 7 SX Phe (7 new)

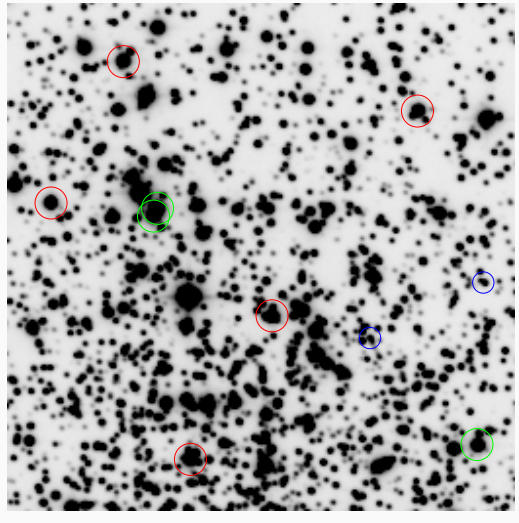

reference frame

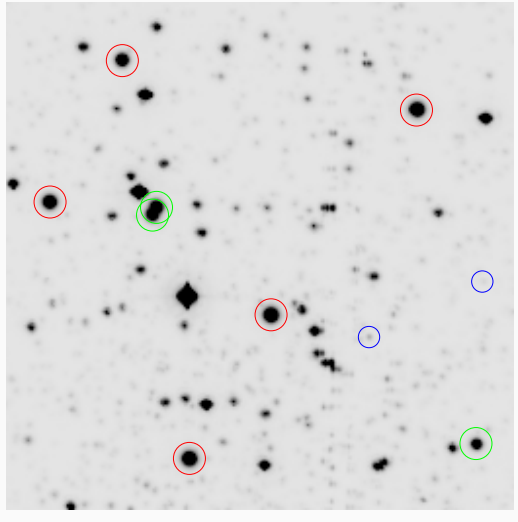

variability map

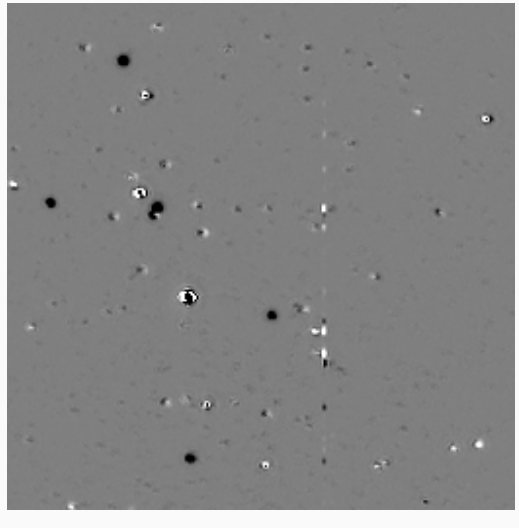

difference image t = 0.50 d

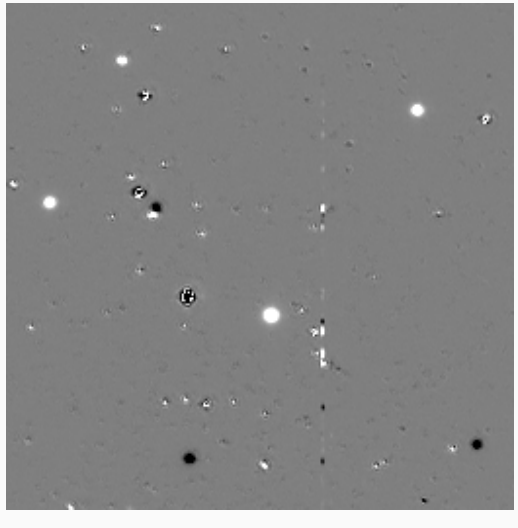

difference image t = 0.65 d

CMD of globular cluster

- main sequence (MS) + turn-off point (TO)
- subgiant branch (SGB)
- red giant branch (RGB) + tip of RGB (TRGB) + red bump (RB)
- horizontal branch (HB) + extreme blue HB (EBHB)
- asymptotic giant branch (AGB)
- blue stragglers (BS)

Pulsational instability strip

- region of the H-R diagram where occur (mostly) radial pulsations driven by κ mechanism in the H/He ionization zone
- SX Phoenicis stars (BS)
- RR Lyrae stars (HB)
- Population II Cepheids (blue loop from AGB)

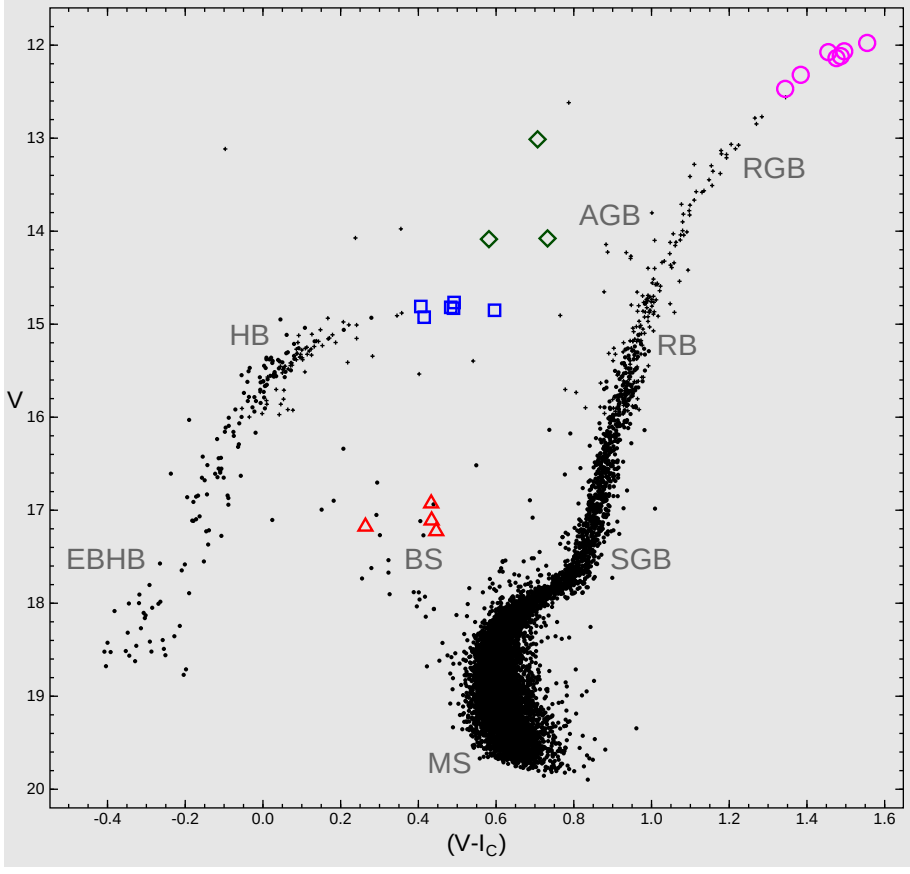

The colour – magnitude diagram for M 13 (Kopacki et al. 2003). SX Phoenicis stars are indicated with triangles, RR Lyrae variables with open squares, Population II Cepheids with diamonds, and variable red giants with circles.

Classification of globular clusters according to properties of their RR Lyrae stars

- Oosterhoff's dichotomy
  - ***OoI*** :
    $\langle P \rangle_{\rm ab} = 0.55$, $N_{\rm c}/(N_{\rm ab} + N_{\rm c}) = 20$ %
  - ***OoII*** :
    $\langle P \rangle_{\rm ab} = 0.65$, $N_{\rm c}/(N_{\rm ab} + N_{\rm c}) = 50$ %
- $[{\rm Fe/H}]_{\rm OoI} > [{\rm Fe/H}]_{\rm OoII}$

Catalogue of Variable Stars in Globular Clusters (CVSGC)

- `www.astro.utoronto.ca/~cclement/read.html`

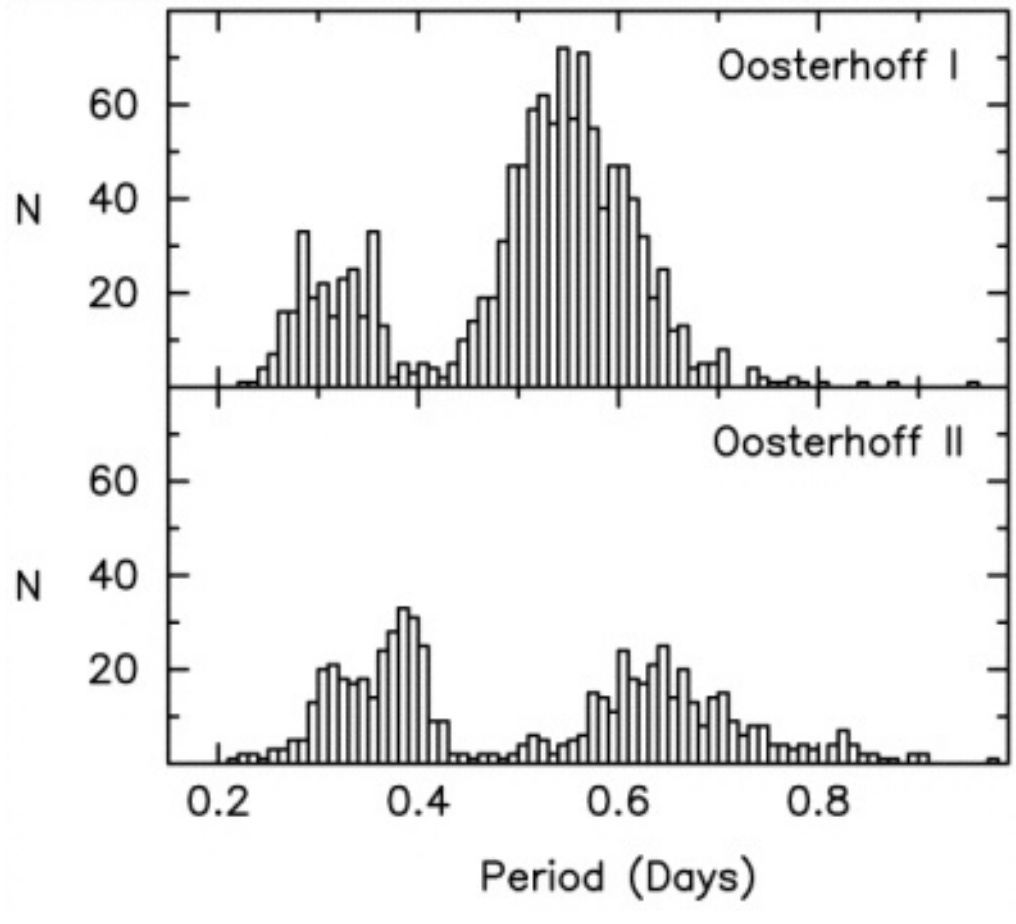

Period distribution for RR Lyrae variables in clusters of Oosterhoff type I (top) and Oosterhoff type II (bottom). Clement et al. (2001, AJ 122, 2587).

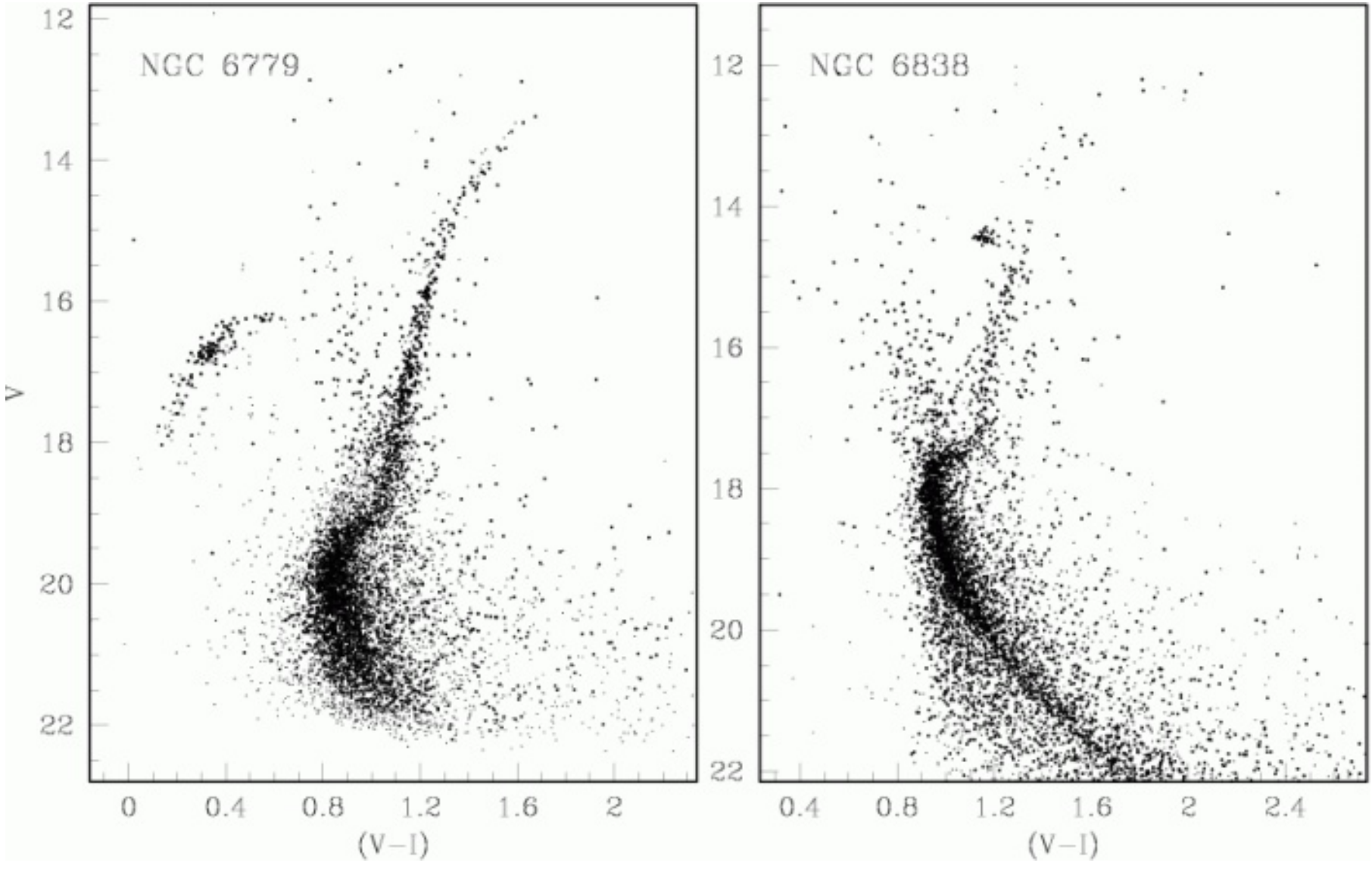

CMDs for two GCs: M56 (left) and M71 (right) showing completely different HB colours. M56 is metal-poor ([Fe/H] = −1.94) and M71 is metal-rich ([Fe/H] = −0.58). Rosenberg et al. (2000, AApSS 145, 451).

Classification of globular clusters according to colour and shape of their HB

- HB morphology
  - metallicity effect
  - age effect (second parameter)
  - HBR $= (N_{\rm B} - N_{\rm R})/(N_{\rm B} + N_{\rm RR} + N_{\rm R})$
  - BHB – HBR < 0
  - RHB – HBR < 0
- mass loss on RGB $\Rightarrow$ colour (mass) spread on HB
- ***synthetic HB*** from Gaussian mass distribution along HB; $\langle M \rangle$ $+\sigma_M$
- bimodal HBs
- HBs with long blue tails with gaps

- high-metallicity GC have RHB
- low-metallicity GC have mostly BHB, but some have RHB
- none high-metallicity GC with BHB

- OoI – RHB
- OoII – BHB (+ RHB)

- NGC6388 and NGC6441 have RHB (normal for their [Fe/H]) and BHB/EBHB
- two populations of RR Lyr stars, both OoI and OoII, in ω Cen

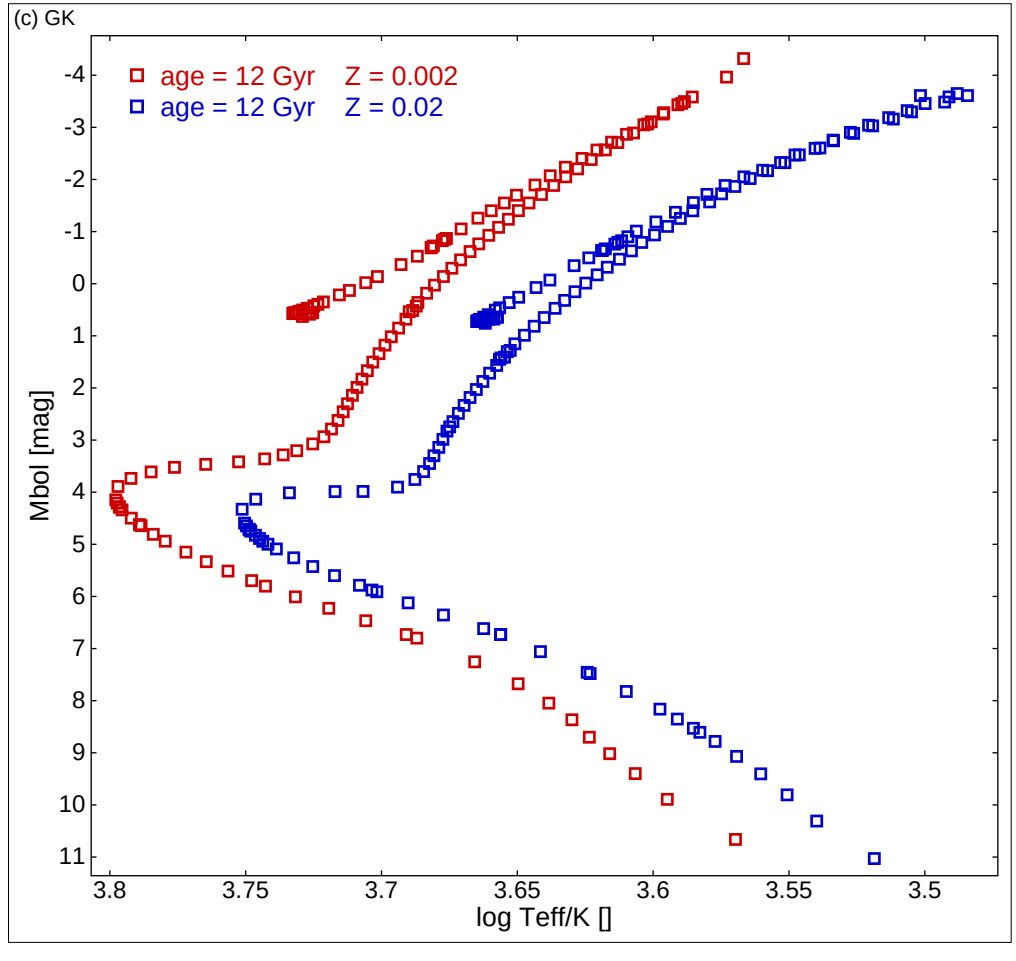

Effect of metallicity on the shape of GCs CMD. Isochrones are taken from Marigo et al. (2008, AAp 482, 883). Generated with `http://stev.oapd.inaf.it/cmd`.

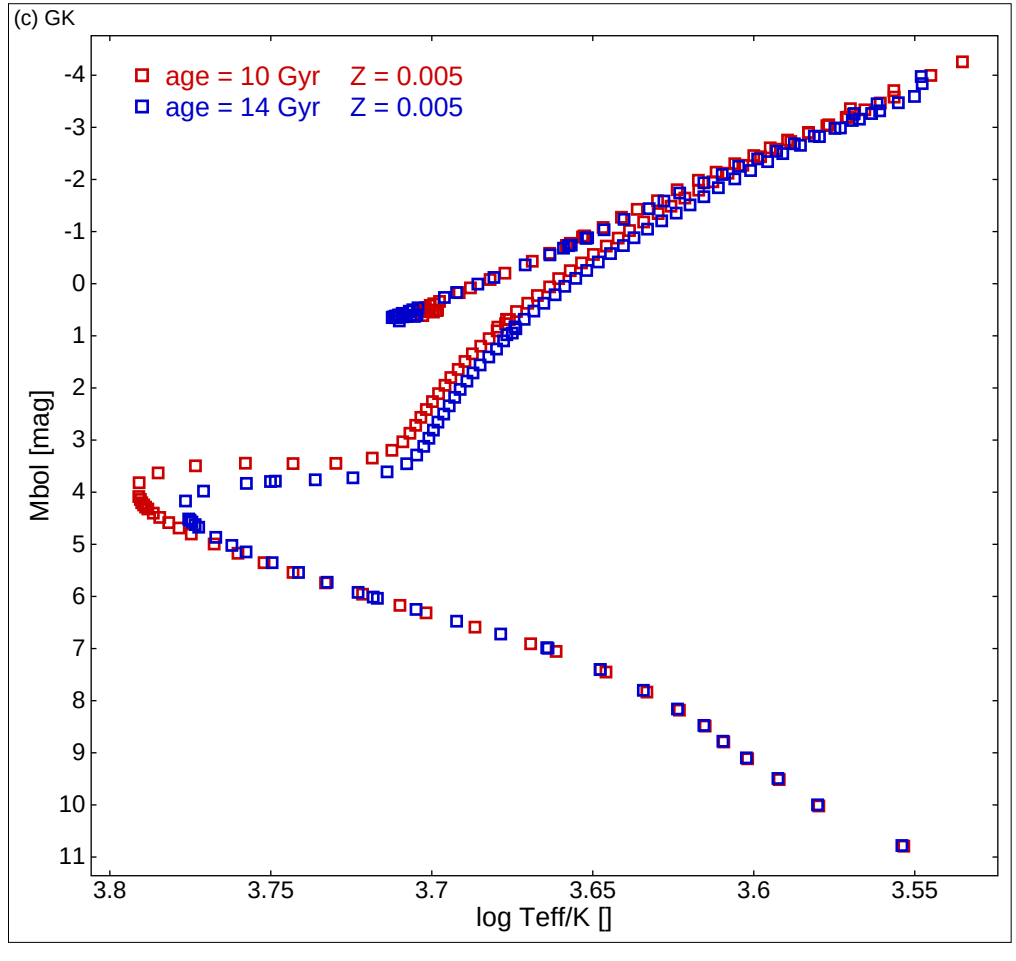

Effect of age on the shape of GCs CMD. Isochrones are taken from Marigo et al. (2008, AAp 482, 883). Generated with `http://stev.oapd.inaf.it/cmd`.

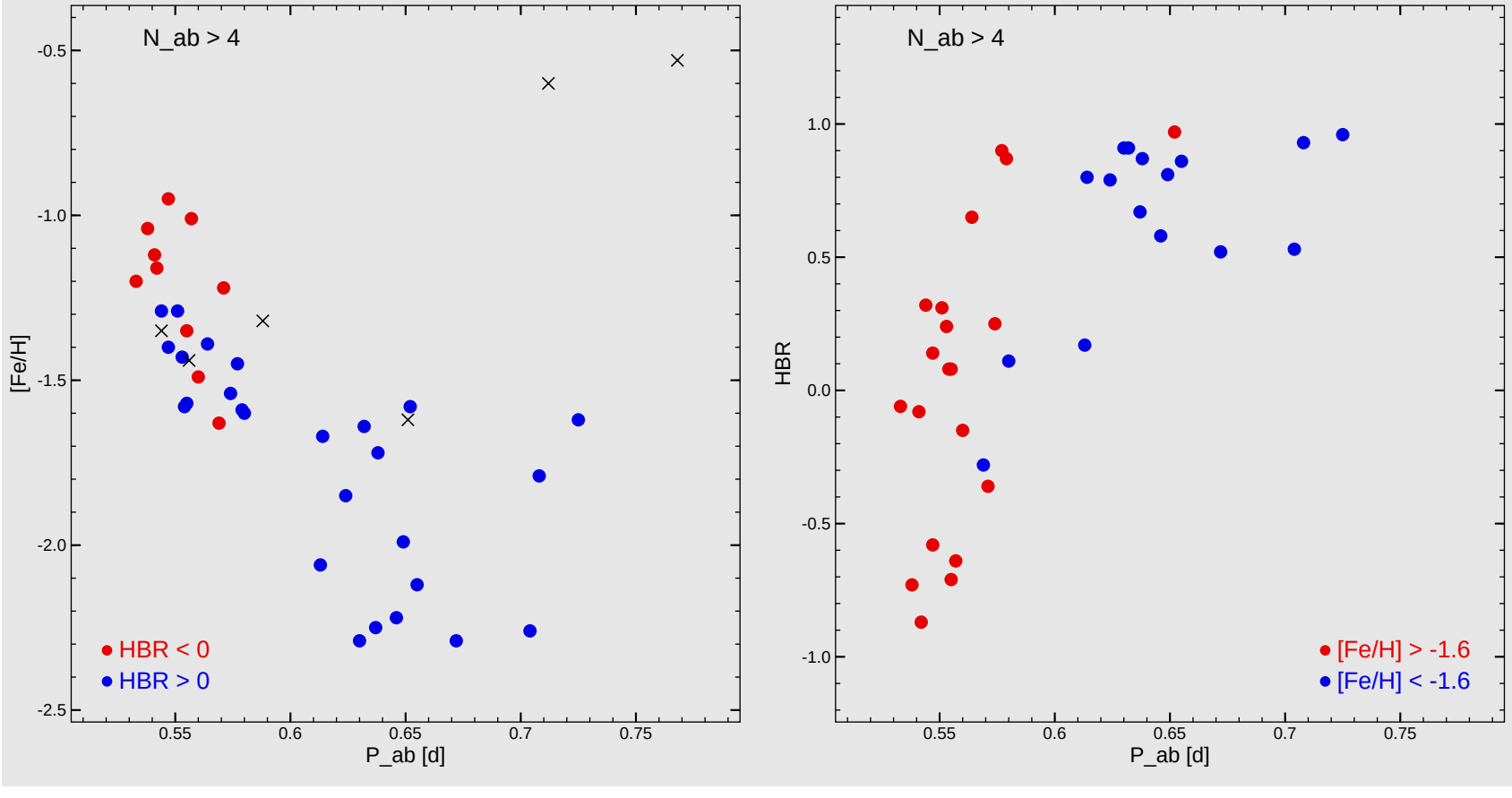

Left panel: [Fe/H] vs. mean period of cluster RRab stars. Right panel: HBR vs. mean period of cluster RRab stars. Only the data for Galactic globular clusters are shown. Data taken from Clement et al. (2001, AJ 122, 2587).

HB in colour – magnitude diagram

- Blazhko RRc stars have bluest colours

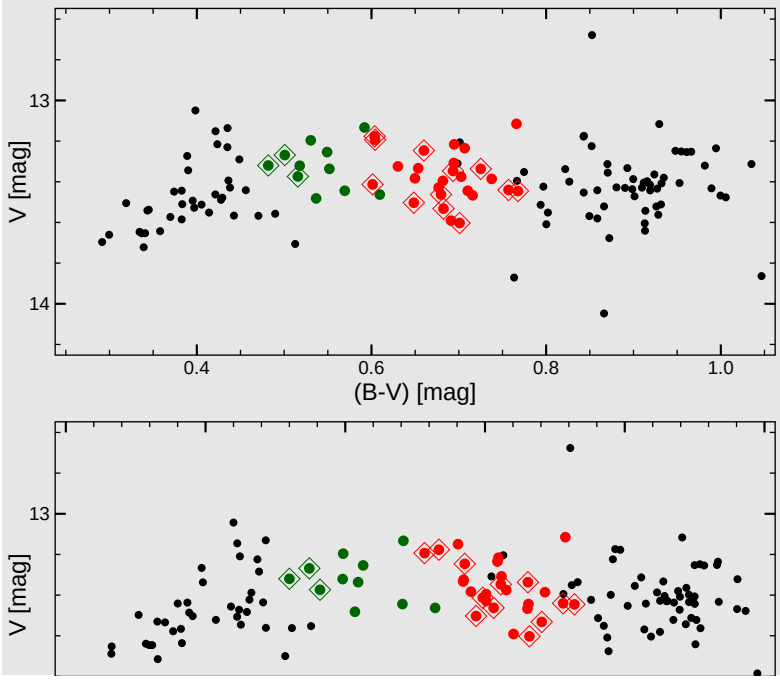

Parts of colour – magnitude diagrams for M 4 showing horizontal branch only. RRab stars are indicated with red dots, RRc stars, with green dots. They are represented by the intensity-weighted mean brightnesses and magnitude-weighted mean colour indices. Variables exhibiting the Blazhko effect are indicated with diamond symbols.

Period – amplitude diagram

- Blazhko RRc stars have smallest periods and amplitudes

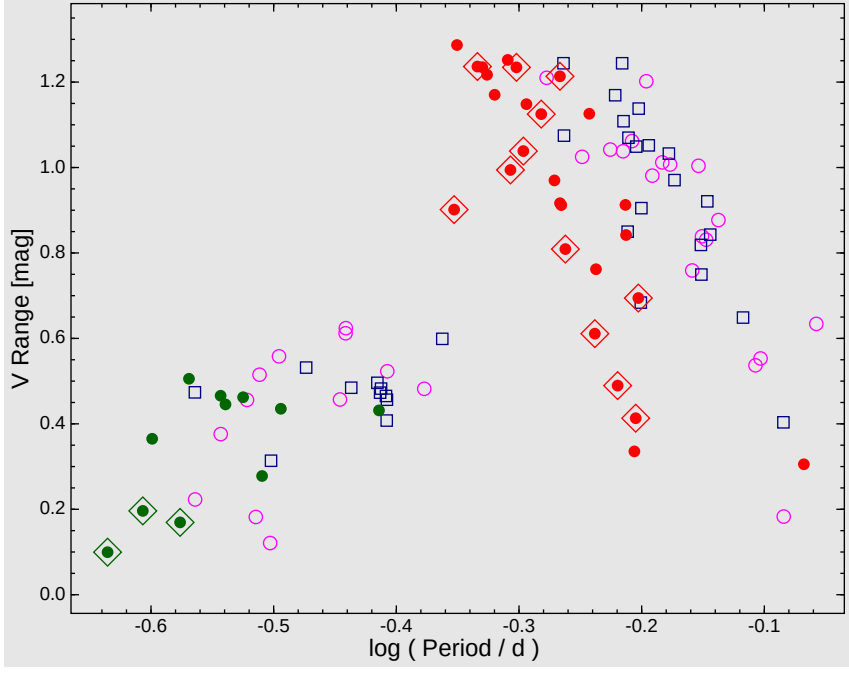

V ranges of variability as a function of period for RR Lyrae stars in M 4. RRab stars are shown with red dots, RRc stars, with green dots. Variables exhibiting the Blazhko effect are indicated with diamond symbols. For comparison, RR Lyrae stars of M 53 are shown with blue squares and RR Lyrae stars in M 2 are indicated with pink circles.

System of GCs of MW

- two distinct subpopulations in the GGCS
  - based on metallicity and kinematics
- ***metal-poor component*** (MPC)
  - 3/4 of all clusters
  - spread throughout the halo
- ***metal-rich component*** (MRC)
  - 1/4 of all clusters
  - restricted to the Solar sphere
  - thick disk population (high metallicity and large systemic rotation)
  - space density resembles bulge-like population

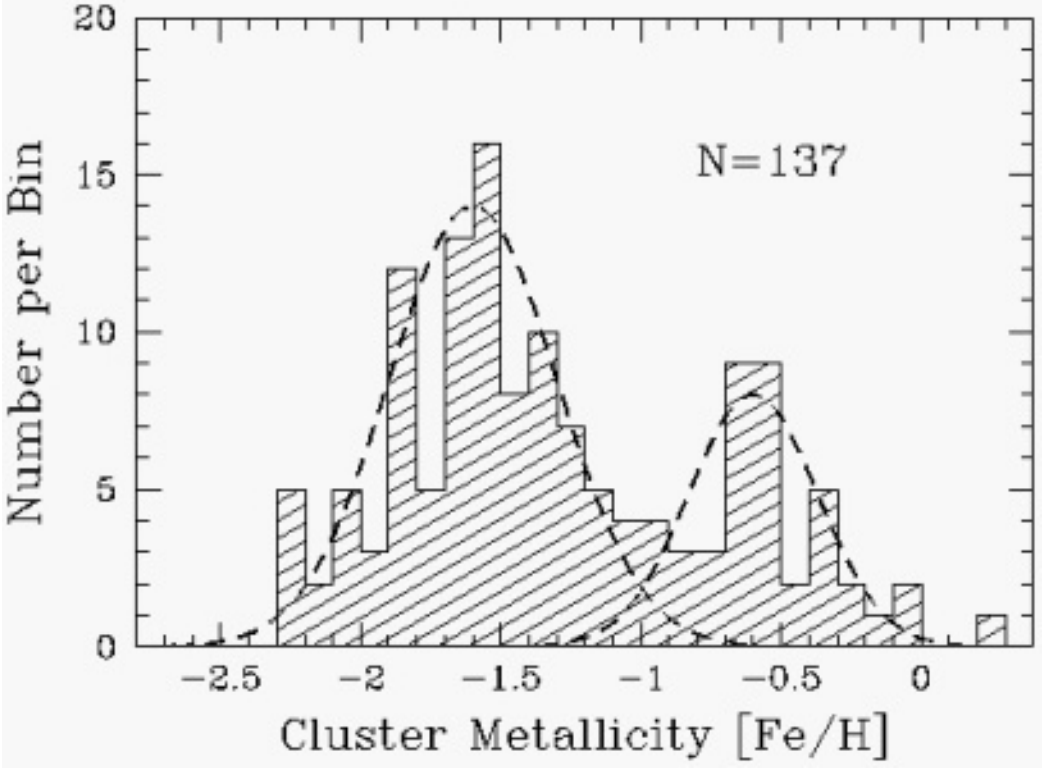

Metallicity distribution function for the GGCs. The two Gaussian curves have means and standard deviations of $(-1.6, 0.30)$ and $(-0.6, 0.23)$ and define the metal-poor (MPC) and metal-rich (MRC) components. Harris (1999, Globular Clusters).

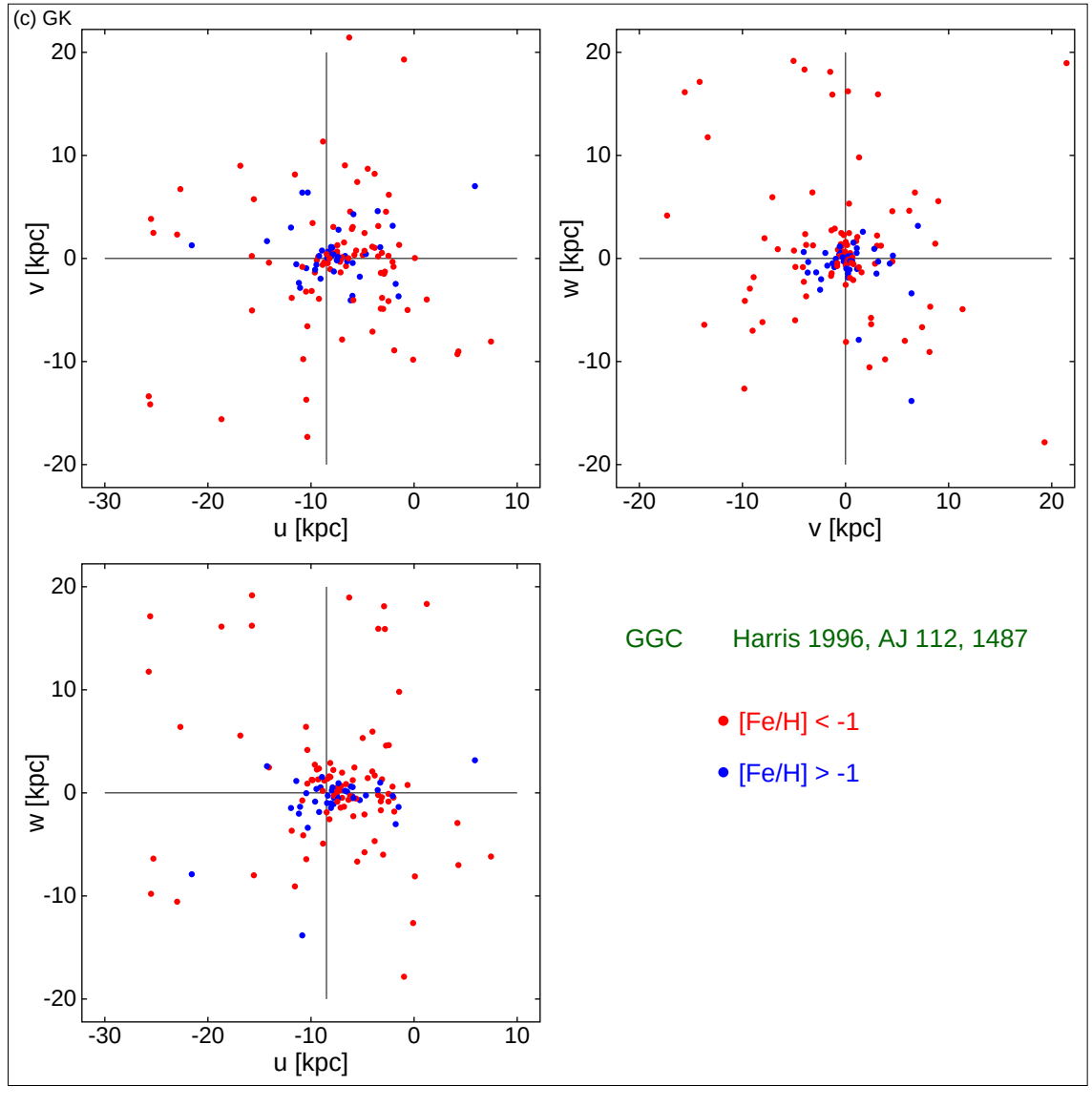
(c) GK
v [kpc]
u [kpc]
w [kpc]
v [kpc]
w [kpc]
u [kpc]
GGC Harris 1996, AJ 112, 1487
[Fe/H] < -1
[Fe/H] > -1

Models of Galaxy formation

- ***ELS*** model
  - Eggen, Lynden-Bell & Sandage (1962, ApJ 136, 735)
  - among high-velocity stars, those with lower abundances possess more halo-like orbits
  - monolithic rapid ***collapse*** followed by dissipational formation of disk with ***spin-up***
- ***SZ*** model
  - Searle & Zinn (1978, ApJ 225, 357)
  - no correlation between metallicity and Galactocentric distance for GCs more distant than $R_{\rm GC} = 8$ kpc
  - anomalies in CMDs of distant GCs
  - outer halo created by ***accretion*** and merger of many dwarf-like pregalactic fragments having different ages and metallicities

Low-luminosity dSph galaxies vs. globular clusters

- have similar luminosities, stellar masses, generally no gas or recent star formation, and contain metal-poor, old stellar populations
- but GCs are small ($1-10$ pc) and do not contain much DM, while dSph galaxies are much larger (> 100 pc) and are dominated by DM as indicated by their large $[M/L]$
- two structurally distinct populations

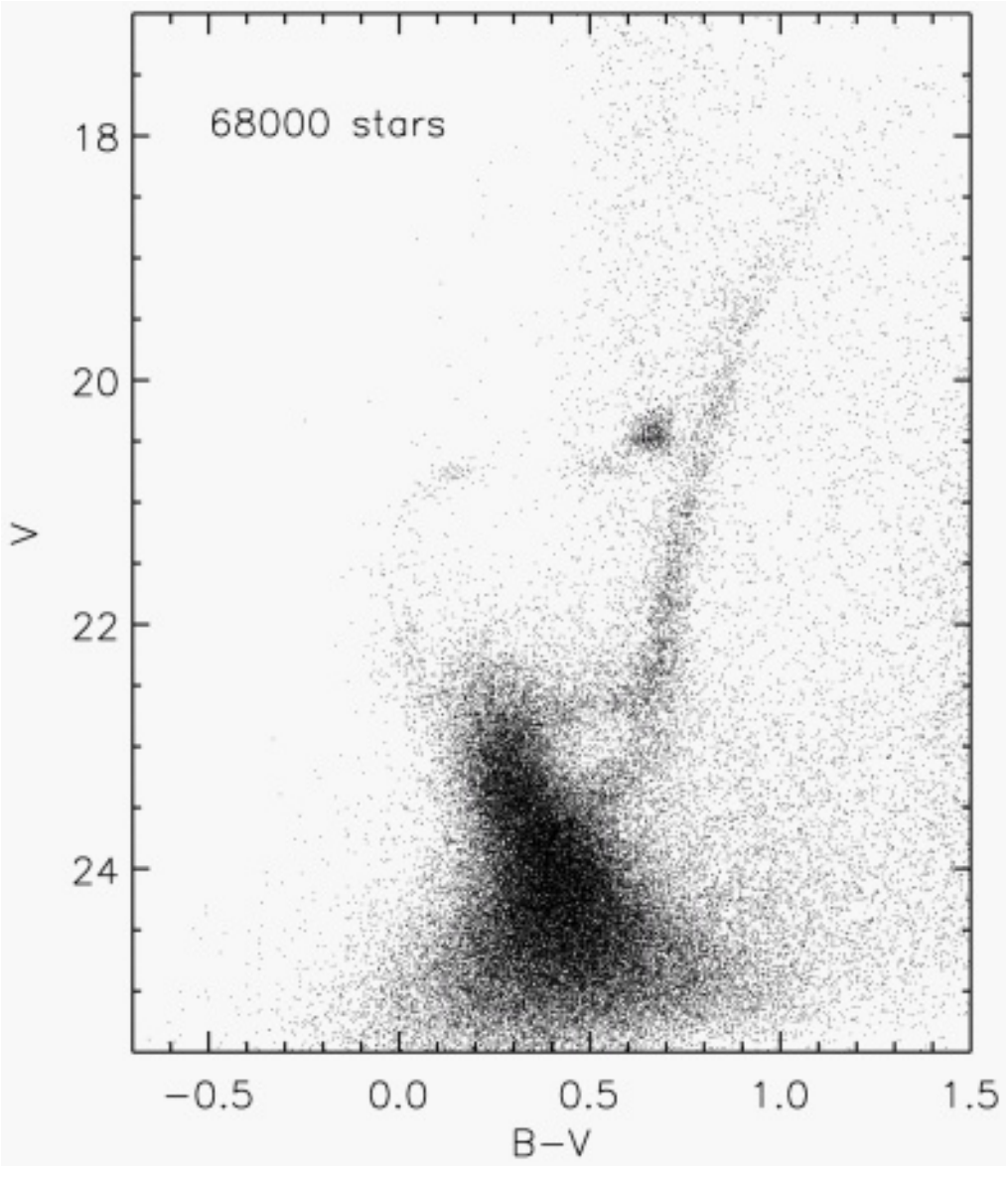

CMD for the Carina dSph galaxy. Note three populations: old with age of 12 Gyr (faint turnoff at $V = 23.5$ mag, BHB, RHB, RR Lyrae "gap"), intermediate with age of 5 Gyr (bright turnoff at $V = 22.5$ mag, red clump) and even young with age of 0.6 Gyr (blue MS). Monelli et al. (2003, AJ 126, 218).

Formation of galaxies

- buildup of massive galaxies via major merging events
- buildup via more continuous accretion process
- tidal disruption of smaller galaxies in the gravitational field of our Galaxy leaves very extended and long-lasting trails of stars

Accretion of DG by MW

- Sagittarius Dwarf Galaxy (SDG)
  - discovered by Ibata et al. (1995, MNRAS 277, 781)
  - stellar abundance and kinematics survey of K and M stars in the galactic bulge
  - M54, Arp2, Ter7, Ter8, Pal12, and NGC 4147 seem to be associated with SDG

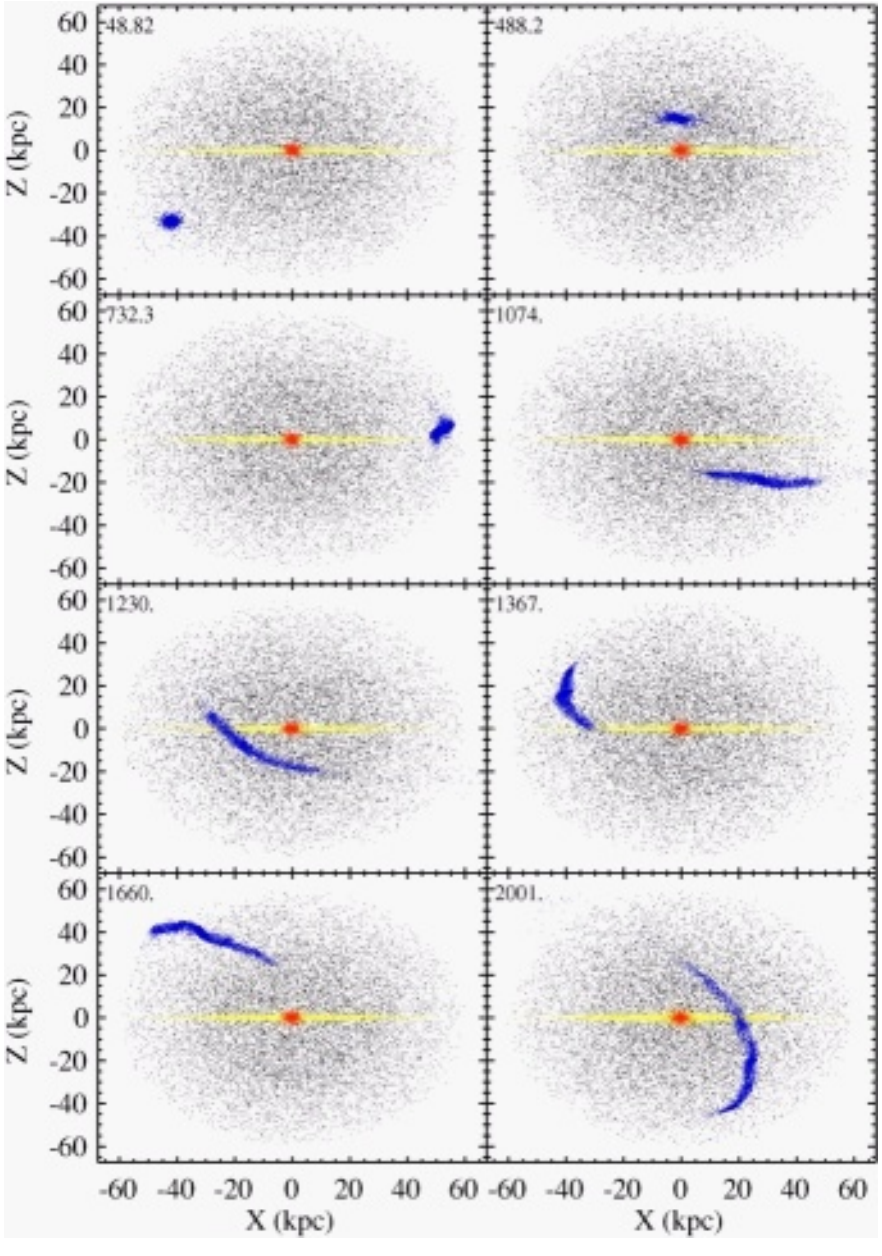

Time series of MW and SDG particles (blue) from the start of the simulation to 2.0 Gyr The label on the panels shows the time in units of Myr. The fifth panel (at 1230 Myr) is closest to the present time. Myers et al. (2010, ApJ 723, 1057).

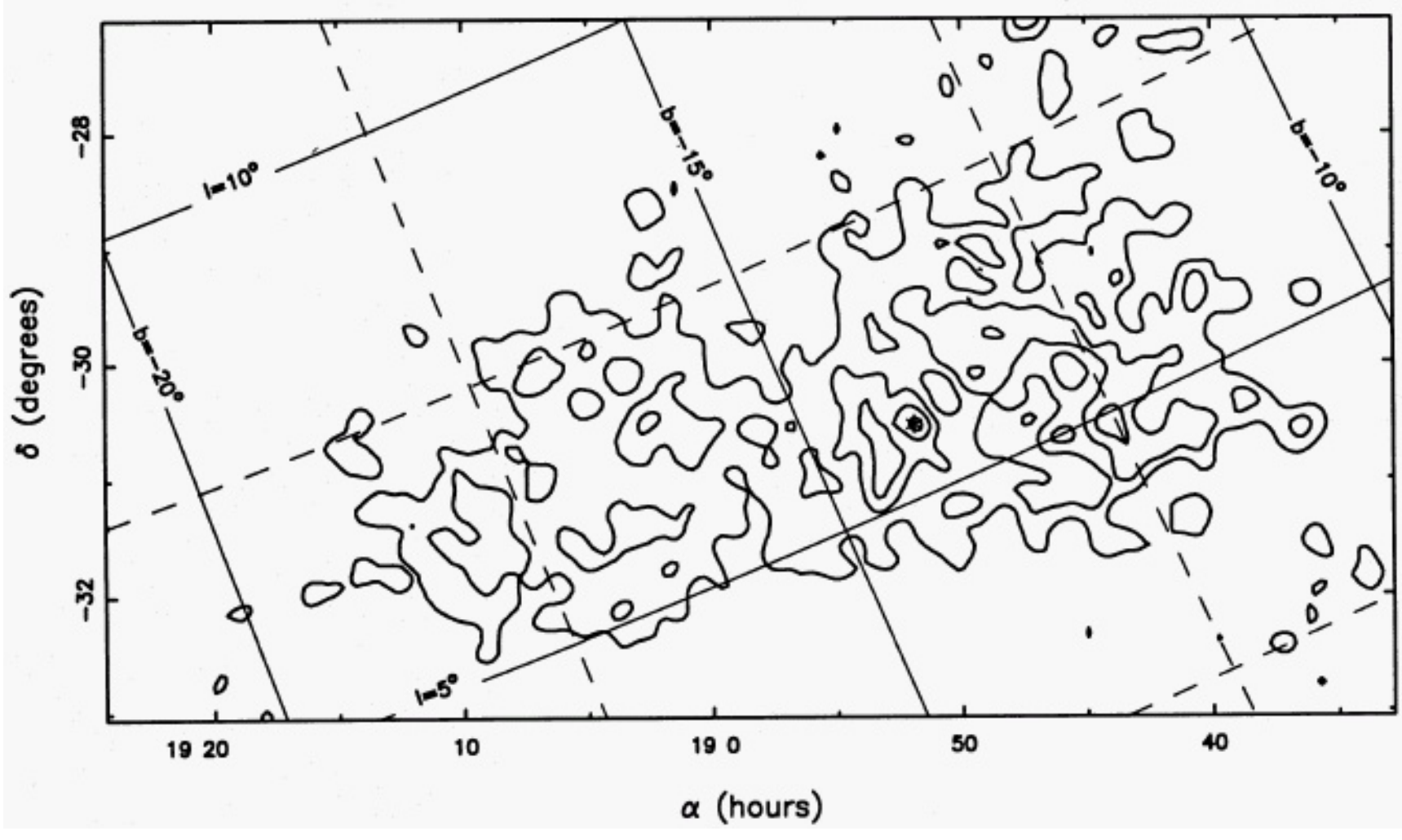

Isodensity map for the UKST field of SGD, constructed from the excess of images present at the HB magnitude. Globular cluster M54 is represented with a 'star' symbol. Ibata et al. (1995, MNRAS 277, 781).

System of GCs of the MW Halo

- two subpopulations in the Galactic halo (+ disk/bulge population)
  - based on the position in the HBR vs. [Fe/H] plane
- van den Bergh (1993, ApJ 411, 178), Zinn (1993, ASPCS 48, 38)
  - "BHB" GCs
  - "RHB" GCs (second-parameter GCs)
  - ***age*** as second parameter
  - "old halo" (OH) GCs (inner halo GCs)
  - "young halo" (YH) GCs (outer halo GCs)
  - bulge/disk (BD) GCs
- both halo populations present Oosterhoff dichotomy
- $[\mathrm{Fe/H}]_{\mathrm{YH}} < [\mathrm{Fe/H}]_{\mathrm{OH}}$ (by ≈ 0.25)

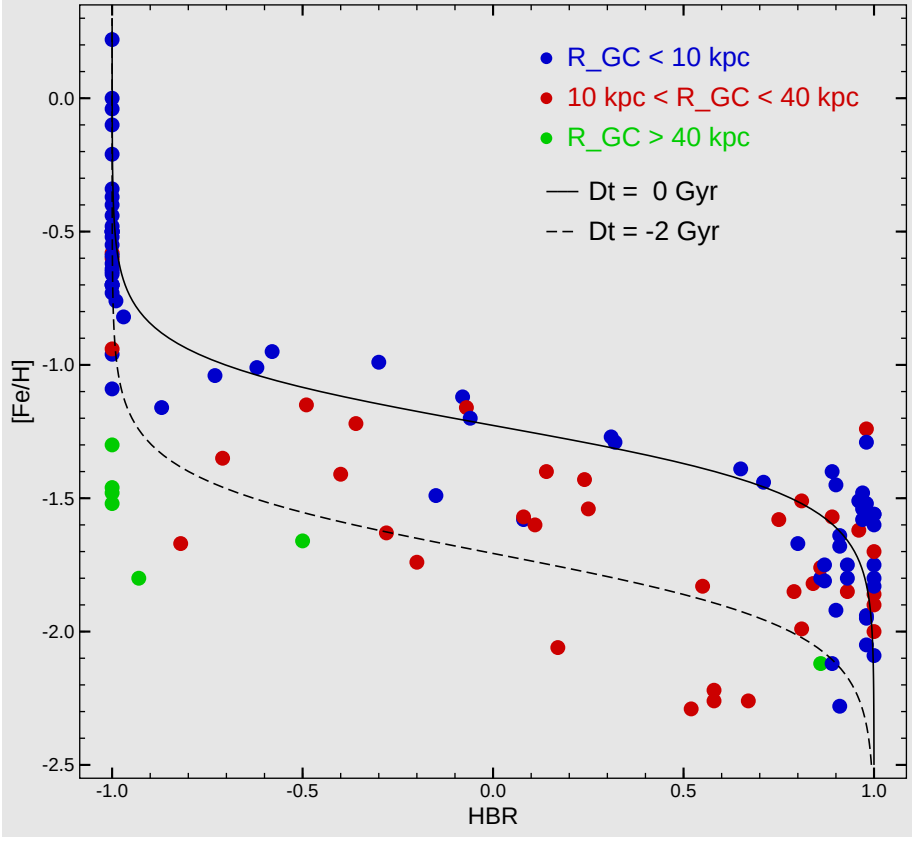

The HB morphology index HBR vs. metallicity [Fe/H] plane for Galactic globular clusters. The solid and dashed lines are theoretical isochrones produced with the synthetic HB code with fixed mass-loss. Note the systematic variation of the HB type with Galactocentric distance.

- Mackey & Gilmore (2004, MNRAS 355, 504)
  - fiducial line defined by HBR – [Fe/H] correlation for inner halo GCs ([Fe/H] < -0.8, $R_{\rm GC} < 6$ kpc) (Zinn 1993)
  - fiducial line defined by top isochrone
  - ΔHBR – difference in HB index between GC and the fiducial line at given metallicity
  - YH for $\Delta{\rm HBR} < -0.3$ ($\Delta\tau = 0.6$ Gyr)
- zone of avoidance (for GGCs) occupied by external GCs
- external systems fall along the trend defined by YH GCs

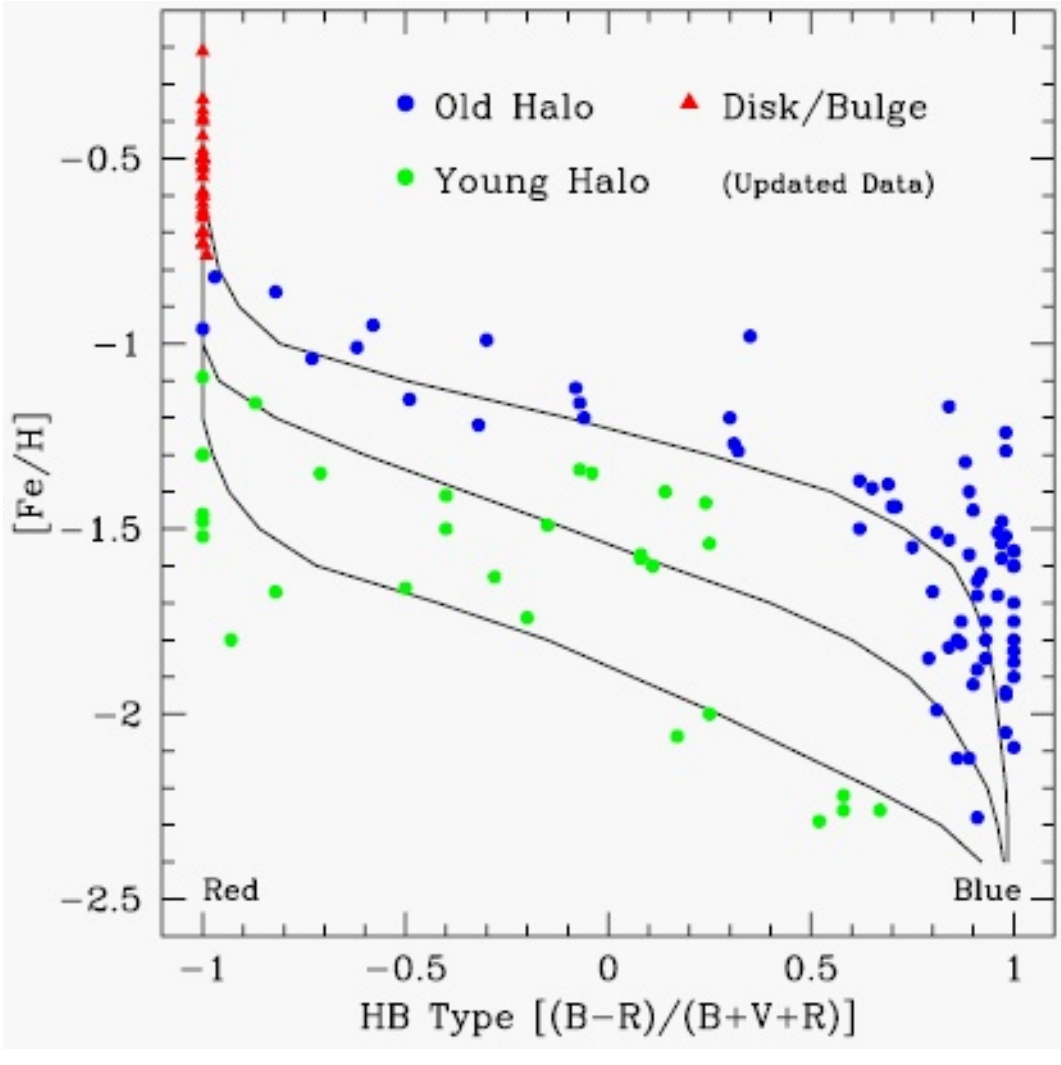

HB-type vs. metallicity diagram for 137 Galactic globular clusters. The clusters have been divided into three subsystems according to similar criteria of Zinn (1993). The isochrones are from Rey et al. (2001) and are based on the Lee et al. (1994) synthetic HB models. The two lower isochrones are, respectively, 1.1 Gyr and 2.2 Gyr younger than the top isochrone. Mackey & Gilmore (2004, MNRAS 355, 504).

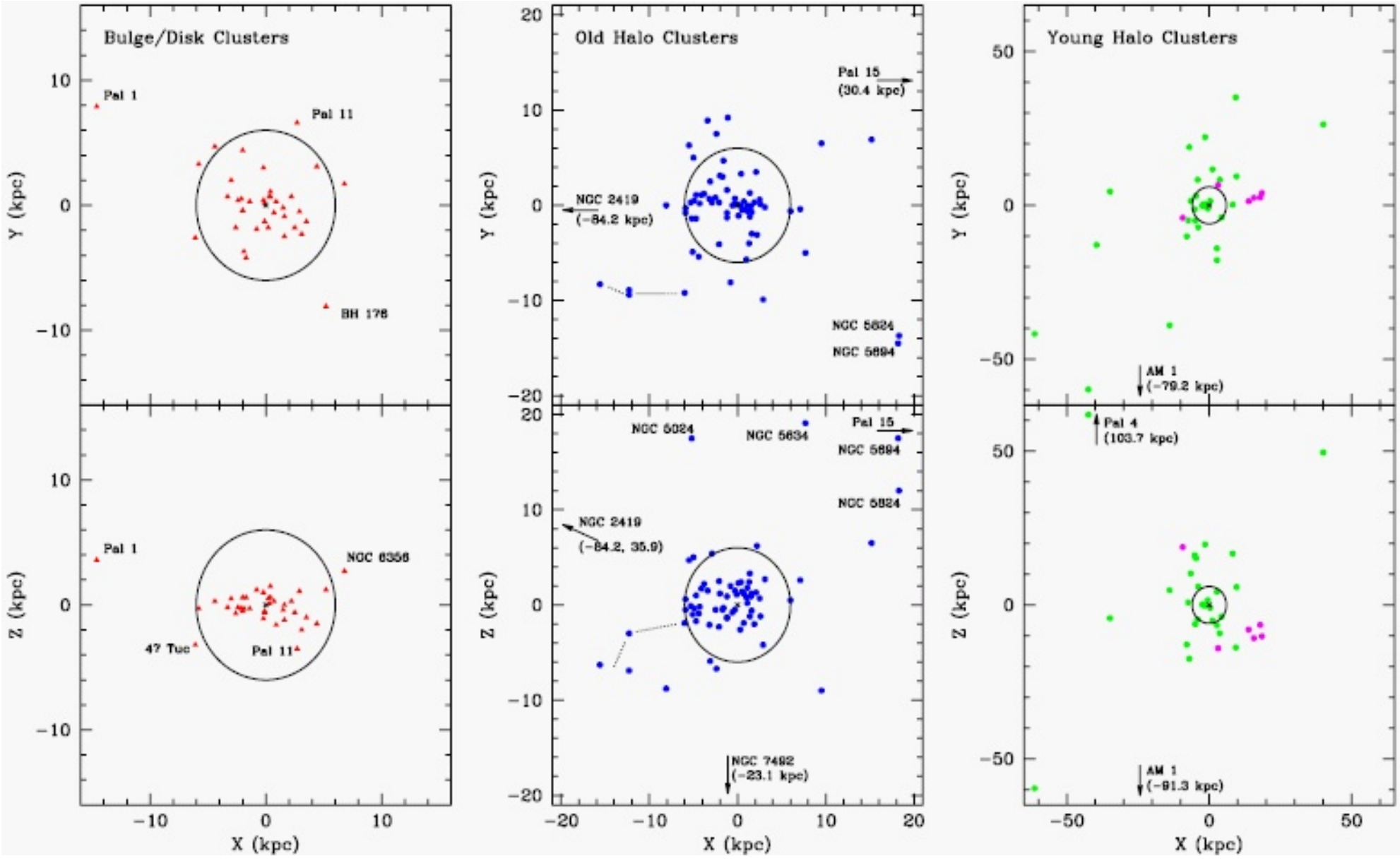

Spatial positions of GGCs in each of the Galactic subsystems. The Sun is at $(X, Y, Z) = (-8, 0, 0)$. In each diagram a circle of radius 6 kpc is marked. The six Sagittarius GCs are marked with magenta points in the YH diagram, while the four GCs linked with the Canis Major dwarf are joined with a dotted line in the OH plot. Mackey & Gilmore (2004, MNRAS 355, 504).

Zinn (1993)

- three groups of GCs are quite distinct in terms of their typical ages, spatial distributions and mean dynamical characteristics
- BD+OH GCs formed during a dissipative collapse of the ELS type
- YH GCs (and some metal-poor OH GCs) formed in external dwarf galaxies and later accreted into the Galactic halo as suggested by SZ model
- YH GCs must bear some resemblance to the GCs observed in the MW DGs

GCSs of the MW dwarf galaxies

- 13 dwarf companions to the Milky Way
- Mackey & van den Bergh (2005, MNRAS 360, 631)
- Mackey & Gilmore (2004, MNRAS 355, 504)
  - only the four most massive – LMC, SMC, Fornax and Sagittarius dSphs – contain globular cluster systems
  - young massive GCs in MCs (age of few Myr)
  - updated database of (Galactic and external) GCs parameters (mostly HB type)

GCSs of dSph galaxies in HBR – [Fe/H] diagram

- **SMC**
  - classic second-parameter effect
  - metal-intermediate OH GCs have BHBs, whereas the SMC GCs have entirely RHBs
  - it is consistent with SMC GCs beeing $\approx$ 3 Gyr younger than the OH GCs
- **LMC**, **Fornax dSph**, and **Sagittarius dSph**
  - contains only/mostly YH-type clusters
  - but many of them seem to be coeval with the oldest GGCs
- discrepant and uncertain age ($\sigma_\tau \approx 1$ Gyr) and metallicity measurements

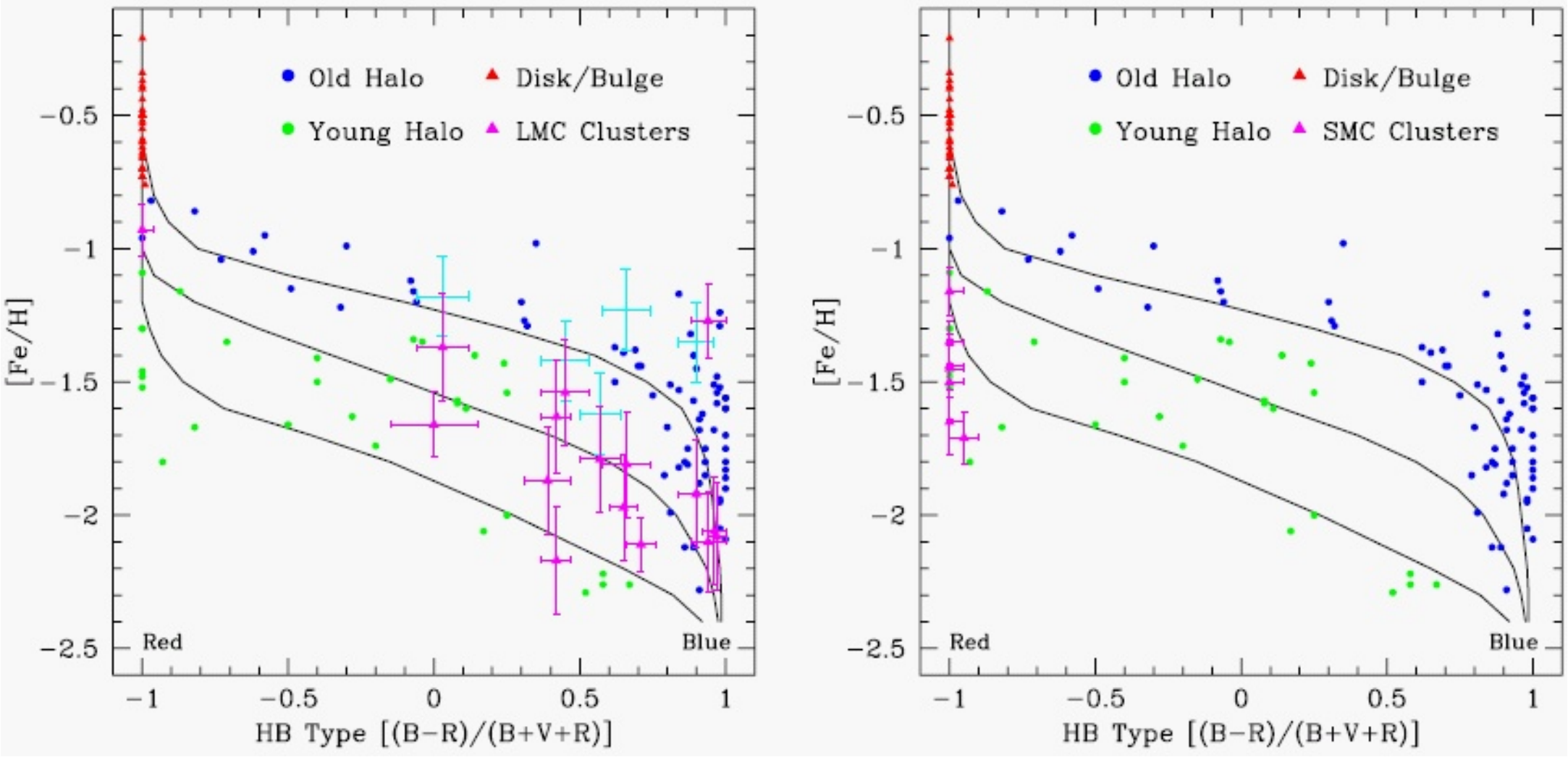

HB-type vs. metallicity diagrams for the LMC (left) and SMC (right), cluster systems. Points for the three Galactic globular cluster subsystems are also plotted. Cyan points represent alternative (higher) metallicity measurements for the clusters directly below them. The overplotted lower isochrones are 1.1 Gyr and 2.2 Gyr younger than the top isochrone. Mackey & Gilmore (2004, MNRAS 355, 504).

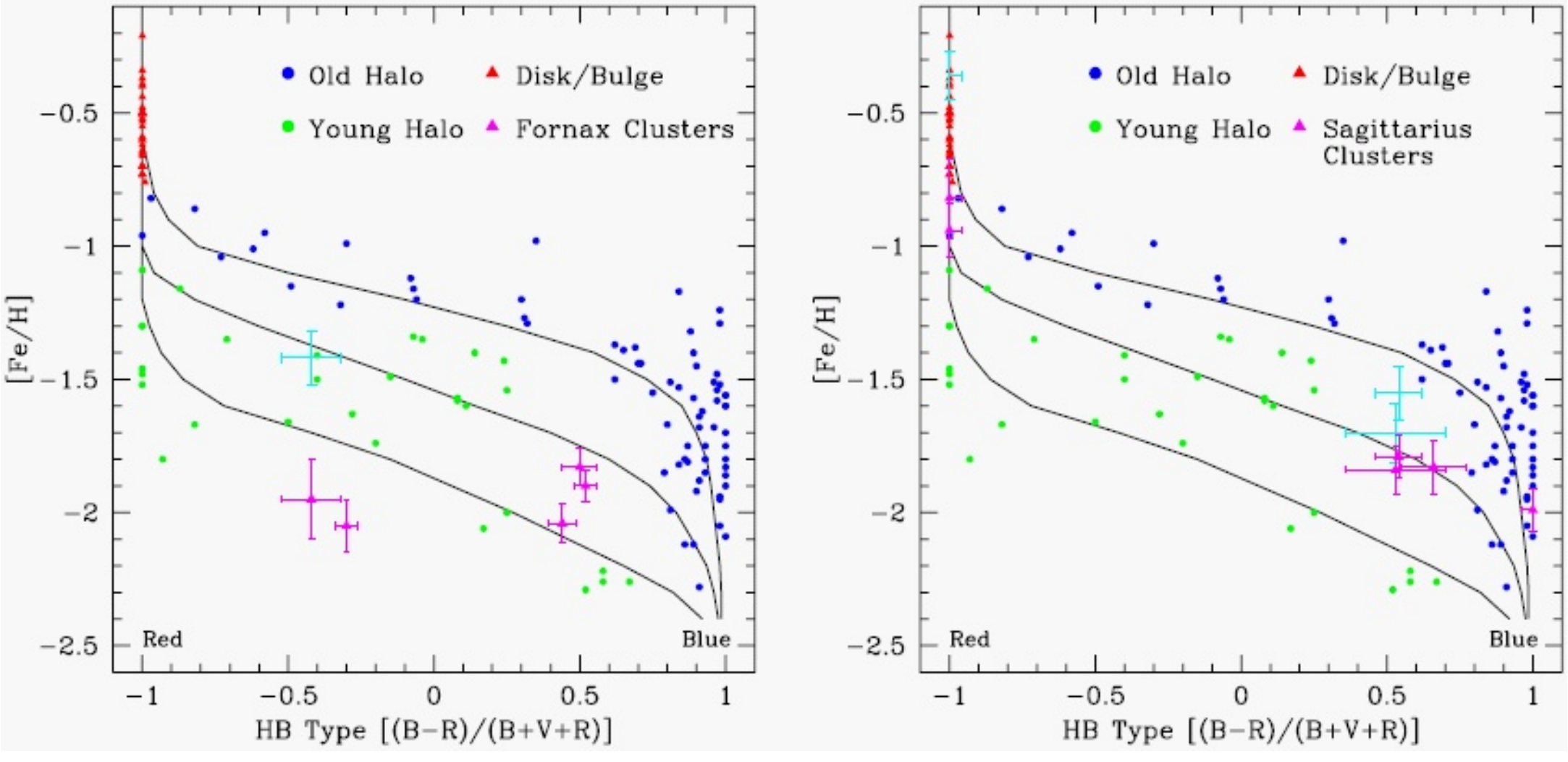

HB-type vs. metallicity diagrams for Fornax dSph (left) and Sagittarius dSph (right) cluster systems. Points for the three Galactic globular cluster subsystems are also plotted. Cyan points represent alternative (higher) metallicity measurements for the clusters directly below them. The overplotted lower isochrones are 1.1 Gyr and 2.2 Gyr younger than the top isochrone. Mackey & Gilmore (2004, MNRAS 355, 504).

Conclusions

- in terms of HBR – [Fe/H] plot majority of the external GCs is indistinguishable from YH GGCs
- BD and OH possess mostly compact clusters, and YH possesses a large fraction of very expanded clusters; the distribution of core radii for the external GCs matches the YH distribution
- YH GCs have large values of RR Lyrae specific frequency $S_{\rm RR}$; in this they strongly resemble the external GCs; in contrast OH and BD GCs have small specific frequencies.
  - $S_{\rm RR} = N_{\rm RR} \times 10^{0.4(M_V+7.5)}$

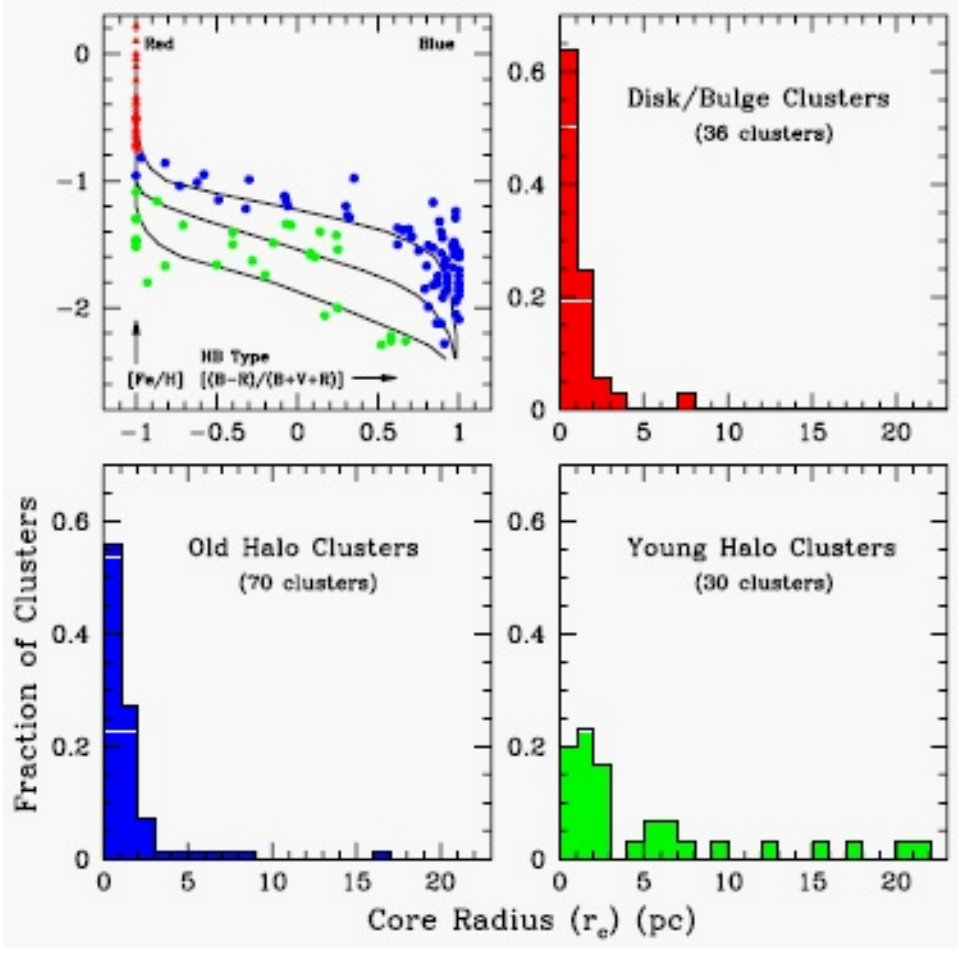

The distribution of core radii for the three Galactic globular cluster subsystems. Mackey & Gilmore (2004, MNRAS 355, 504).

Age differences between clusters

- Do GGCs differ in age by ≈ 2 Gyr?
- Do Galactic OH and extragalactic GCs differ in age by ≈ 2 Gyr?
- second-parameter GC pairs
  - the same metallicity
  - very different HBs (RHB and BHB)
- turnoff ages and reddening uncertainties
- **Review by Catelan** (2009, ApSS 320, 261)
  - age may be the the global second parameter driving the mean HB colour for some GCs, but for many GCs environmental effects might be a local second parameter generating dispersion in colour
- NGC288 (BHB) – NGC362 (RHB)
  - [Fe/H] ≈ -1.3 (ZW), ≈ -1.1 (CG)
- M13 (EBHB) – M3 (BHB+RHB, HBR ≈ 0)
  - [Fe/H] ≈ -1.5 (ZW)
  - no significant age difference for whole HB in M13
  - origin of EBHB stars may not be linked to the GC age, but rather to other processes that may trigger enhanced mass loss on RGB
  - after removing all M13 EBHB stars the different HB types can be explained entirely in terms of turnoff age differences

The relative age that is required to explain the difference in HB type between M3 and M13 entirely in terms of age (lines corresponding to different mass loss formula) plotted as a function of the M3 absolute age for two determinations of turnoff age difference, by Salaris & Weiss (2002) and by Rey et al. (2001). Catelan (2009).

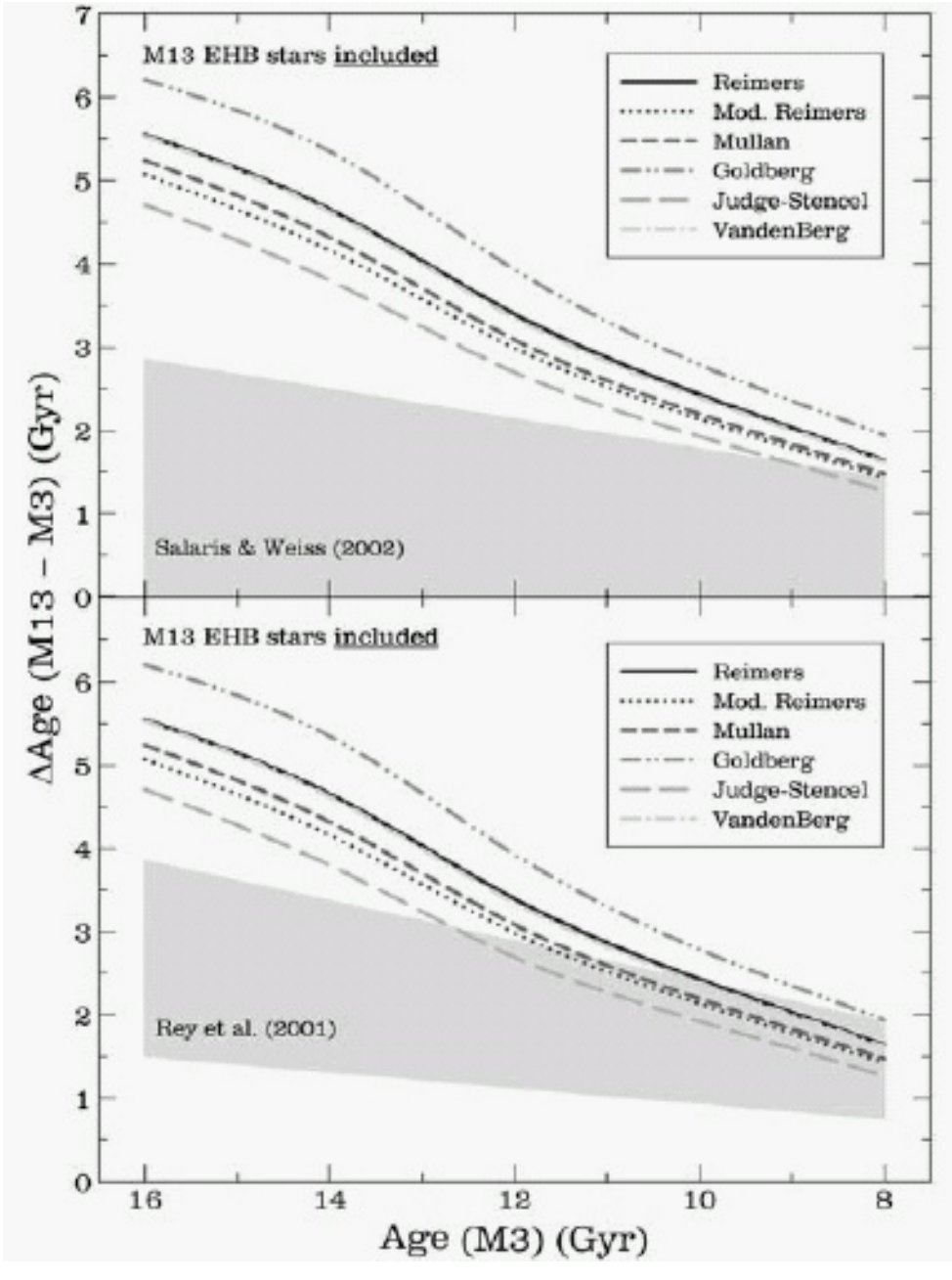
M13 EHB stars included
Reimers
Mod. Reimers
Mullan
Goldberg
Judge-Stencel
VandenBerg
Salaris & Weiss (2002)
M13 EHB stars included
Reimers
Mod. Reimers
Mullan
Goldberg
Judge-Stencel
VandenBerg
Rey et al. (2001)
ΔAge (M13 – M3) (Gyr)
Age (M3) (Gyr)

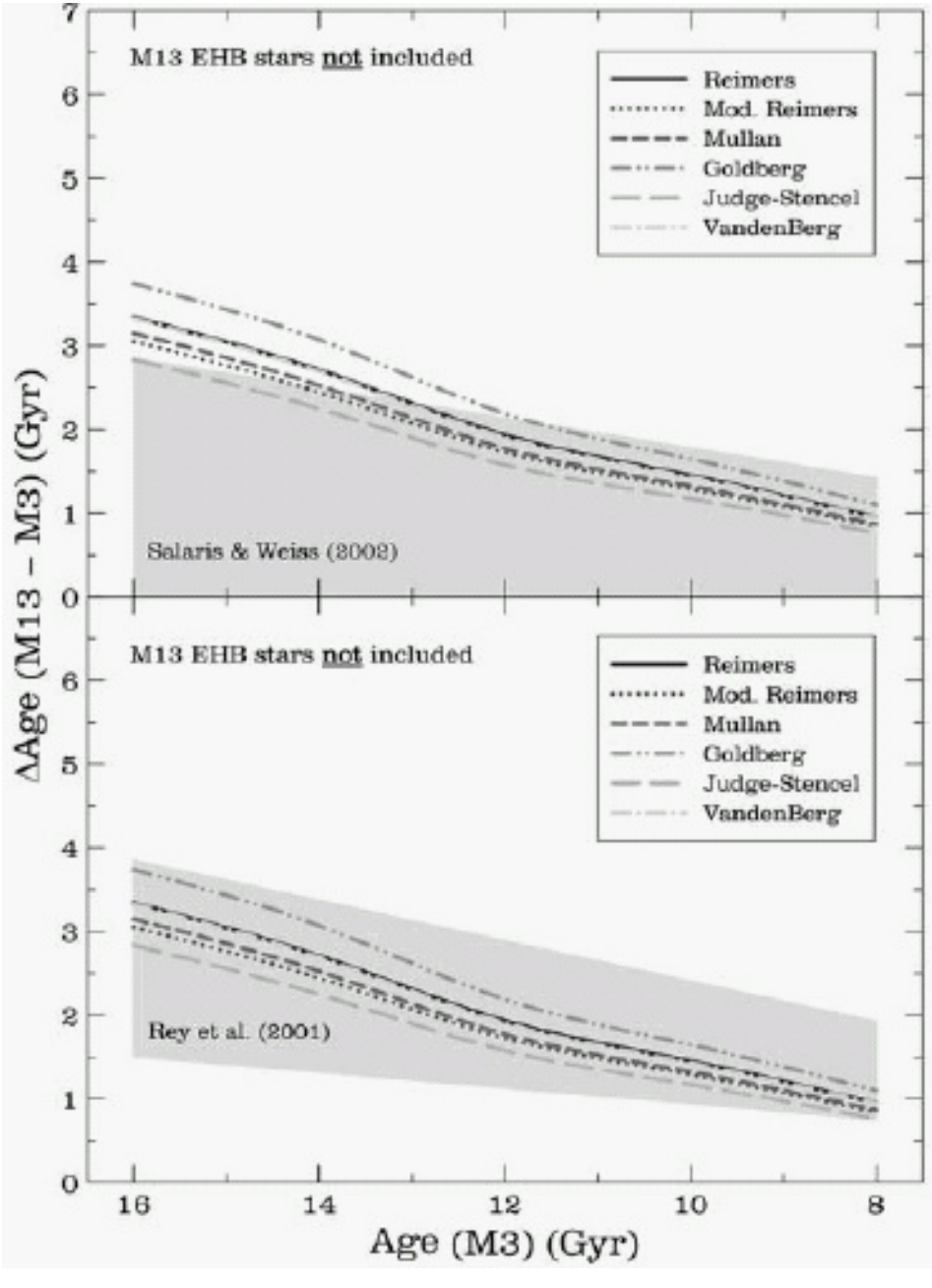
M13 EHB stars not included
Reimers
Mod. Reimers
Mullan
Goldberg
Judge-Stencel
VandenBerg
Salaris & Weiss (2002)
M13 EHB stars not included
Reimers
Mod. Reimers
Mullan
Goldberg
Judge-Stencel
VandenBerg
Rey et al. (2001)
ΔAge (M13 – M3) (Gyr)
Age (M3) (Gyr)

Oosterhoff type of dSph galaxies

- GGCs show Oosterhoff dichotomy
  - OoI and OoII + OoInt + OoIII
  - Galactic halo field seems to show this effect too (see Miceli et al. 2008, ApJ 678, 865)
- dSph galaxies and their GCs are predominantly OoInt
- If the halo was accreted from "protogalactic fragments" like present-day dSph satellite galaxies, the Galactic halo ***should not*** display the Oosterhoff dichotomy!
- Galactic halo cannot have been assembled by the accretion of dwarf galaxies resembling MW satellites as proposed by SZ model!

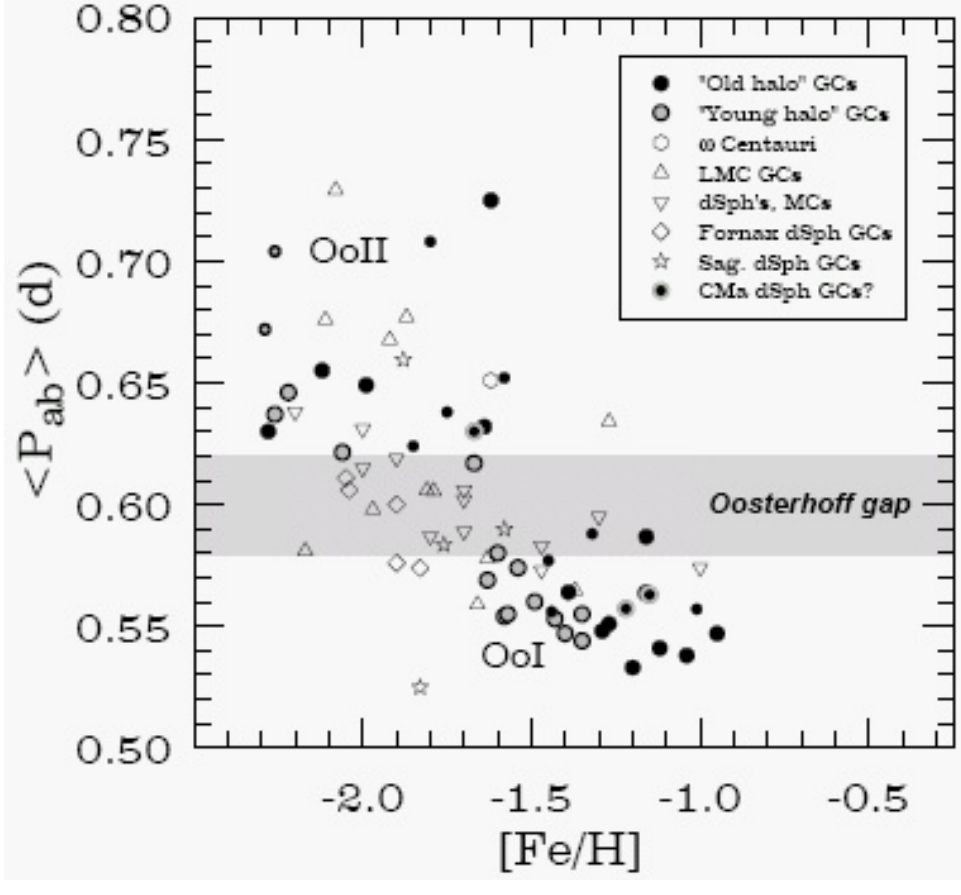

Secular period-changes of RR Lyrae stars

Secular period-changes of RR Lyrae stars

- pulsation period is related to the structure of the star
  - $P\sqrt{\varrho} = \text{const}$
  - $M = \text{const} \quad \Rightarrow \quad dP/dt = 1.5 \times (P/R) \times dR/dt$
  - period changes $\rightarrow$ evolutionary changes of radius
- direction and speed of evolution in HR diagram

Theoretical predictions

- two basic types of evolutionary tracks from HB depending on core-mass and metallicity
  - slow evolution to the blue, away from ZAHB, followed by more rapid evolution to the red at higher luminosities
  - slow evolution redward from ZAHB, followed by more rapid evolution to the red at the end of the HB phase
- most HB stars are expected to be in slow early stages of evolution from ZAHB
  - $|\beta| < 0.03$ d/Myr

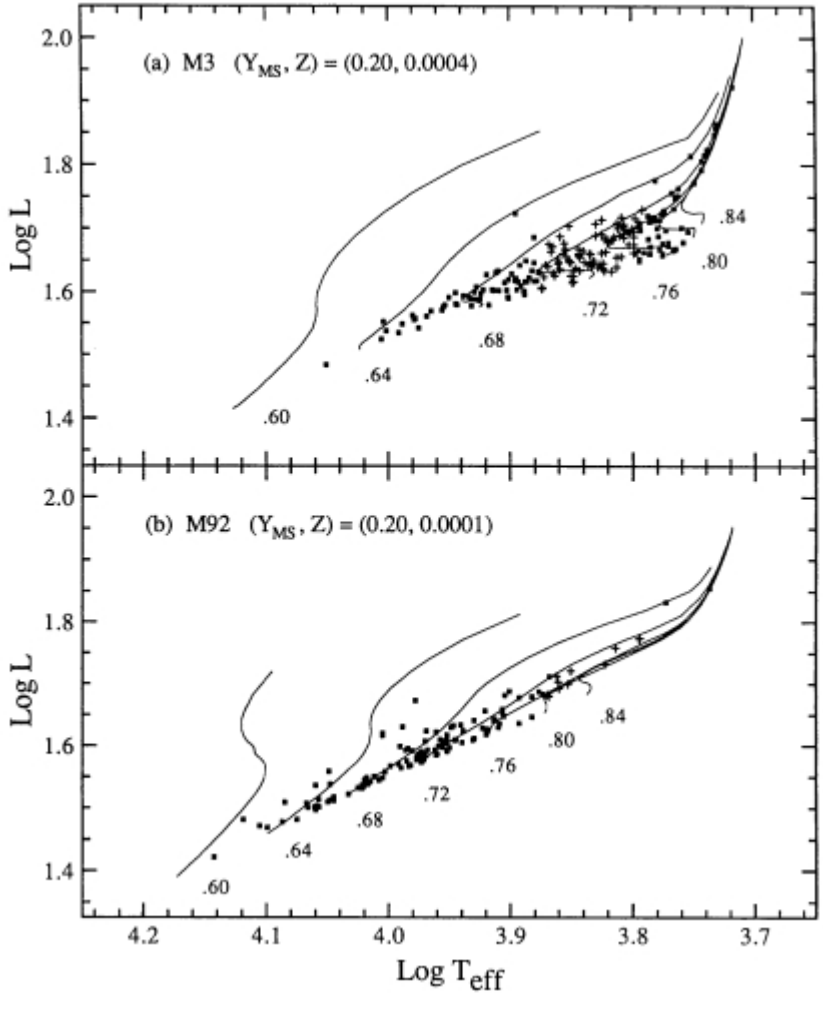

Synthetic models of HB for M 3 (OoI) and M 92 (OoII) with evolutionary tracks from HB. RR Lyrae stars are represented with plus signs. Each track is labeled with total mass in solar units (Lee et al. 1990).

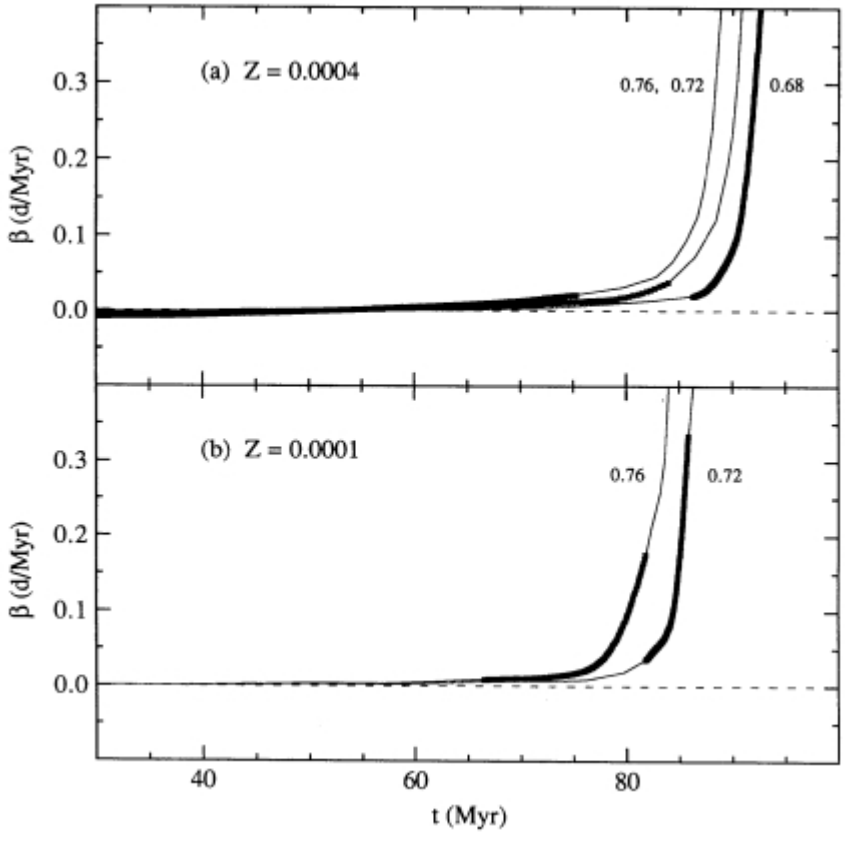

Evolutionary rates of period change $\beta = dP/dt$ along the HB tracks as a function of time elapsed from ZAHB. Each track is labeled with total mass. The heavy lines show the approximate range of the instability strip (Lee 1991).

Evolution from ZAHB in HR diagram

- redward $\Rightarrow \beta > 0$ d/Myr (increase of P)
- blueward $\Rightarrow \beta < 0$ d/Myr (decrease of P)
- $\langle\beta\rangle$ depends on the HB type
  - more RR Lyrae stars with positive β than with negative values in GCs with blue HB (mostly OoII)

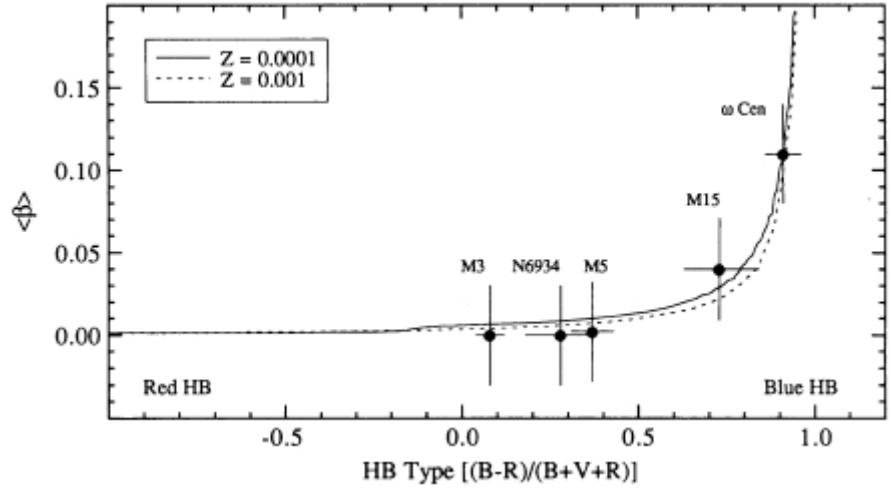

Synthetic HB calculations of the mean period-change rate $\langle\beta\rangle$ as a function of HB type. Filled circles show observational results for the five best-studied globular clusters (Lee 1991).

O-C diagram

- comparison of the observed (O) times of brightness maximum with those calculated (C) according to the adopted ephemeris with constant period

  $$T_{\max} = T_0 + P \times E$$

  E is cycle number from epoch T_0
- if P is constant the $O-C$ diagram is a ***straight line***
- if P is changing with a slow and constant rate a good approximation for the $O-C$ diagram is a ***parabola***

  $$P(t) = P_0 + \beta \times t \qquad \beta = dP/dt$$
- ***sine curve*** in the $O-C$ diagram indicates periodic variations of P
  - light-time effect caused by orbital motion in binary system

Warning

- cumulative effect of period 'noise' on the $O-C$ diagram

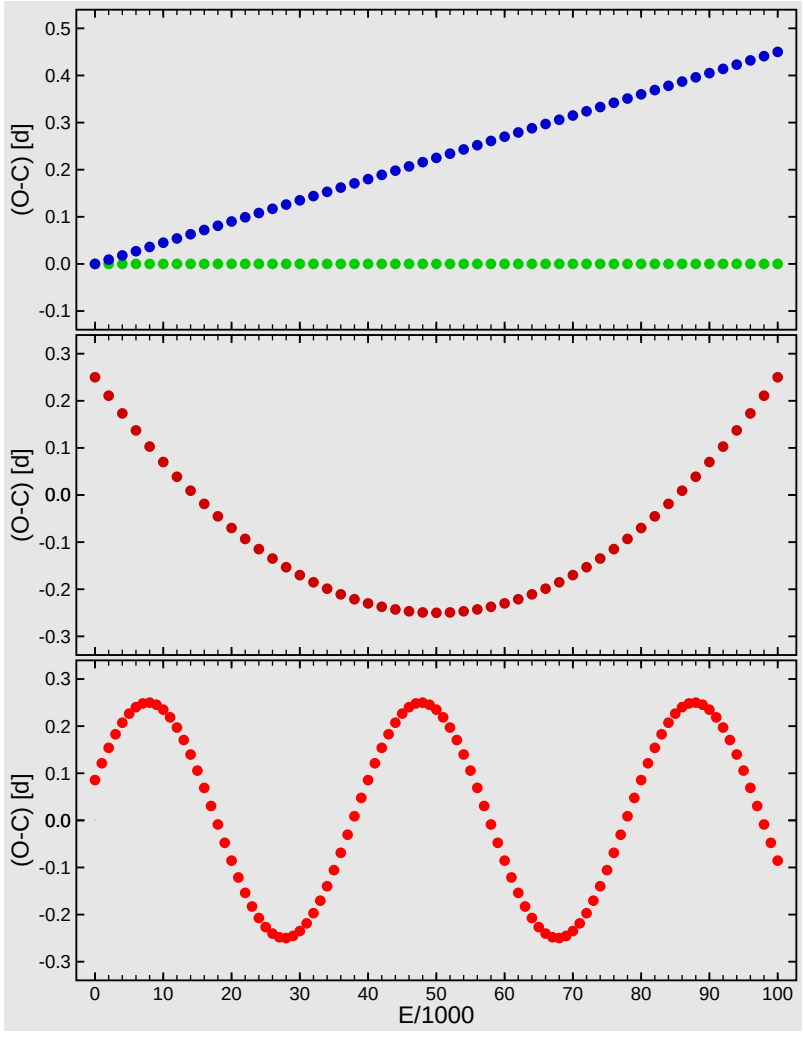

Different types of the $O-C$ diagram: upper panel – constant period, middle panel – constant rate of period change, bottom panel – cyclic period changes.

Observed period changes in RR Lyrae stars

- evolutionary period changes in RR Lyrae stars are masked by 'noise' of irregular character
- random and/or abrupt period changes
- changes (one order) too fast for evolutionary origin

Mean rate of period change for RR Lyrae stars from a single globular cluster

- uniform sample of RR Lyrae stars
- ω Cen – Jurcsik et al. (2001)
  - period changes of most RRab stars are in agreement with theoretical predictions for late redward phase of the HB evolution
    $\beta = 10^{-11} - 10^{-9}$ d/d
  - period changes of most RRc stars show more complex irregular behaviour
  - irregular period changes and large period decrease rates without satisfactory explanation

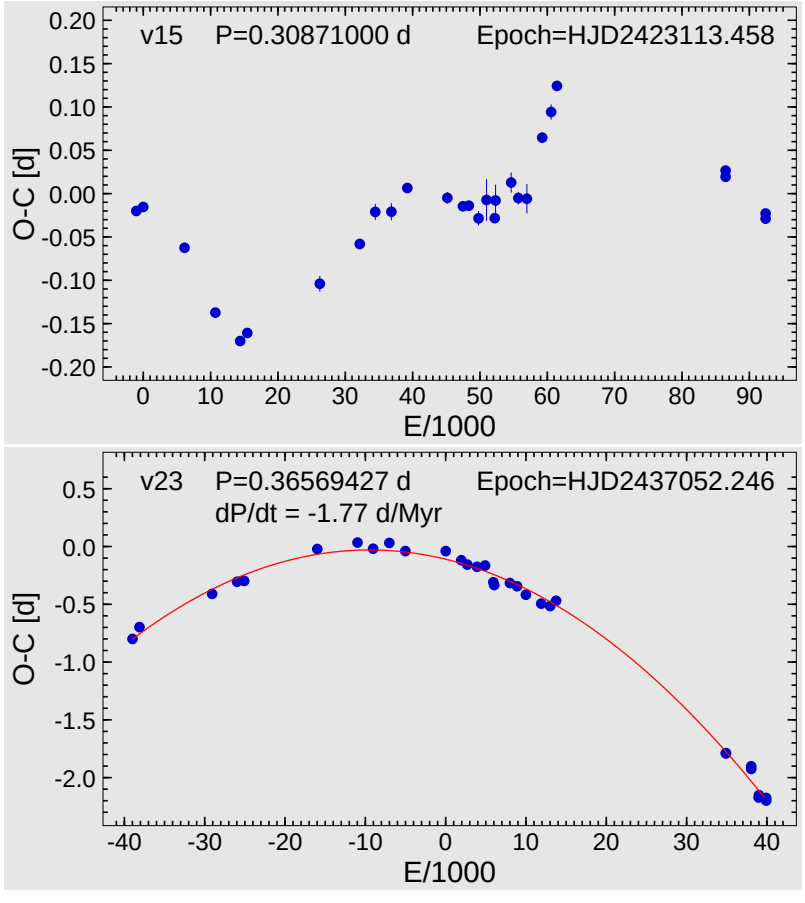

Examples of $O - C$ diagrams for RR Lyrae stars from M 53

Blazhko effect in RR Lyrae stars

Fourier analysis of LCs of RR Lyrae stars

- galactic globular clusters
- MACHO and OGLE data on Galactic Bulge and LMC

Types of the multiperiodic behaviour observed in RR Lyrae stars

- Alcock et al. (2000)
  - RR01 – RRd
  - RR12
  - RR0/1-**v1** – one close component
  - RR0/1-**BL** – two symmetric close components
  - RR0/1-v2 – two asymmetric close components
  - RR0/1-vM – multifrequency close components
  - RR0/1-PC – period change
- period ratio from 0.95 to 1.05
- side-frequencies of a triplet have different amplitudes

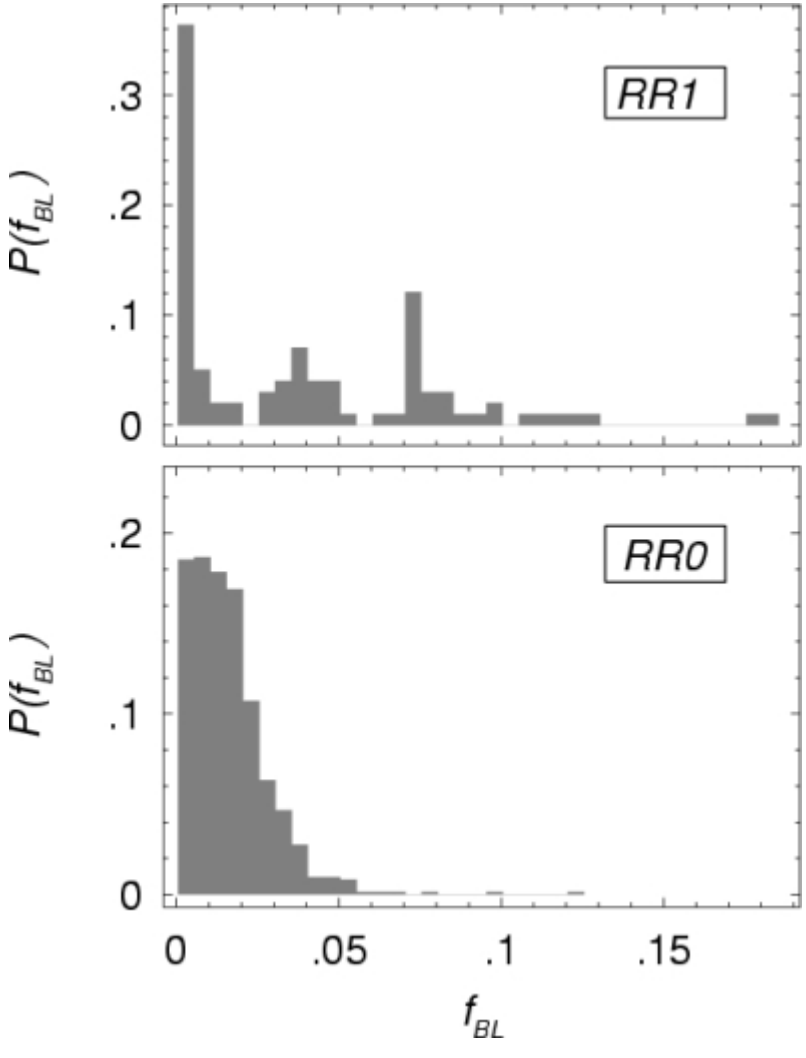

Histograms of modulation frequencies for Blazhko RRab (upper panel) and RRc (bottom panel) stars in LMC (Nagy and Kovács 2006).

RR0-BL

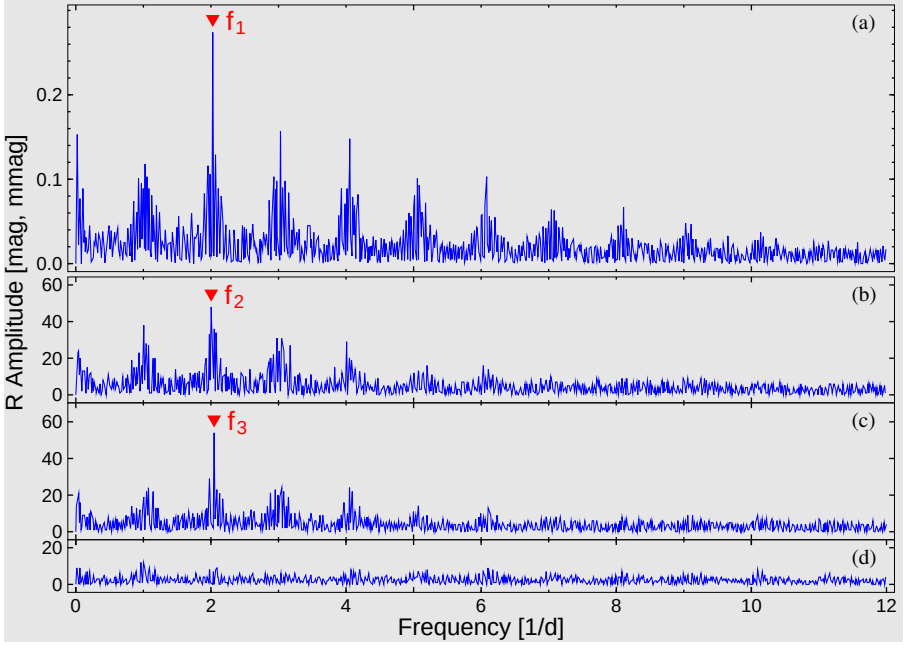

Fourier spectra for the Blazhko RRab star v11 exhibiting frequency triplet (RR0-BL). Subsequent stages of prewithening are shown: (a) original R-filter data, (b) after prewhitening with frequency $f_1 = 2.027521$ 1/d, (c) after removing frequencies f_1 and $f_2 = 2.00548$ 1/d, and (b) after prewhitening with frequency f_1, f_2, and $f_3 = 2.04755$ 1/d, The separations between non-radial components and the radial mode are $\Delta f_{21} = f_2 - f_1 = -0.022$ 1/d and $\Delta f_{31} = f_3 - f_1 = 0.020$ 1/d. This translates into the Blazhko modulation period of $P_{\rm BL} \approx 47.6$ d.

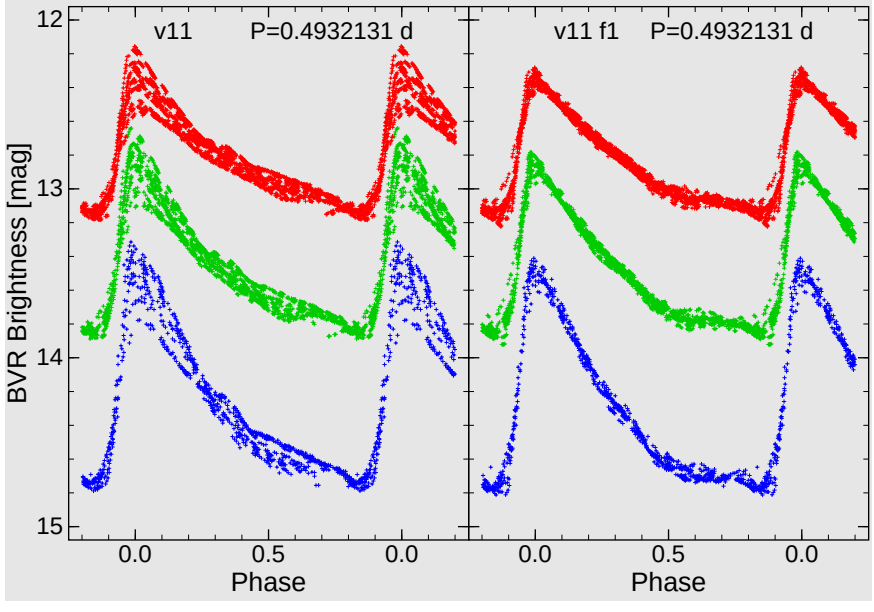

BVR light curves of the Blazhko RRab star v11 with two equally-spaced non-radial component (RR0-BL). Blue symbols show B-filter magnitudes, green symbols show V-filter magnitudes, and red symbols show R-filter magnitudes. Left panel presents original data and right panel shows oscillations in the fundamental radial mode only, that is after removing non-radial and combination frequencies.

RR0-v1

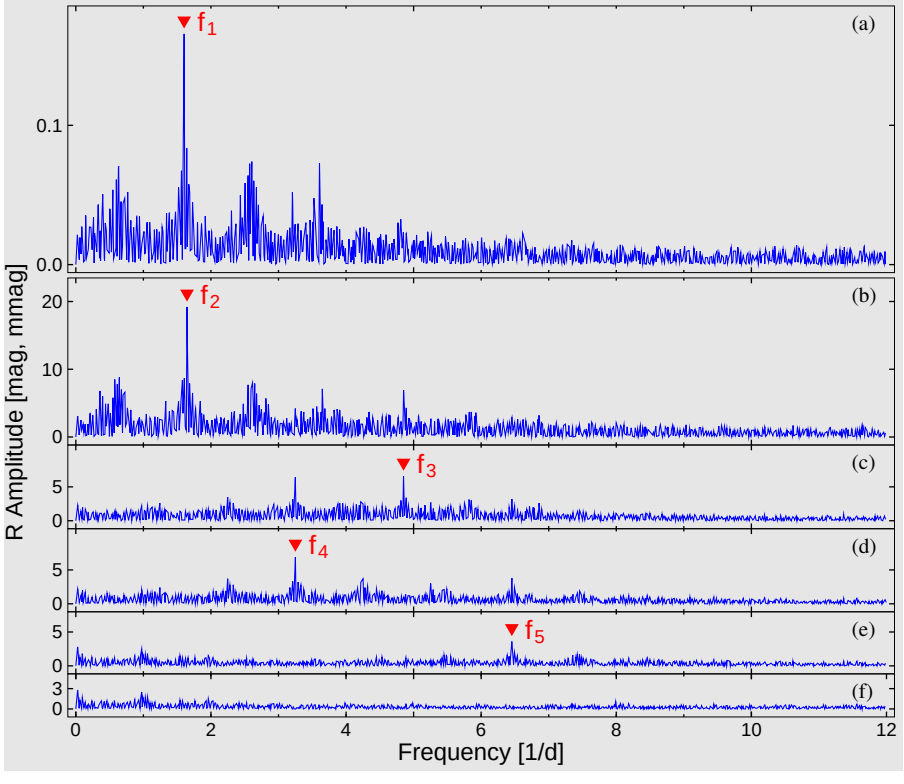

Fourier spectra for the Blazhko RRab star v39 showing frequency doublet (RR0-v1): (a) for original V-filter data, (b) after prewhitening with primary frequency $f_1 = 1.602700$ 1/d, (c) after removing f_1 and secondary frequency $f_2 = 1.64631$ 1/d. Remaining components are combination frequencies of f_1 and f_2: (c) $f_3 = 2f_1 + f_2 = 4.8519$ 1/d, (d) $f_4 = f_1 + f_2 = 3.2493$ 1/d, and (e) $f_5 = 3f_1 + f_2 = 6.4542$ 1/d. The separation of the two main frequencies is $\Delta f = f_2 - f_1 = 0.044$ 1/d, which translates into modulation period of $P_{\rm BL} = 22.9$ d.

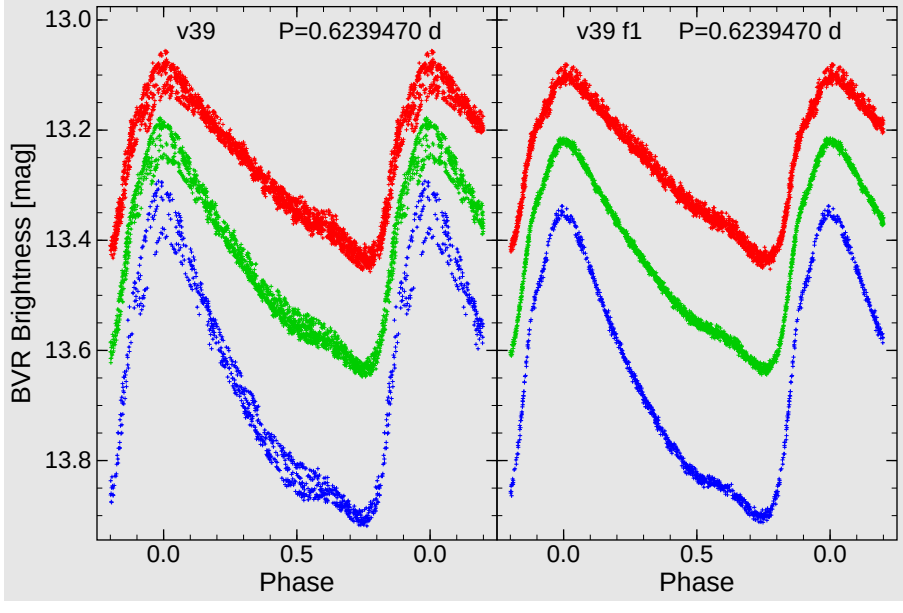

BVR light curves of the Blazhko RRab star v39 with one non-radial component (RR0-v1). Blue symbols show B-filter magnitudes, green symbols show V-filter magnitudes, and red symbols show R-filter magnitudes. Left panel presents original data and right panel shows oscillations in the fundamental radial mode only, that is after removing non-radial and combination frequencies.

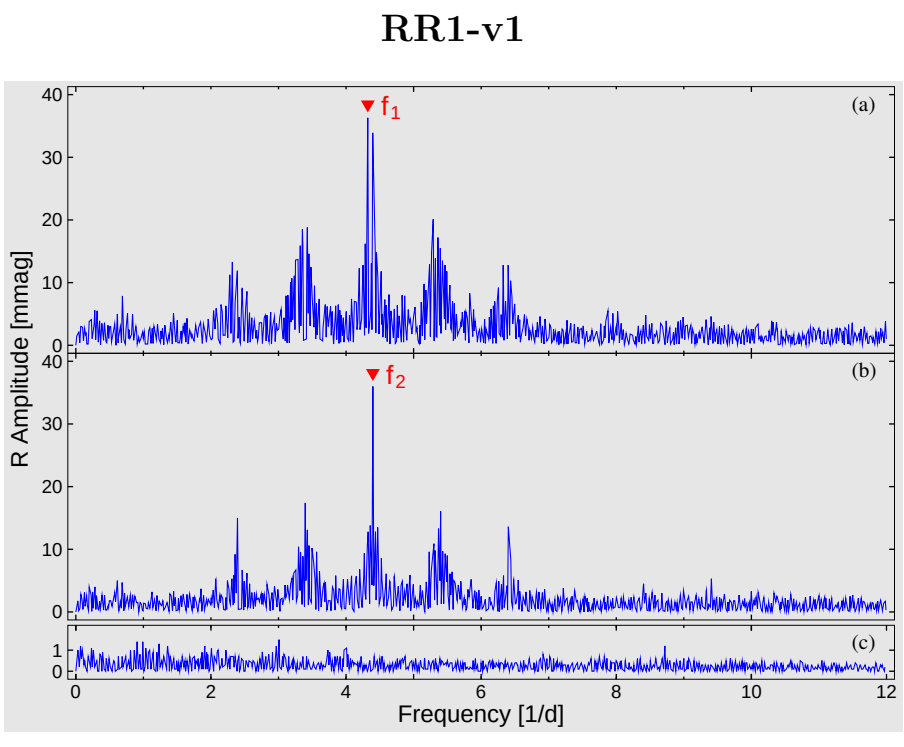

Fourier spectra for the Blazhko RRc star v49 showing frequency doublet (RR1-v1): (a) for original R-filter data, (b) after prewhitening with primary frequency $f_1 = 4.31924$ 1/d, and (c) after removing f_1 and secondary frequency $f_2 = 4.39738$ 1/d. The amplitude scale is the same in every panel. The separation of the two frequencies is $\Delta f = f_2 - f_1 = 0.078$ 1/d, which translates into modulation period of $P_{\rm BL} = 12.8$ d.

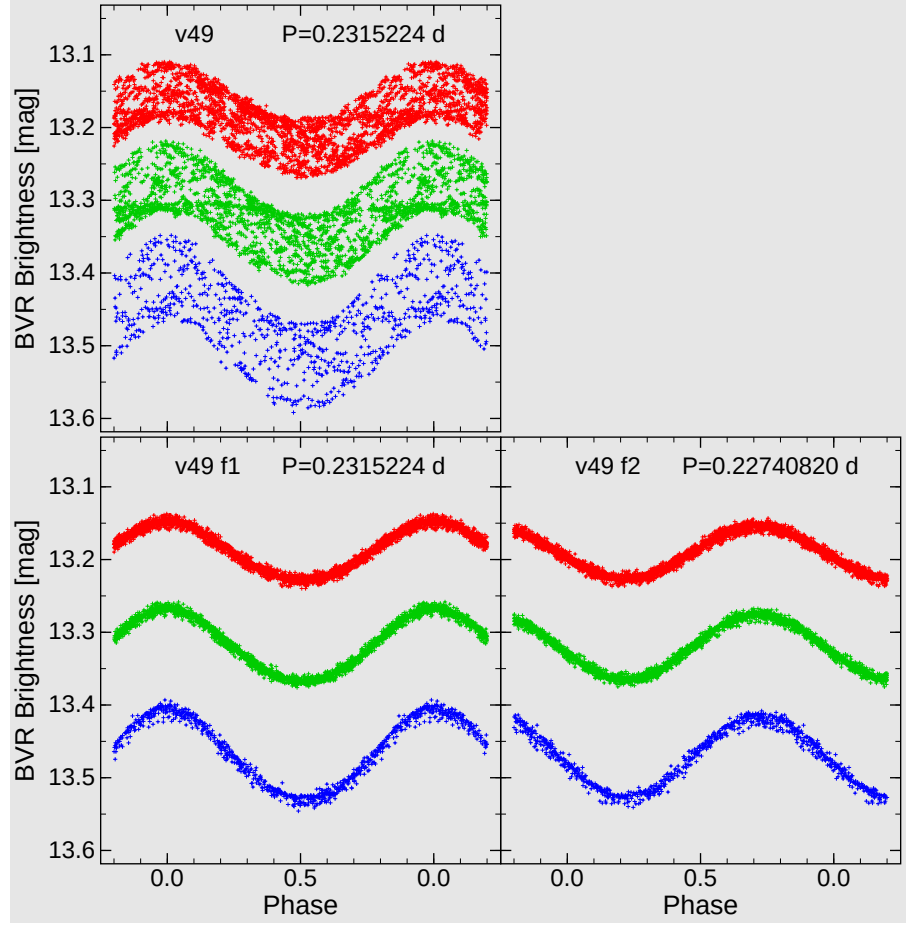

BVR light curves of the RRc Blazhko star v49 with one non-radial component (RR1-v1). Blue symbols show B-filter magnitudes, green symbols show V-filter magnitudes, and red symbols show R-filter magnitudes. Upper panel presents original data and bottom panels show separated oscillations in detected two modes.

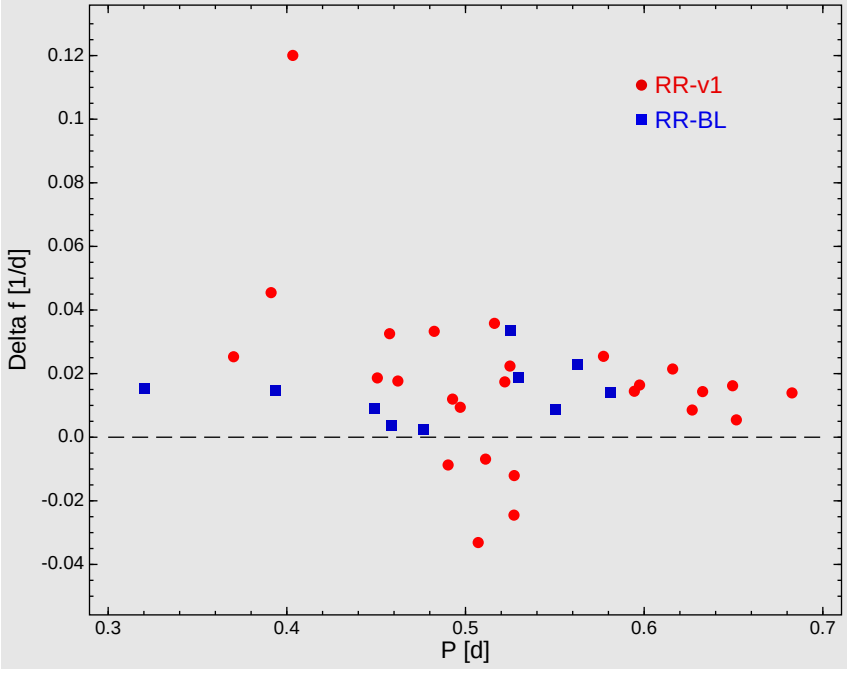

Frequency difference Δf as a function of a period P for OGLE-1 Blazhko RR Lyrae stars. RR-v1 stars are marked with circles and RR-BL variables with squares (Moskalik and Poretti 2003).

- most RR-v1 stars have positive frequency separation, meaning that secondary frequency is higher than the primary one

Non-radial pulsations in RR Lyrae stars

- additional frequencies in very close vicinity to the main radial mode
  - frequency doublets and triplets
- while frequency triplet can be generated from periodic modulation of a purely radial oscillation, such a process cannot produce a doublet
- secondary component of the dublet must correspond to **non-radial** mode of pulsation

Incidence rates

- in Galactic Bulge only 3 % of RRc and 25 % RRab stars show Blazhko effect
- the fraction of multiperiodic RRab stars is two times higher in Galactic Bulge than in LMC
  - metallicity effect

Origin of Blazhko phenomenon

- non-radial modes as a main agent responsible for the amplitude/phase modulation
- ***resonant excitation of non-radial modes***
  - Dziembowski i Mizerski (2004)
  - excitation of dipole modes
  - nonlinear resonance between radial mode and non radial mode
  - modulation period is determined by rotation rate and Brunt–Väisälä frequency
- ***oblique rotator with magnetic field***
  - Shibahashi (2000)
  - excitation of quadrupole modes
  - strong magnetic field (not detected in RR Lyr, Chadid et al 2004)
  - radial mode is deformed by magnetic field to give non-radial mode which symmetry axis coincides with magnetic axis
  - modulation period is equal to one or half rotation period

- ***turbulent convection model***
  - Stothers (2006, ApJ 652, 643)
  - transient magnetic field generated by turbulent or rotational dynamo mechanism
  - cyclic changes of the strength of the envelope convection gives rise to the modulation of periodic oscillation
  - strengthening of convection is expected to lower the pulsation amplitude
  - stochastic character

Mode identification

- amplitude ratio – phase shift method
- moment method
- identification of non-radial modes in the brightest RR Lyrae star (RR Lyr, Kolenberg 2002)
  - not conclusive, but favours dipole modes

Problems

- deviations from stricly periodic modulation
- additional long modulation cycles (order of yr)
- unequal amplitudes of side frequencies of triplet structure
- different incidence rates for Blazhko RRab and RRc stars
- effect of metallicity and convection

Simulation of Blazhko modulation

- Periodic changes with modulation
  - amplitude modulation
  - phase modulation
  - period modulation (phase modulation with variable amplitude)

$$m(t) = A[1 + A_A \sin(\omega_B t + \varphi_A)] \sin[\omega t + \varphi + A_\varphi \sin(\omega_B t + \varphi_\varphi)]$$

- Szeidl & Jurcsik (2009, CAs 160, 17)
  - multiplets
  - decrease of amplitude with increase of harmonic order
  - asymmetry of side-frequency amplitudes

  (depends basically on $\Phi = \varphi_A - \varphi_\varphi$)
  - ***symmetric triplets*** ($A_A = 0$ or $A_\varphi = 0$ or $\Phi = 0$ or π)
  - ***doublets*** ($A_A = A_\varphi$ and $\Phi = \pi/2$ or $3\pi/2$)

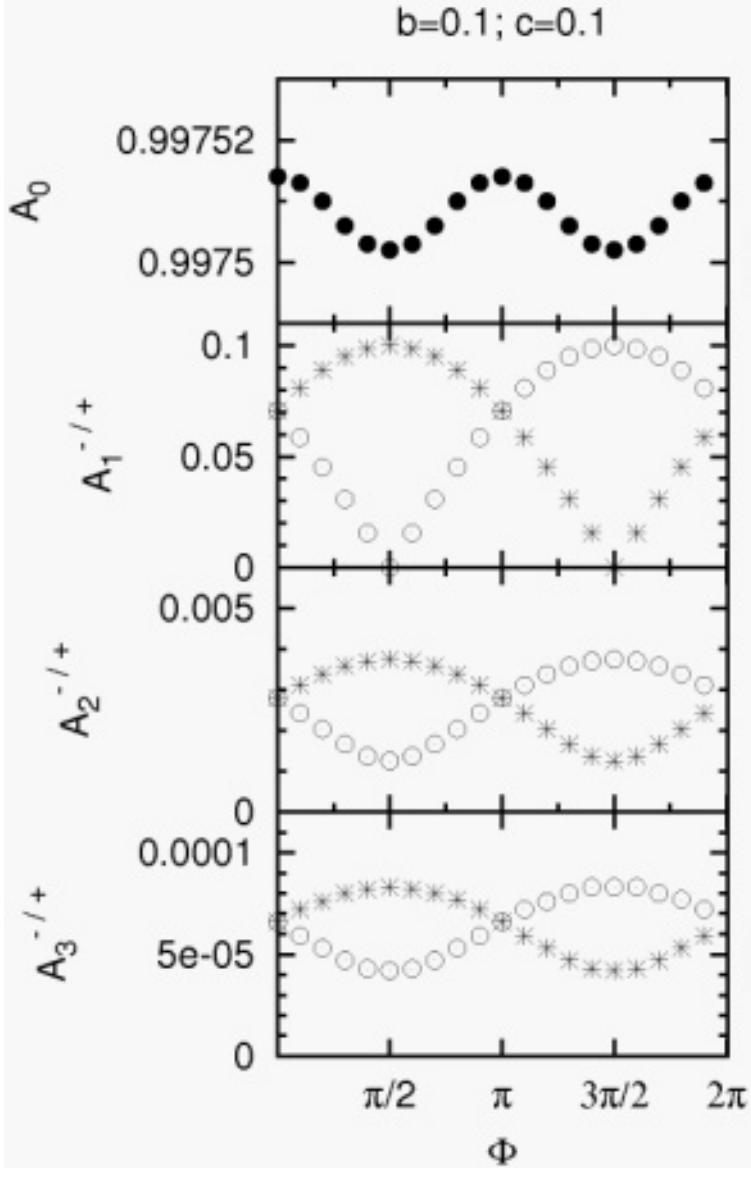

Blazhko effect in RR Lyrae stars: Kepler's view

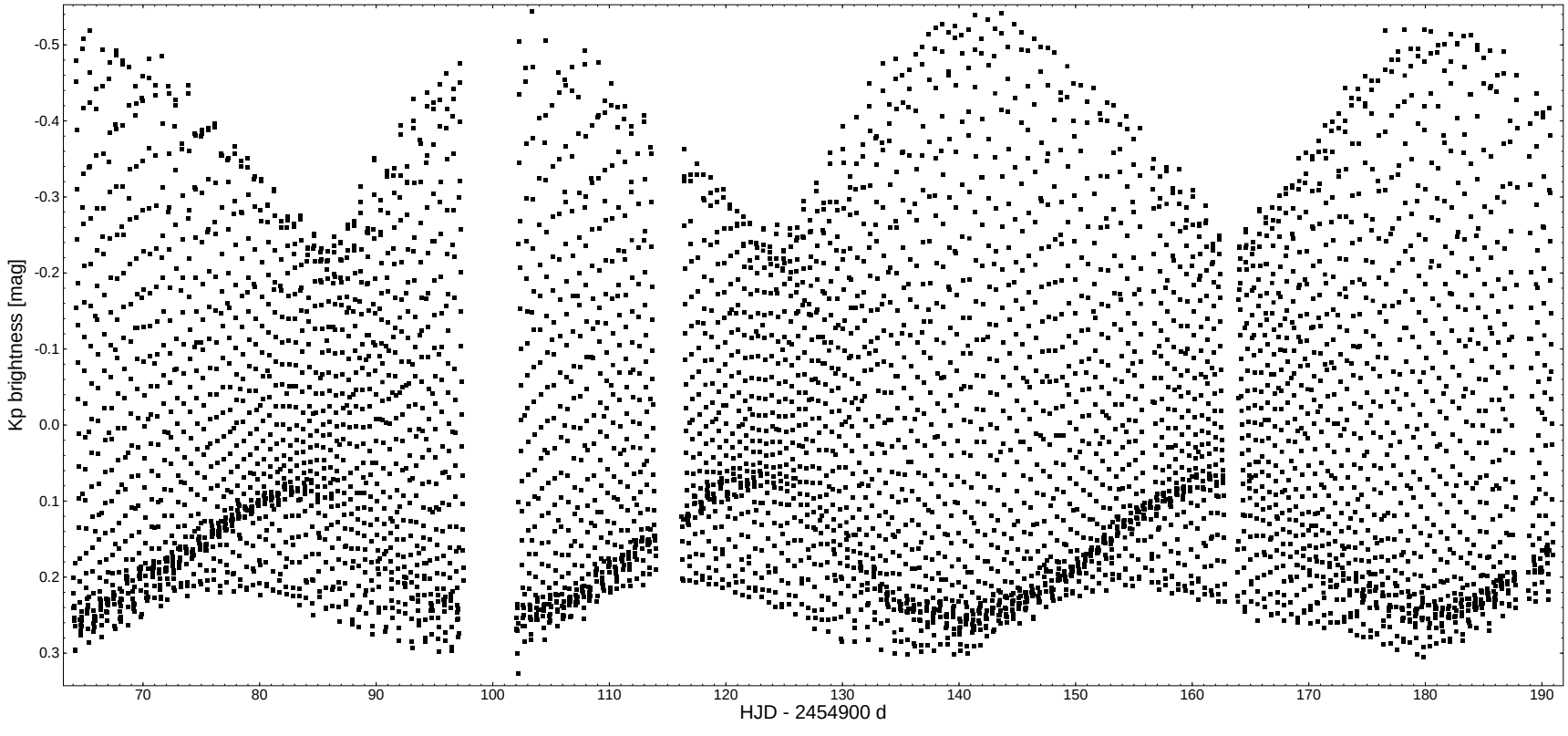
Kp brightness [mag]
-0.5
-0.4
-0.3
-0.2
-0.1
0.0
0.1
0.2
0.3
70
80
90
100
110
120
130
140
150
160
170
180
190
HJD - 2454900 d

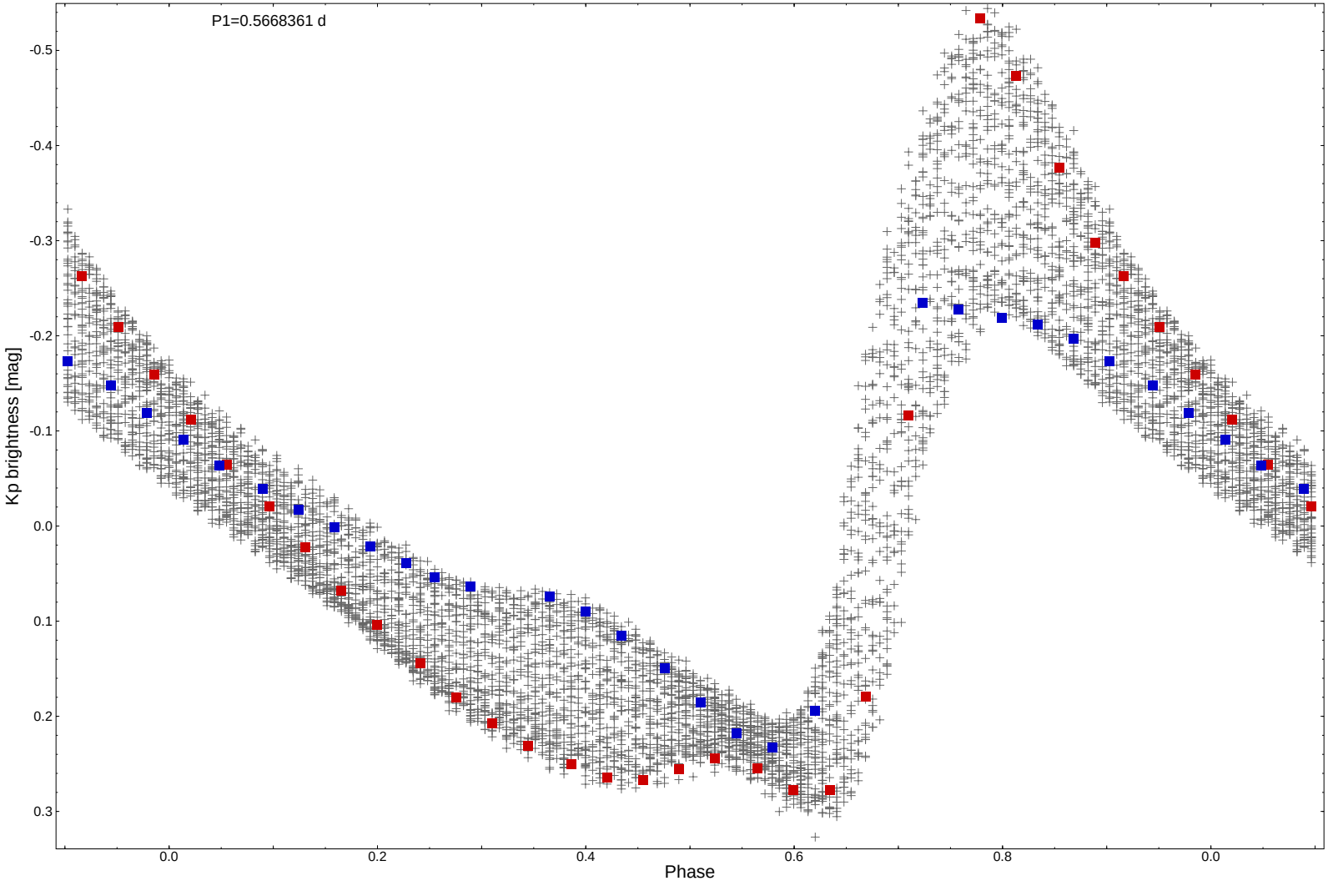
P1=0.5668361 d
Kp brightness [mag]
-0.5
-0.4
-0.3
-0.2
-0.1
0.0
0.1
0.2
0.3
0.0
0.2
0.4
0.6
0.8
0.0
Phase

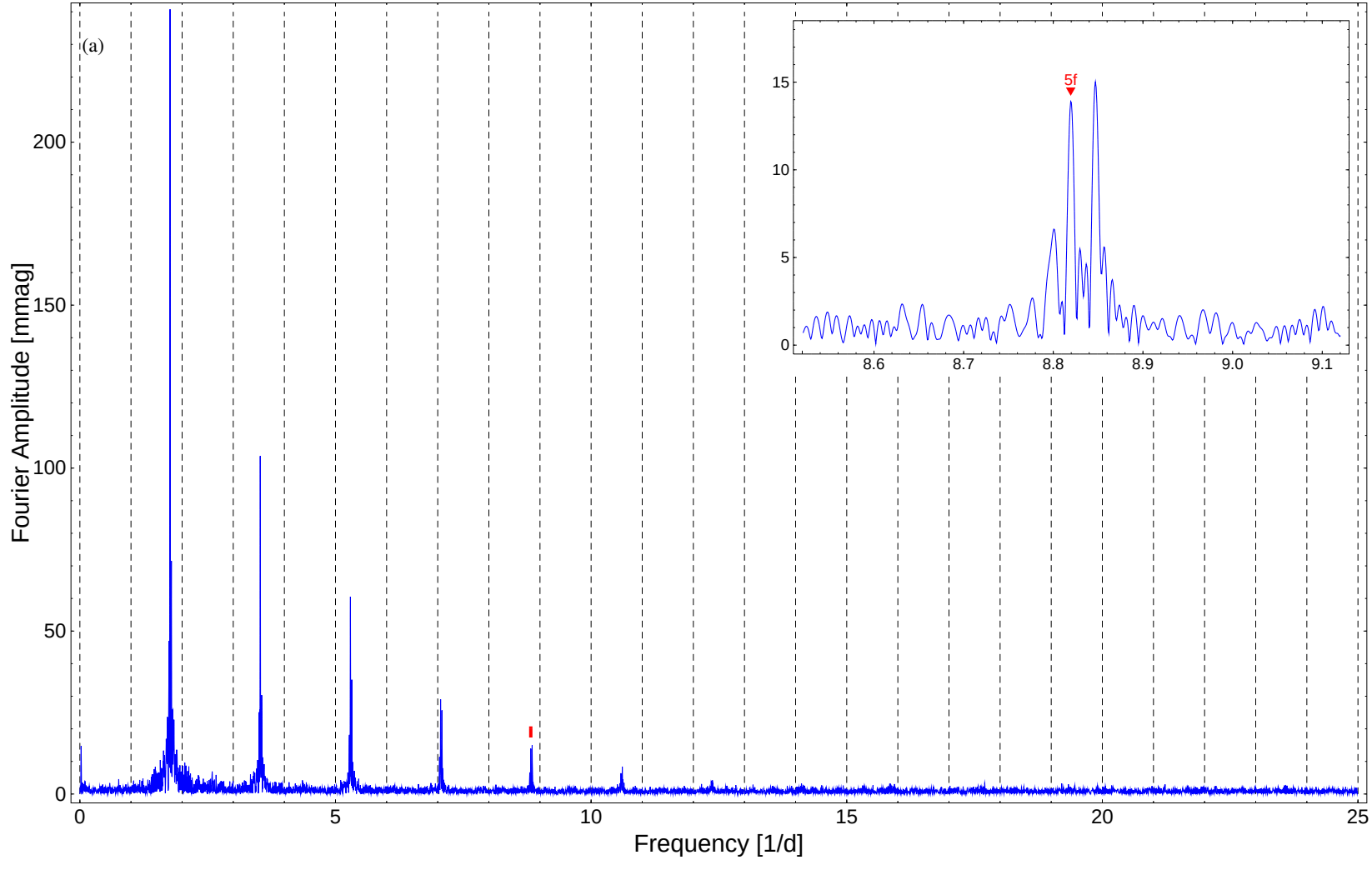
(a)
Fourier Amplitude [mmag]
Frequency [1/d]
0
50
100
150
200
0
5
10
15
20
25
5f
15
10
5
0
8.6
8.7
8.8
8.9
9.0
9.1

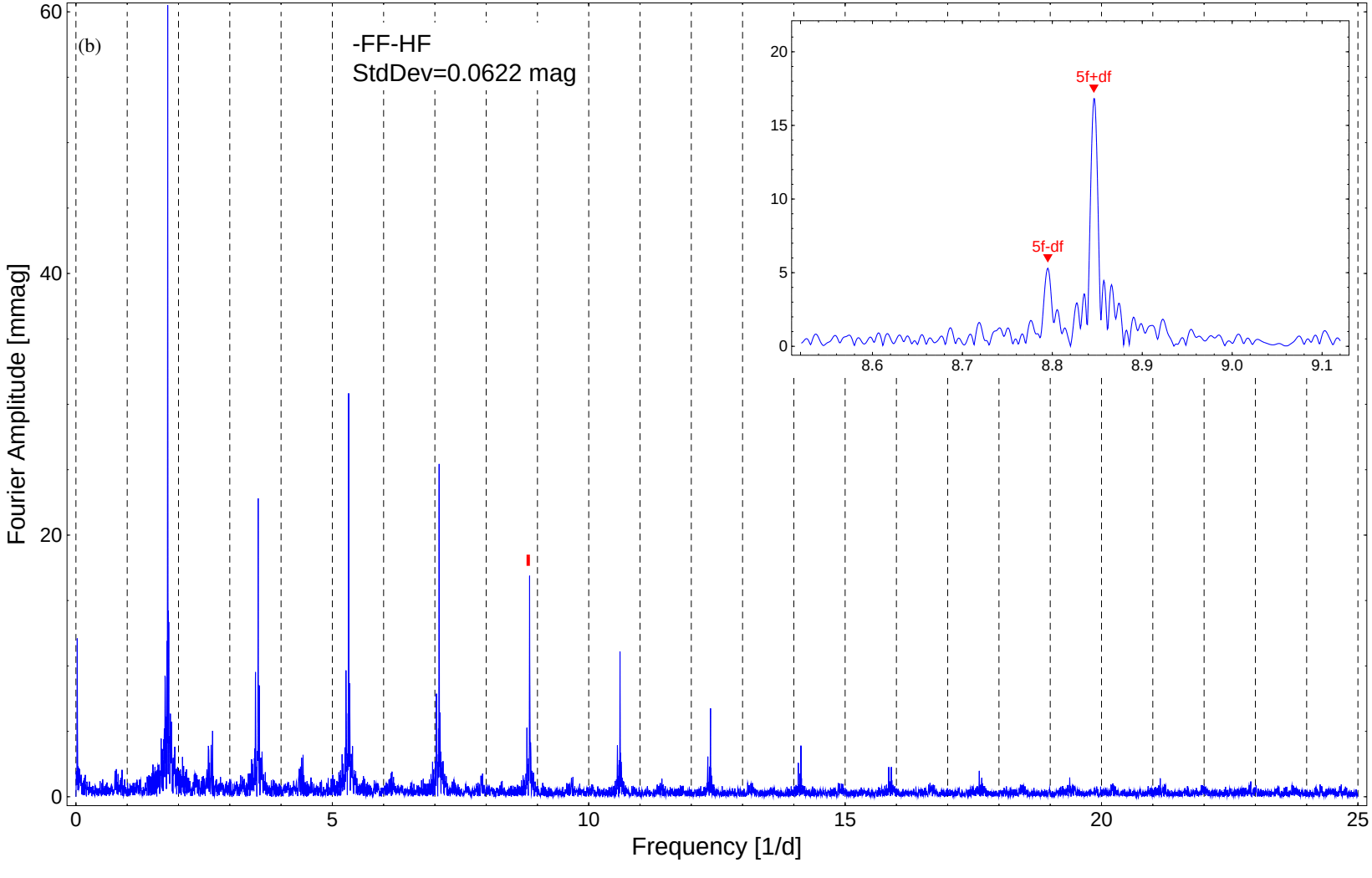
(b)
-FF-HF
StdDev=0.0622 mag
5f+df
5f-df
Fourier Amplitude [mmag]
Frequency [1/d]
0
20
40
60
0
5
10
15
20
25
8.6
8.7
8.8
8.9
9.0
9.1

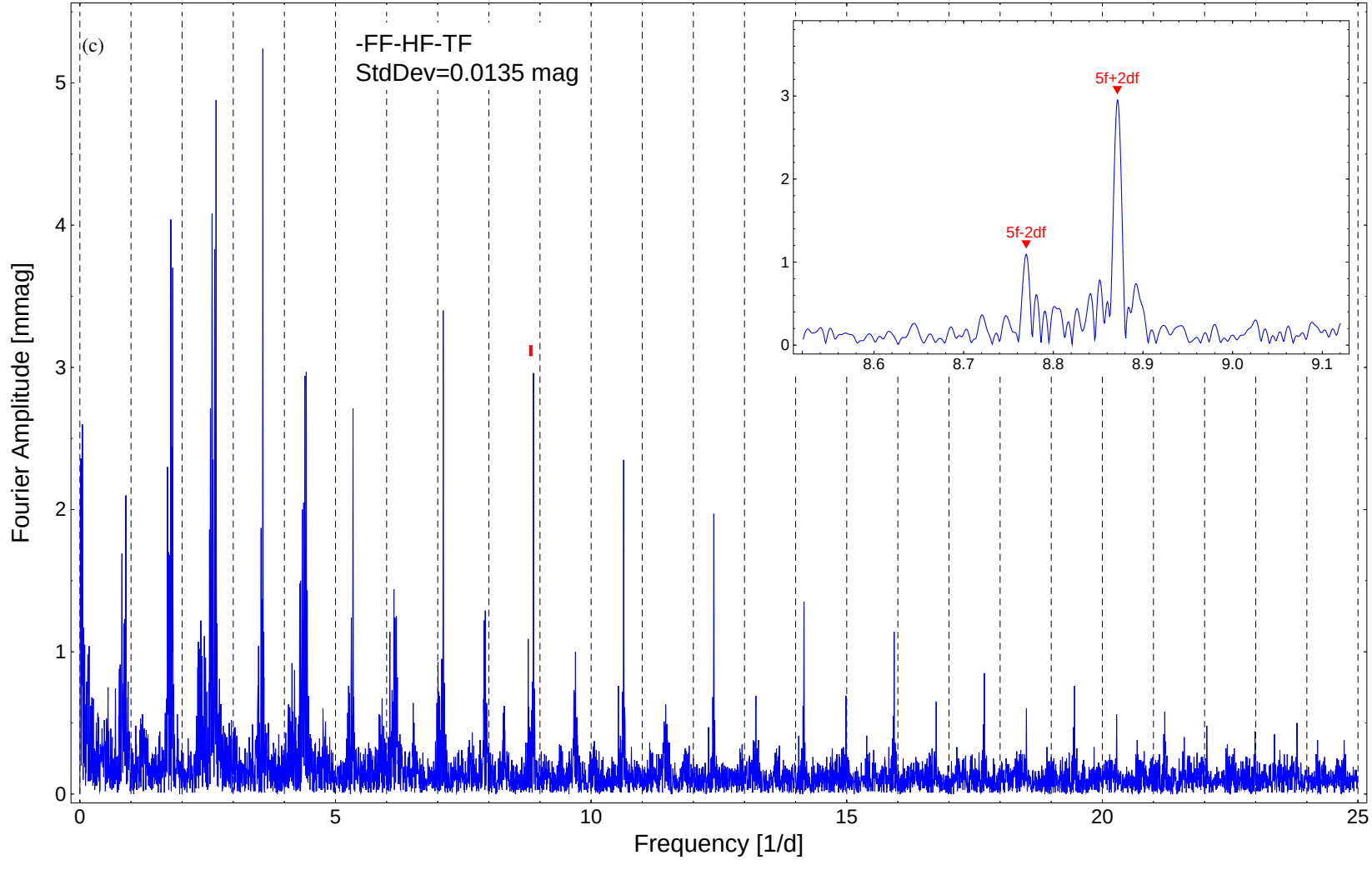
(c)
-FF-HF-TF
StdDev=0.0135 mag
5f+2df
5f-2df
Fourier Amplitude [mmag]
Frequency [1/d]
0
1
2
3
4
5
0
5
10
15
20
25
8.6
8.7
8.8
8.9
9.0
9.1

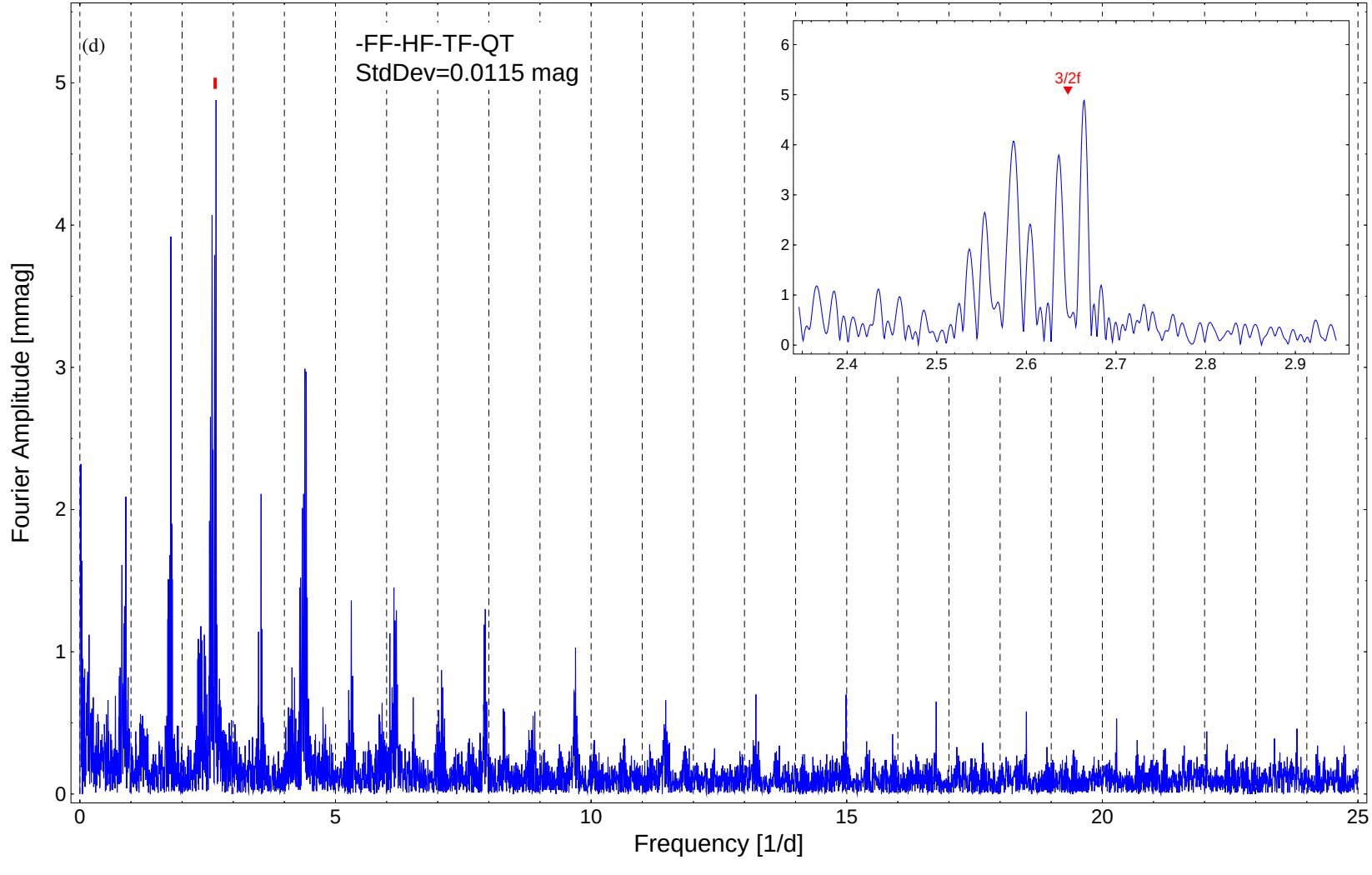
(d)
-FF-HF-TF-QT
StdDev=0.0115 mag
3/2f
Fourier Amplitude [mmag]
Frequency [1/d]
0
1
2
3
4
5
0
5
10
15
20
25
2.4
2.5
2.6
2.7
2.8
2.9
6

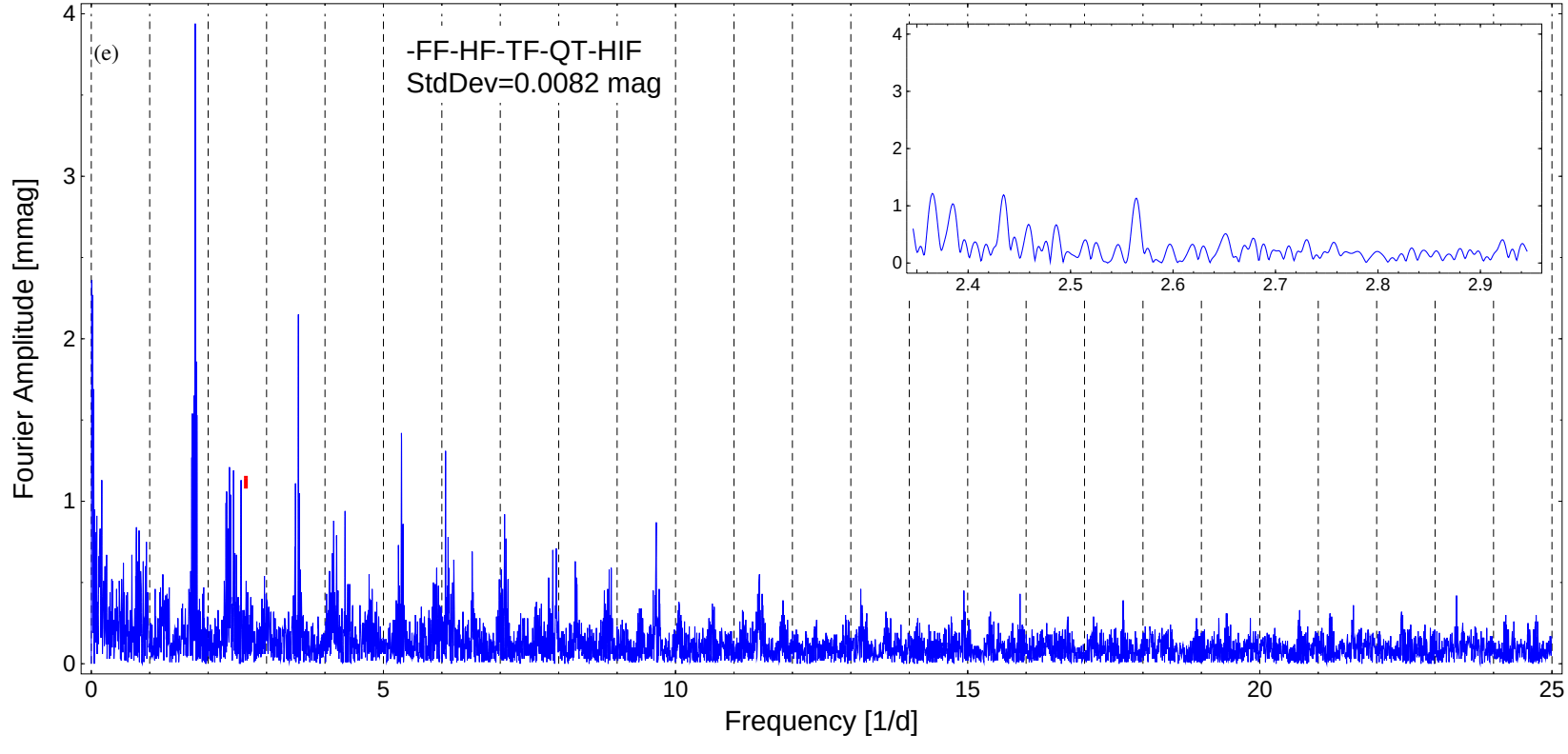
(e)
-FF-HF-TF-QT-HIF
StdDev=0.0082 mag
Fourier Amplitude [mmag]
Frequency [1/d]
0
1
2
3
4
5
10
15
20
25
2.4
2.5
2.6
2.7
2.8
2.9

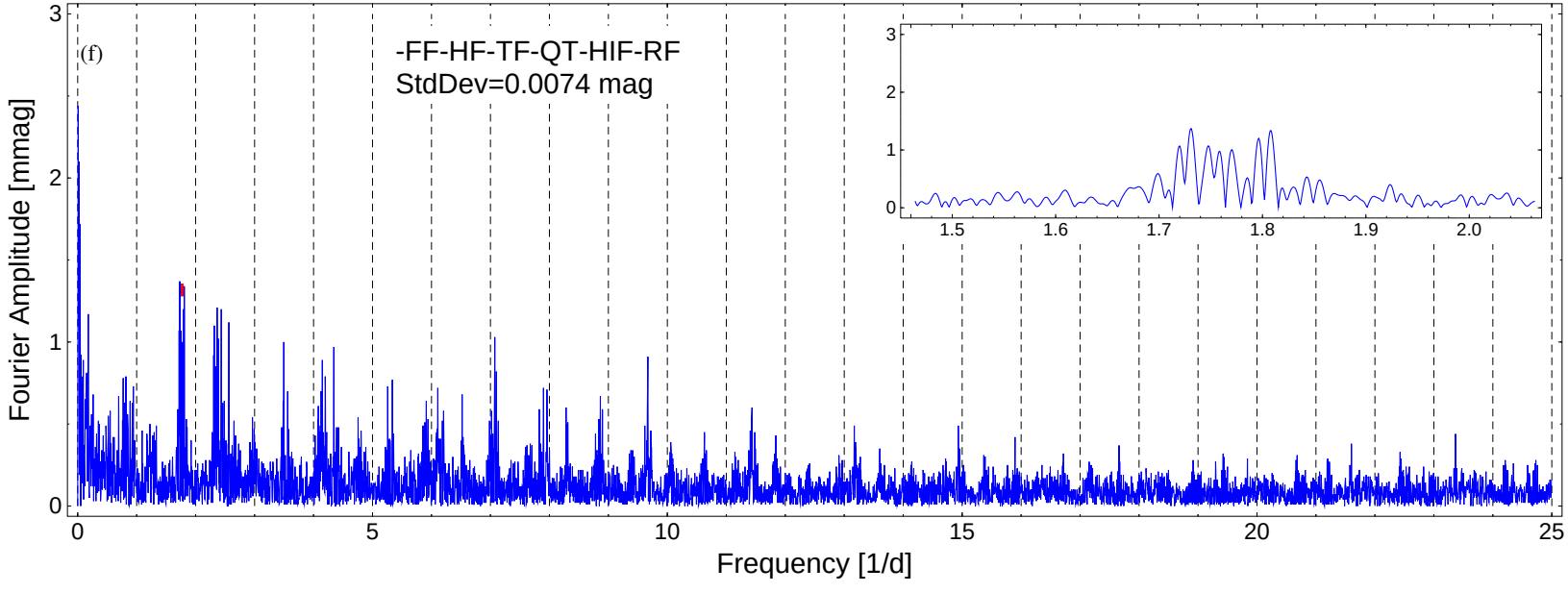
(f)
-FF-HF-TF-QT-HIF-RF
StdDev=0.0074 mag
Fourier Amplitude [mmag]
Frequency [1/d]
0
1
2
3
0
5
10
15
20
25
1.5
1.6
1.7
1.8
1.9
2.0

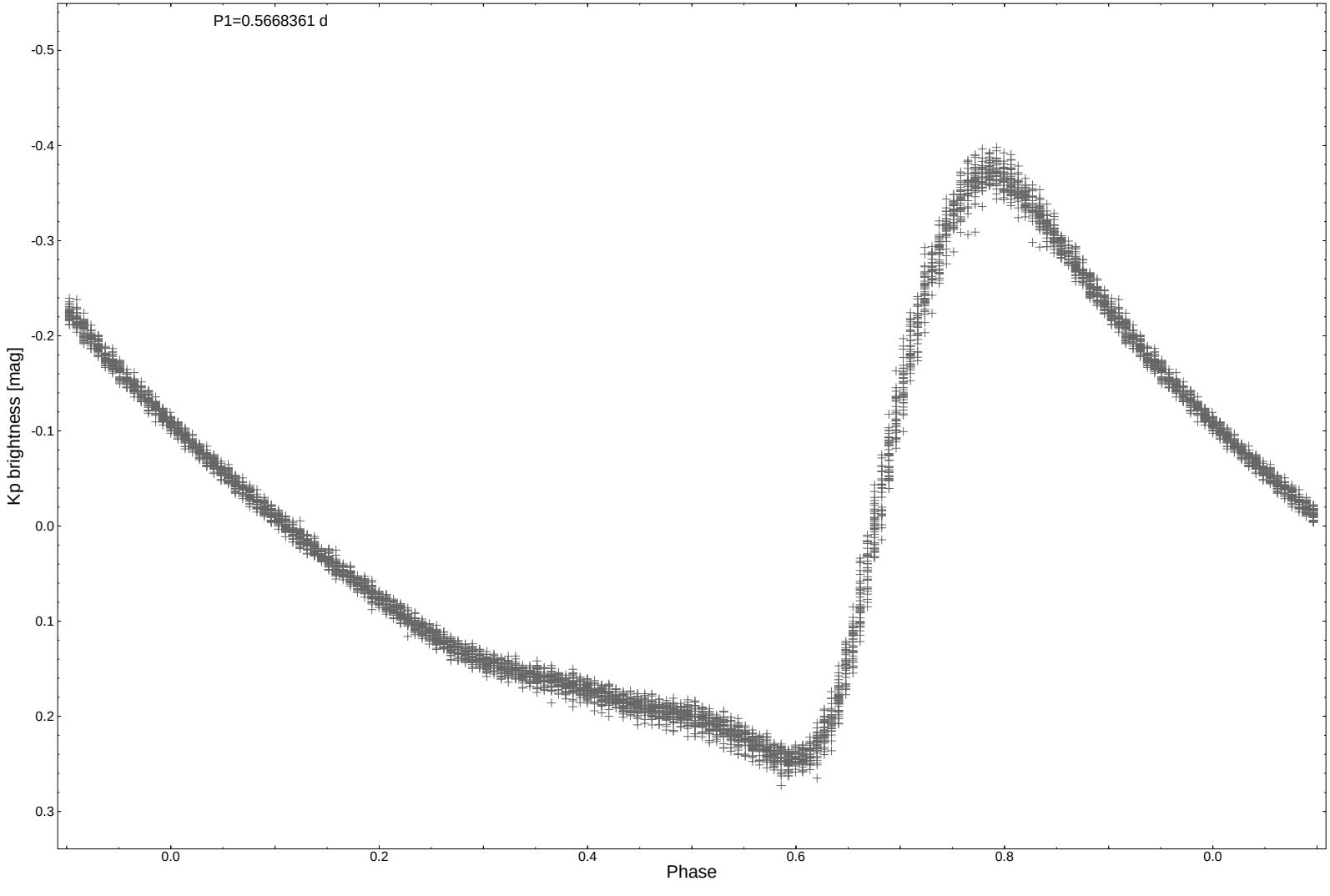
P1=0.5668361 d
Kp brightness [mag]
-0.5
-0.4
-0.3
-0.2
-0.1
0.0
0.1
0.2
0.3
0.0
0.2
0.4
0.6
0.8
0.0
Phase

Period doubling

- Szabo et al. (2010): RR Lyr, V808 Cyg, V355 Lyr
- PD – period doubling
- alternating maxima and minima of the pulsational cycles
- HIF – half-integer frequencies $(2n+1)/2f_0$
- $A_{3/2} > A_{5/2} > A_{1/2}$
- $A_{\rm HIF}$ changes, but not with modulation period
- many peaks around expected HIFs
  – varying pulsational period throughout the Blazhko cycle and
  – transient nature of the PD phenomenon
- PD only in stars with Blazhko effect

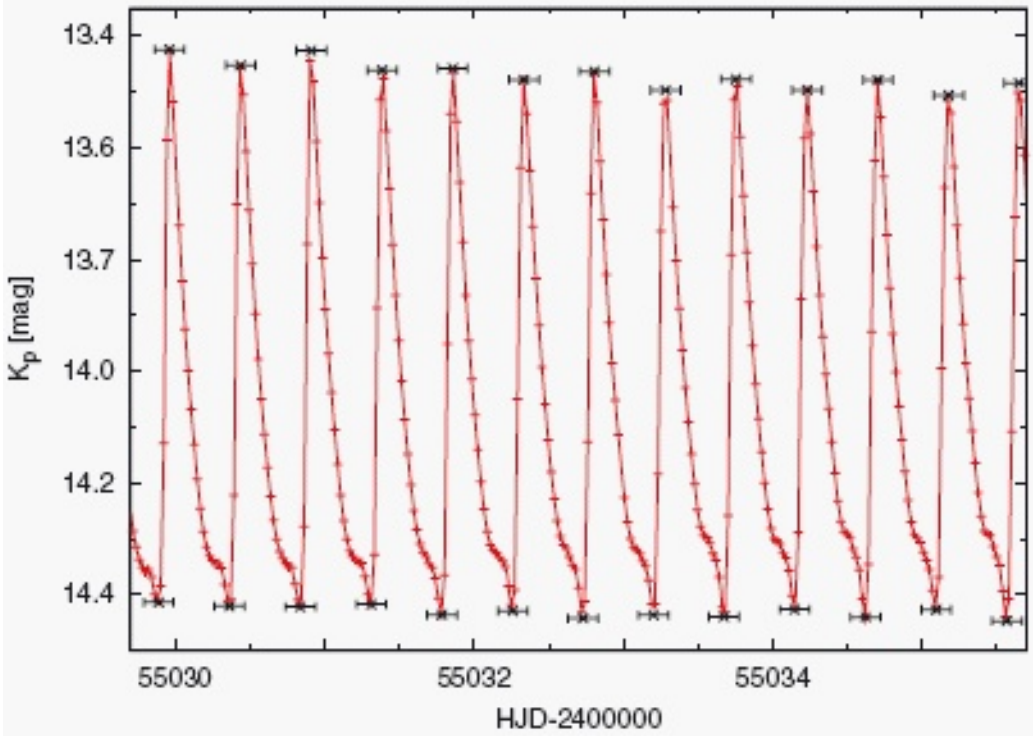

6-d segment of the V355 Lyr light curve showing small PD effect, i.e. alternating maxima and minima. Szabo et al. (2010).

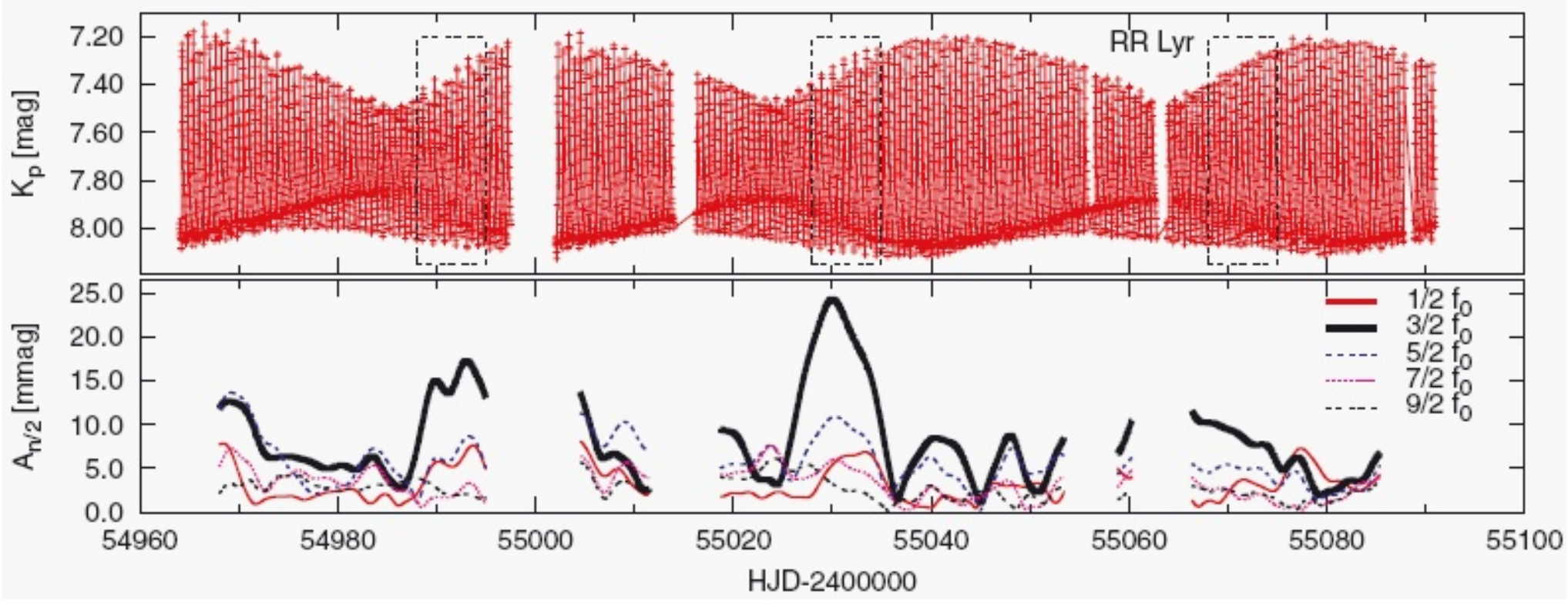

Upper panel: Q1+Q2 light curve of RR Lyr. Note that the individual pulsational cycles are hardly discernible, while the long period (39.6 d) Blazhko modulation clearly stands out. Bottom panel: amplitudes of the HIFs. Szabo et al. (2010).

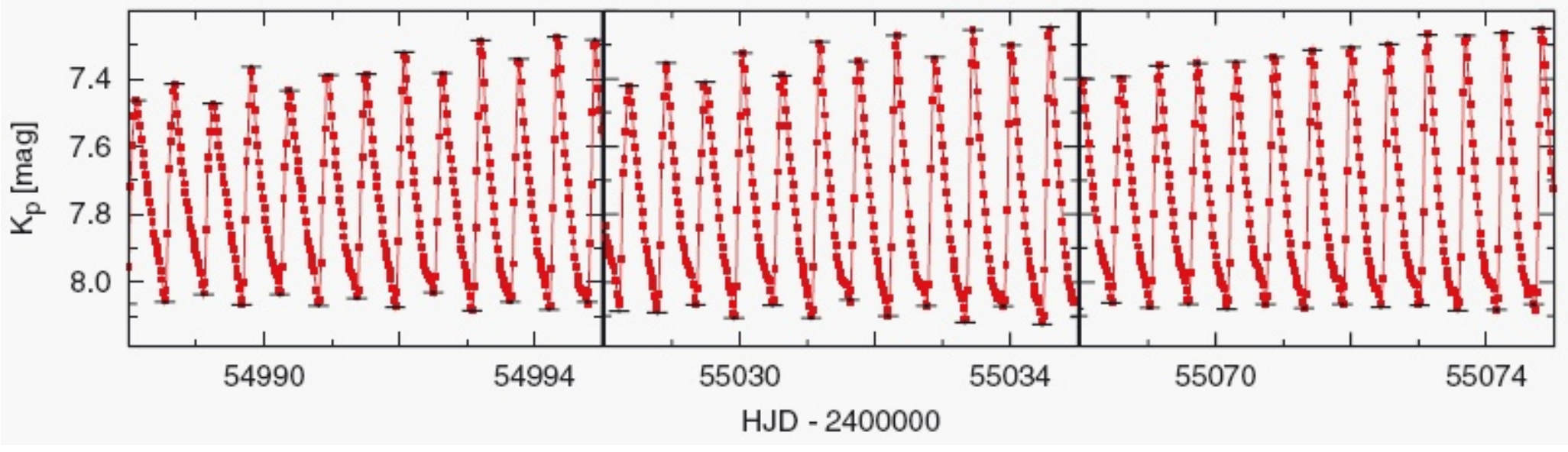

7-d segments of the Kepler light curve of RR Lyr showing different degrees of PD effect at the same Blazhko phase. The maxima and the minima were fitted with a ninth-order polynomial and the small horizontal bars drawn through the extrema are plotted to guide the eye. Szabo et al. (2010).

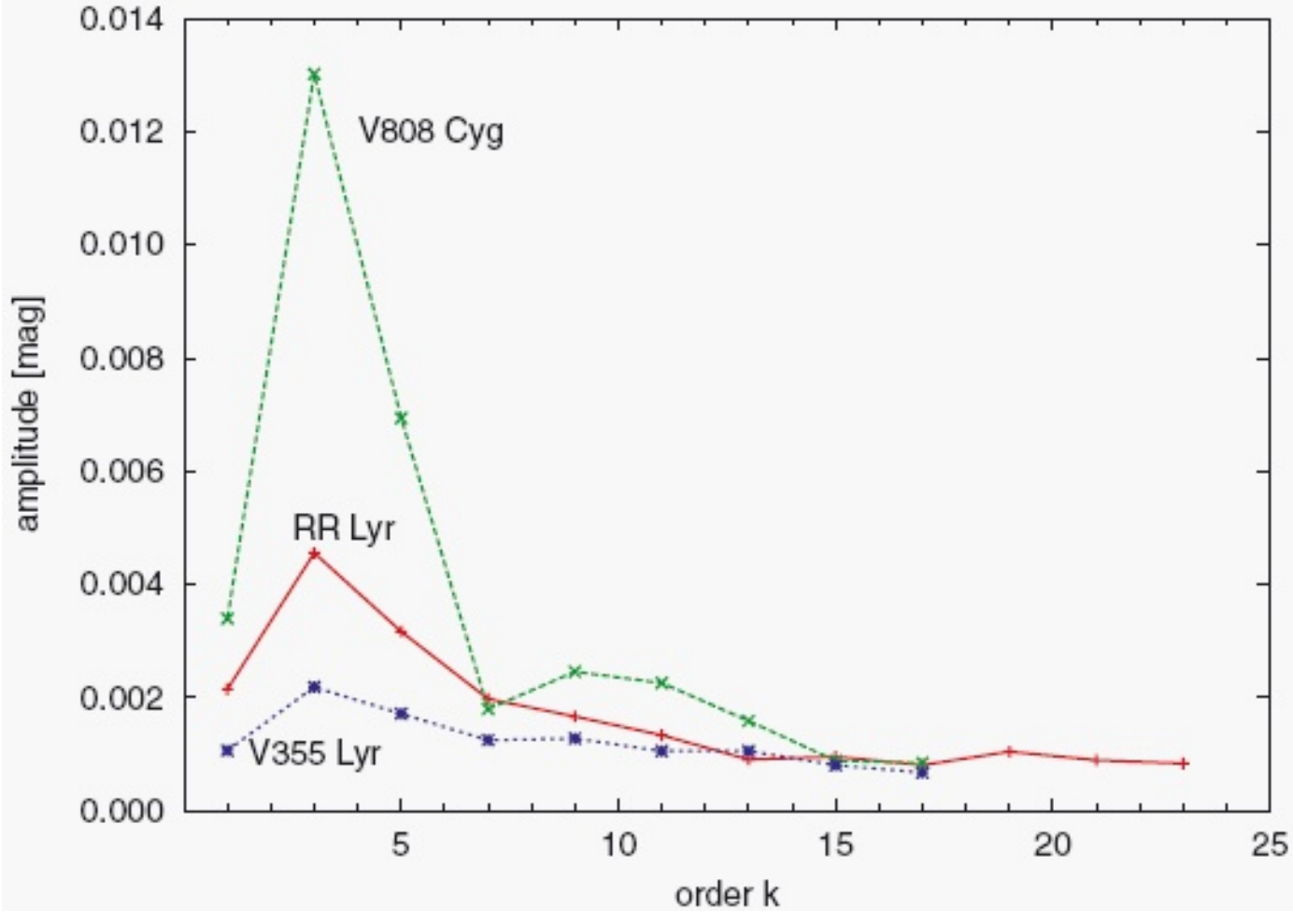

Amplitudes of the HIFs as a function of the order k, where k denotes the $(k/2)f_0$ frequency. Note the significant bump seen around $k = 9$ as a sign of the 9:2 resonance with the ninth (strange) overtone for V808 Cyg and the change of slope for the other stars. Szabo et al. (2010).

Hydrodynamical models

- turbulent convective stellar pulsation hydrocode (Florda-Budapest code; Kolláth et al. 2002)
- destabilization of the fundamental mode leading to the PD bifurcation
- coupling/resonance with the ninth overtone $P_0/P_9 = 9/2$ in a wide temperature range
- strange mode: with a non-normal damping rate and eigenfunction, without adiabatic counterpart and having energy associated with its pulsation confined to the outer zones of the star
- reproduction of the time-scale of the PD occurance (~ 10 d)
- PD strongly depends on the parameters of turbulent convection

Summary

- stars with the strongest PD show also strong amplitude/phase modulation.
- assuming that during the Blazhko cycle the turbulent/convective structure of the star varies (Stothers 2006), in certain Blazhko phases the PD effect appears, because PD strongly depends on the parameters of turbulent convection

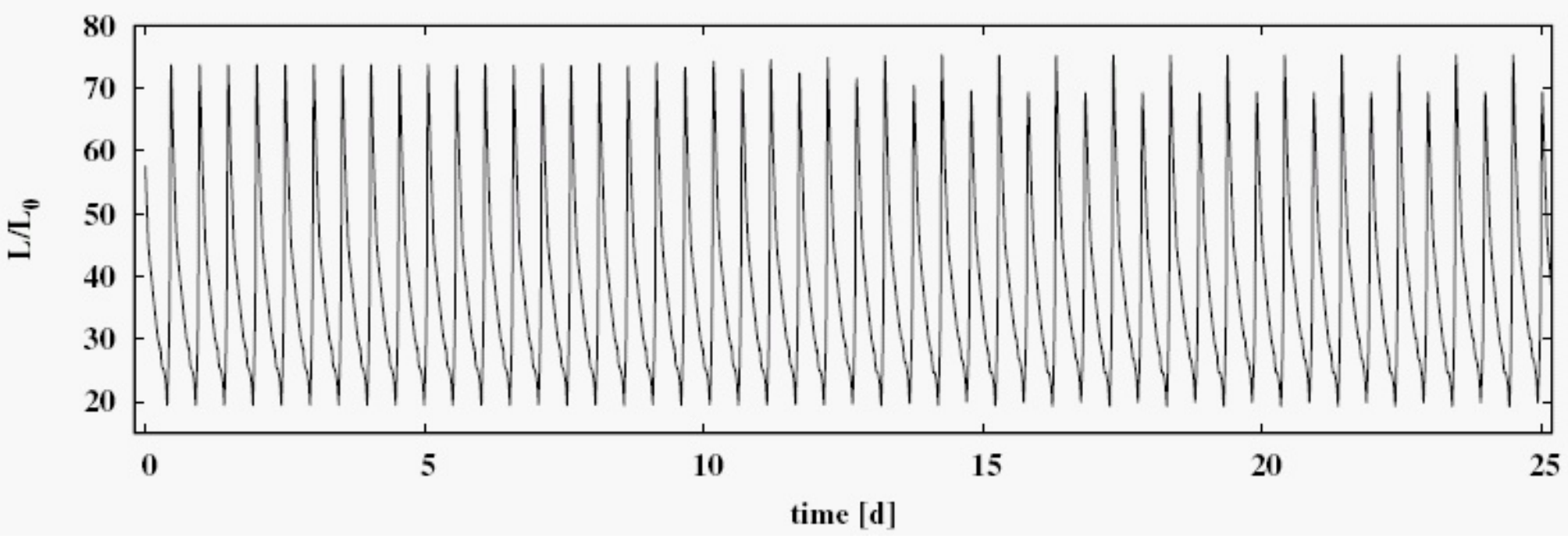

Results of a hydrorun showing the onset of the PD phenomenon. Szabo et al. (2010).

Period – luminosity relation for Population II pulsating stars

Introduction

- standard candles for old stellar systems
- independent test of the Cepheid distance scale
- calibration of secondary distance indicators (GC LF or RG tip)
- distance is a fundamental step to determine ages of GCs
- absolute ages ⇒ cosmological implications
- relative ages ⇒ formation process of galaxies
- review papers:
  - LNP, vol. 635 (2003)
  - Sandage and Tammann (2006, ARAAp 44, 93)

Pulsational instability strip

- region of the H-R diagram where occur (mostly) radial pulsations driven by κ mechanism in the H/He ionization zone
- RR Lyrae stars (HB)
- Population II Cepheids
  - BL Herculis (AHB1) stars (evolution from BHB)
  - W Virginis stars (blue loop from AGB)
  - RV Tauri stars (post AGB)
- Anomalous Cepheids
- SX Phoenicis stars (BS)

BL Her is the population I analog of the AHB1 (XX Vir) population II variables

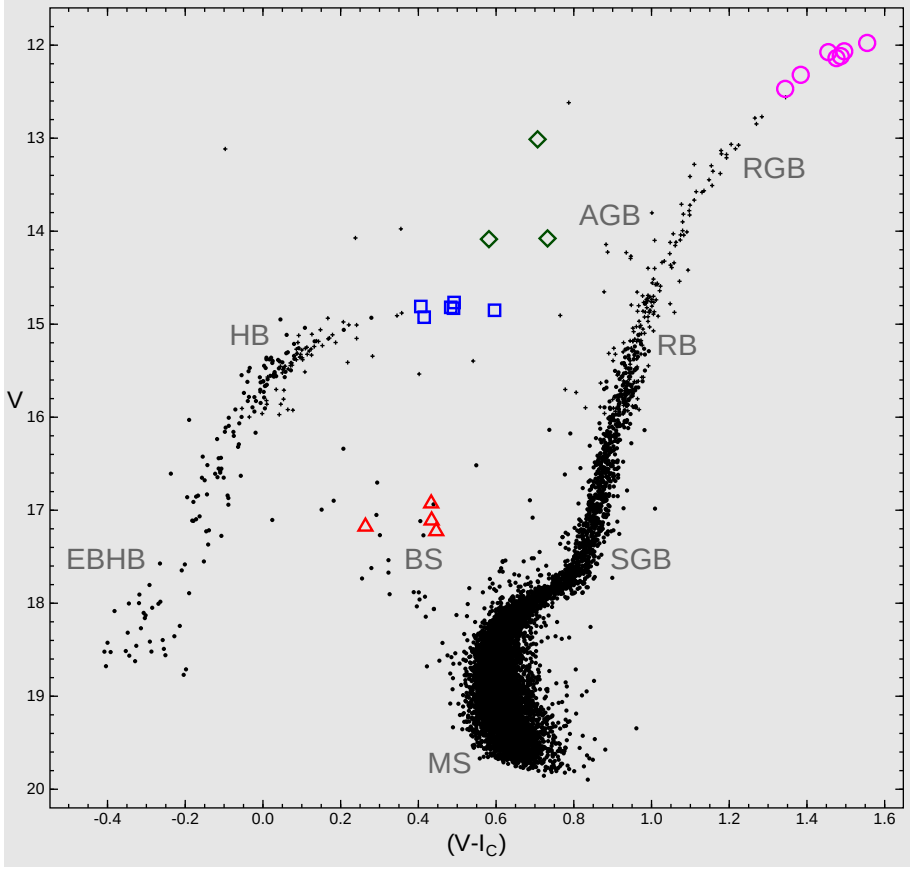

The colour – magnitude diagram for M 13 (Kopacki et al. 2003). SX Phoenicis stars are indicated with triangles, RR Lyrae variables with open squares, Population II Cepheids with diamonds, and variable red giants with circles.

PL relations for Pop. II variables

Period vs. adjusted-magnitude diagrams and fitted PL relations for SX Phe, RR Lyr, Pop. II and anomalous Cepheids and for V and K passbands. The magnitudes have been dereddened, normalized to the metallicity of M15, and shifted to the distance of M15. The slopes of the PL relations for the assumed F and FO modes for each kind of variable stars are parallel. Note that the slopes of the PL relations are different for various types of stars. The assignment of pulsation modes was based on PL, PA, and PC diagrams. Nemec et al. (1994, AJ 108, 222).

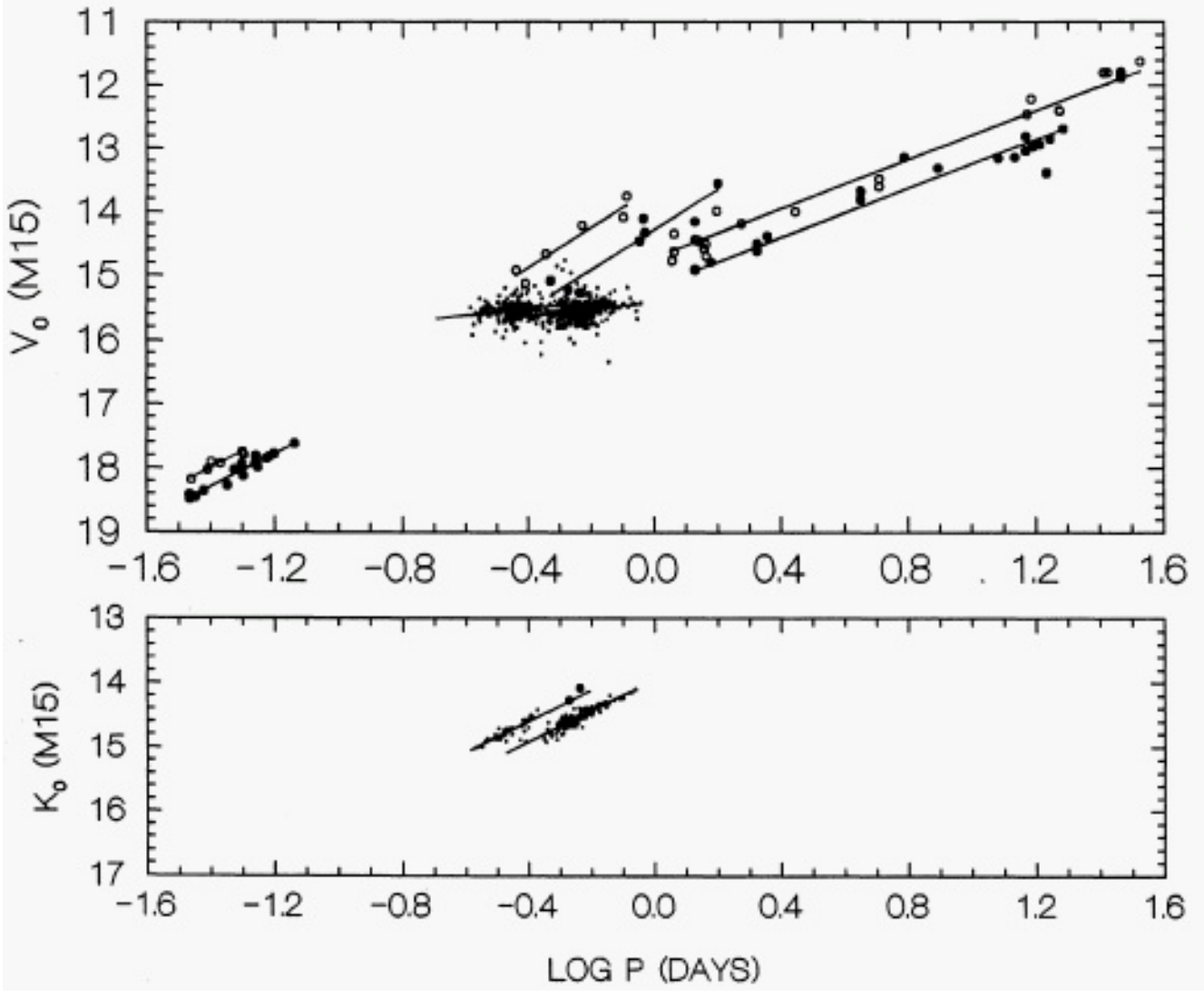

Period – metallicity relation for RR Lyrae stars

Predicted brightness of the HB

- the higher [Fe/H], the fainter ZAHB
- the higher [α/Fe], the fainter ZAHB

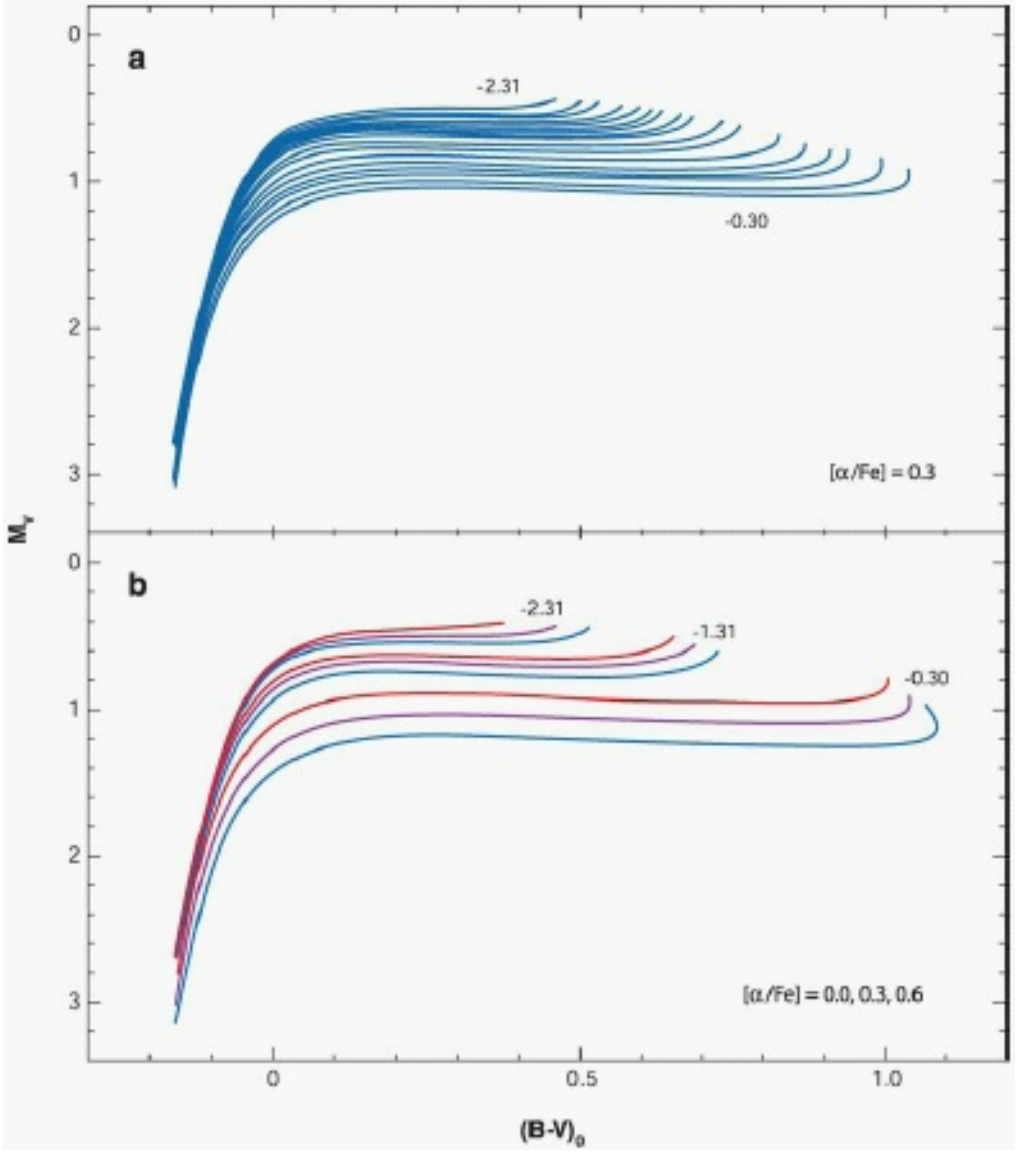

(a) Predicted level of the ZAHB by VandenBerg et al. (2000, ApJ 532, 430) for 17 different metallicities in step of 0.15 in [Fe/H] for an α element enhancement [α/Fe] = 0.3. (b) The sensitivity of the HB level to changes of [α/Fe].

M_V calibration for RR Lyrae stars

- $M_V(RR) = \alpha([\mathrm{Fe/H}] + 1.5) + \beta$
- $\alpha = 0.20$: Baade-Wesselink analysis of field RR Lyrae stars (Fernley et al. 1998, MNRAS 293, L61)
- $\alpha = 0.18$: main sequence fitting for GCs (Carretta et al. 2000, ApJ 533, 215)
- $\alpha = 0.22$: HB luminosity of 19 GCs in M 31 (Rich et al. 2001)
- $\alpha = 0.21$: RR Lyraes in bar of the LMC (Gratton et al. 2004)
- no clear break in the slope around [Fe/H] $= -1.5$ as proposed by the theoretical models
- luminosity-metallicity relation can be different in various locations
- $\alpha = 0.09$: Sculptor dSph galaxy (Clementini et al. 2005, MNRAS 363, 734)
- β from trigonometric, statistical and pulsational parallaxes
- $M_V = 0.54$ at [Fe/H] $= -1.4$ (HST and Hipparcos parallax for RR Lyr; Benedict et al. (2002))
- $M_V = 0.77$ at [Fe/H] $= -1.6$ (statistical parallax; Popowski and Gould (1998))
- $M_V = 0.73$ (pulsational parallax)
- $M_V = 0.52$ (MS fitting)
- good agreement except statistical parallax

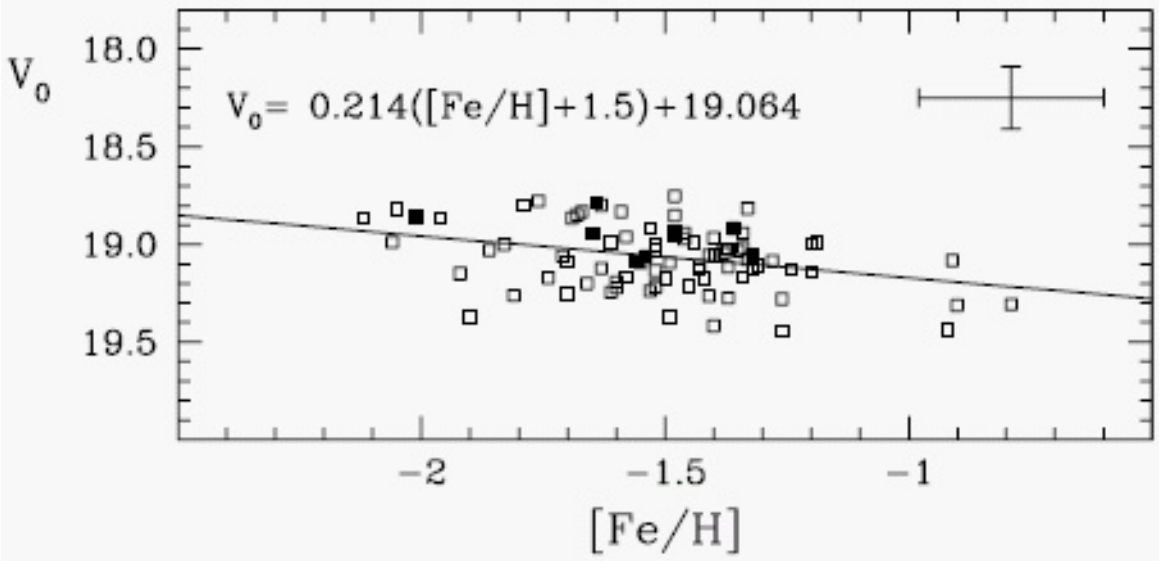

Run of the dereddened mean magnitude of the RR Lyrae stars in the bar of the LMC as a function of the metallicity [Fe/H]. Filled symbols are double-mode pulsators, open symbols ab- and c-type RR Lyrae stars. Gratton et al. (2004, AAp 421, 937).

Remarks on the M_V calibration

- theoretical predictions of nonlinearity of $M_V(\mathrm{ZAHB}) - \log Z$ relation
- solar-scaled mixture seems inappropriate for GC
- $[\alpha/\mathrm{Fe}]$ enhancement ($\sim$0.3) in GC and field metal-poor stars
- RR Lyrae samples contain stars evolved off ZAHB
- evolutionary correction $\Delta M_V(\mathrm{ZAHB} - \mathrm{HB}) \approx 0.08$ mag
- evaluation of the evolutionary effects (through synthetic HB simulations)
- predicted $M_V(\mathrm{RR})$ depends on the HB morphology

Pulsational $M_V - [\mathrm{Fe/H}]$ relation for GC RR Lyrae stars

- Caputo et al. (2000, MNRAS 316, 819)
  - non-linear convective HD code for pulsating models (Bono at al.)
  - M_V and P of models at FOBE for suitable Z, μ, L, and Y
  - $M_{\mathrm{bol}}(\mathrm{FOBE}) = a \log P(\mathrm{FOBE}) + b \log Z + c$
  - $M_{\mathrm{bol}} \Rightarrow M_V$
  - $\log Z$ $(+[\alpha/\mathrm{Fe}]) \Rightarrow [\mathrm{Fe/H}]$
  - 'pulsational' distance modulus from matching the predicted FOBE with observed distribution of RRc stars

Name	[Fe/H]	HB	$\langle V_{RR} \rangle$	$\sigma_{\langle V_{RR} \rangle}$	Ref. (RR Lyrae)
NGC 1851	−1.05	−0.36	16.03	0.09	Walker (1998)
NGC 4147	−1.54	+0.55	16.98	0.08	Newburn (1957)
IC4499	−1.26	+0.11	17.64	0.08	Walker & Nemec (1996)
NGC 4590 M68	−1.99	+0.17	15.64	0.04	Walker (1994)
NGC 4833	−1.58	+0.93	15.33	0.15	Demers & Wehlau (1977)
NGC 5053	−1.98	+0.52	16.64	0.11	Nemec, Mateo & Schombert (1995)
NGC 5272 M3	−1.34	+0.08	15.63	0.10	Carretta et al. (1998)
NGC 5466	−2.14	+0.58	16.46	0.07	Corwin, Carney & Nifong (1999)
NGC 5904 M5	−1.11	+0.31	15.06	0.08	Caputo et al. (1999)
NGC 6171 M107	−0.91	−0.73	15.60	0.10	Dickens (1970)
NGC 6333 M9	−1.56	+0.87	16.26	0.07	Clement & Shelton (1999)
NGC 6362	−0.96	−0.58	15.25	0.07	Walker (in preparation)
NGC 6809 M55	−1.61	0.87	14.37	0.06	Olech et al. (1999)
NGC 7006	−1.35	−0.28	18.79	0.14	Wehlau, Slawson & Nemec (1999)
NGC 7078 M15	−2.12	+0.67	15.83	0.06	Bingham et al. (1984)
NGC 7089 M2	−1.31	+0.96	15.97	0.09	Lee & Carney (1999)

Observed parameters of the GCs selected by Caputo et al. (2000).

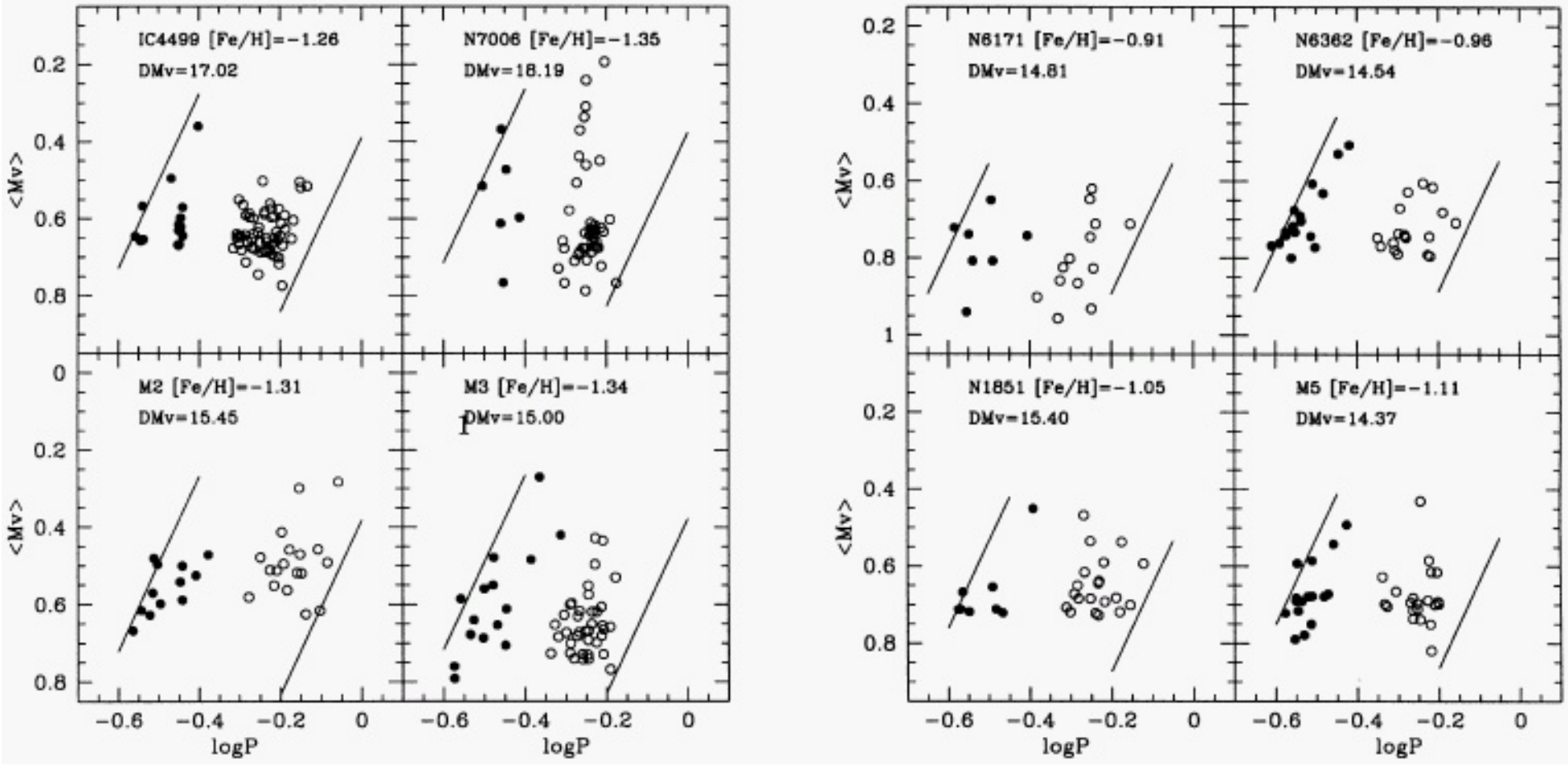

Globular cluster RR Lyraes in the $M_V - \log P$ plane. Filled and open circles are RRc and RRab pulsators, respectively, while the solid lines are the theoretical boundaries of the instability strip. The labeled apparent distance moduli are obtained by constraining the observed RRc distribution to match the predicted blue limit of the pulsation region, under the assumption of solar-scaled chemical composition. Caputo et al. (2000, MNRAS 316, 819).

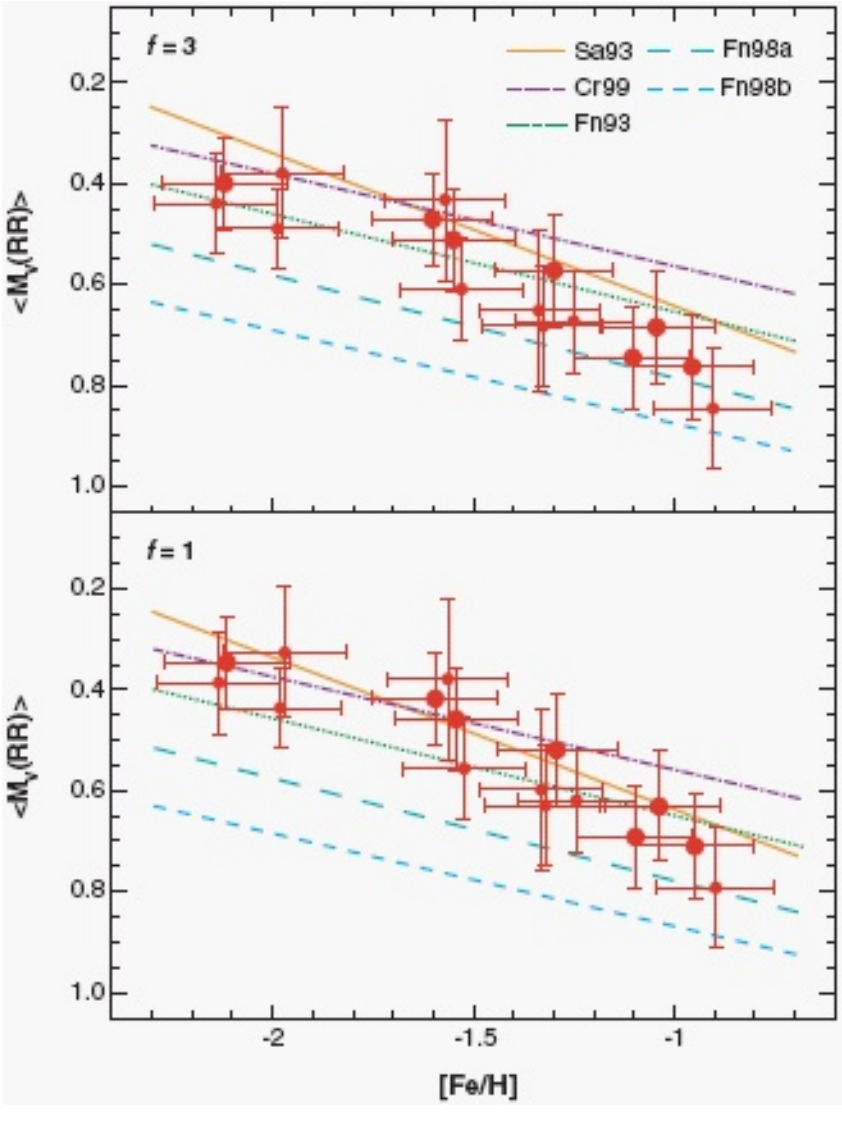

The dependence of M_V(RR) on [Fe/H] for the selected GCs (filled circles: the size of the circle is proportional to the weight), in comparison with empirical calibrations. Caputo et al. (2000, MNRAS 316, 819).

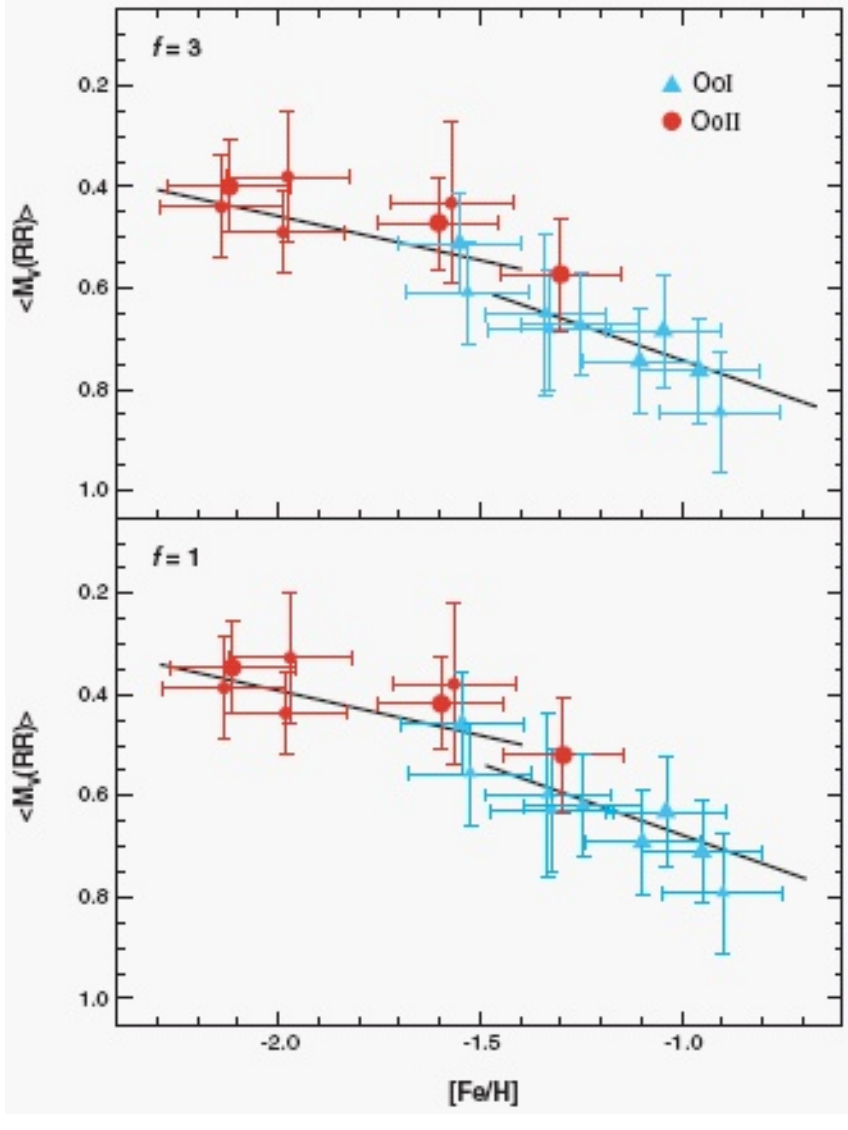

As in previous figure, but distinguishing between OoI (triangles) and OoII (circles) globular clusters. The solid lines are relations for clusters with [Fe/H] < -1.5 and [Fe/H] > -1.5. Caputo et al. (2000, MNRAS 316, 819).

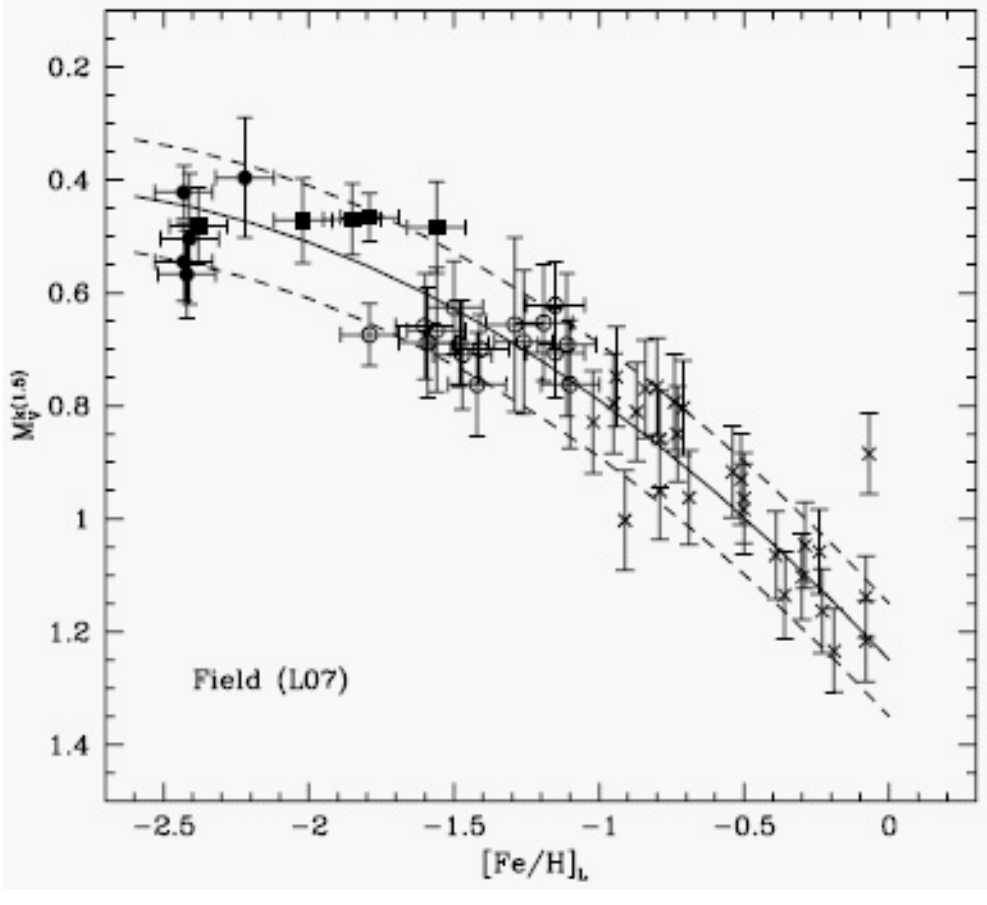

Mean absolute visual magnitude of RRab stars in Galactic globular clusters (open circles for OoI and filled squares for OoII clusters) and of field RRab stars (crosses) versus metallicity.

Metallicity–luminosity relation from Fourier decomposition of the RR Lyrae's LCs

- different calibrations for RRab and RRc stars
- $[\mathrm{Fe/H}] = f(P, \varphi_{31})$
- $M_V = f(P, \varphi_{31})$ (RRc) or
  $M_V = f(P, A_1, A_3)$ (RRab)

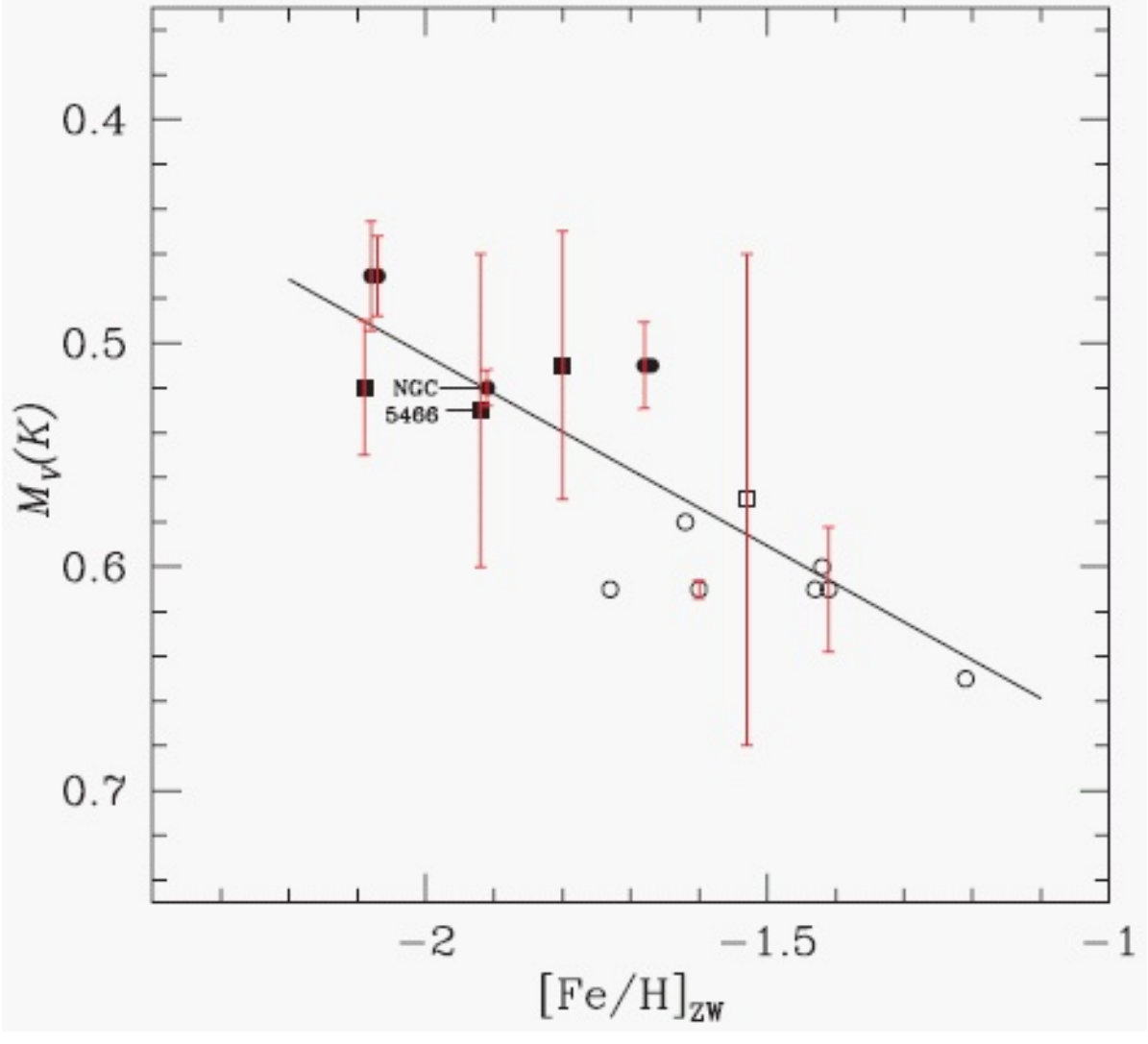

The $M_V - [\mathrm{Fe/H}]$ relationship from the RR Lyrae Fourier light-curve decomposition for a family of 11 globular clusters. Circles represent the results from the RRab stars while squares are from the RRc stars. Open symbols are used for Oo I clusters and filled symbols for Oo II clusters. The fitting line has the form $M_V = +(0.18 \pm 0.03)[\mathrm{Fe/H}] + (0.85 \pm 0.05)$. Arellano Ferro et al. (2008, MNRAS 384, 1444).

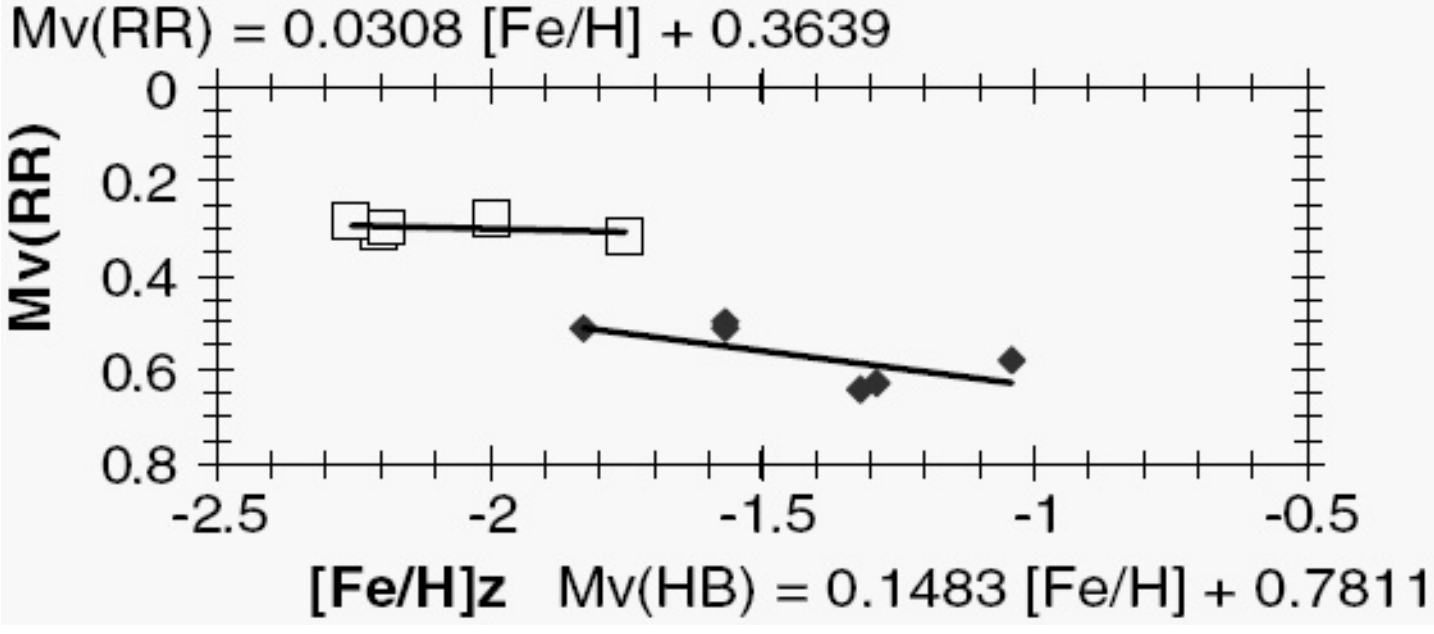

Mean absolute magnitudes of RR Lyrae variables in Oosterhoff II globular clusters (open squares) and Osterhoff I globular clusters (solid diamonds). The equation in the upper left is the fitting equation to the data plotted as open squares and the equation in the lower right to the data plotted as solid diamonds. McNamara (2011, AJ 142, 110).

- an abrupt increase in the $\langle M_V \rangle_{\rm RR}$ values of RR Lyrae stars or the $\langle M_V \rangle_{\rm HB}$ values of the HB of about 0.2 mag during transition from Oo I GCs to Oo II GCs at [Fe/H] ≈ -1.5

M_V [Fe/H] -1.5	M_V [Fe/H] -1.0	Reference
0.55	0.72	McNamara et al. (2004)
0.51	0.65	Bono et al. (2007)
0.52	0.75	Sandage & Tammann (2006)
0.51	0.65	Catelan et al. (2004)
0.5	0.68	Bono et al. (2003)
0.54	0.68	Caputo et al. (2000)
0.52		Benedict et al. (2002)
0.59		Cacciari & Clementini (2003)
$0.53 \pm .010$	$0.69 \pm .016$	Avg

Absolute magnitudes of RR Lyrae stars as inferred by calibrations of various investigators. McNamara (2011, AJ 142, 110).

Exceptions to the RR Lyr M_V calibration

- NGC6388 and NGC6441
  - metal-rich GCs ([Fe/H] ≈ -0.6)
  - RHB (normal for their [Fe/H]) + (E)BHB
  - average period of RRab stars too long even for OoII type GCs
  - RR Lyraes overluminous in M_V for their metallicity
  - connection to the second parameter effect
- not all RR Lyrae stars follow the same luminosity–metallicity relation

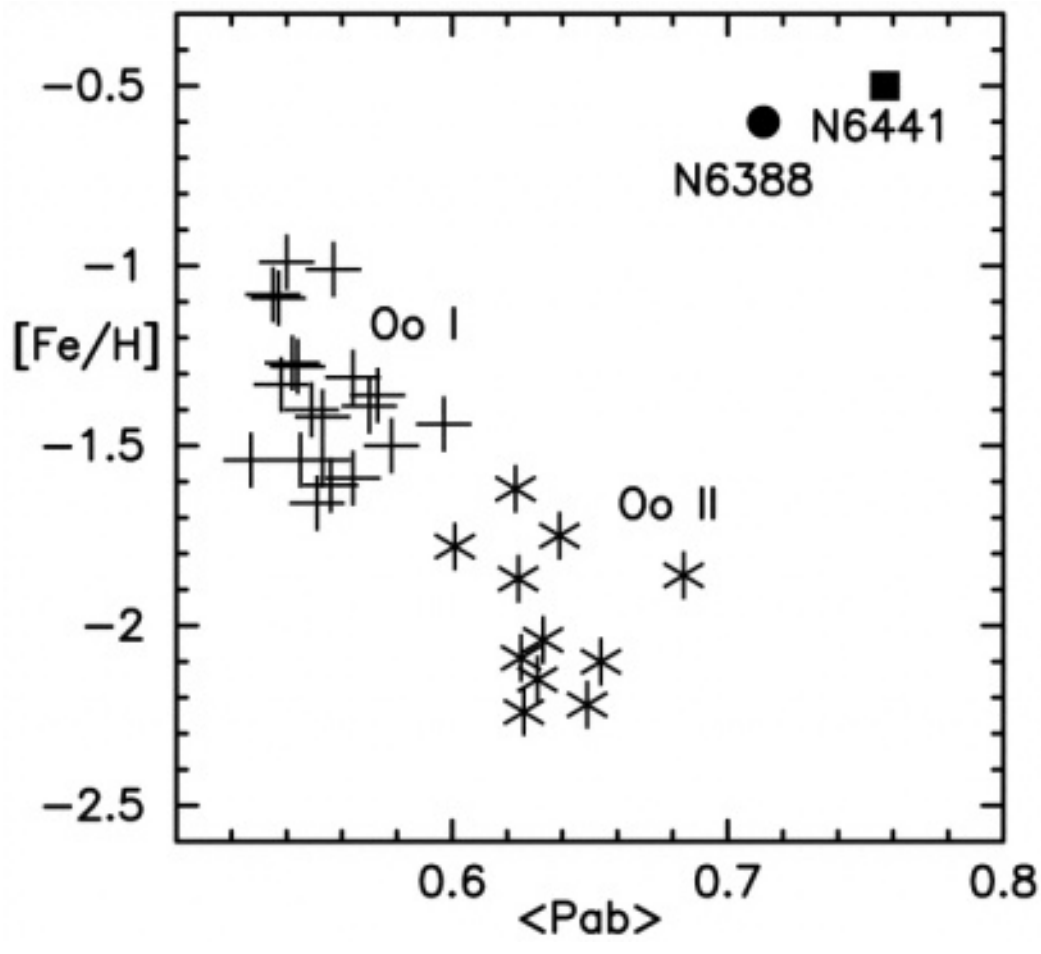

Metallicity vs. mean period of RRab stars diagram for Galactic GCs. Pritzl (2001).

Period – luminosity relation for RR Lyrae stars

Period – luminosity relationship

- average relation between M_V and metallicity [Fe/H]
  - $M_V(RR) = 0.22([\mathrm{Fe/H}]_{1.5}) + 0.56$ (Gratton et al. (2003)
  - strong dependence on evolutionary effects
  - possible nonlinearity
- Cepheids present a tight PL relation irrespective of bandpass
  - large range in L but only a modest range in T_{eff}
- RR Lyrae PL relation tight only at IR
  - small range in L
  - strong dependence of period on temperature
  - BC at IR leads to a large range in absolute magnitudes across instability strip along HB

Theoretical calibration of PL relationship

- HB simulations
  - RGB and HB evolutionary tracks for $Z = 0.001 - 0.006$
  - main-sequence helium abundance $Y = 0.23$
  - mass distribution on ZAHB with $\sigma_\mu = 0.02\ M_\odot$
  - BE of IS + width of IS $\Delta \log T_{\mathrm{eff}} = 0.075$ => RE of IS
  - periods from $P - \langle \varrho \rangle$ relation, $P = f(M, L, T_{\mathrm{eff}})$
  - mean mass on the ZAHB and mass dispersion => HB type
  - random 'observational scatter'

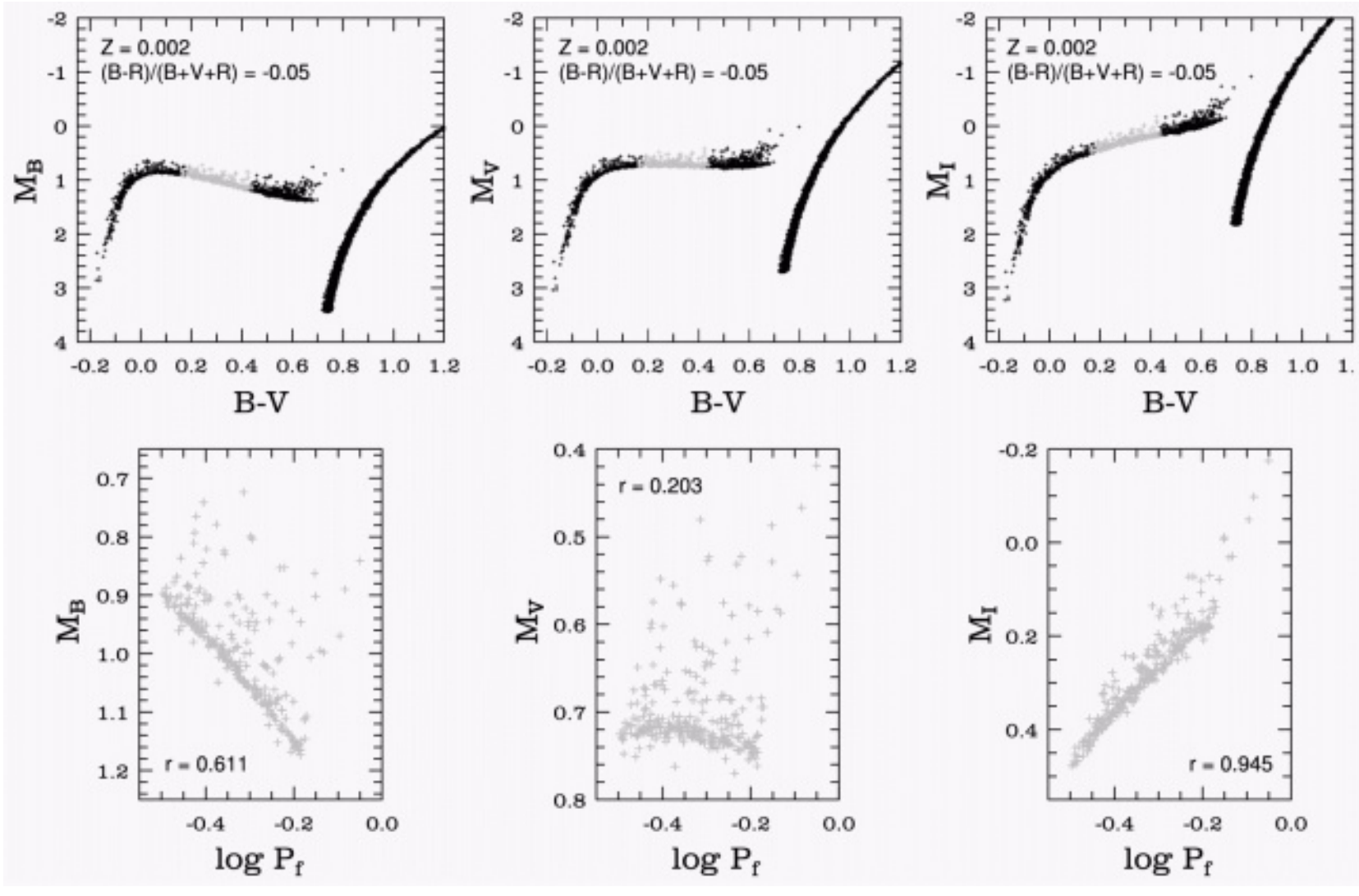

Upper panels: Morphology of the HB in different bandpasses. RRL variables are shown in gray, and nonvariable stars in black. Lower panels: Corresponding RRL distributions in the absolute magnitude – log period plane. r is the correlation coefficient. All plots refer to an HB simulation with $Z = 0.002$ and an intermediate HB type. Catelan et al. (2004, ApJSS 154, 633).

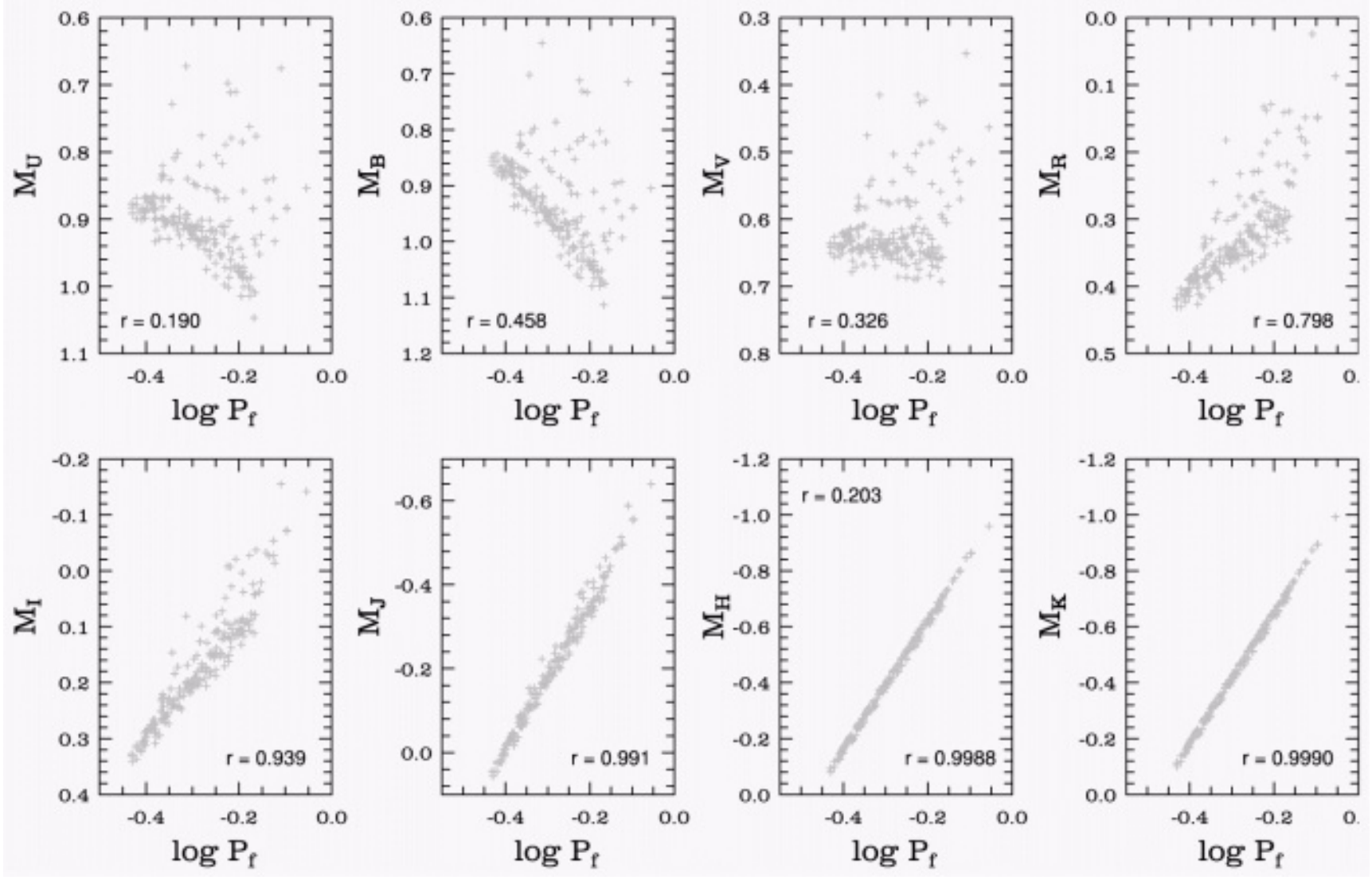

PL relations in several different passbandses. r is the correlation coefficient. All plots refer to an HB simulation with $Z = 0.001$ and an intermediate HB type. Catelan et al. (2004, ApJSS 154, 633).

IR PL relation for RR Lyrae stars in GCs

- Longmore et al. (1986, MNRAS 220, 279)
- NIR observations (K-magnitudes) versus visual data
  - mild dependence on interstellar extinction and metallicity
  - smaller pulsational amplitudes
  - more symmetrical light curves
  - good mean magnitudes
- $M_K = \alpha \log(P_{\rm F}/{\rm d}) + \beta\,[{\rm Fe/H}] + \gamma$
- Sollima et al. (2006, MNRAS 372, 1675)
  - sample of 538 RR Lyrae stars from 16 GC
  - $K - \alpha \log(P_{\rm F}/{\rm d}) = \beta\,[{\rm Fe/H}] + \gamma + (m-M)_K = C$
  - $\alpha = -2.4 \Rightarrow {\rm C} \Rightarrow \alpha \Rightarrow {\rm C} \Rightarrow \alpha$ ...
  - $K_0 = K - C$
  - zero point γ tied to the trigonometric parallax of RR Lyr measured with HST
  - $\alpha = -2.38 \pm 0.04 \qquad \beta = 0.09 \pm 0.14$ (ZW scale)
- metallicity coefficient β is about $2-3$ times smaller than that predicted by theoretical models

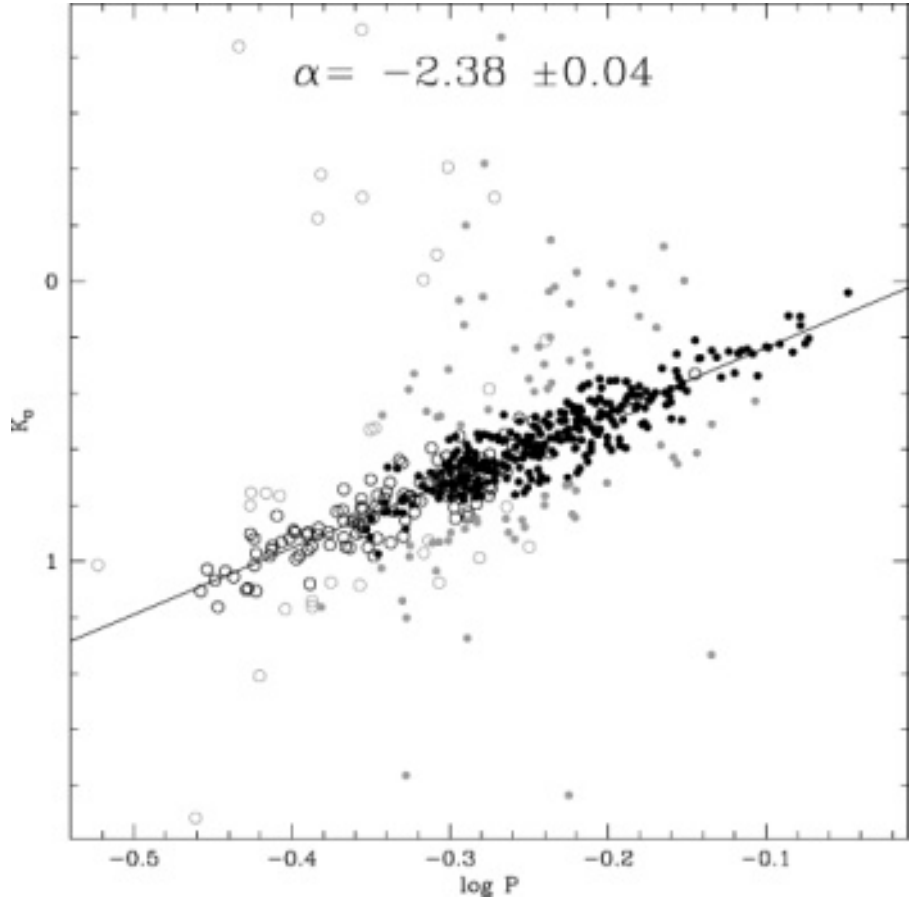

PL$_K$ relation for the 538 RR Lyrae stars from 16 GC. The solid line represents the resulting fit. Filled circles are the RRab variables and open circles are the RRc variables whose periods have been fundamentalized. K magnitude was scaled to the same reference distance and metallicity. Grey symbols mark the points rejected to the fit. Sollima et al. (2006, MNRAS 372, 1675).

Theoretical predictions for IR PL relation of RR Lyrae stars

- Del Principe et al. (2006, ApJ 652, 362)
  - NIR photometry for 180 RR Lyrae stars in ω Cen
  - SHB models of Pietrinferni et al. (2006)
  - pulsation models were used to evaluate periods
  - $M_K = \alpha \log P + \beta + \gamma \tau_{\rm HB}$
  - $\alpha(F) = -2.34$ for $Z = 0.0003$
  - mild dependence on metallicity
  - $(m - M)_0 = 13.7$ in agreement with results from ML relation for RR Lyraes and and eclipsing binary OGLEGC17

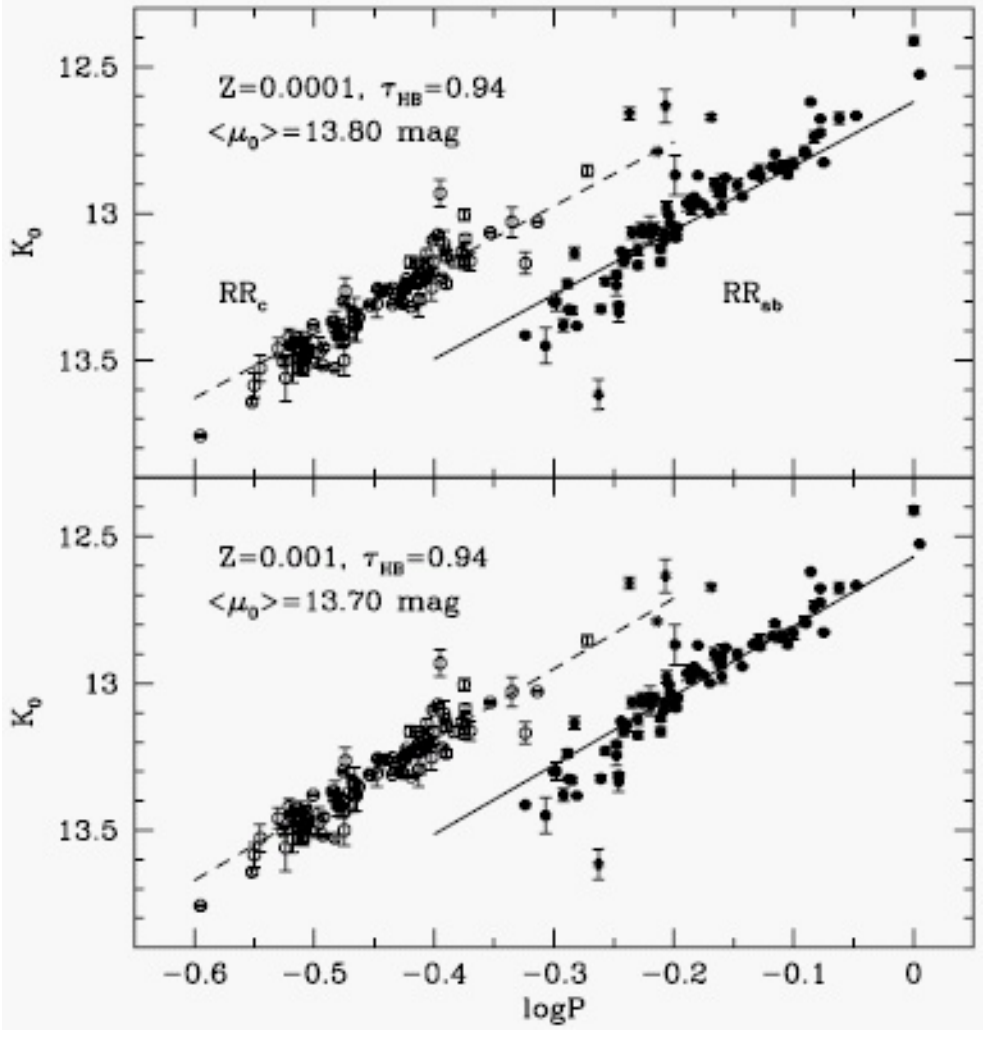

Dereddened K magnitudes of RR Lyrae stars in ω Cen vs. period. Solid and dashed lines display the predicted PL relation for F (filled circles) and FO (open circles) pulsators, respectively. The adopted metallicity and HB type are labeled. Del Principe et al. (2006, ApJ 652, 362).

Period – luminosity relation for Population II Cepheids

Optical period–luminosity relations for type II Cepheids

- Soszyński et al. (2008, AcA 58, 293)
  - OGLE III
  - about 200 type II and 80 anomalous Cepheids from LMC
  - classification based on the position in the PL diagram
  - $W_I = I - 1.55(V - I)$

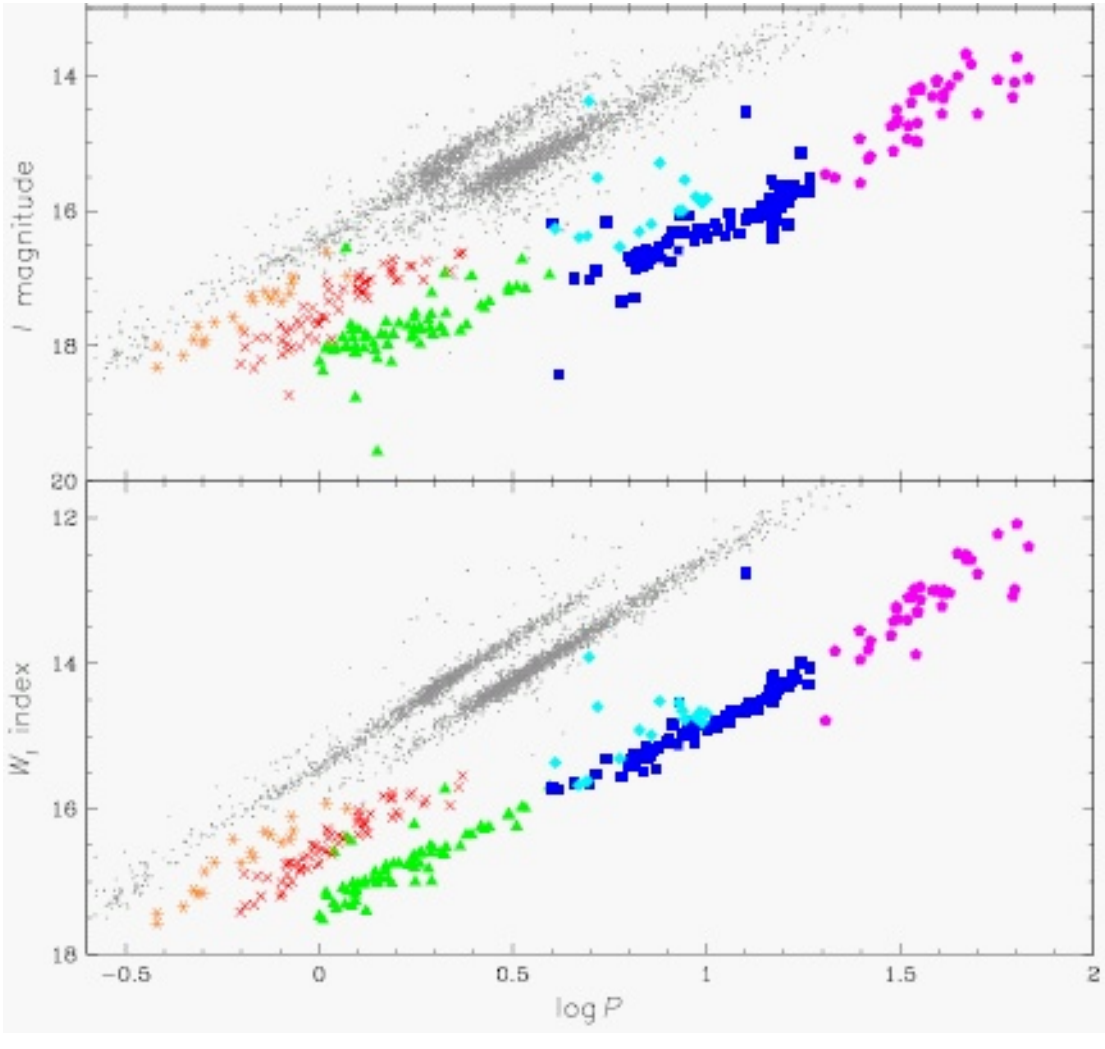

Period–luminosity diagrams for Cepheids in the LMC. Green, blue, cyan and magenta symbols show type II Cepheids, red and orange symbols indicate anomalous Cepheids pulsating in F and FO modes, respectively. Grey points represent calssical Cepheids.

Wesenheit Index

- Wesenheit function of van den Bergh (1968, JRASC 62, 145)
- Madore (1982, ApJ 253, 575), Opolski (1983, IBVS 2425)
- reddening-free parameter
- relatively insensitive to the width of the IS
- $W_V = V - R_V(B-V)$
- $W_I = I - R_I(V-I)$
  - $A_I = R_I E(V-I)$, $I = I_0 + A_I$, $(V-I) = (V-I)_0 + E(V-I)$
  - $W_I = I - R_I(V-I) = I_0 + A_I - R_I(V-I)_0 - R_I E(V-I) =$
    $= I_0 + A_I - R_I(V-I)_0 - A_I = I_0 - R_I(V-I)_0 = W_{I0}$
- PLCR for isolated stellar system (LMC)
  - $I = \alpha \log P + \beta(V-I) + \gamma$
  - $W_I = \alpha \log P + (\beta - R_I)(V-I) + \gamma =$
    $= \alpha \log P + (\beta - R_I)(V-I)_0 + (\beta - R_I)E(V-I) + \gamma$
  - $\log P = \text{const} \Rightarrow$ intrinsic colour spread + differential reddening
  - $\Delta W_I / \Delta I = (\beta - R)/\beta$

Infrared period–luminosity relations for type II Cepheids in globular clusters

- Matsunaga et al. (2006, MNRAS 370, 1979)
  - about 40 (from 80 known) type II Cepheids from GCs
  - $(m - M)_0$ of GCs from $M_V(\mathrm{HB}) = 0.22[\mathrm{Fe/H}] + 0.89$ (Gratton et al. (2003))
  - $M_K = -2.41(\log P - 1.2) - 4.00$
  - $\sigma \approx 0.2$ mag
- no evidence for more than one mode of pulsation
- slope and zero-point of the PLR agree with that of RR Lyraes

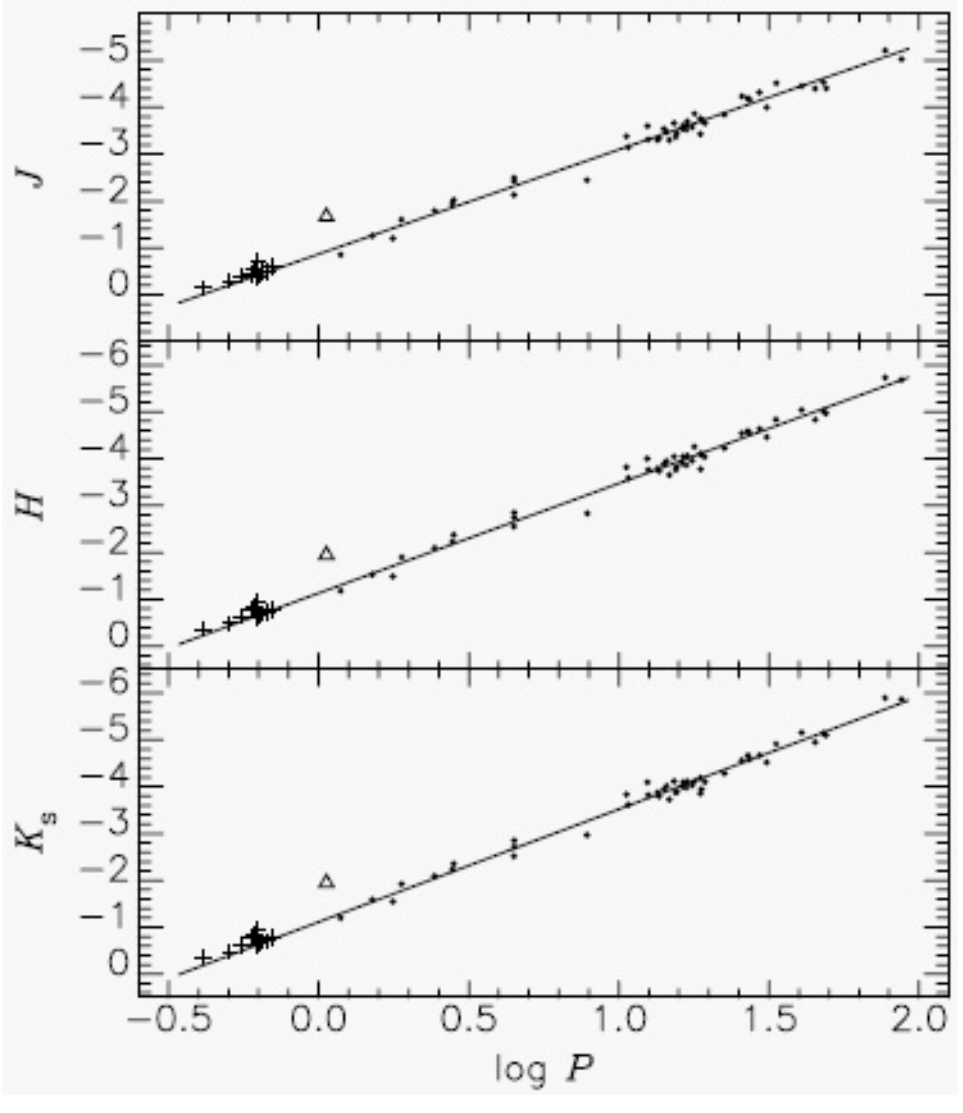

PLR for type II Cepheids from GCs (filled circles). RR Lyrae stars from M92 are plotted as plus symbols. The triangle is for v7 from M92, which can be anomalous Cepheid.

Infrared period–luminosity relations for type II Cepheids in LMC

- Matsunaga et al. (2009, MNRAS 397, 933)
  - 200 Cepheids in LMC from OGLE-III
  - JHK from IRSF at SAAO
  - $K = -2.41(\log P - 1.2) + 14.76$
  - $\sigma \approx 0.2$ mag
- BL Her and W Vir stars follow the same relation
- RV Tau stars do not continue the linear PL relation
- zero-points from BW parallaxes of V553 Cen and SW Tau

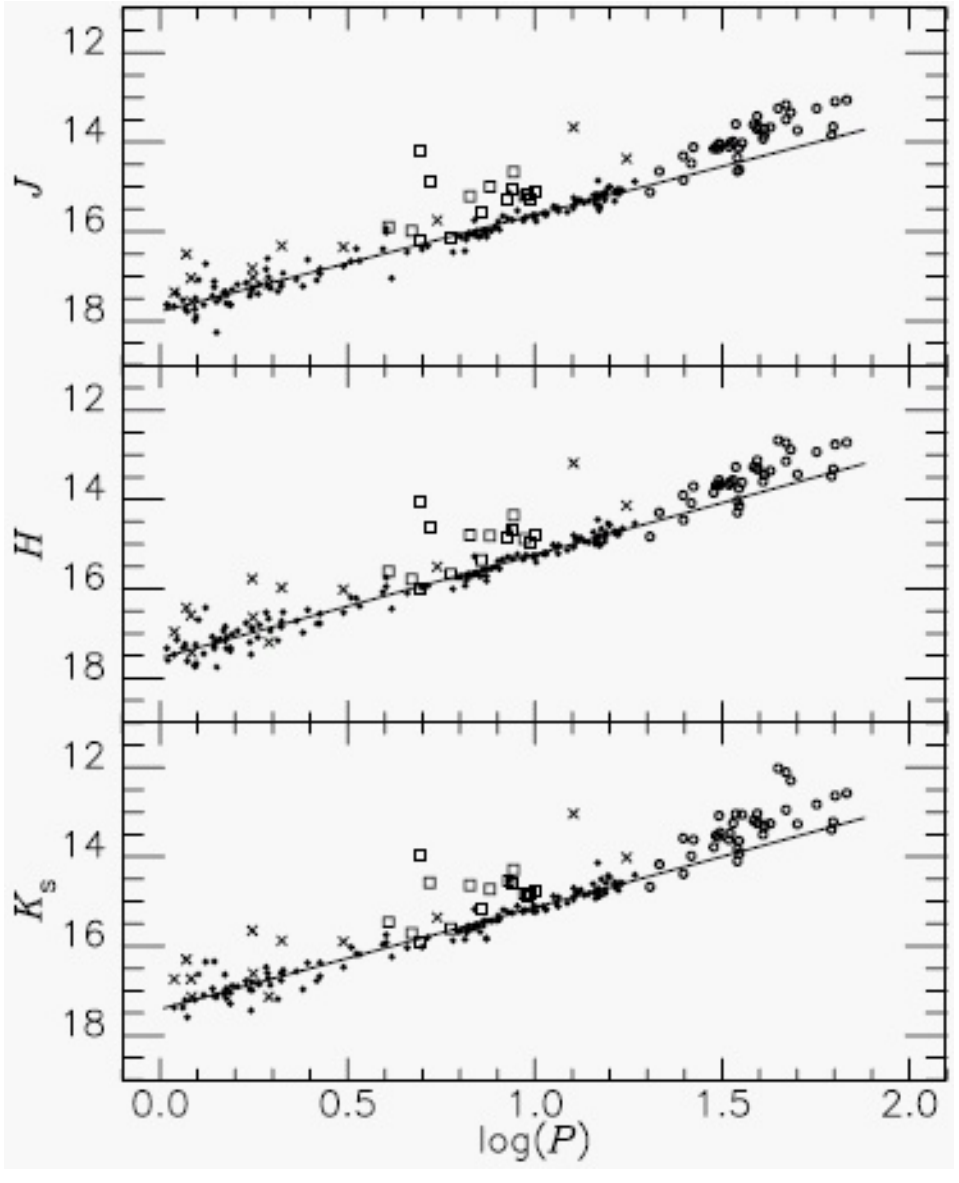

Period–magnitude relation for type II Cepheids in LMC. Filled circles indicate BL Her and W Vir stars used to solve the PL relations, while crosses indicate those excluded, open squares pW and open circles RV Tauri stars. Matsunaga et al. (2009, MNRAS 397, 933).

Test of consistency

- RR Lyr and Pop. II Cepheids scales vs. classical Cepheids scale
- comparison of the distances they imply for the LMC
- Feast (2010)
- various estimates evidently agree well

Method	Modulus
Cepheids (VI) uncorr.	18.52 ± 0.03
Cepheids (K) uncorr.	18.47 ± 0.03
Cepheids (VI) corr.	18.39 ± 0.05
CephII (VI)	$18.46 \pm \sim 0.1$
CephII (K)	$18.50 \pm \sim 0.1$
RR Lyrae (V)	$18.38 \pm \sim 0.1$
RR Lyrae (K)	$18.37 \pm \sim 0.1$

The classical Cepheid results are based on HST and Hipparcos trigonometrical parallaxes together with a period-luminosity-colour (reddening-free) relation in VI and a period-luminosity relation in K. The first two entries have not been corrected for metallicity differences between the LMC Cepheids and the Galactic Cepheid calibrators. The third entry shows the VI result after applying a metallicity correction. Observational estimates of metallicity effects at K are not available. The CephII results are based on the OGLE (VI) and IRSF (JHK) LMC data.

Period – luminosity relation for Anomalous Cepheids

Anomalous Cepheids

- new class of Cepheid-like variables
  - P from 0.8 to 2 d
  - different LCs (small amplitudes, more symmetrical)
  - are brighter than RR Lyr and AHB1 stars, but fainter than classical Cepheids
  - masses of about 1.5 $M_\odot$
  - low metallicity, [Fe/H] < -1.3
  - two known in GGCs (NGC5466 and M92)
- ACs are rare in GGCs and abundant in dSph galaxies
- long-period type II Cepheids are rare in dSph galaxies but present in GGCs

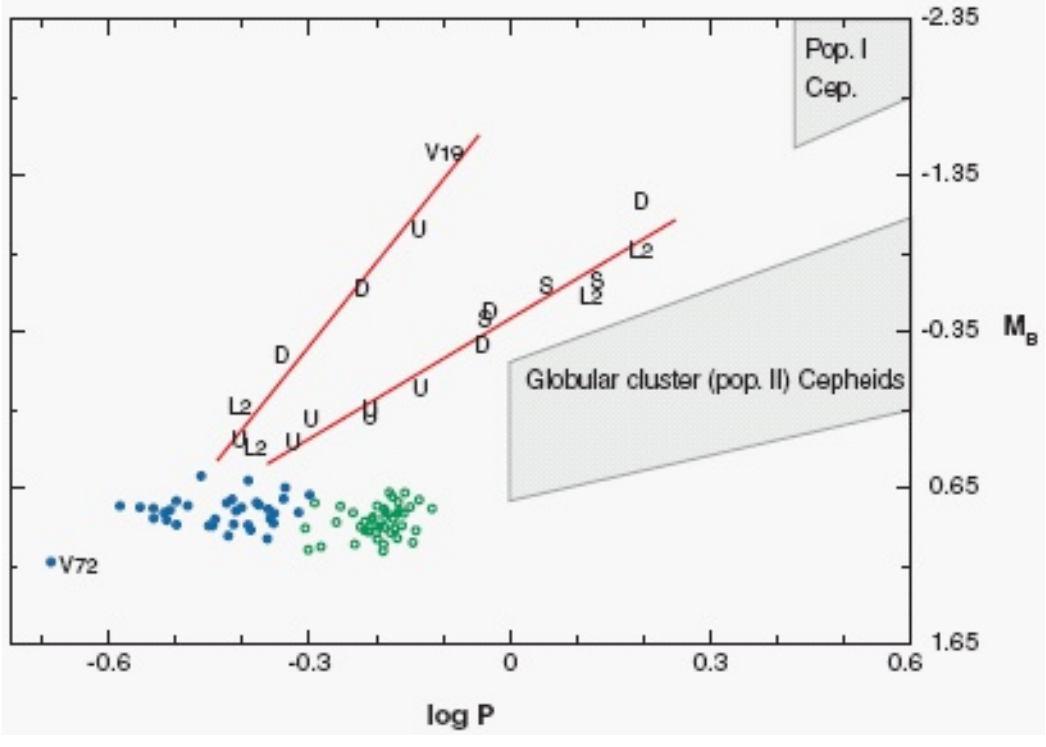

B-band PL relation for anomalous Cepheids compared with the position of the RR Lyraes in the UMi dSph, and compared with the boundary locations of the PL relations for population I and II Cepheids. The symbols are for the dSph galaxies of U = UMi, L2 = Leo II, D = Dra, and S = Scl. The lines through the dSph points are for the fundamental and first overtone pulsators. Nemec et al. (1988, AJ 96, 528).

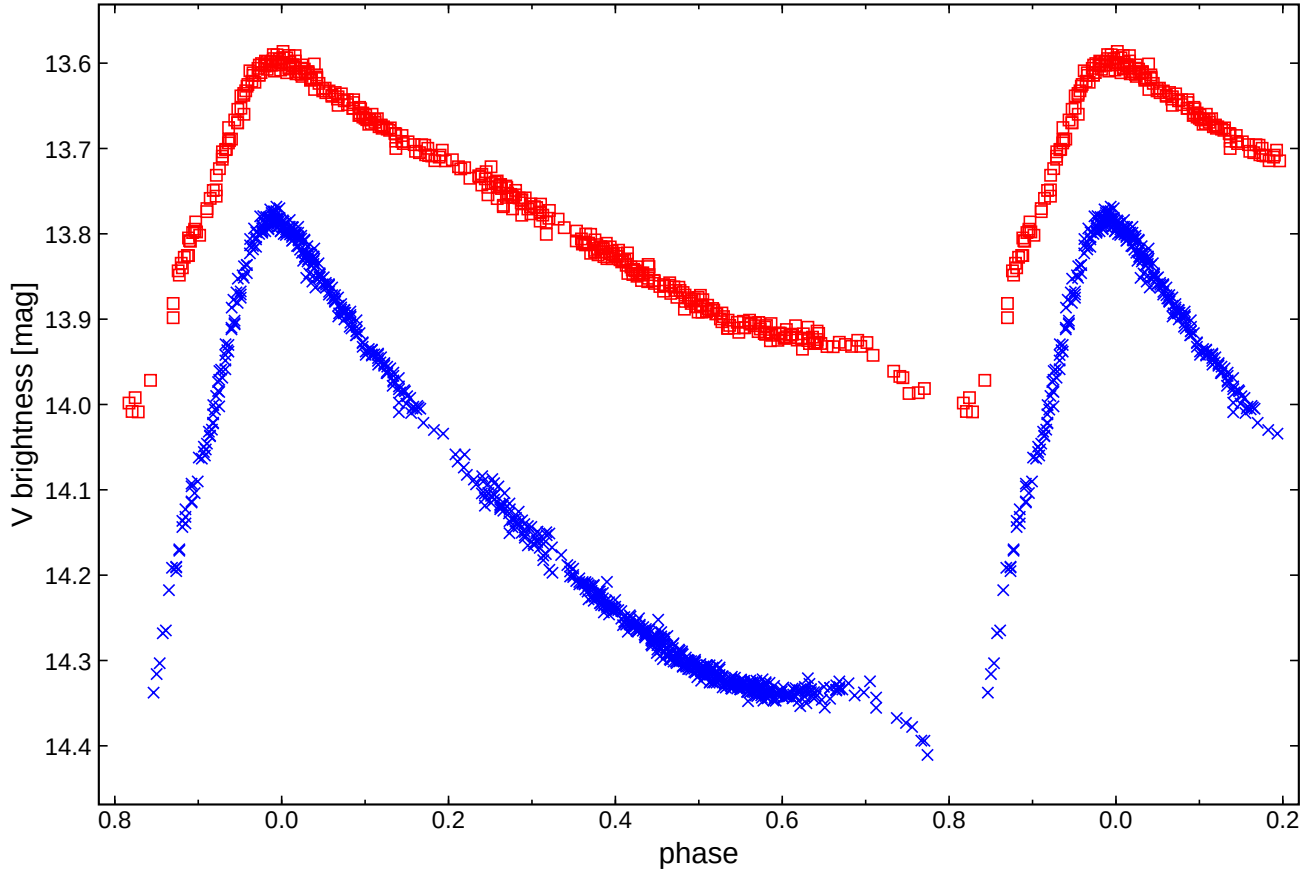

Phased light curves of v7 from M92 obtained the CCD observations. V observations (crosses) are the lower curve and I_C observations (squares) the upper one. I_C magnitudes were shifted by adding 0.2 mag. Osborn *et al.* (2012).

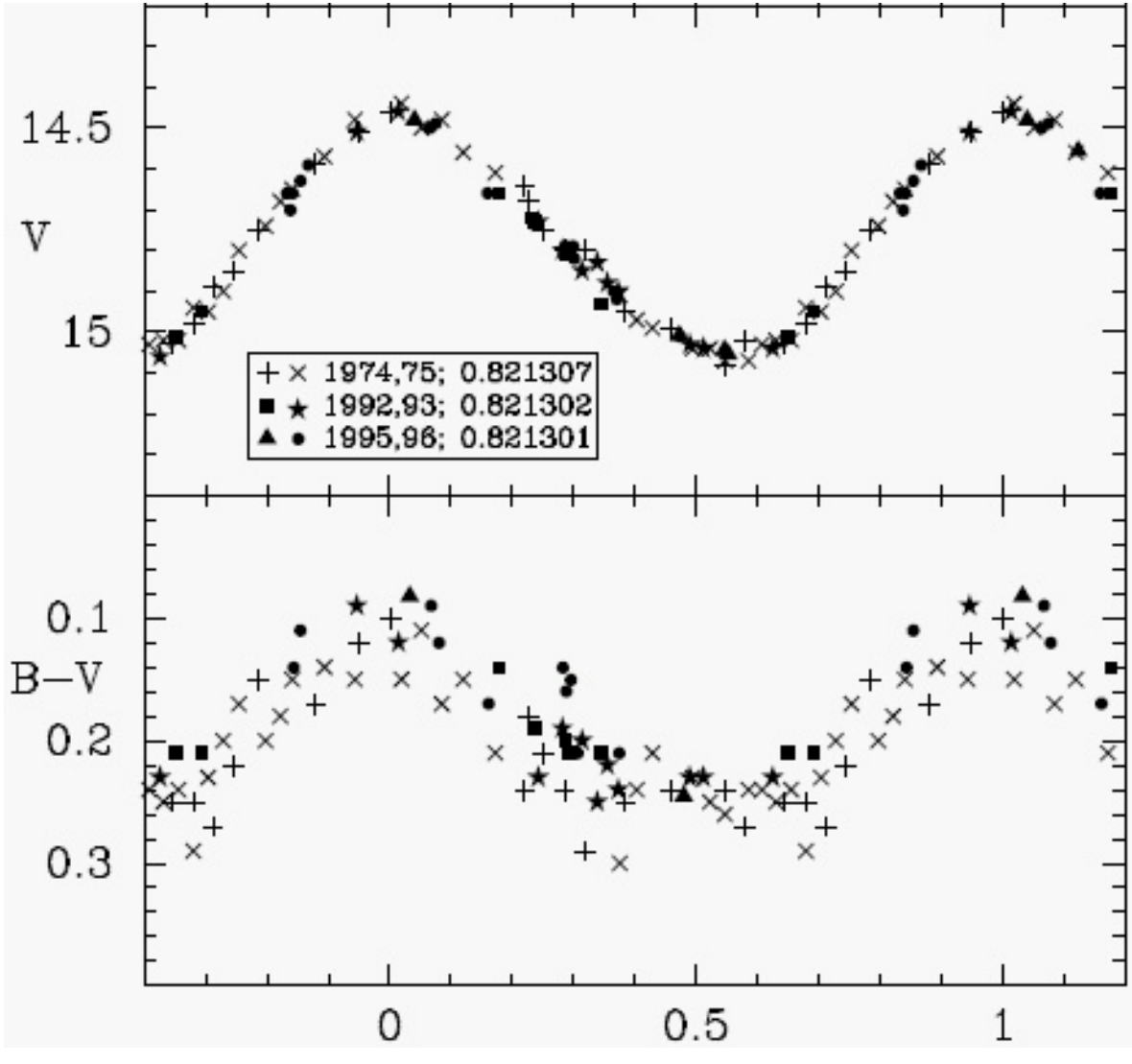

Phased light and colour curves of v19 from NGC5466. McCarthy and Nemec (1997, ApJ 482, 203).

Anomalous Cepheids

- Abundant in dSphGs (old ($\tau > 10$ Gyr), having population of stars with intermediate age ($\tau < 6$ Gyr), rich in gaz), transition-type dSph/dIrr, LMC.
- Absent in dIrrGs.
- Few in Galaxy:
  - NGC5466-V19 and M92-V7 ([Fe/H] ≈ -2),
  - XZ Cet.
- Evolutionary stage:
  - HB after He flash ($1 - 2\ M_{\odot}$, low metallicity)
- Origin:
  - young single star ($\tau < 5$ Gyr) due to recent star formation
  - merger of binary system with old component stars

  (ACs result from the evolution of BSSs)

galaxy	μ_0 (mag)	$EB-V$ (mag)	[Fe/H]	Ref.	Notes
AndI	24.5	0.05	−1.5	1	a
AndII	24.1	0.06	−1.5	2	a
AndIII	24.3	0.06	−1.9	1	a
AndVI	24.5	0.06	−1.6	3	a
Carina	20.1	0.04	−1.6	4	a
Draco	19.5	0.03	−2.1	3	a
Fornax	20.7	0.03	−1.6	5	b, e
LeoII	21.6	0.02	−1.9	3, 6	c
LMC	18.5	0.10	−1.7	7	a, f
Phoenix	23.1	0.02	−1.4	8	d, f
Sculptor	19.6	0.02	−1.8	9, 10	c
Sextans	19.7	0.04	−1.6	11	a

Dwarf galaxies with observed Anomalous Cepheids listed with their intrinsic distance modulus μ_0, $E(B-V)$ reddening, and metal abundance [Fe/H]. Fiorentino *et al.* (2006, AAp 460, 155)

Host galaxy	AC number	Observed quantities	μ_0	$E(B-V)$	Source
And VI	6	V, B, A_V	24.45 mag	0.06 mag	Pritzl et al. (2002)
Leo II	4	V, A_V	21.59 mag	0.02 mag	Pritzl et al. (2002)
Draco	8	V, B, A_V	19.49 mag	0.03 mag	Pritzl et al. (2002)
Carina	8	V, B, A_V	20.14 mag	0.04 mag	Dall'Ora et al. (2003)
Sculptor	3	V, A_V	19.56 mag	0.02 mag	Kaluzny et al. (1995)
Sextans	6	V, B, A_V	19.74 mag	0.03 mag	Mateo et al. (1995)
Fornax	17	V, I	20.70 mag	0.03 mag	Bersier & Wood (2002)

Selected parameters of anomalous Cepheids in dwarf spheroidal galaxies. Marconi *et al.* (2004, AAp 417, 1101).

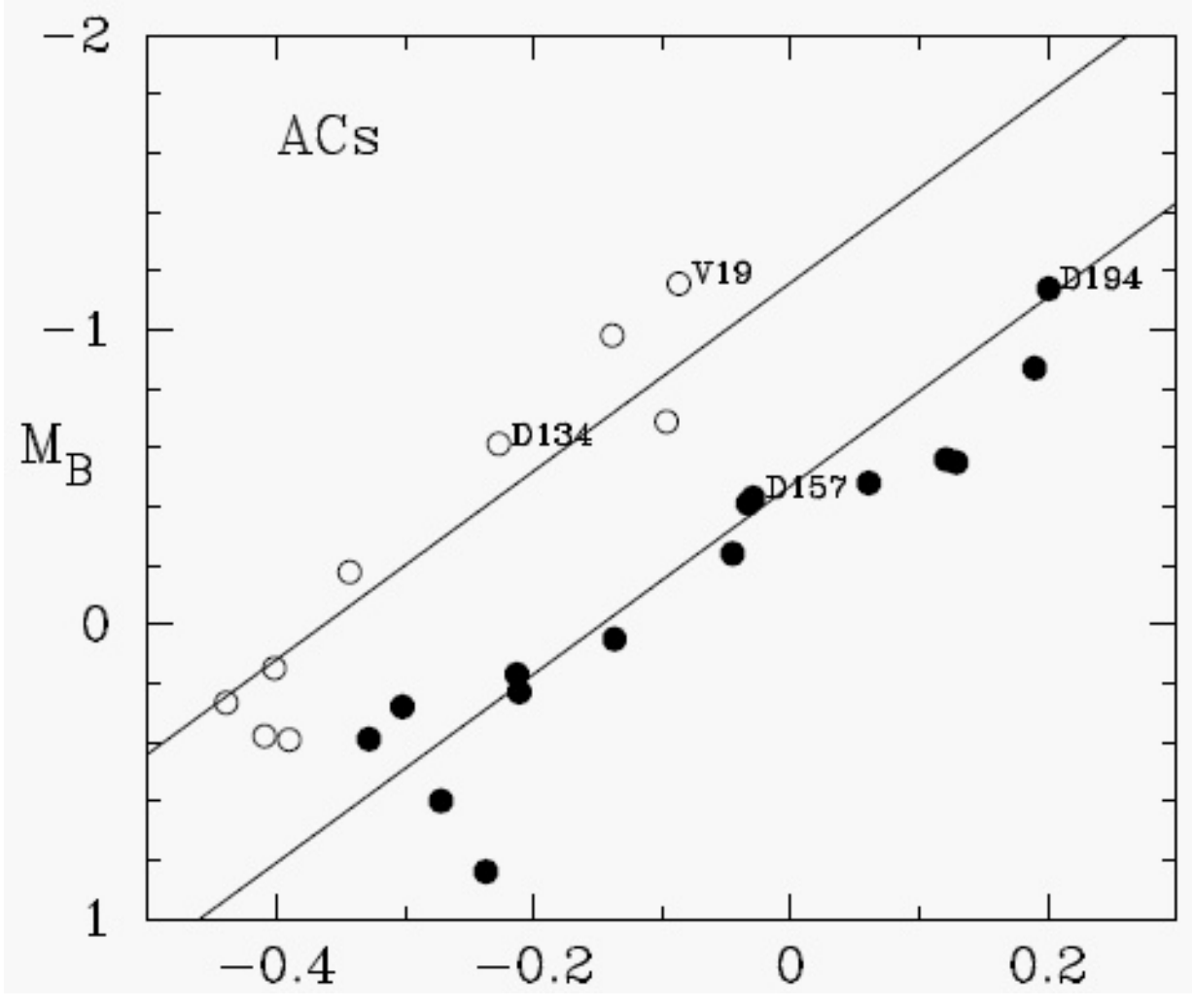

Period – luminosity diagram for all the known anomalous Cepheids. The solid dots are the fundamental mode (F) pulsators, and the open circles are the first-overtone (H) pulsators. NGC5466-V19 and three of the Draco ACs are labelled. The diagonal lines are the P-L relations derived by NNL for [Fe/H] = −2. McCarthy and Nemec (1997, ApJ 482, 203)

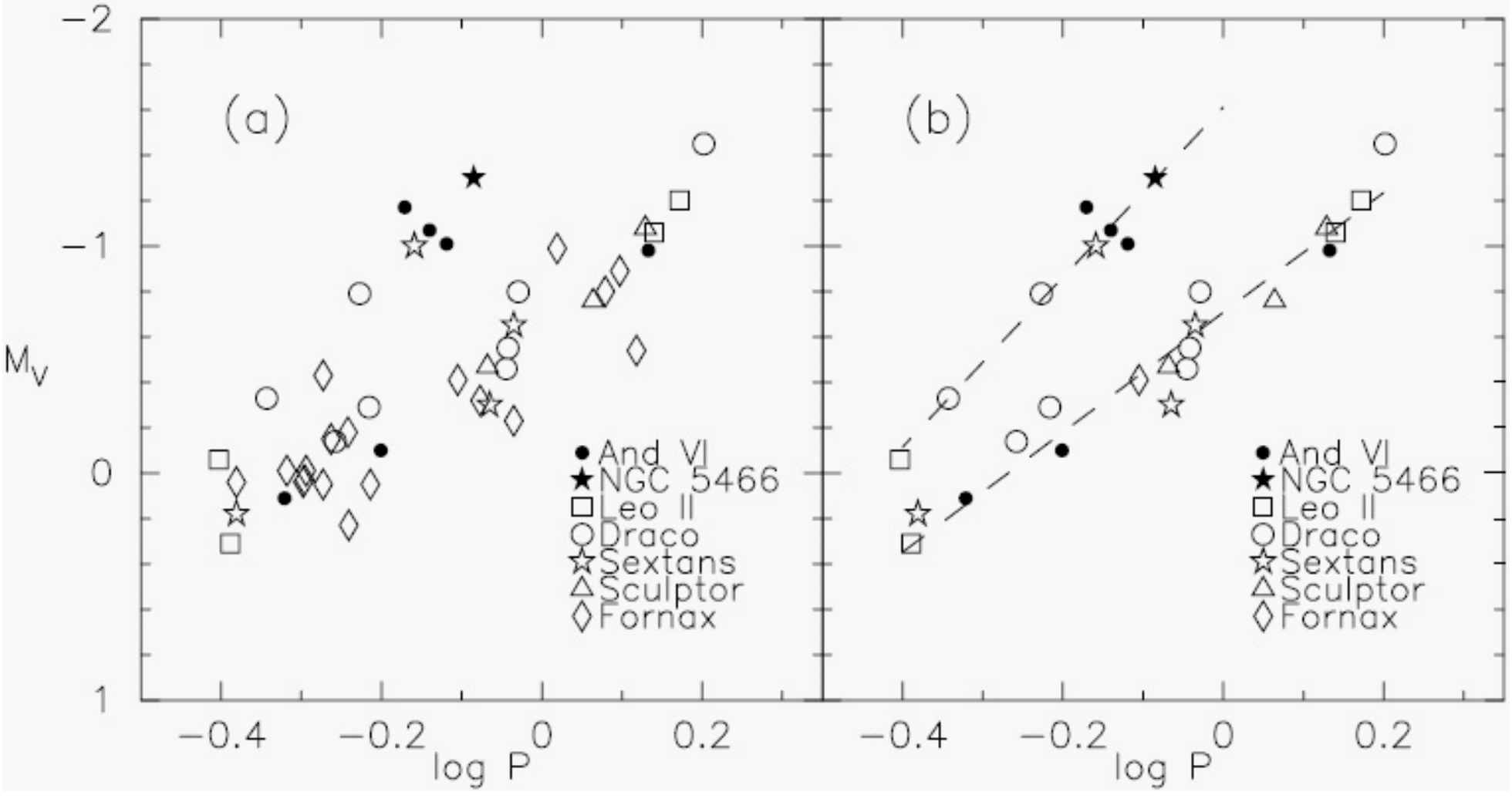

M_V vs. period for anomalous Cepheids: (a) all data; (b) the data with the Fornax data from Bersier and Wood (2002) removed. Pritzl *et al.* (2002, AJ 124, 1464)

• no clear difference between fundamental and first-overtone ACs in a period-amplitude diagram

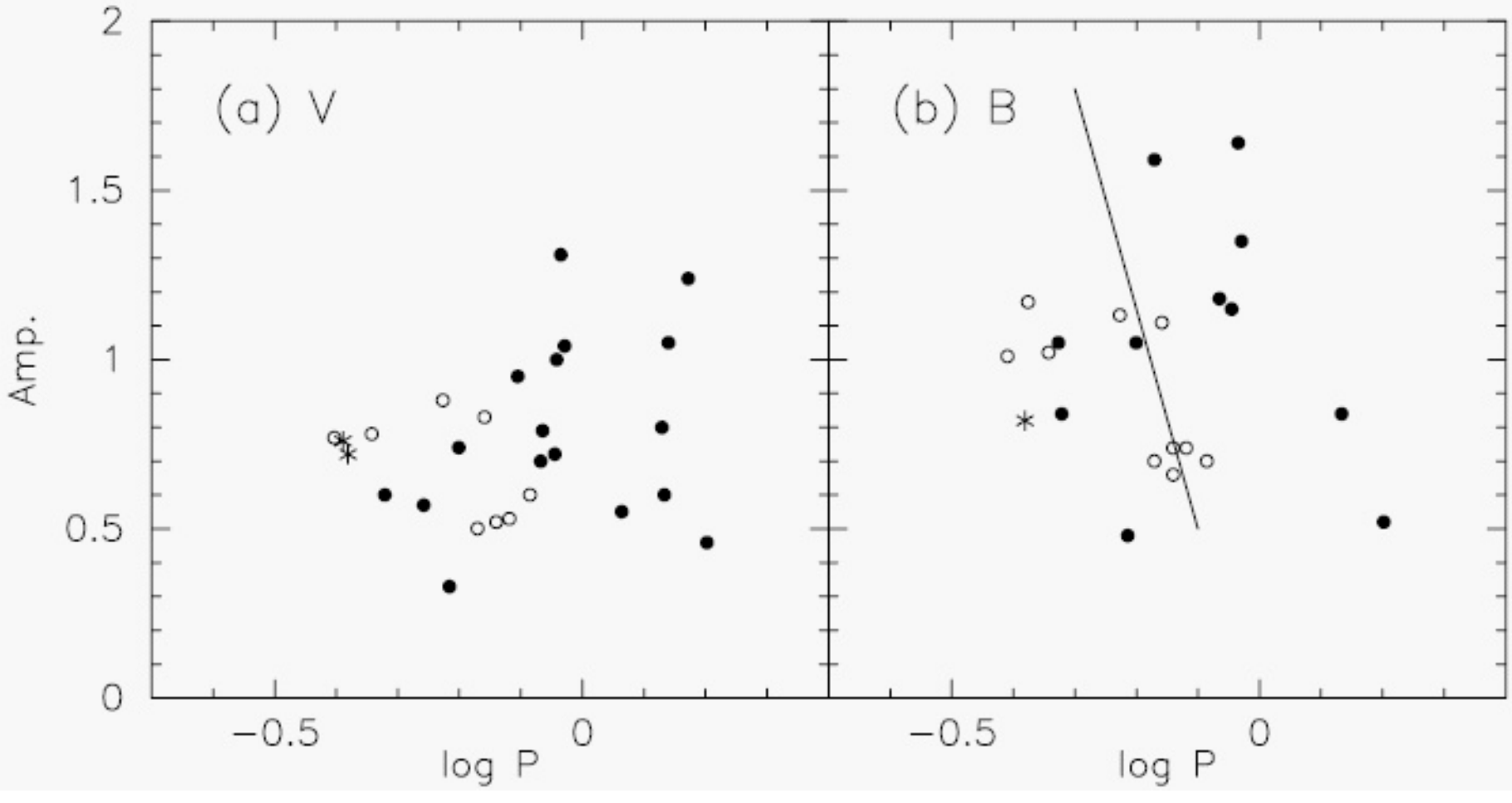

Period – amplitude diagram for anomalous Cepheids, showing first-overtone stars (open circles) and fundamental mode stars (filled circles). Asterisks denote ACs with uncertain classification. The line in (b), taken from Fig. 7 of Bono et al. (1997), represents the predicted location of the ZAHB fundamental mode pulsators and is meant to divide fundamental mode from first-overtone pulsators. Pritzl *et al.* (2002, AJ 124, 1464)

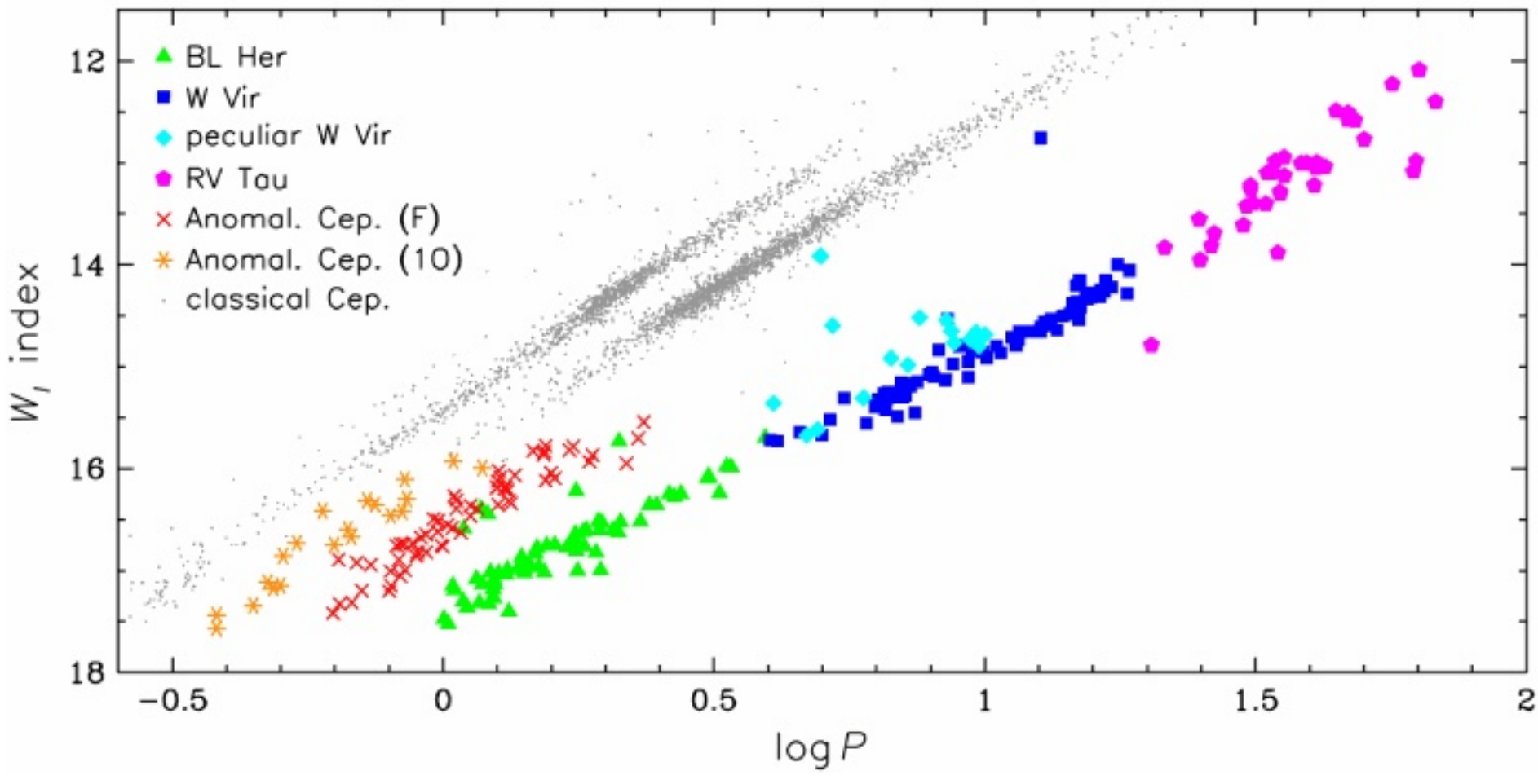

LMC, Soszyński *et al.* (2008, AcA 58, 293)

- for low metal abundances ($Z < 0.0004$) and relatively young ages (< 4 Gyr) the effective temperature of ZAHB models reaches a minimum for a mass of about $1.0-1.2\ M_{\odot}$, while if the mass increases above this value, both the luminosity and the effective temperature start increasing, forming the so called 'ZAHB turnover'.
- within such an evolutionary scenario, ACs appear to belong to the post-turnover portion of the ZAHB which crosses the instability strip at luminosity higher than RR Lyrae pulsators.

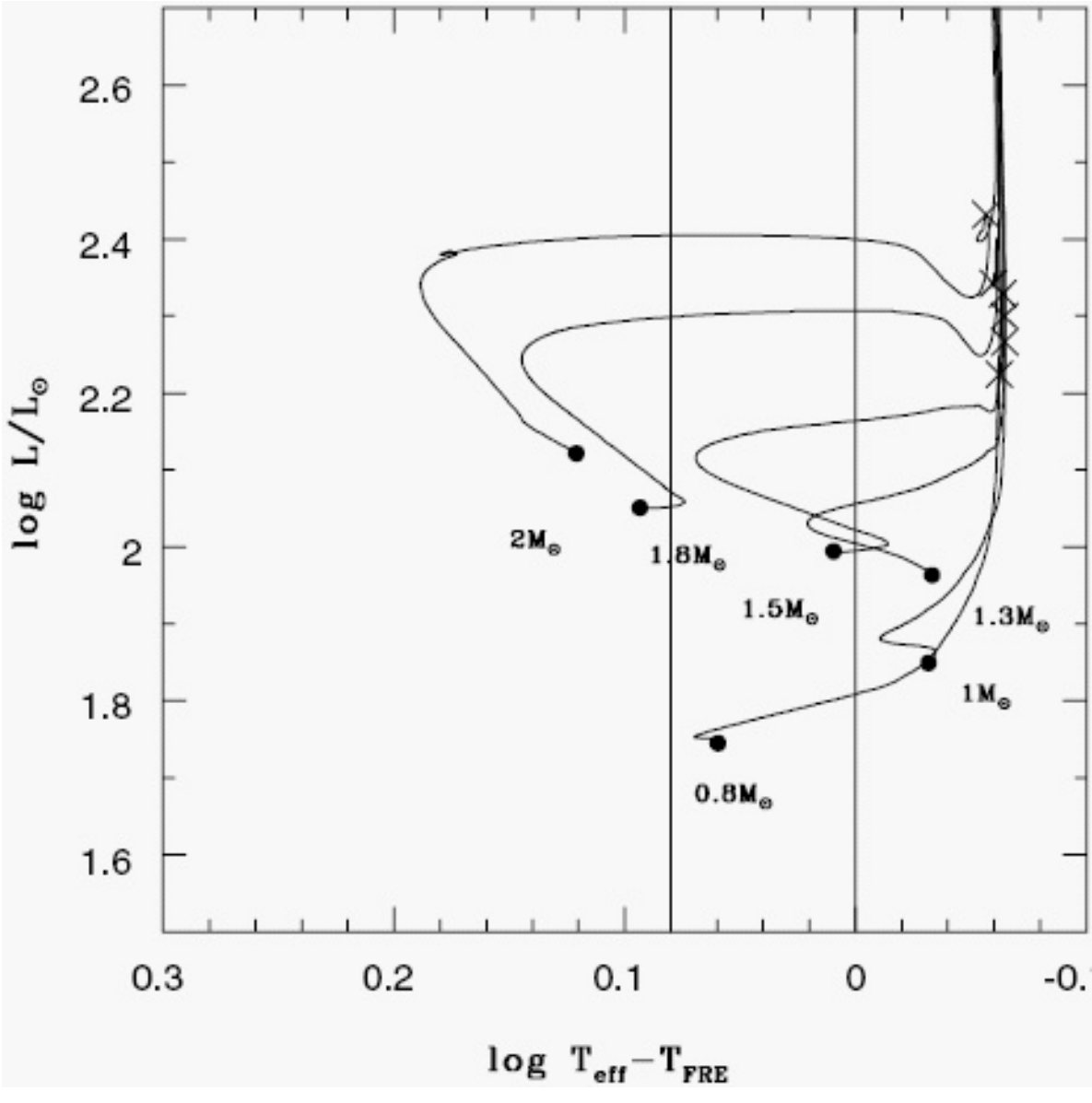

Canonical (no mass-loss) evolutionary tracks of central He-burning models with $Z = 0.0001$, $Y = 0.24$ and the labeled masses. In order to point out the connection of evolution with pulsation, we subtract the value at the red edge (FRE) of the pulsation region from the effective temperature of each model. Dots indicate the initial central He-burning phase, crosses indicate the central He-exhaustion phase corresponding to $t_{\rm He}$, as the vertical lines represent the predicted boundaries of the instability strip. Fiorentino *et al.* (2006, AAp 460, 155)

M	t	$M_{\rm He}$	$t_{\rm He}$ + $t_{\rm EAGB}$	$t_{\rm IS}$	$\langle \log L_{\rm IS} \rangle$	$\langle \log T_{\rm e}({\rm FOBE}) \rangle$	$\langle \log T_{\rm e}({\rm FRE}) \rangle$
2.0	0.7	0.416	98 + 6	0.5	2.40	3.84	3.76
1.8	1.0	0.425	104 + 7	3.2	2.30	3.84	3.76
1.5	1.8	0.463	92 + 8	87.6	2.09	3.85	3.77
1.3	2.8	0.483	76 + 9	35.0	2.03	3.85	3.77
1.0	6.6	0.501	80 + 10	–	–	–	–
0.8	14.5	0.508	79 + 11	69	1.77	3.86	3.78

Selected parameters of the $Z = 0.0001$ evolutionary tracks without mass-loss. Mass (M) and luminosity (L) are in solar units. We give the evolutionary age (t, in 10^9 yr) and the He-core mass ($M_{\rm He}$) at the beginning of the central He-burning phase, the duration ($t_{\rm He}$, in 10^6 yr) of the central He-burning phase and the time ($t_{\rm EAGB}$, in 10^6 yr) elapsed from the central He-exhaustion and the beginning of the EAGB phase. For the models which evolve into the IS, the last three columns give the average luminosity and effective temperature at the blue and the red edge of the IS. Fiorentino *et al.* (2006, AAp 460, 155)

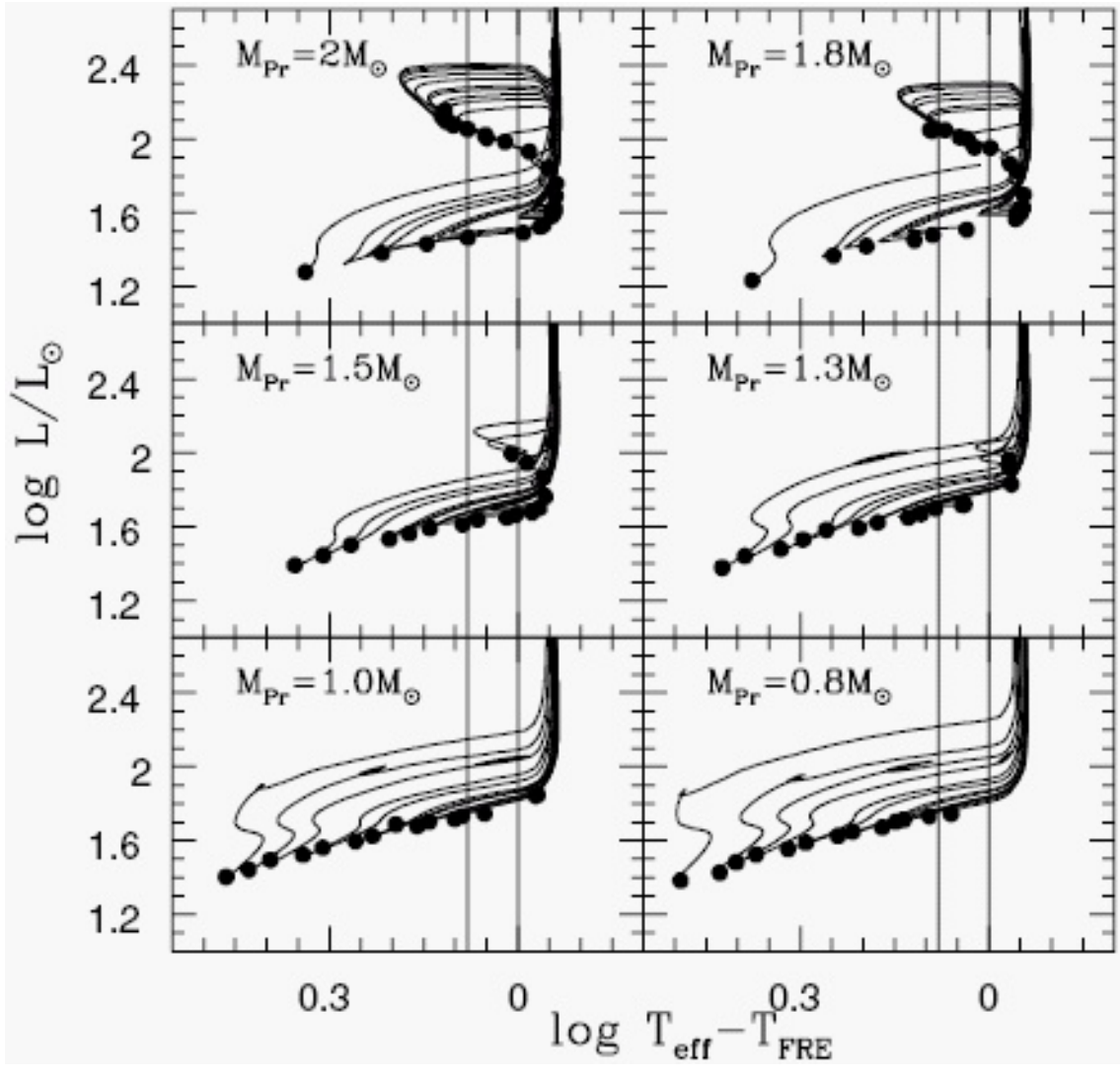

Evolutionary tracks of the ZAHB models with $Z = 0.0001$, $Y = 0.24$, and mass-loss, generated from the labeled progenitor mass. In each panel the mass changes from $M_{\rm He}$ to $M_{\rm pr}$. Fiorentino *et al.* (2006, AAp 460, 155)

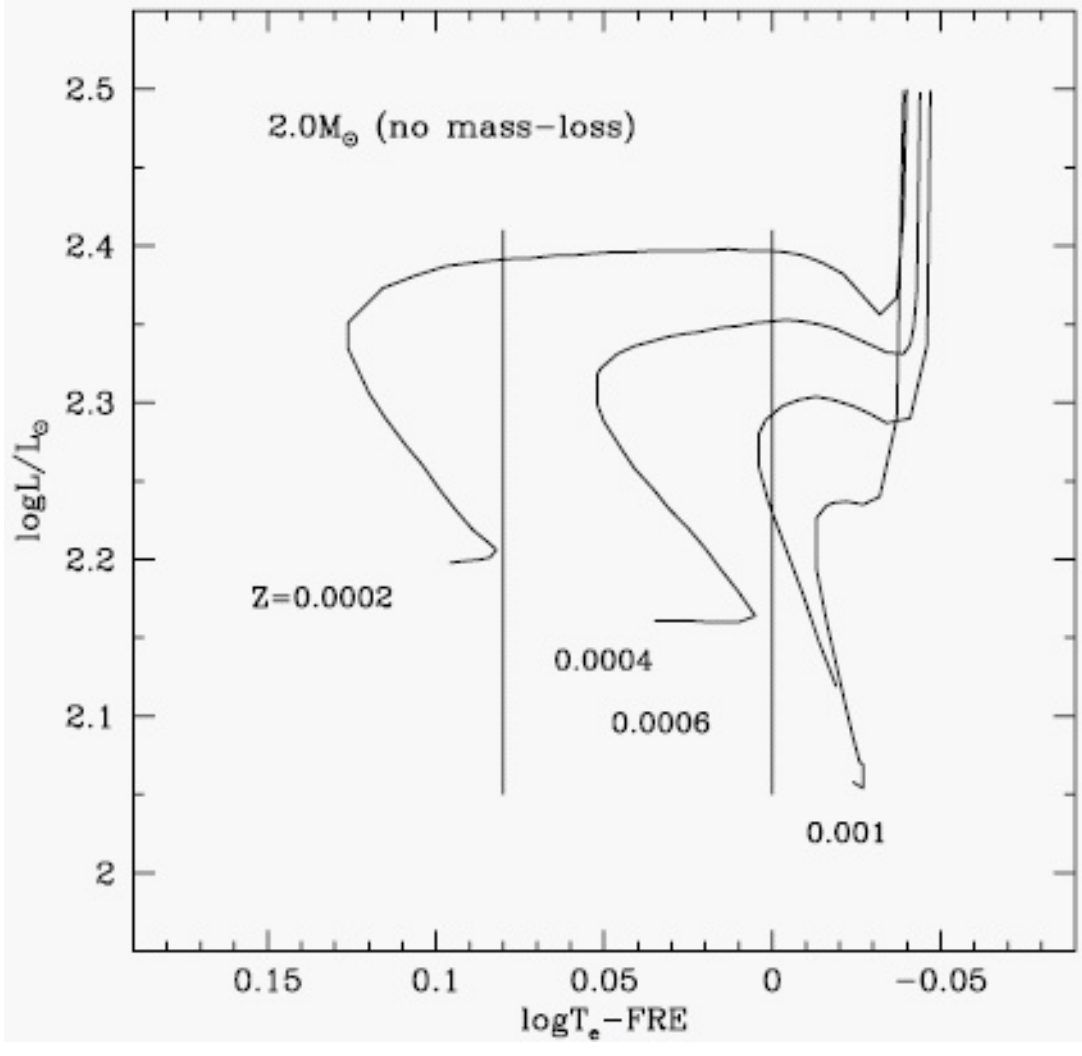

Evolutionary tracks for HB models with mass of 2.0 $M_{\odot}$ and the labeled metal content, in absence of mass loss. Fiorentino *et al.* (2006, AAp 460, 155)

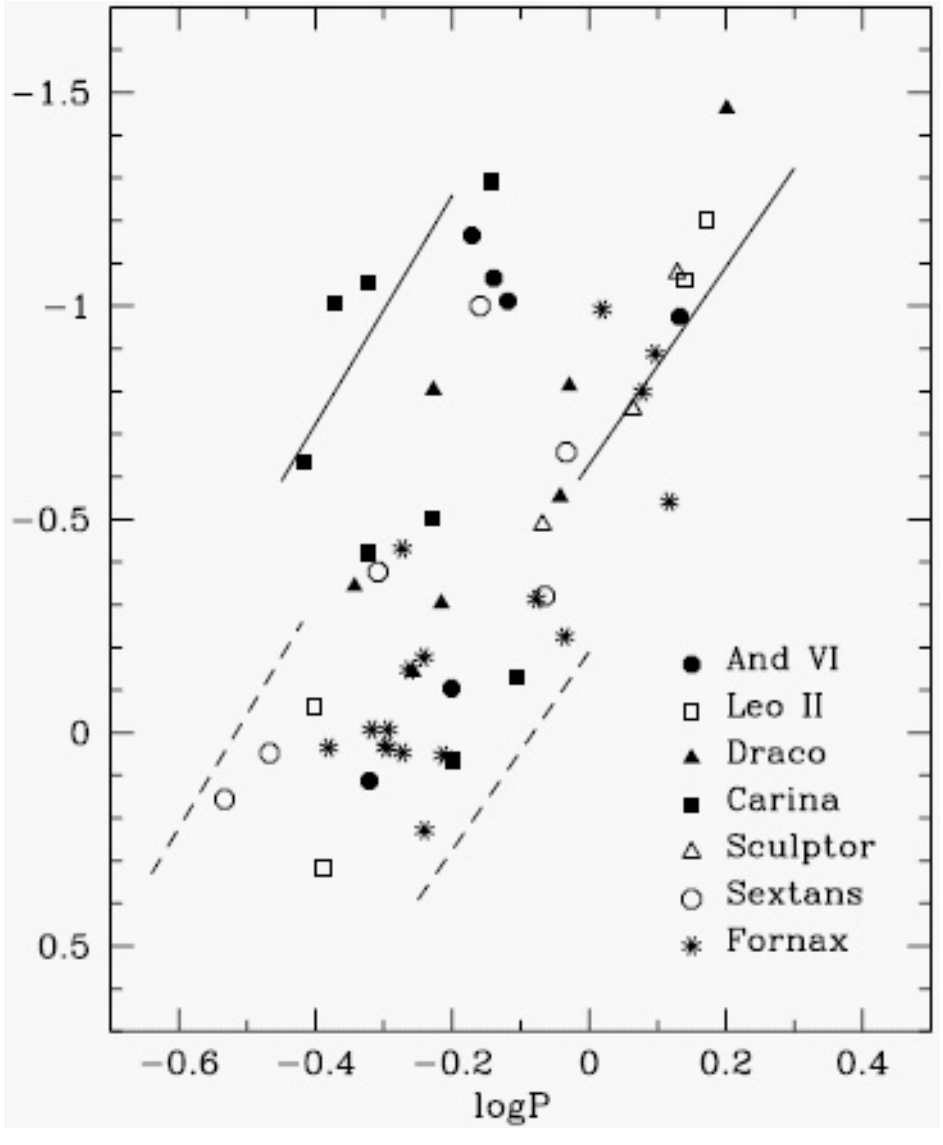

Comparison between the location of observed ACs in the M_V – $\log P$ diagram and the predicted boundaries of the instability strip at 1.3 $M_\odot$ (dashed line) and 2.2 $M_\odot$ (solid line). Marconi *et al.* (2004, AAp 417, 1101)

Short-period Classical Cepheids

Short-period Classical Cepheids, s-pCC

- Found in dIrrGs , absent in dSphGs.
- Periods about 1 d.
- Young stars burning He in the core (without He flash).
- Stars with low metallicity, for which evolutionary tracks have a blue loop extending to the blue far enough to intersect IS.
- dSph/dIrr
    - low metallicity
    - several populations of stars with different age
    - simultaneous occurance of ACs and s-pCCs.

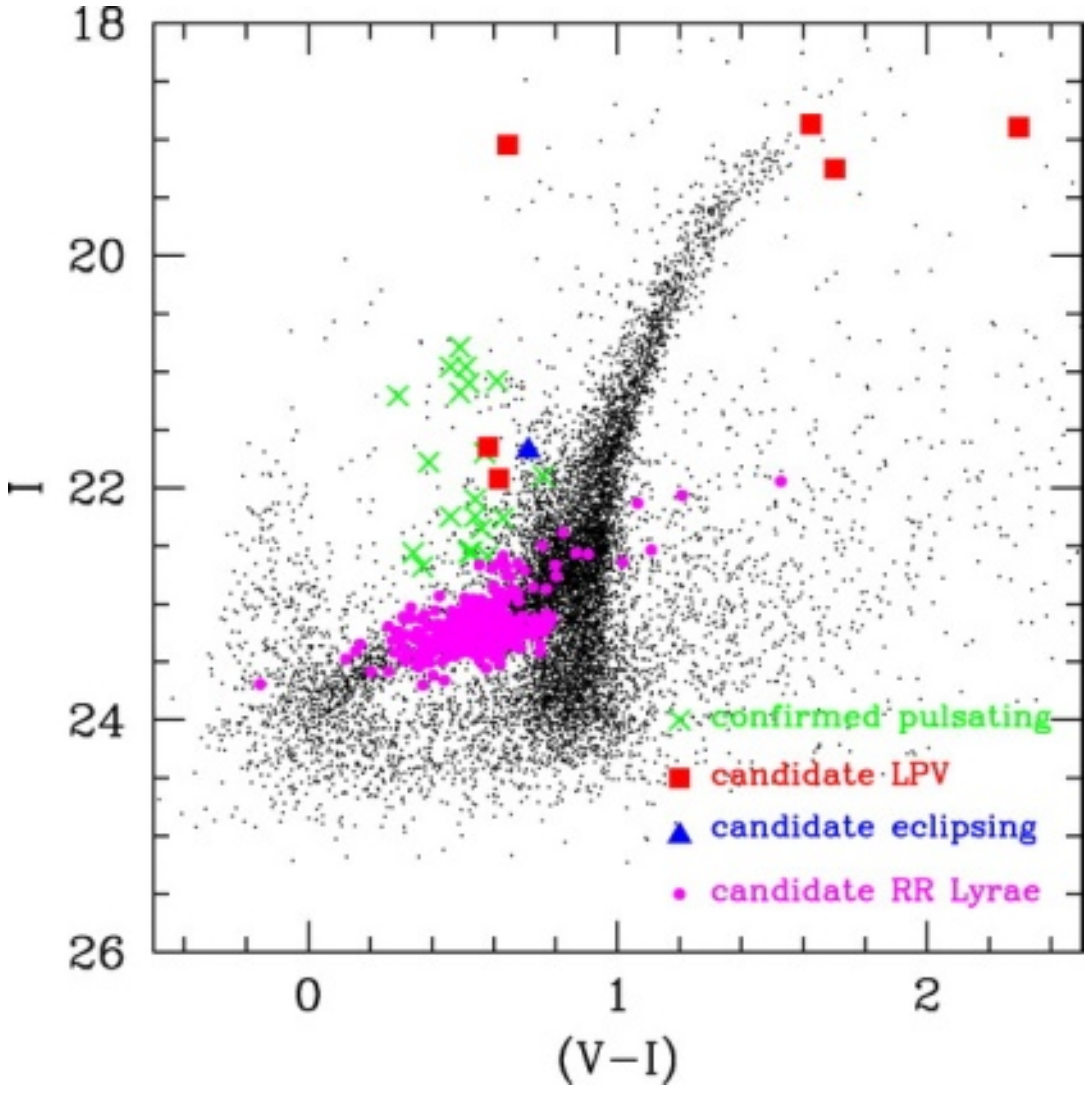

$(V-I, I)$ CMD of Phoenix dIrrG with confirmed pulsating (crosses) and long-period (squares) variables and the candidate eclipsing binary star (triangle). The 396 candidate RR Lyrae stars are shown as small circles. Gallart *et al.* (2004, AJ 127, 1486).

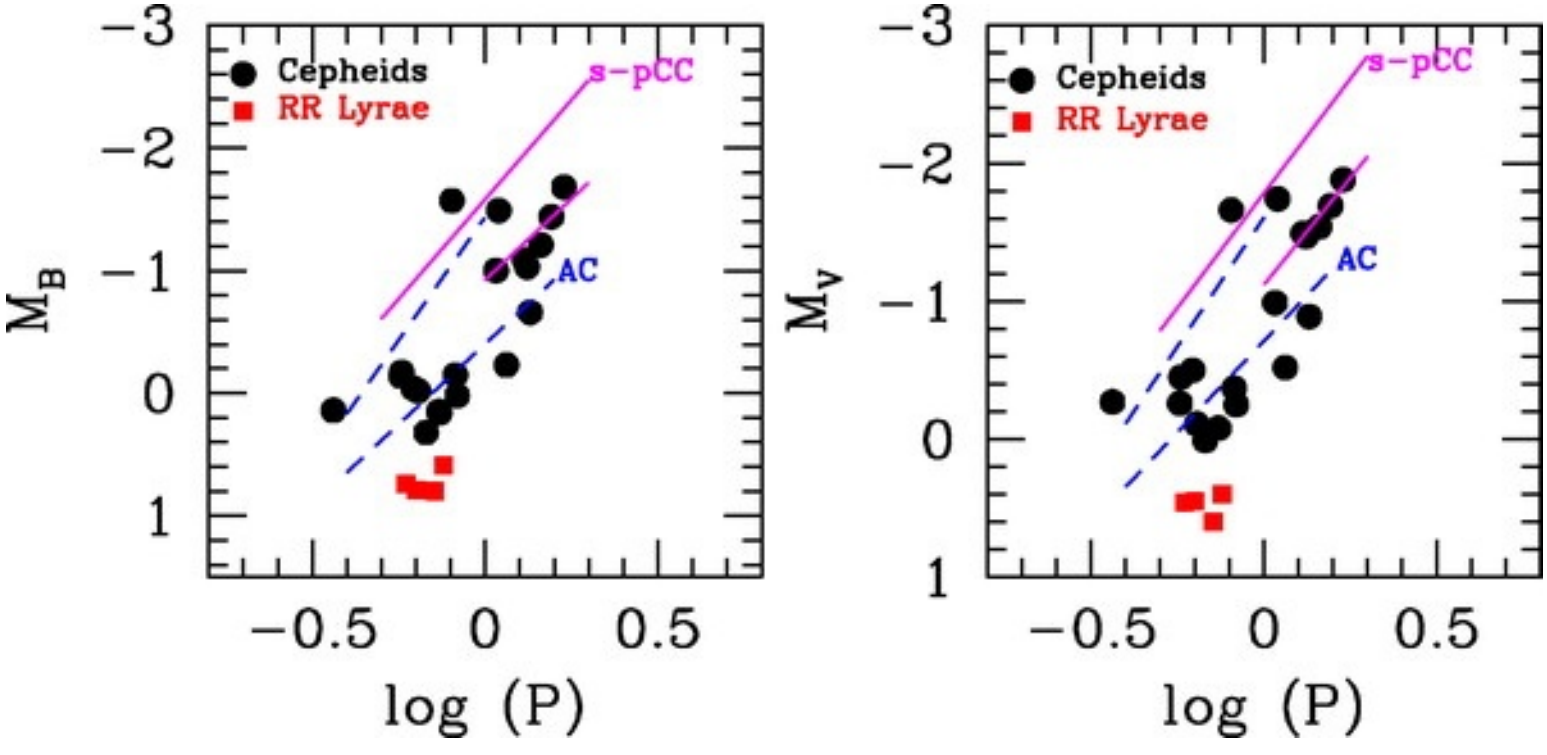

PL diagrams (in the B and V bands) for the Phoenix Cepheids. The PL relations obtained for dSph ACs by Pritzl et al. (2002) are represented as dashed lines, and the PL relations for ($P < 2$ d) OGLE SMC s-pCC's as solid lines. The four RR Lyrae variables for which periods have been obtained are included in the plot. Gallart *et al.* (2004, AJ 127, 1486)

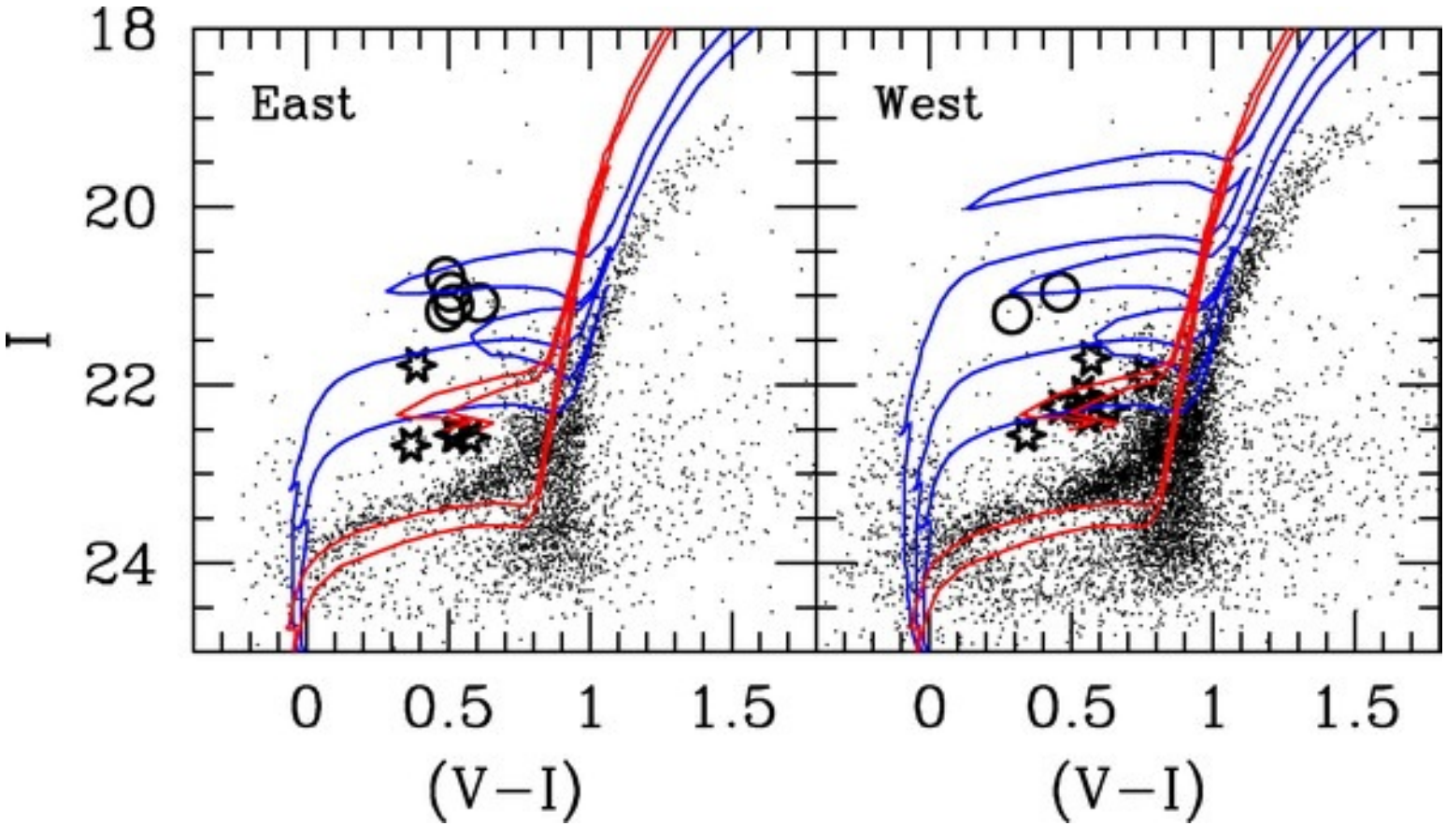

CMDs of the eastern and western parts of Phoenix. The east/west division has been made in order to keep separate the stars belonging to the young association located in the west part. It does not divide the galaxy exactly in half, and thus the sequences appear more populated in the west CMD. The ratio of main-sequence plus blue-loop stars ($-0.5 < (V-I) < 0.1$, $21 < I < 23.5$) to stars near the tip of the RGB ($(V-I) > 1.0$, $I < 20$) is, however, significantly larger in the west part (1.1 ± 0.2 vs. 0.4 ± 0.2), where the blue stars also extend to brighter magnitudes, indicating younger ages. Short-period classical Cepheids and ACs are represented as circles and stars, respectively. Isochrones from Bertelli et al. (1994) for $Z = 0.001$ and ages 200, 400, and 600 Myr, and for $Z = 0.0001$, and 1.3 and 1.6 Gyr have been superposed. Note how the position of the s-pCC's are well fitted by the younger isochrones, while the ACs are best fitted by the isochrones older than 1 Gyr. Gallart *et al.* (2004, AJ 127, 1486)

Secular period changes for ACs

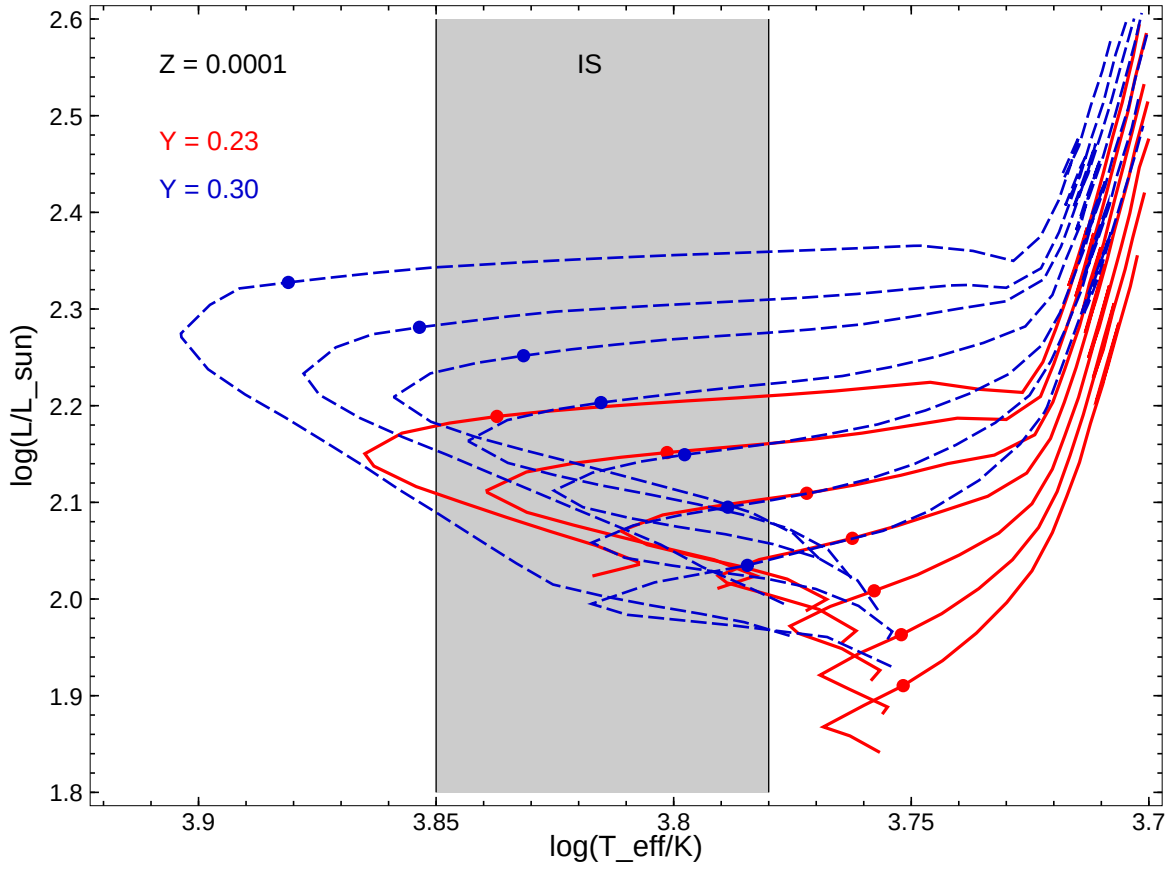

Evolutionary tracks of HB stars for $Z = 0.0001$, $Y = 0.23$ (continous lines) and $Y = 0.30$ (dashed lines), and masses from 1.0 to 1.6 $M_{\odot}$. The approximate boundaries of the instability strip (IS) are shown with two vertical lines. Dots indicate an approach to central He exhaustion (less than 10 % of the initial abundance). Osborn *et al.* (2012).

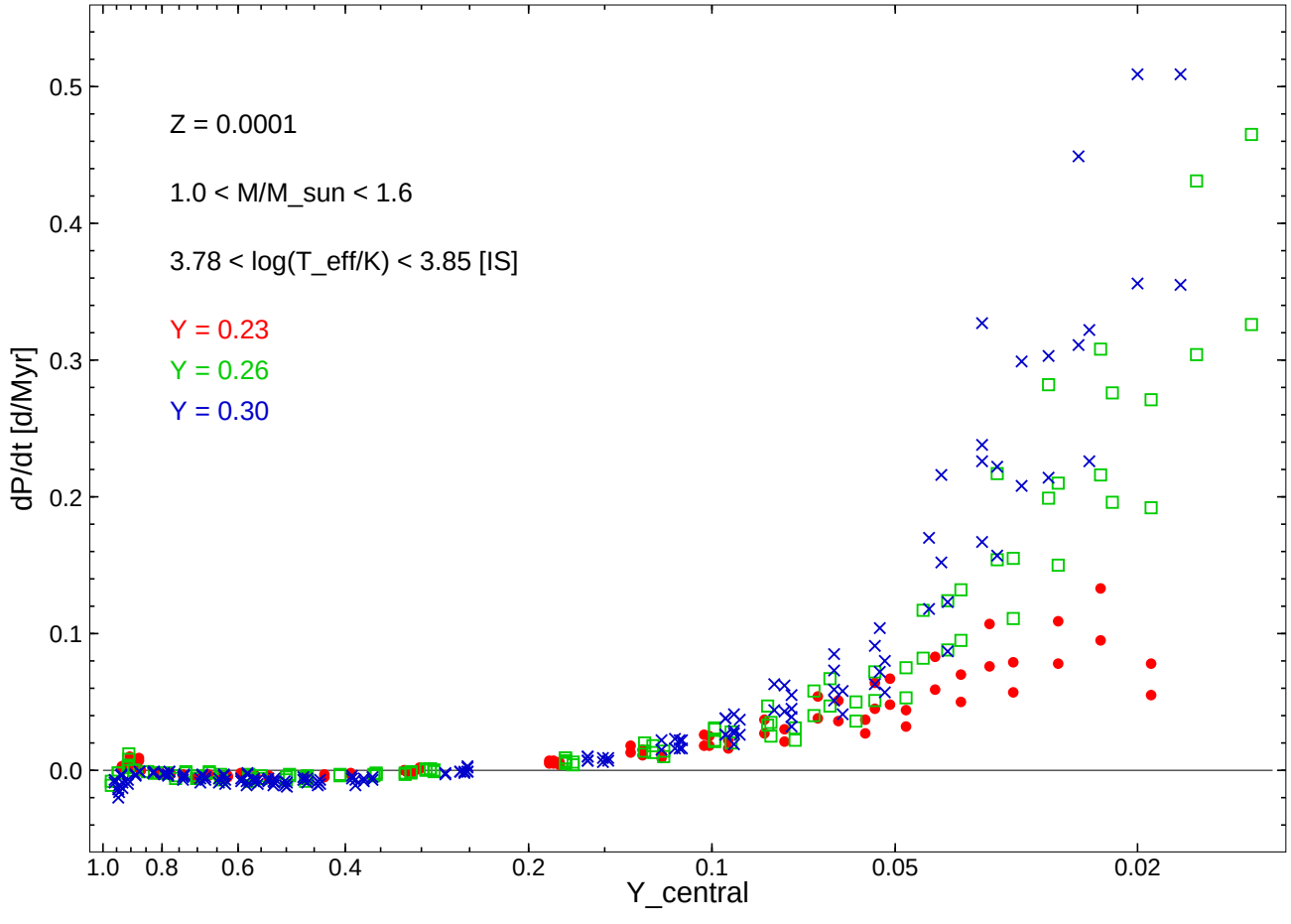

Evolutionary rates of the period change, dP/dt, for models of HB stars within the instability strip as a function of the central helium abundance, Y_c. Models for envelope helium abundances of $Y = 0.23$, 0.26, and 0.30 are indicated with filled circles, squares, and crosses, respectively. Osborn *et al.* (2012).

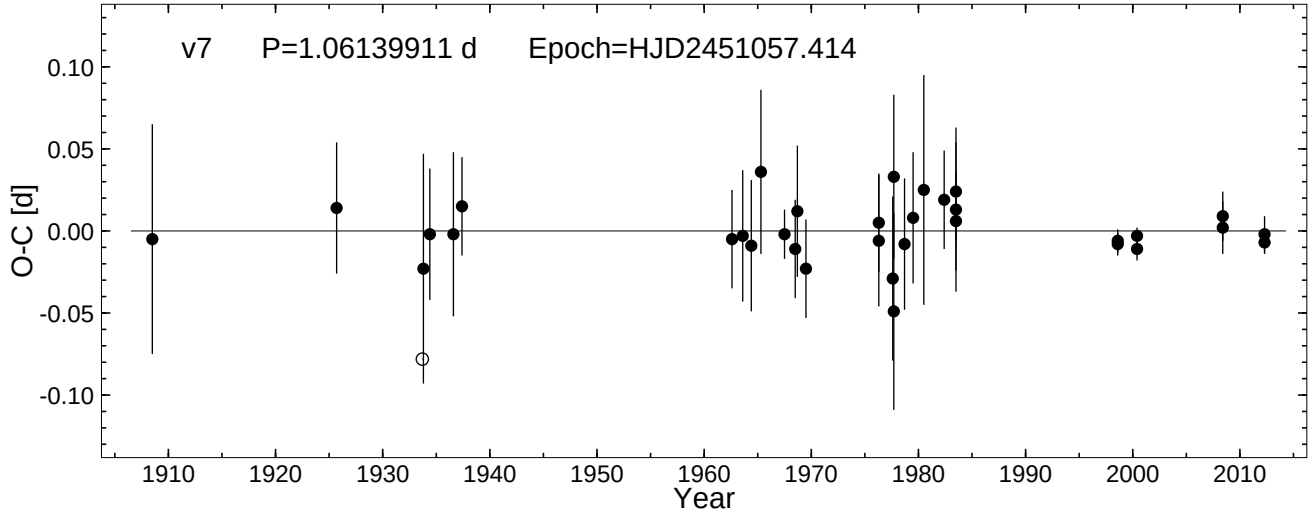

The derived $O-C$ diagram for v7 from M92. The open circle is from Hachenberg's published time of maximum. Osborn *et al.* (2012).

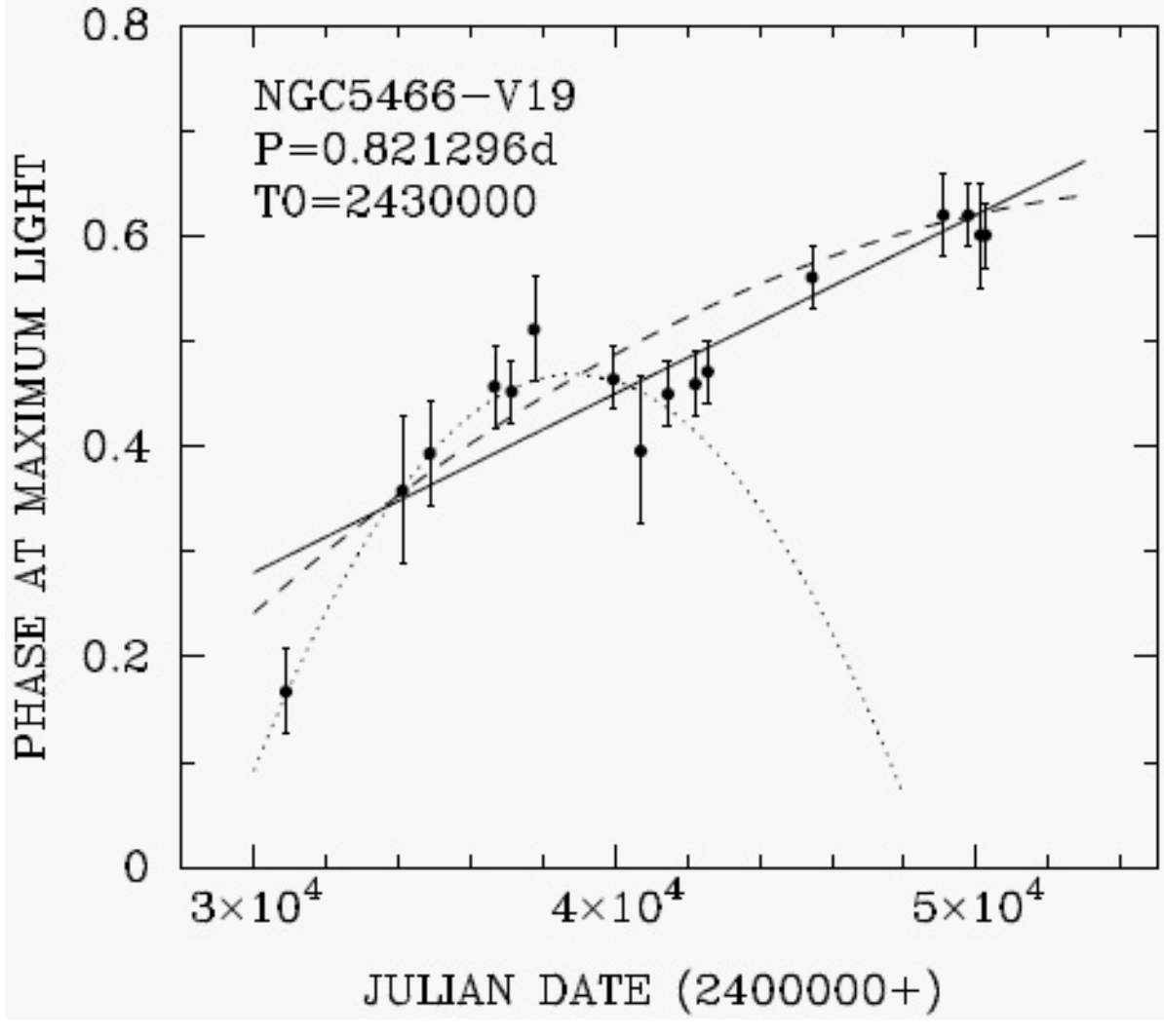

$O-C$ diagram for V19 from NGC5466. The dashed-line parabola suggests a decreasing period with $dP/dt = -0.3 \pm 0.19$ d/Myr, and the dotted-line corresponds to $dP/dt = -2.4 \pm 0.19$ d/Myr. McCarthy i Nemec (1997, ApJ 482, 203)

Period – luminosity relation for SX Phoenicis stars

SX Phoenicis stars

- short-period pulsating stars
- Pop. II analogues of the Pop. I δ Scuti stars
- lower part of the classical instability strip just above ZAMS
- blue stragglers
- few known in the field but many in GCs
- $P < 0.2$ d
- $\Delta V < 1$ mag
- HADS ($\Delta V > 0.3$ mag)

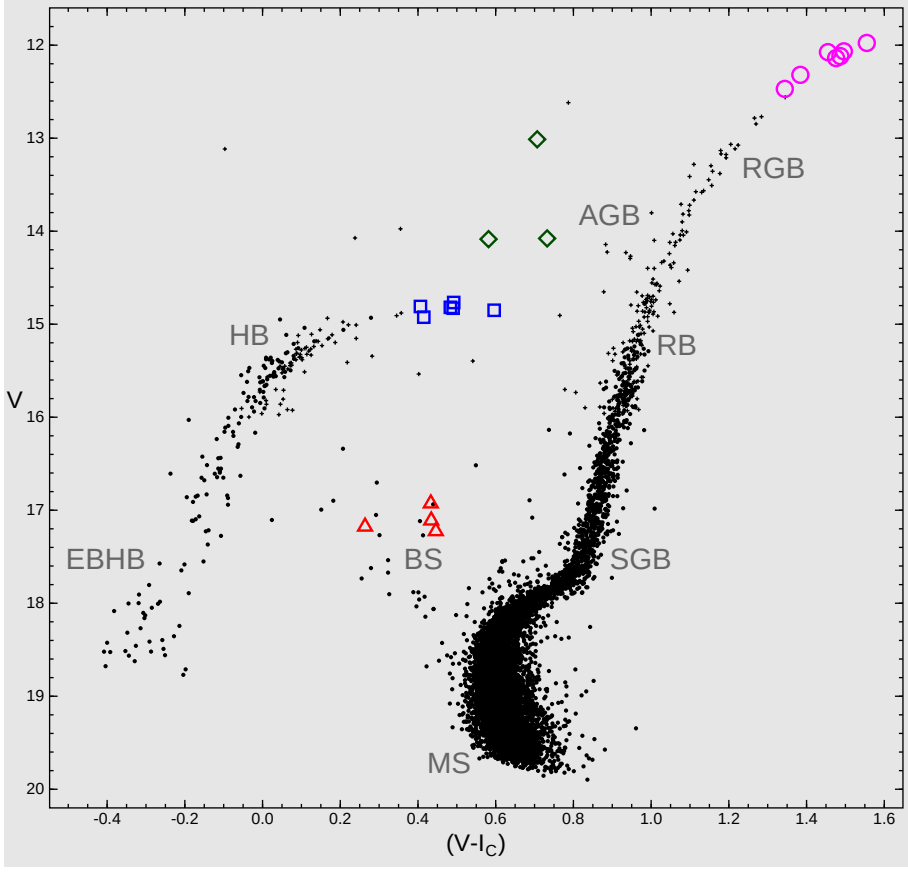

The colour – magnitude diagram for M 13 (Kopacki et al. 2003). SX Phoenicis stars are indicated with triangles, RR Lyrae variables with open squares, Population II Cepheids with diamonds, and variable red giants with circles.

PLM relations for Pop. II variables

- Nemec et al. (1994, AJ 108, 222)
  - 20 field and cluster SX Phe stars
  - assignment of pulsation modes based on the PL, PA, and PC diagrams
  - $M_{STC} = a_T + b_T \log P_{STC} + c[\mathrm{Fe/H}]_C$ where S stands for star, T, type of variability (including F and FO modes), and C, cluster
  - $(m - M)_{0,\mathrm{M15}} = 15.03$ mag
  - $M_V(F) = -2.56 \log P + 0.32[\mathrm{Fe/H}] + 0.36$

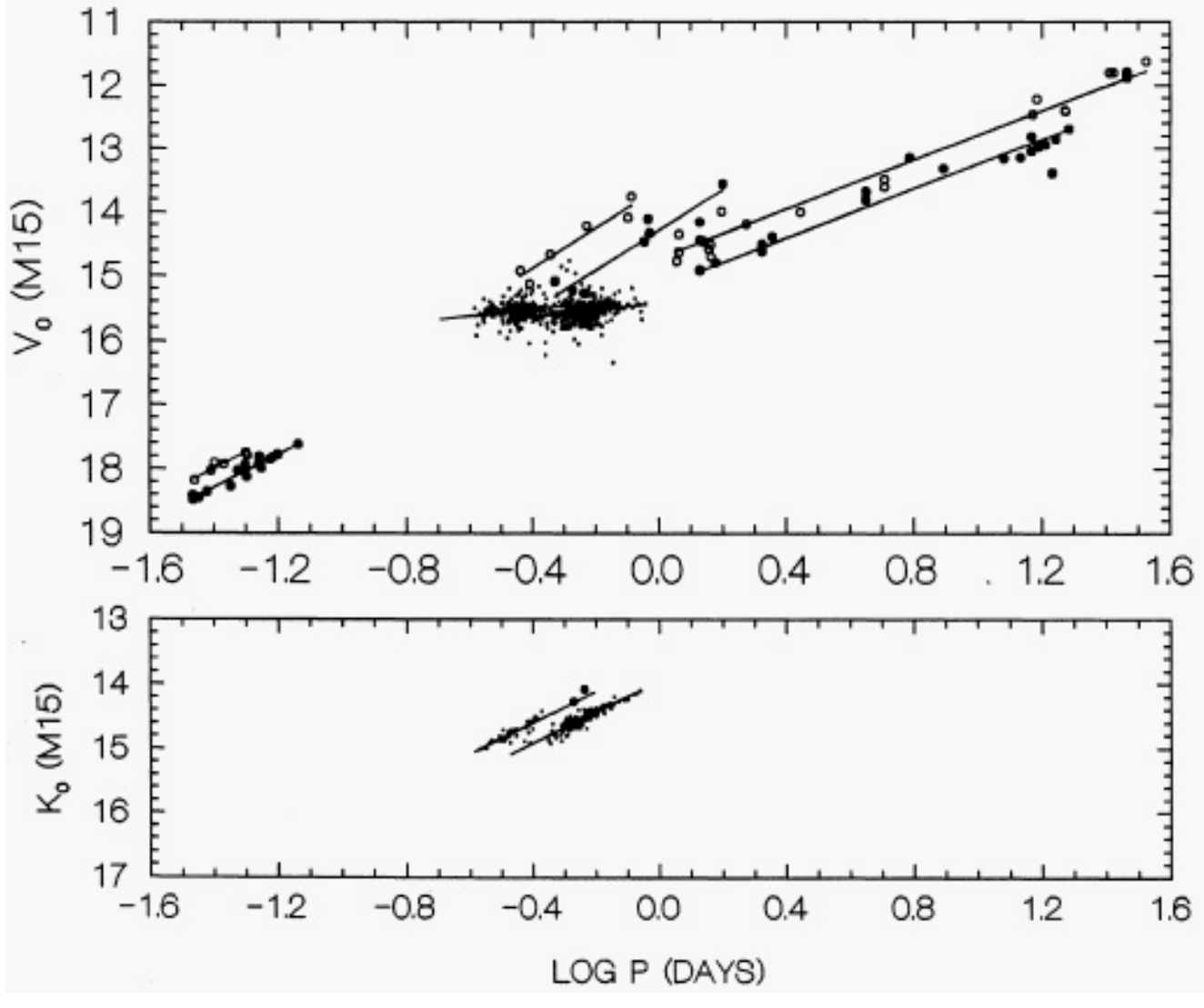

Period vs. adjusted-magnitude diagrams and fitted PL relations for SX Phe, RR Lyr, Pop. II and anomalous Cepheids and for V and K passbands. The magnitudes have been dereddened, normalized to the metallicity of M15, and shifted to the distance of M15. The slopes of the PL relations for the assumed F and FO modes for each kind of variable stars are parallel. Note that the slopes of the PL relations are different for various types of stars. Nemec et al. (1994, AJ 108, 222).

PL relation for SX Phoenicis stars

- McNamara (1995, AJ 109, 1751)
  - sample of field and GCs stars
  - data from McNamara (1992)
  - F pulsators have asymmetrical LCs and $\Delta V > 0.25$ mag
  - FO pulsators have symmetrical LCs and $\Delta V < 0.2$ mag
  - $P\sqrt{\varrho} = Q \;\Rightarrow M_{\rm bol} = f(P, \mu, T_{\rm eff}, Q)$
  - $T_{\rm eff}(P)$ and $\mu(P)$ from field SX Phe stars
  - $Q = -1.495 \quad M_{\rm bol} = M_V - 0.2$
  - $M_V(F) = -3.29 \log P - 1.38$
  - needs to be shifted by 0.22 mag to match observed PL relation

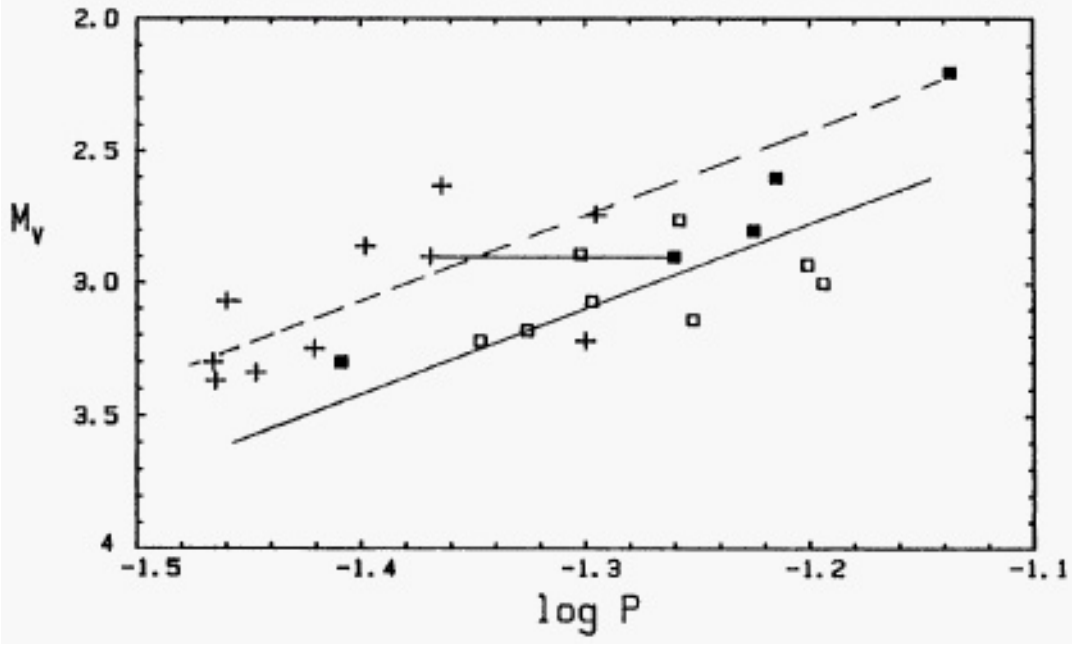

The PL relation of SX Phe variables. The open squares and crosses represent stars in GCs pulsating in F and FO mode, respectively; solid squares indicate field SX Phe stars. SX Phe star is a radial double-mode pulsator and is represented with two symbols connected with the horizontal line. The solid and dashed lines are PL relations derived from pulsation equation for F and FO pulsating stars, respectively. McNamara (1995).

PL relation for SX Phe and HADS stars

- McNamara (1997, PASP 109, 1221)
  - semiempirical PL relation for SX Phe and HADS stars
  - Strömgren $uvby\beta$ photometry
  - $T_{\rm eff}$ and P_0 are used with the pulsation equation and stellar models to derive $M_{\rm bol}$
  - $T_{\rm eff}$ from Kurucz (1994) models
  - $M_{\rm bol}$ from evolutionary tracks in the $\log T_{\rm eff}$ vs. $\log P_{\rm F}$ diagram
  - $M_V = -3.72 \log P - 1.99$
  - $\sigma = 0.1$ mag

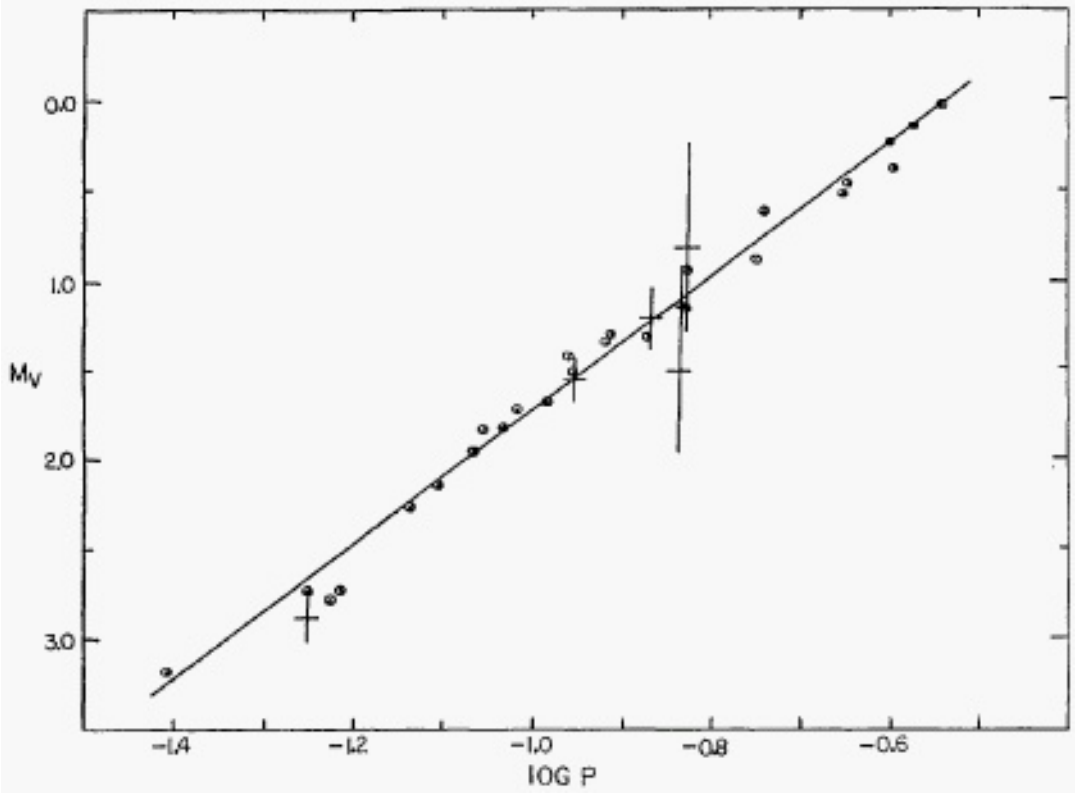

Semiempirical PL relation of SX Phe (short-period) and HADS (long-period) variables. The crosses are M_V values of several stars inferred from Hipparcos data. McNamara (1997).

Problems with mode identification in SX Phe stars

- no clear separation of F and FO pulsators in the Bailey diagram
- large amplitude indicates fundamental mode
- double-mode variables
  - F+FO ($P_{\rm FO}/P_{\rm F} = 0.77 - 0.79$)
  - FO+SO ($P_{\rm SO}/P_{\rm FO} = 0.81 - 0.83$)
  - F mode has the largest amplitude
- recent discovery of many SX Phe stars in BS population of GCs
  - multiperiodicity
  - very small amplitudes
  - non-radial modes

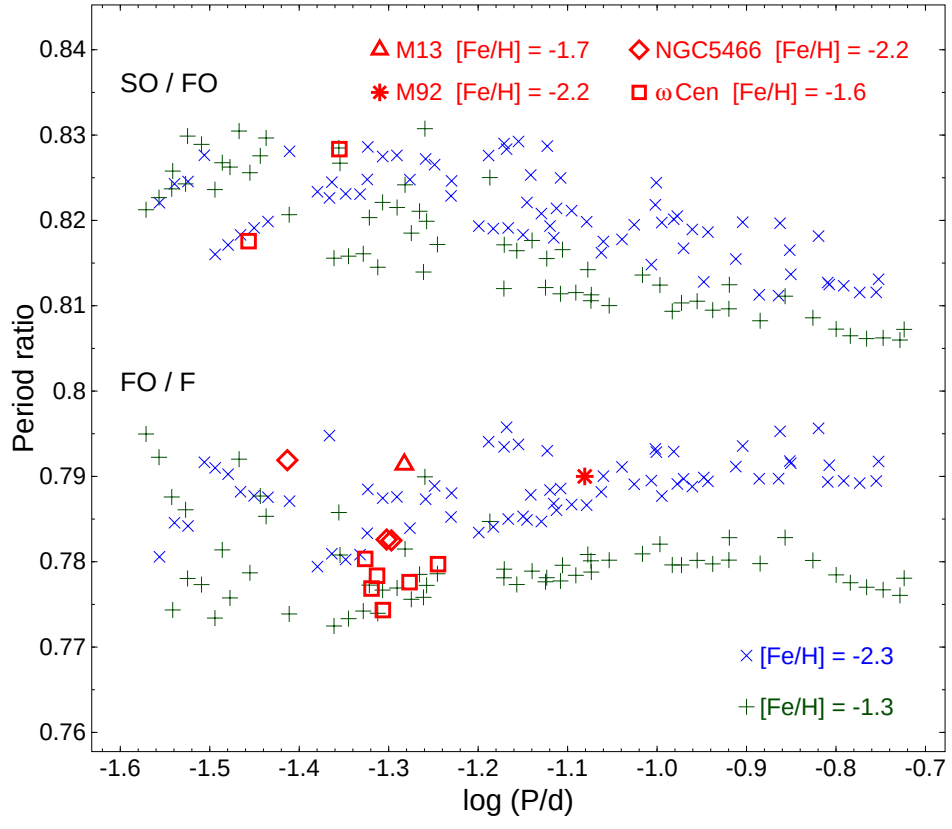

The period-period ratio diagram for the fundamental (F), first overtone (FO) and second overtone (SO) radial modes as a function of period of the fundamental mode. Theoretical period ratios given by Santolamazza et al. (2001) for metallicities [Fe/H] $= -1.3$ (pluses) and [Fe/H] $= -2.3$ (crosses) are shown for various model masses, luminosities and effective temperatures. Observed period ratios for radial double-mode SX Phoenicis stars in ω Cen (Olech et al. 2005; squares), NGC5466 (Jeon et al. 2004; diamonds), and M13 (Kopacki 2005; triangle) are also indicated. A possible period ratio for v34 in M92 is shown with asterisk.

Theoretical predictions for SX Phe stars

- Santolamazza et al. (2001, ApJ 554, 1124)
  - linear nonadiabatic radiative models
  - $Y = 0.24$; $Z = 10^{-4}, 10^{-3}$; $M/M_{\odot} = 1.0, 1.2, 1.4$; $\log L/L_{\odot} = 0.6{-}1.4$
  - dispersion of the PL relation is reduced by including colour and metallicity terms
  - $M_{\rm bol}(F) = -3.69 \log P - 11.17 \log T_{\rm eff} + 41.06 \quad (\sigma = 0.08$ mag)
  - $M_{\rm bol}(F) = -3.73 \log P - 11.37 \log T_{\rm eff} - 0.07 \log Z + 41.60 \quad (\sigma = 0.06$ mag)
  - comparison with observations (117 SX Phe stars from GGCs)
  - $M_V^{\rm BE}(F) = -3.05 \log P - 1.32$

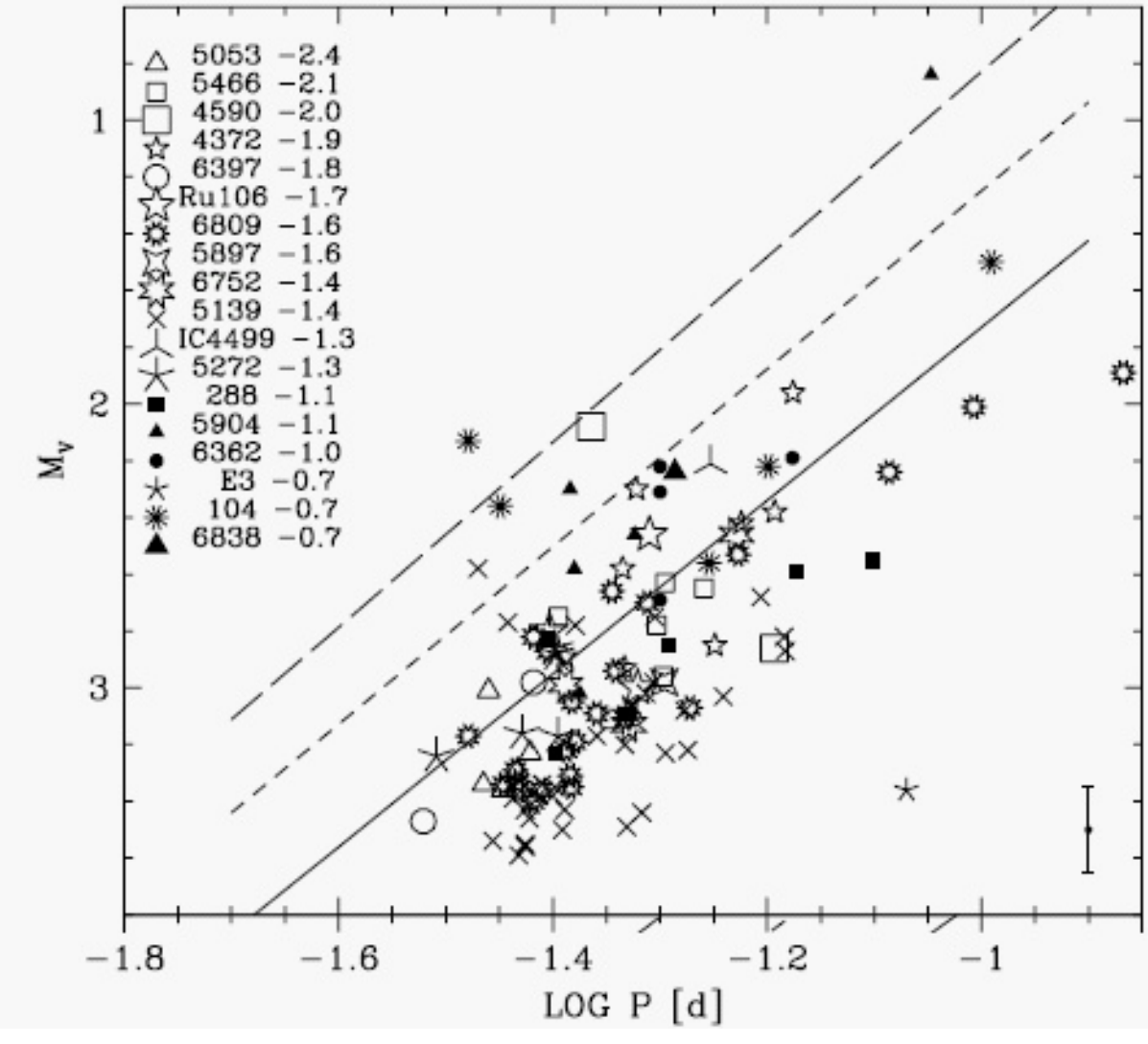

Comparison in the M_V – $\log P$ plane between predicted blue edges for the first three radial modes (solid line is for fundamental mode) and available data for SX Phe stars in GGCs. Santolamazza et al. (2001, ApJ 554, 1124).

SX Phe stars in NGC5466

- Jeon et al. (2004, AJ 128, 187)
- $(m-M)_V = 16$ mag ; $E(B-V) = 0$ mag (Harris 1996)
- $M_V(F) = -3.25 \log P - 1.30$
- $\sigma = 0.04$ mag

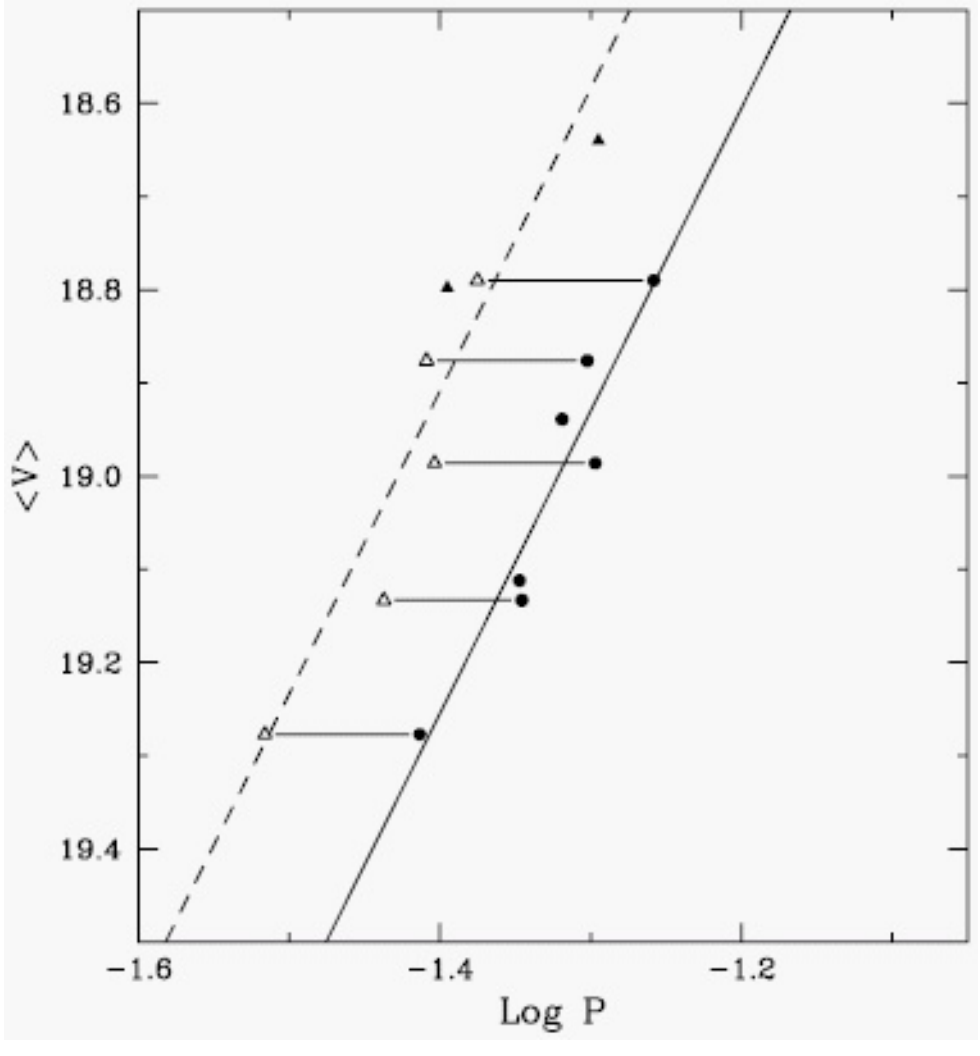

Diagram of $\log P$ vs. mean V magnitude showing fundamental (filled circles) and first-overtone (filled triangles) modes of SX Phe stars in NGC5466, and the first-overtone modes for five radial double-mode stars (open triangles). The solid line represents the PL relation for SX Phe stars pulsating in F mode, and the dashed line shows the same relation shifted by the period ratio $P_{\rm FO}/P_{\rm F} = 0.783$, representing the PL relation for FO pulsators. Jeon et al. (2004, AJ 128, 187).

SX Phe stars in NGC5053

- Arellano Ferro et al. (2010, MNRAS 402, 226)
- $M_V = -2.56 \log P + 0.32[\mathrm{Fe/H}] + 0.36$ from Nemec et al. (1994)

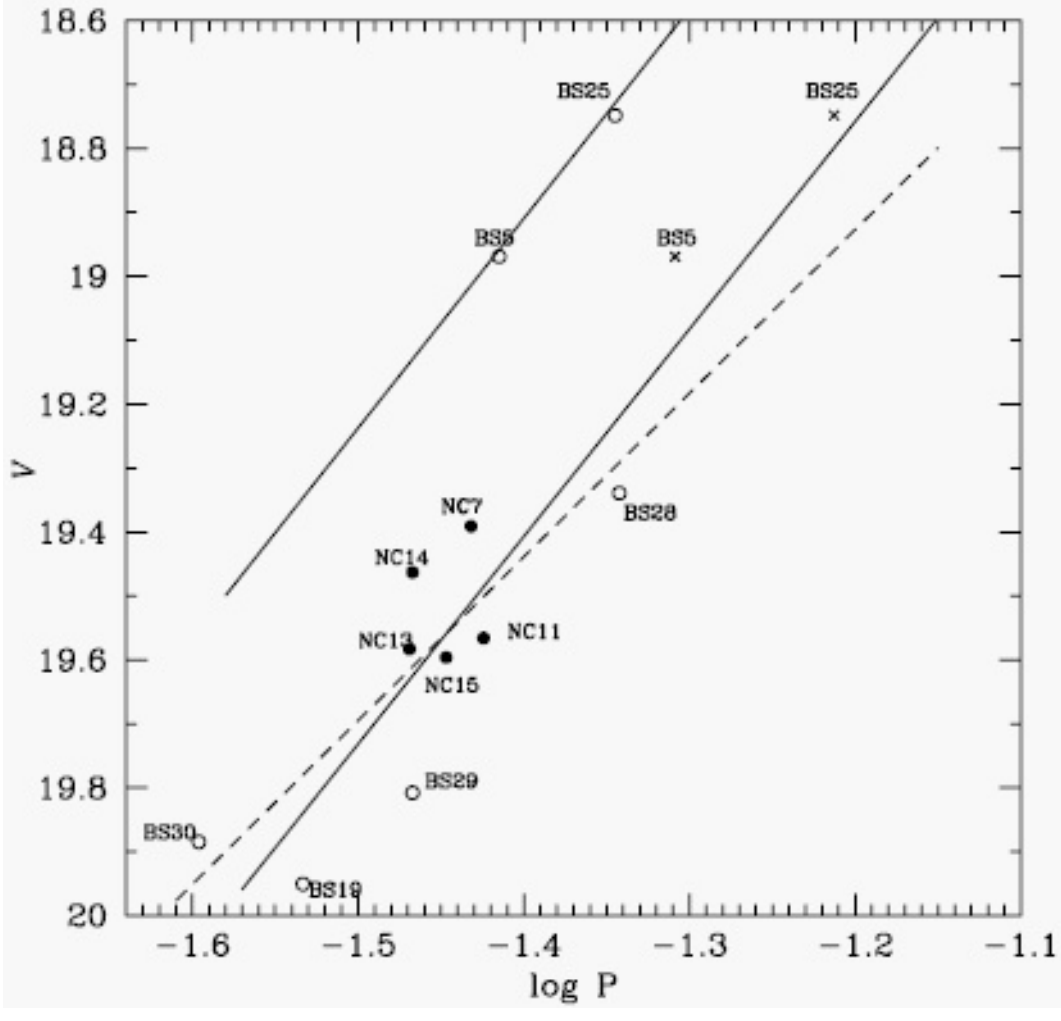

PL relation for SX Phe stars in NGC5053. Filled and open circles represent known and new SX Phe stars, respectively. Two symbols are shown for BS5 and BS25 for F (circles) and FO (crosses) periods. The two solid lines correspond to the F and FO relations of Jeon et al. (2004) and the dashed line shows the relation of Nemec et al. (1994). Arellano Ferro et al. (2010, MNRAS 402, 226).

Database of SX Phoenicis stars in GGCs

- P, $\langle V \rangle$, ΔV for SX Phe stars
- Catalogue of SX Phe Stars in GCs by Rodríguez and López-González (2000, AAp 359, 597)
  - 122 stars in 18 GGCs
- CVSGC by Clement et al. (2001, AJ 122, 2587)
  - revised version of 2010 but not complete
- search in literature
- ***232 SX Phe stars in 29 GGCs***
- ***15 stars with two radial modes***
- [Fe/H], $(m - M)_V$ for GCs
- Catalogue of Parameters for MW GCs by Harris (1996, AJ 112, 1487)
  - electronic version of December 2010
- $(m - M)_V$ from
  HB (or RR Lyrae) V-magnitude ($V_{\rm HB}$) and M_V(HB) calibration of Gratton et al. (2003, AAp 408, 529)
  - $M_V(\mathrm{HB}) = 0.22[\mathrm{Fe/H}] + 0.89$ (MS fitting)

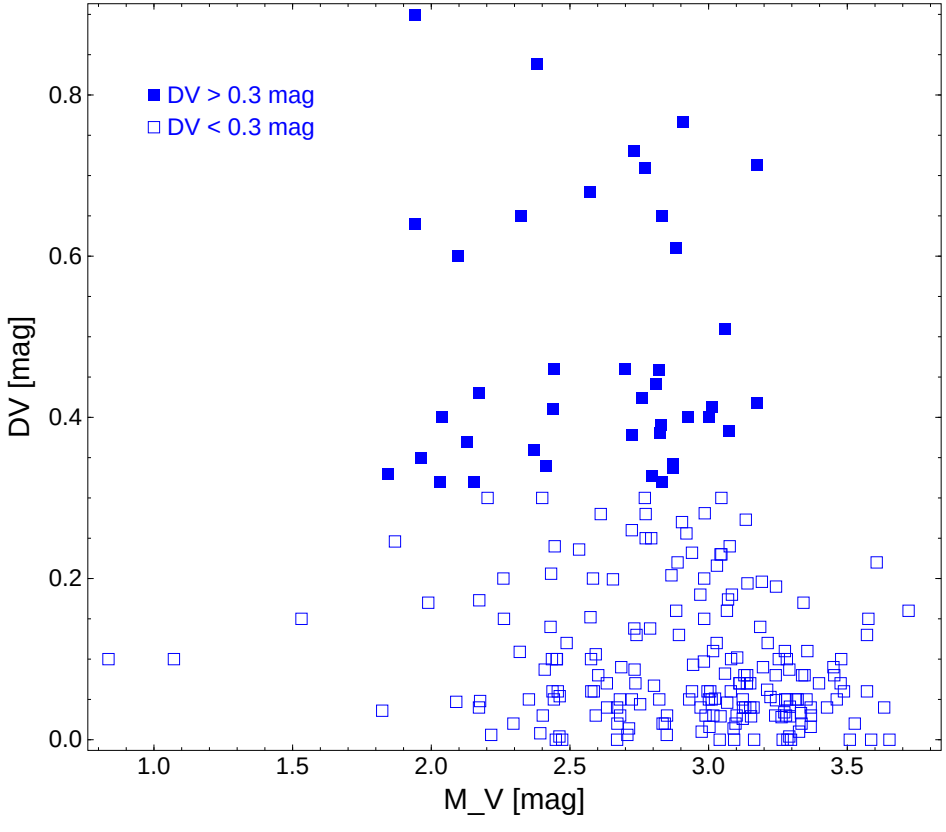

V-filter range of variability ΔV vs. derived absolute magnitude M_V for analyzed SX Phoenicis stars. Stars with $\Delta V > 0.3$ mag are indicated with filled squares.

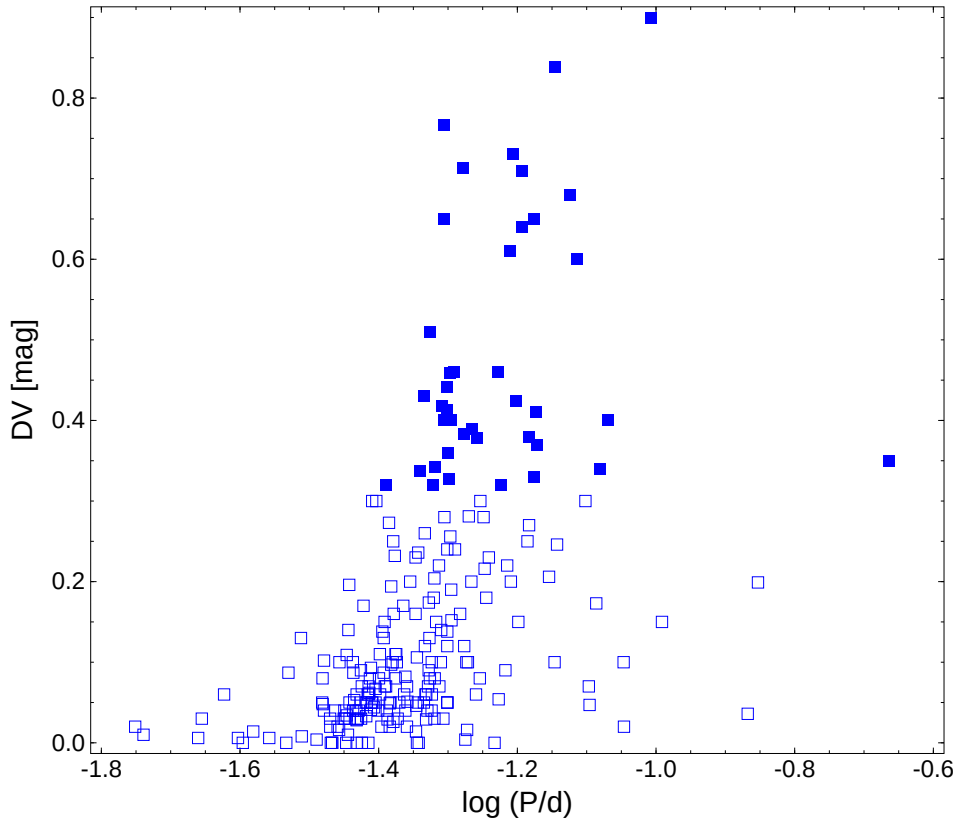

V-filter range of variability ΔV vs. $\log P$ for analyzed SX Phoenicis stars. Stars with $\Delta V > 0.3$ mag are indicated with filled squares.

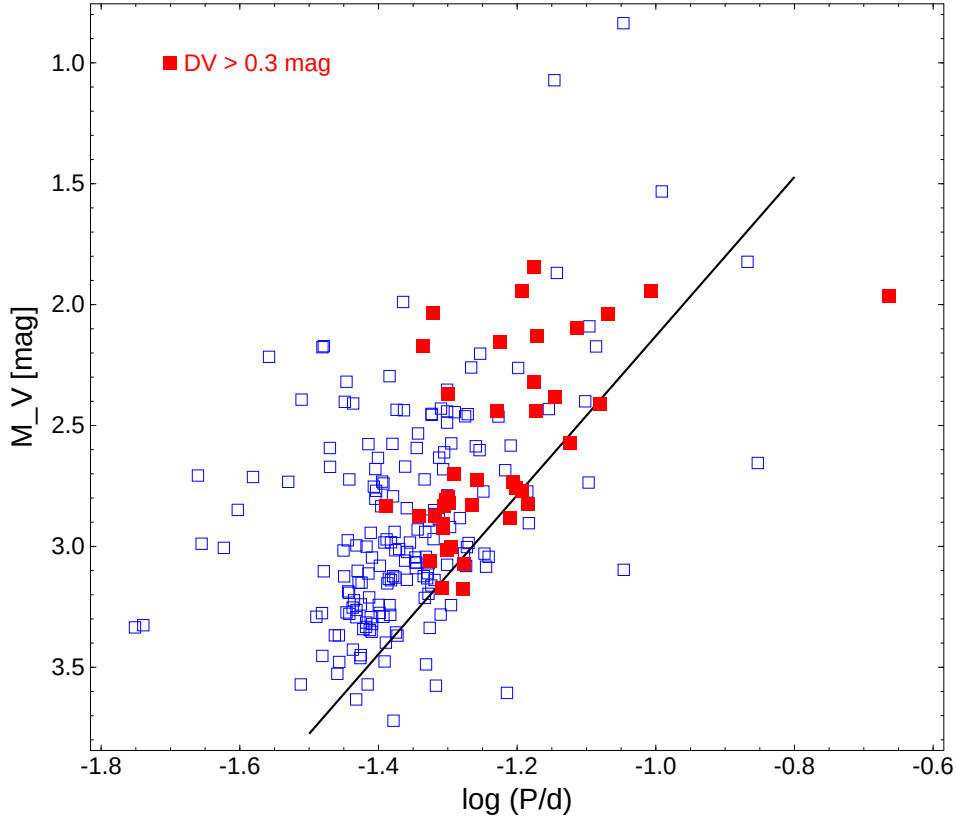

The period – luminosity diagram for analyzed SX Phoenicis stars. Stars with $\Delta V > 0.3$ mag are indicated with filled squares. The solid line shows PL relation for fundamental mode taken from McNamara (1995).

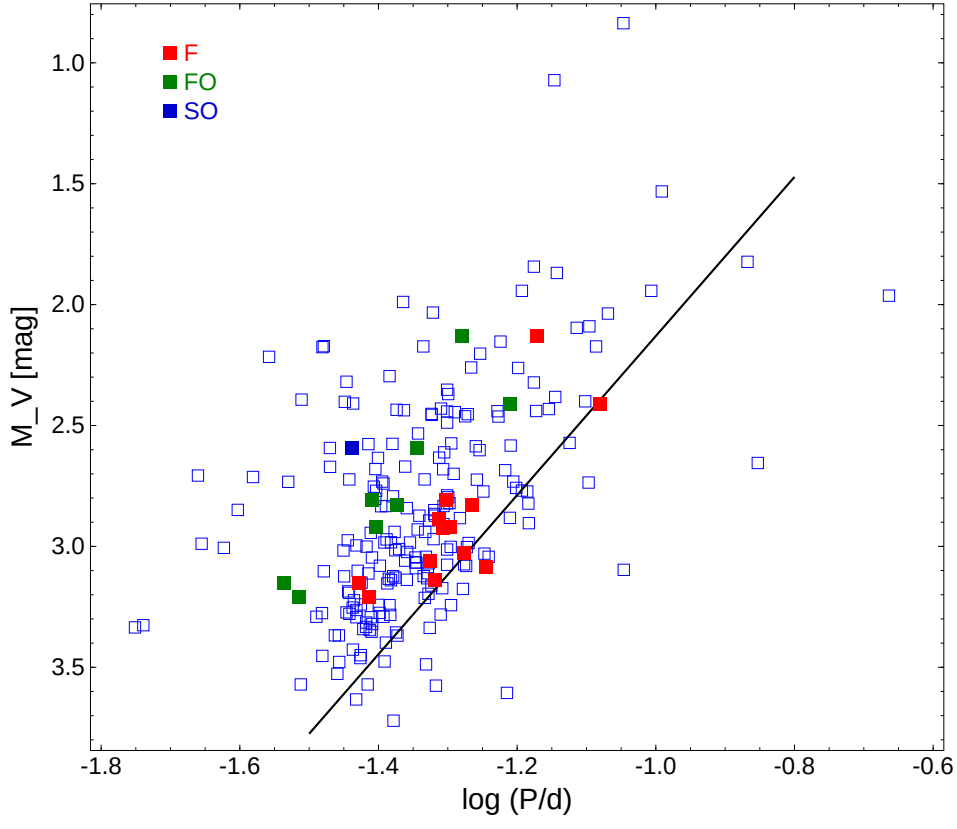

The period – luminosity diagram for analyzed SX Phoenicis stars. Double radial-mode stars are indicated with filled squares. The solid line shows PL relation for fundamental mode taken from McNamara (1995).

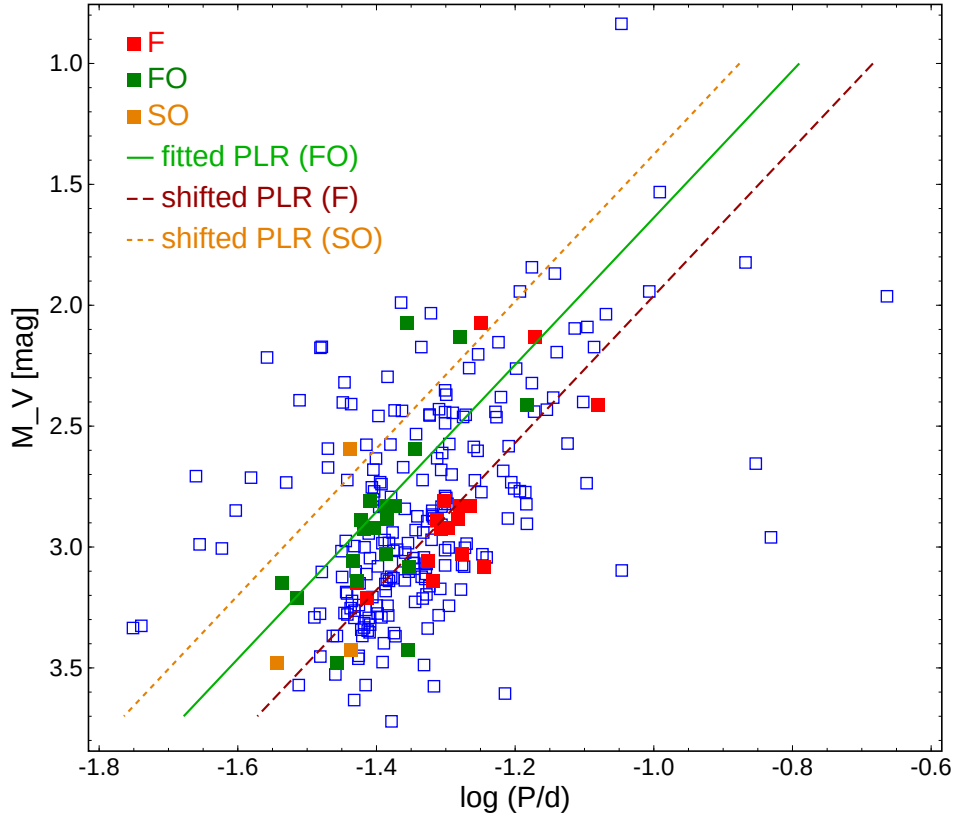

The period – luminosity diagram for analyzed SX Phoenicis stars. Double radial-mode stars are indicated with filled symbols. The solid line shows PL relation (PLR) for the first overtone (FO) mode obtained from the linear fit for the observed F/FO and FO/SO stars excluding two faintest stars (FO/SO pulsators from ω Cen), which seem to be too faint for their periods.

Summary

- observed (P)L(M) relations for a given class of pulsating stars are in agreement with each other; slopes are very similiar, only zero-points can differ
- theoretical predictions are mostly in agreement with observed relations
- beside RR Lyrae stars, also other types of Population II variables are gaining more attention in application to distance determination
- IR spectral range holds several advantages over optical range

Multiple stellar populations of ω Cen

ω Cen

- the most massive and luminous GGC
  - $M \approx 3 - 7 \times 10^6\ M_\odot$ ($\approx 0.8 M_{\rm dSph} \approx 10 M_{\rm GGC}$)
- elliptical shape (rotational)
- differential rotation
  - $v_{\rm rot}^{\rm max} \approx 8$ km/s, $v_{\rm rot}/v_{\rm rand} \approx 0.4$, $i \approx 45^\circ$
- large metallicity spread, $-2.2 <$ [Fe/H] < -0.6
- large population of variable stars
  - 180 RR Lyr, 70 SX Phe, 10 Cep, 60 EB
  - large number of Blazhko stars
  - overluminous RR Lyrae stars
- two populations of RR Lyr stars, both OoI and OoII

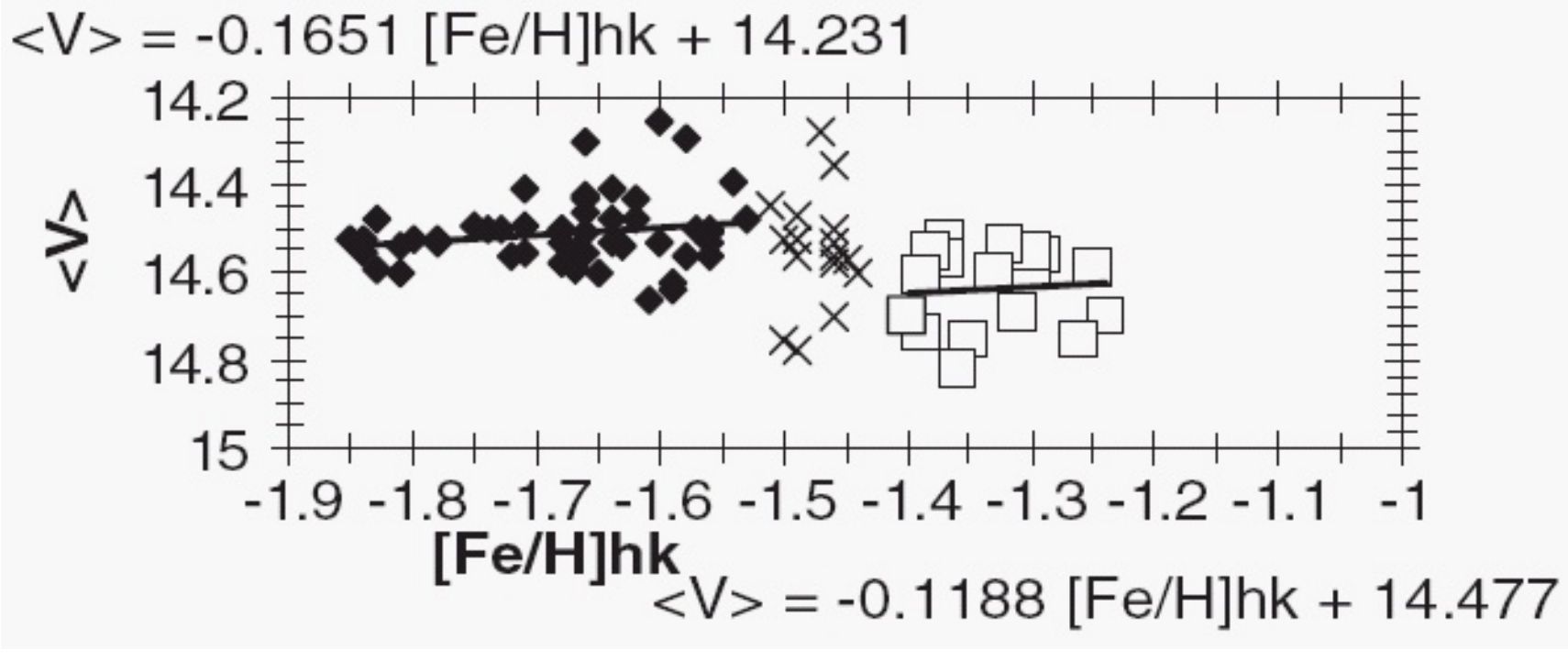

Mean V magnitudes of RR Lyrae stars in ω Cen vs. $[\mathrm{Fe/H}]_{\mathrm{hk}}$. Note the systematic difference between variables with $[\mathrm{Fe/H}]_{\mathrm{hk}} < -1.5$ and $[\mathrm{Fe/H}]_{\mathrm{hk}} > -1.5$. The equation in the upper left is a linear regression solution to the data points plotted as solid diamonds and the equation in the lower right to data points plotted as open squares. The x's are stars in the transition region that were not included in either of the two solutions. McNamara (2011, AJ 142, 110).

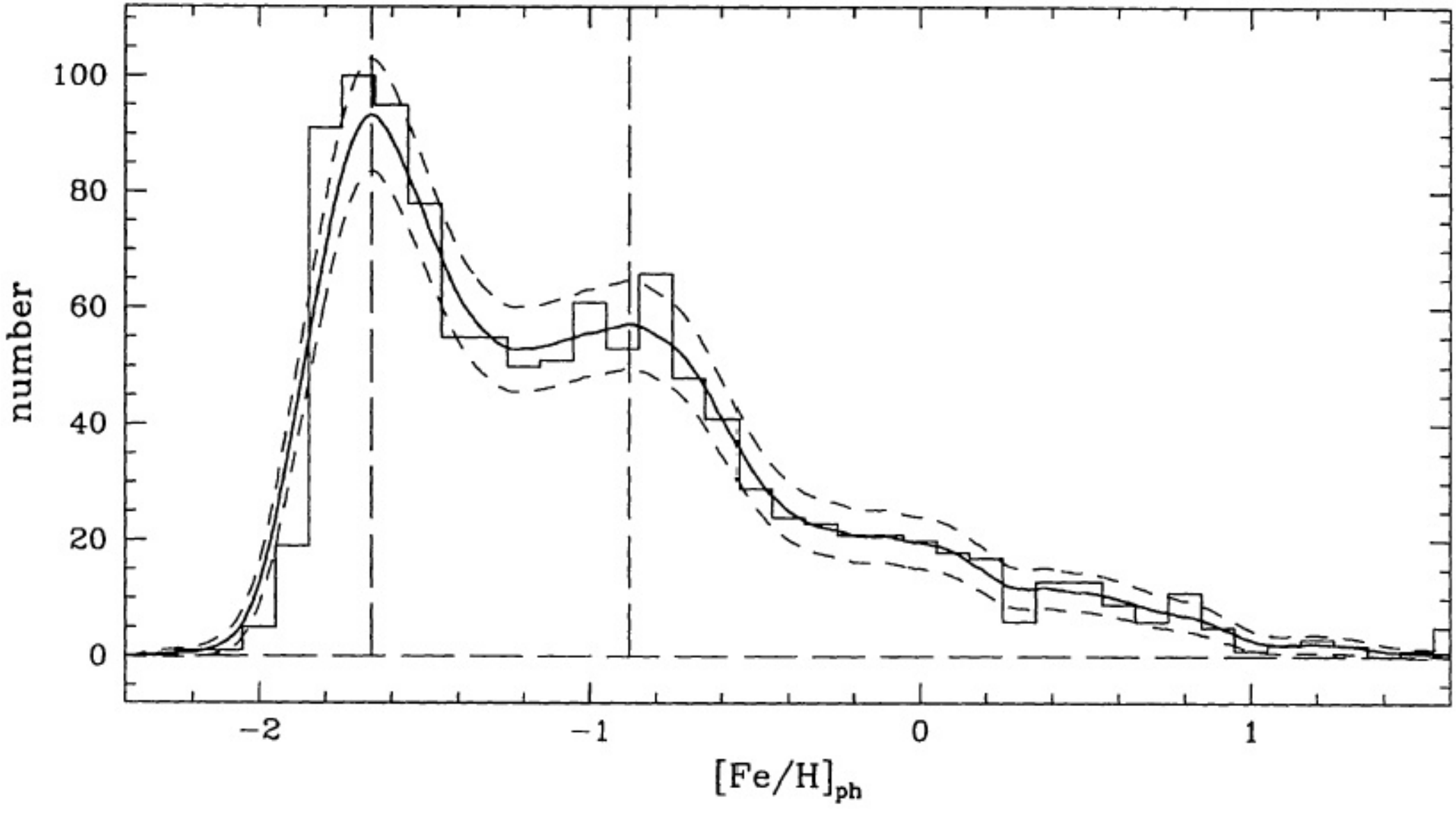
number
100
80
60
40
20
0
−2
−1
0
1
[Fe/H]ph

Stellar populations in the CMD: RGB/SGB

- unusually broad RGB, photometric errors
  - Dickens and Woolley (1967, ROB 128)
- wide RGB due to metallicity spread
  - Cannon and Stobie (1973, MNRAS 162, 207)
- several RGB populations
  - Lee et al. (1999, N 402, 55), Pancino et al. (2000, ApJ 534, L83)
- populations of the SGB and TOPS
- three main populations of the RGB/SGB
  - Hilker et al. (2004, AAp 422, L9)
  - MPP, $-2.0 <$ [Fe/H] < -1.5, 70 %
  - IMP, $3 \times$ MINT, $-1.5 <$ [Fe/H] < -0.9, 25 %
  - MRP, RGB-a, $-0.9 <$ [Fe/H] < -0.6, 5 %
- metal-rich ([Fe/H] > -1.4) RGB stars are more concentrated than the dominant metal-poor population

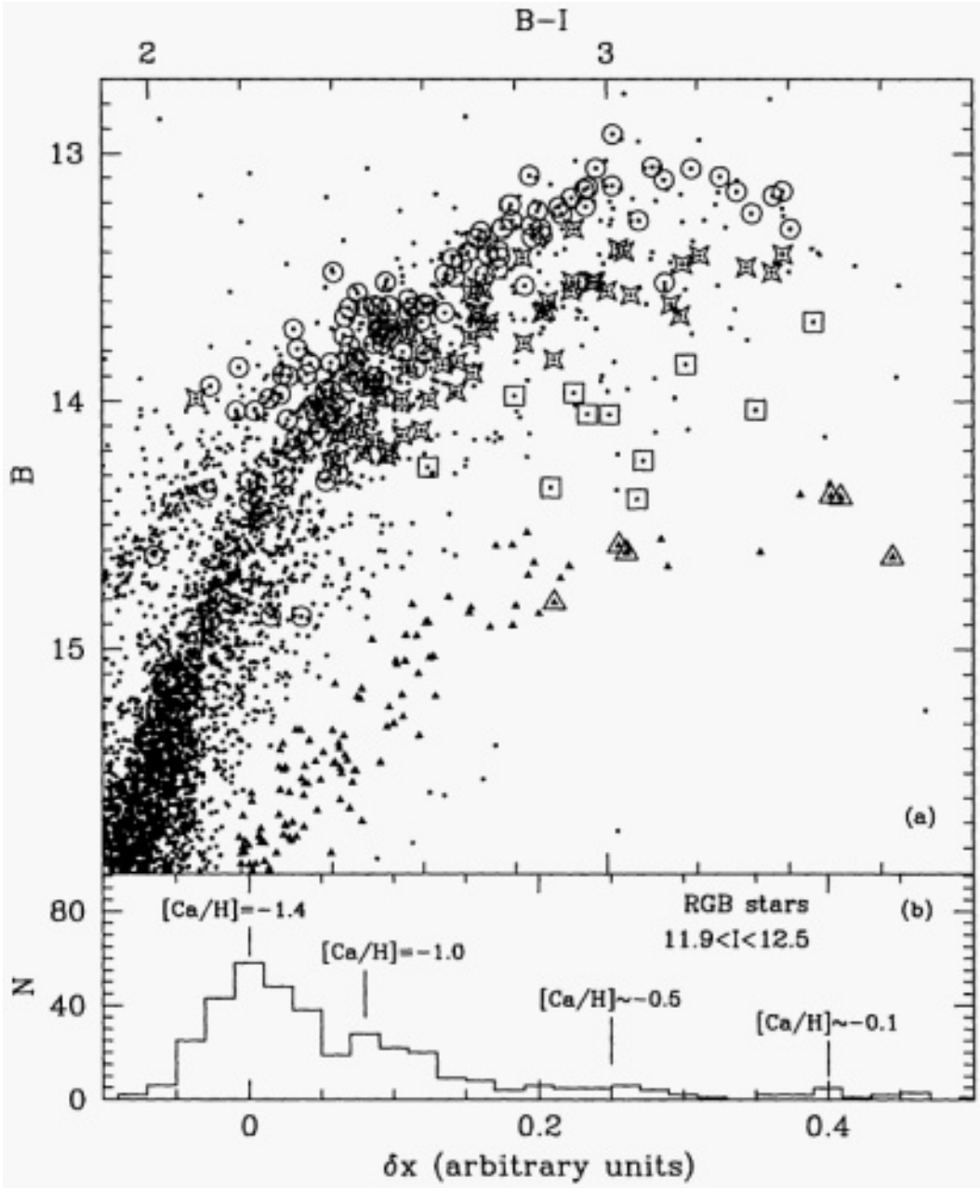

Pancino (2002, ASPC 265, 31)

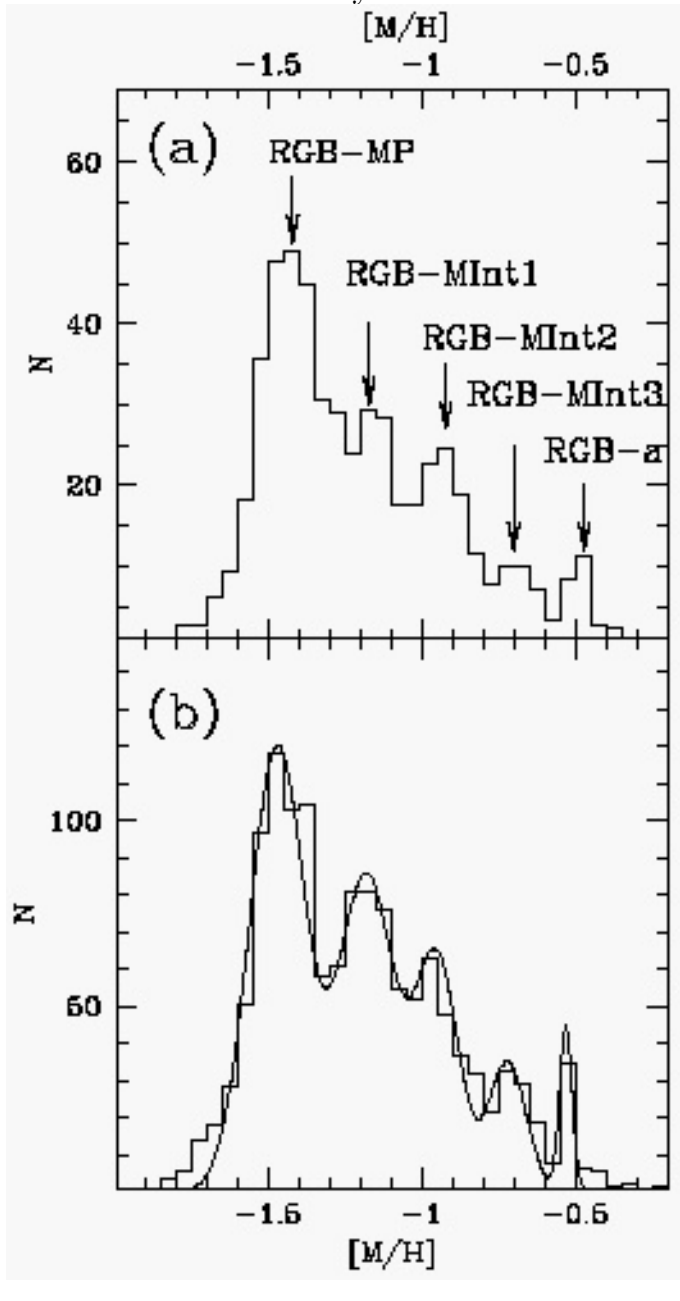

Sollima et al. (2005, MNRAS 357, 265)

Top panel: Zoomed CMD of the upper RGB region. Stars in the RBG-a have been plotted as small filled triangles. Large empty symbols show the position in the CMD for stars with known metallicity. Different symbols refer to stars with different metallicities: large open circles for stars with $-1.5 <$ [Ca/H] < -1.3, large open stars for $-1.1 <$ [Ca/H] < -0.85, large open squares for $-0.65 <$ [Ca/H] < -0.4, large open triangles for [Ca/H] > -0.3, respectively. Bottom panel: Histogram of the distribution of the distances from the mean ridge line of the dominant, metal-poor RGB. The mean [Ca/H] abundances for the four main components of the RGB are also marked. Pancino (2002, ASPC 265, 31)

The derived MDF for a sample of RGB stars from ω Cen. The significant peaks of the distribution are indicated in (a) and interpolated with a multiburst enrichment model (b). Sollima et al. (2005, MNRAS 357, 265)

Table 2. Relative frequency of the main populations of ω Cen.

	[M/H]	per cent
RGB-MP	−1.4	42 ± 8
RGB-MInt1	−1.2	28 ± 6
RGB-MInt2	−0.9	17 ± 5
RGB-MInt3	−0.7	8 ± 3
RGB-a	−0.5	5 ± 1

Sollima et-al. (2005, MNRAS 357, 265)

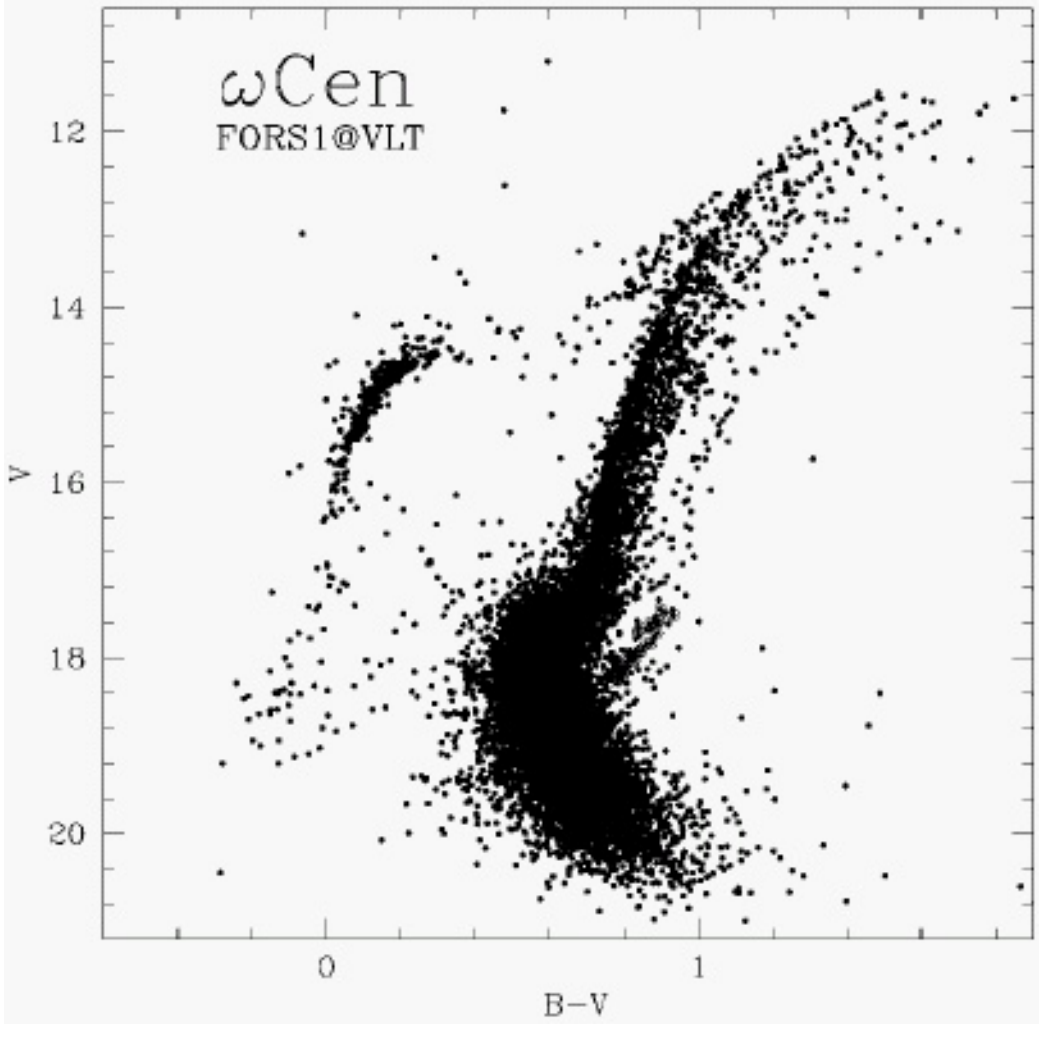

$(V,B-V)$ CMD for stars identified in the nine fields observed with FORS1 at the ESO/VLT. About 14,000 stars with the lowest photometric error have been plotted. The SGB-a population, merging into the cluster MS, is clearly visible. Stars marked with large open circles are identified as SGB-a stars in both the FORS1 and the ACS catalogs. Ferraro et al. (2004, ApJ 603, 81)

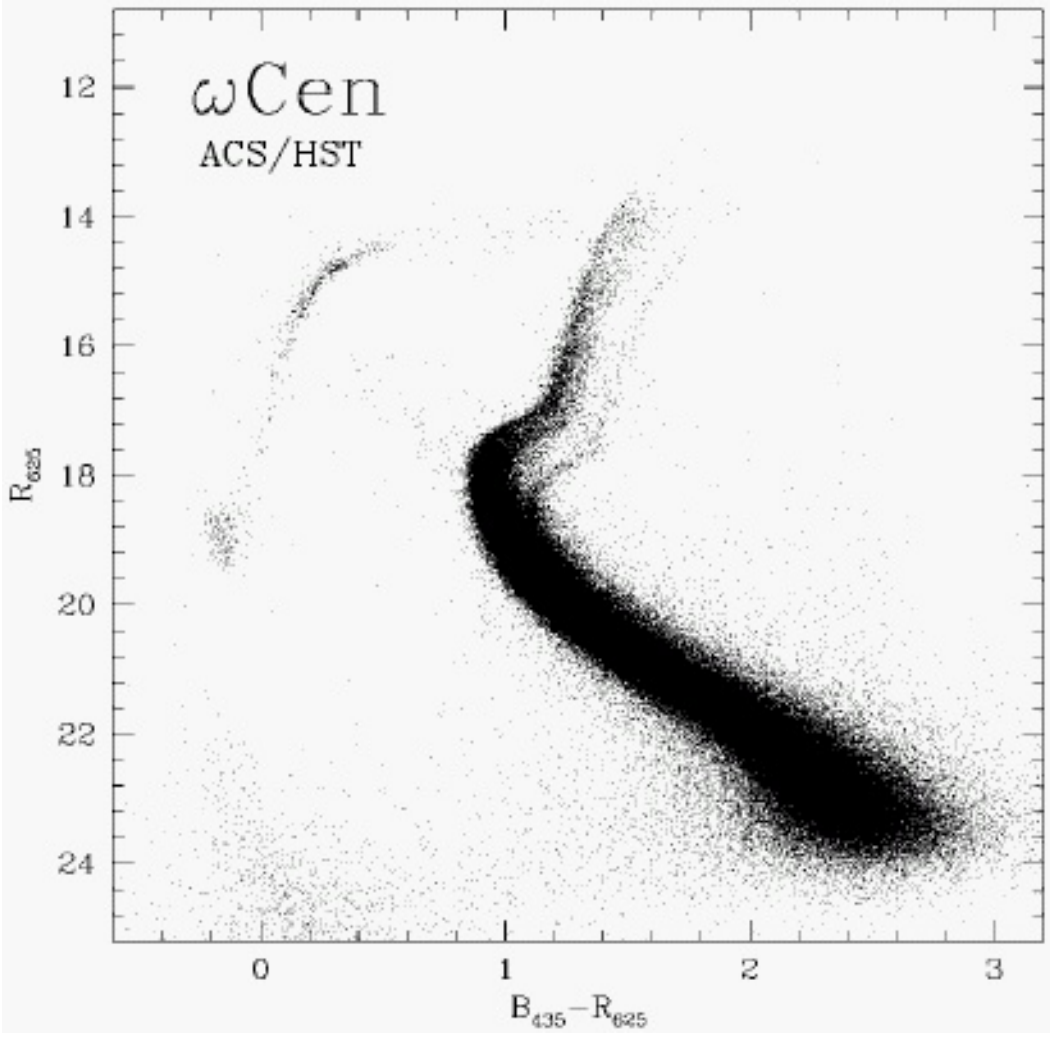

$(R_{625}, B_{435} - R_{625})$ CMD for more than 400,000 stars identified in the nine ACS fields. The SGB-a is clearly visible, along with the complex substructures of the TO-SGB region of ω Cen. Ferraro et al. (2004, ApJ 603, 81)

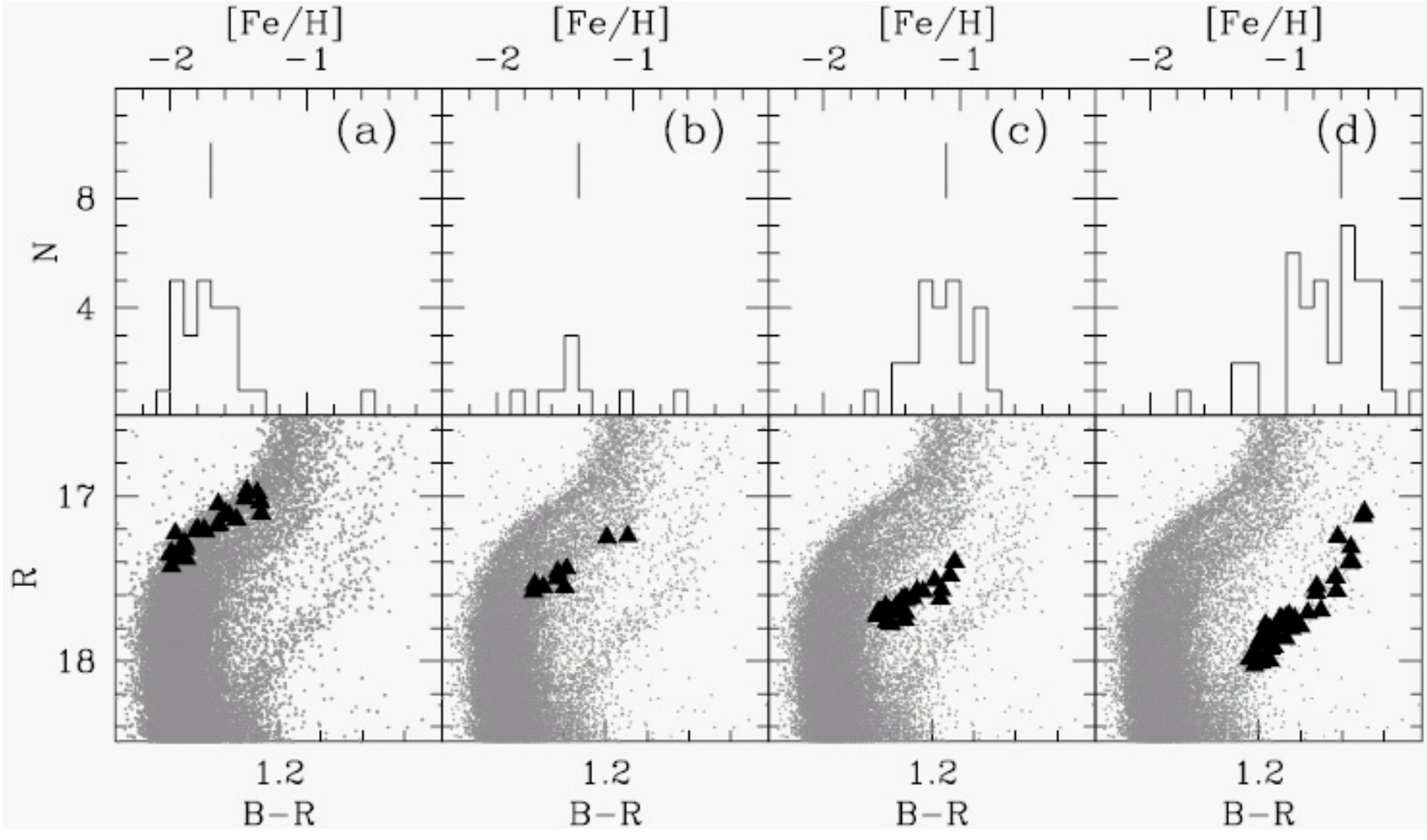

Metallicity distributions for the four groups of stars selected in ω Cen sample (top panels). The peak metallicity of each group is indicated. The positions of the selected stars are marked on the ACS CMD in the corresponding bottom panels.

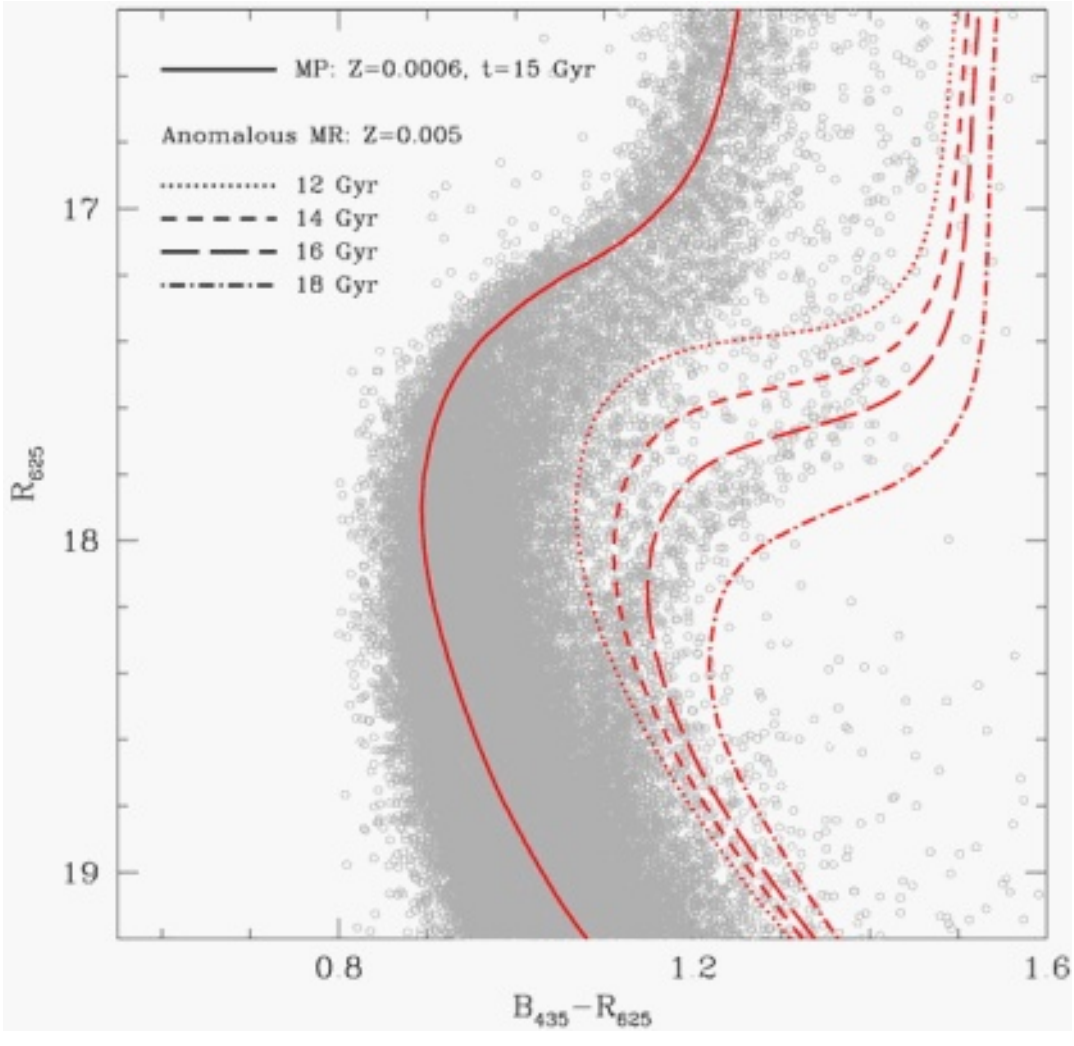

Zoomed (R_{625}, $B_{435} - R_{625}$) CMD of the TO region. Two isochrone sets are overplotted. The metal-poor dominant population is well reproduced by a $Z = 0.0006$ ([M/H] = [(Fe+α)/H] = -1.5) isochrone of 15 Gyr (heavy solid line). A set of $Z = 0.005$ ([M/H] = -0.6) isochrones in the $12 - 18$ Gyr age range is also shown. While the metal-poor population is well reproduced, the observed morphology of the anomalous SGB/TO is not correctly reproduced by any $Z = 0.005$ isochrone, regardless of age. Although the MS-TO level of the anomalous population appears consistent with an age of 17 Gyr (i.e., $\Delta\tau = 2$ Gyr older than the metal-poor component), the TO color is significantly bluer than the corresponding isochrone. Ferraro et al. (2004, ApJ 603, 81)

Stellar populations in the CMD: MS

- MS splitting
  - Anderson (2002, ASPC 265, 87)
- two populations of the MSS
  - Sollima et al. (2007, ApJ 654, 915)
  - rMS, [Fe/H]≈ -1.6, 75 %
  - bMS, [Fe/H]≈ -1.3, 25 %
- bMS has larger metallicity than rMS
- bMS stars are more concentrated toward the cluster center than rMS stars

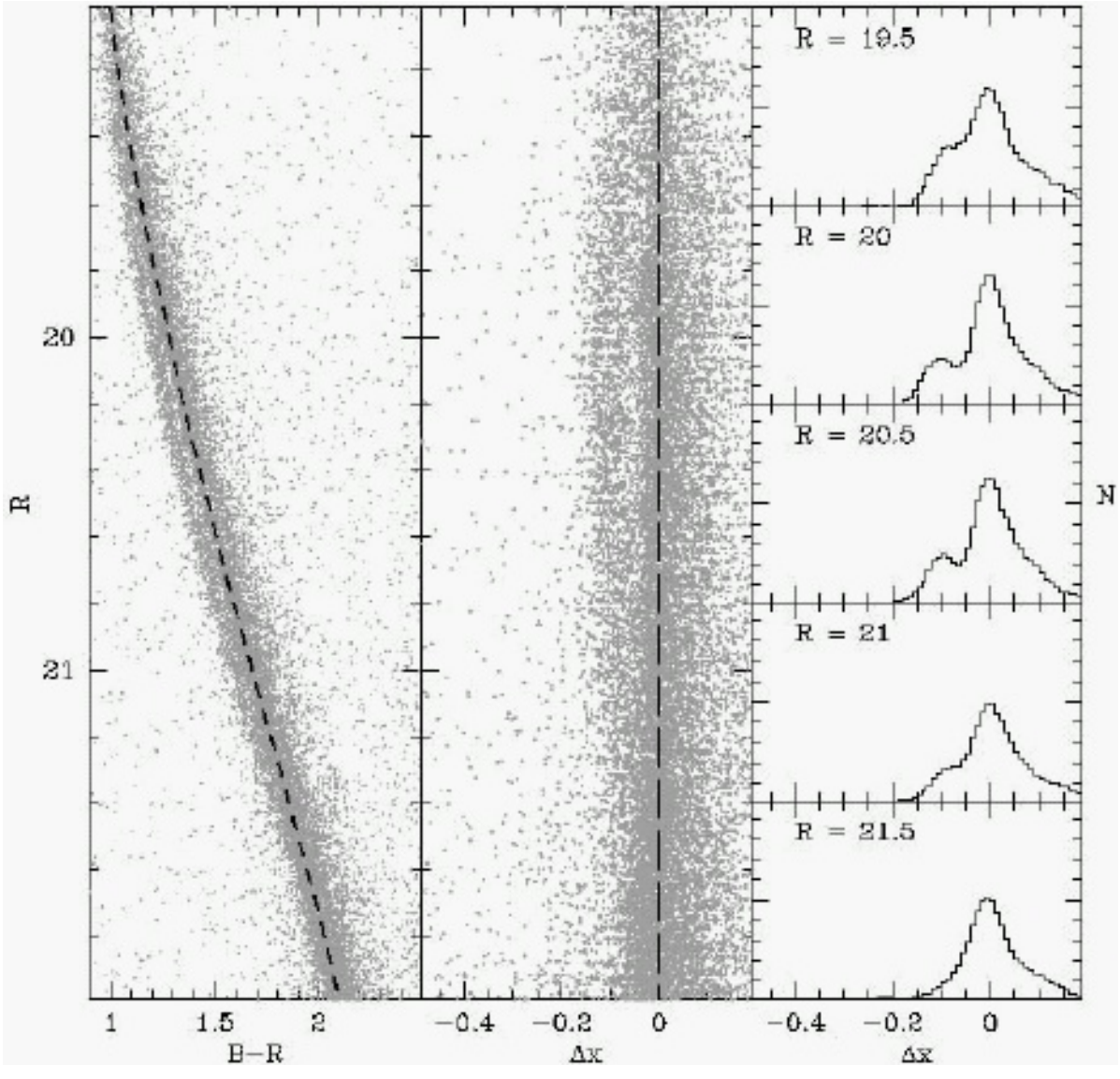

Zoomed (R,$B-R$) CMD of ω Cen in the bMS region (left panel). The mean ridgeline of the rMS population is overplotted to the CMD as a dashed line. The distribution of MS stars with respect to the reference mean ridgeline is shown in the middle panel. In the right panel the histograms of the distances from the mean ridgeline at different magnitude levels are shown. Sollima et al. (2007, ApJ 654, 915)

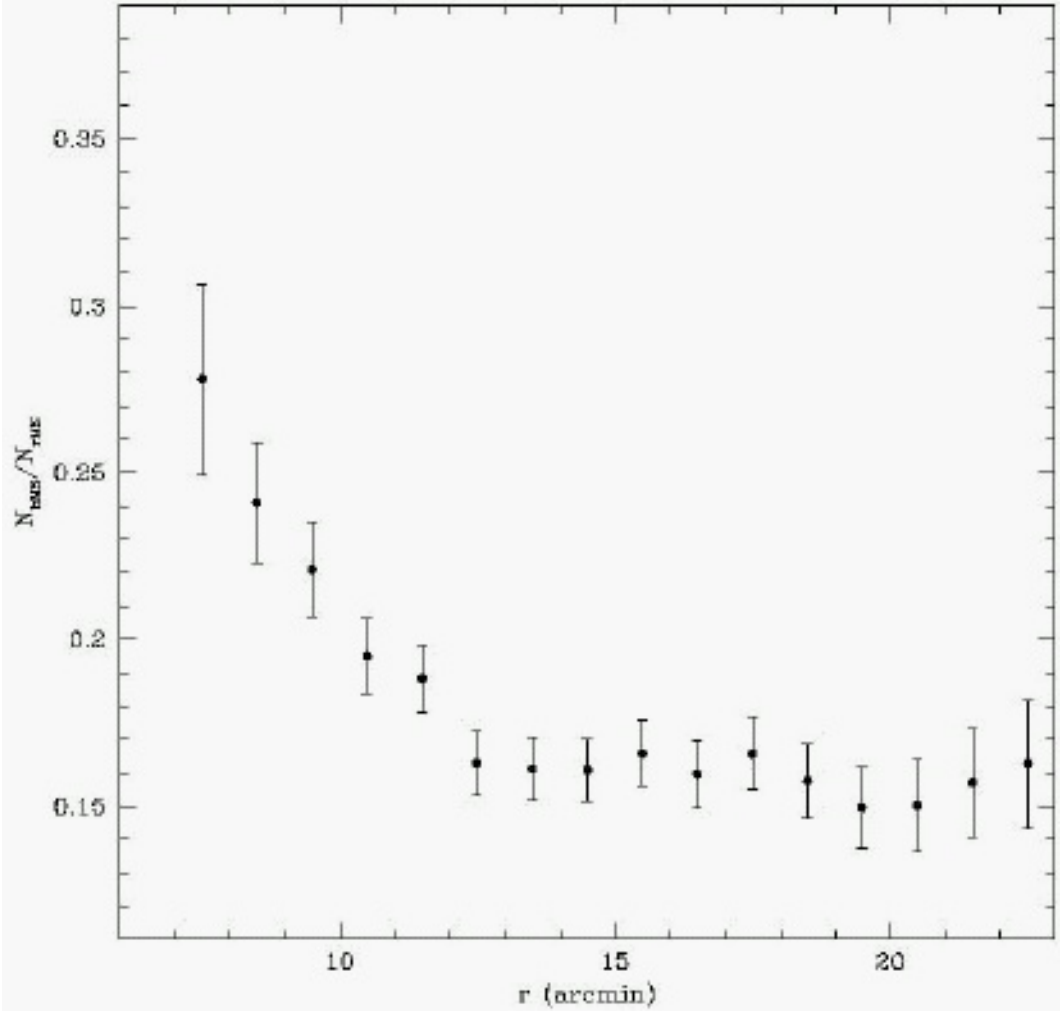

Corrected for contamination effects ratio between the number of bMS and rMS stars at different distances from the cluster center. Sollima et al. (2007, ApJ 654, 915)

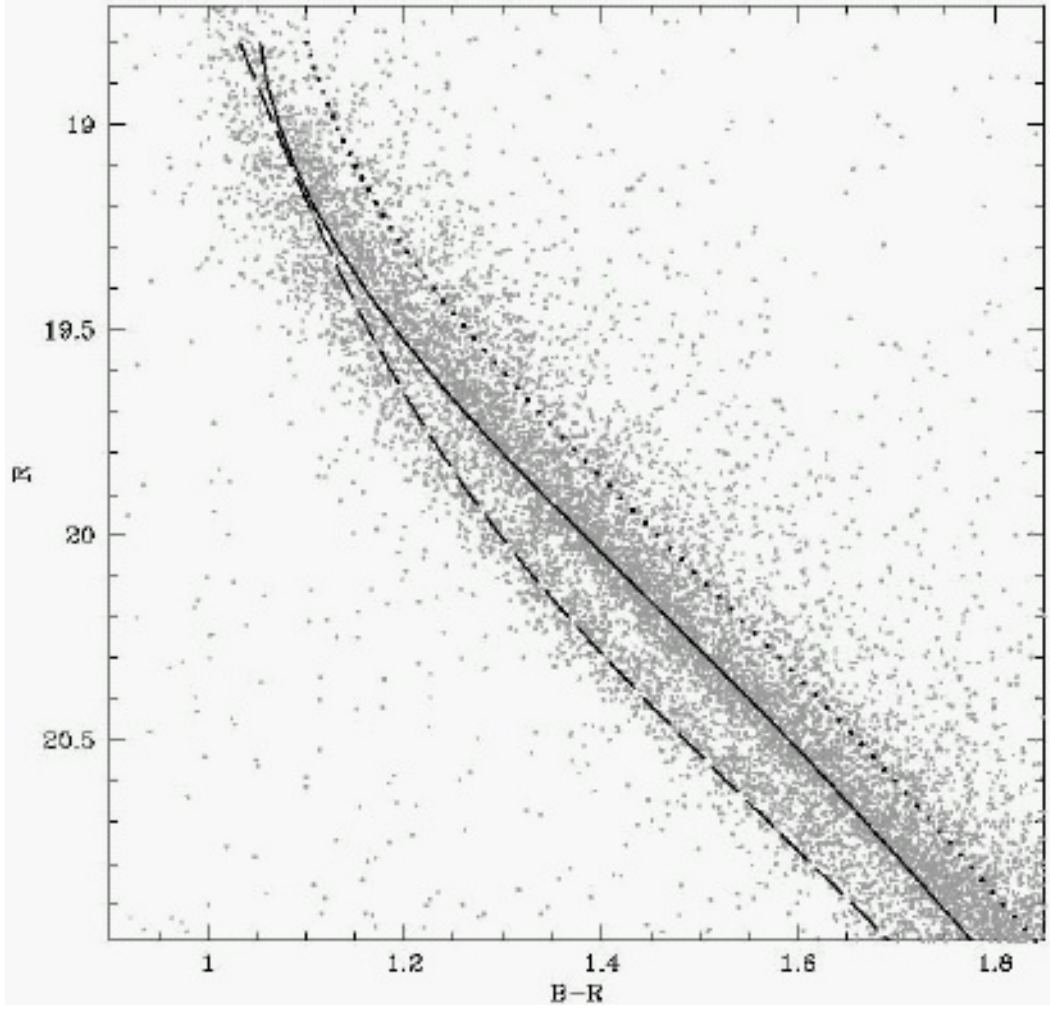

Isochrone fitting of the MS populations of ω Cen. Theoretical isochrones with appropriate metallicity and helium abundance ([Fe/H] $= -1.6$ and $Y = 0.246$, solid line; [Fe/H] $= -1.3$ and $Y = 0.246$, dotted line; $Y = 0.40$, dashed line) are overplotted. Sollima et al. (2007, ApJ 654, 915)

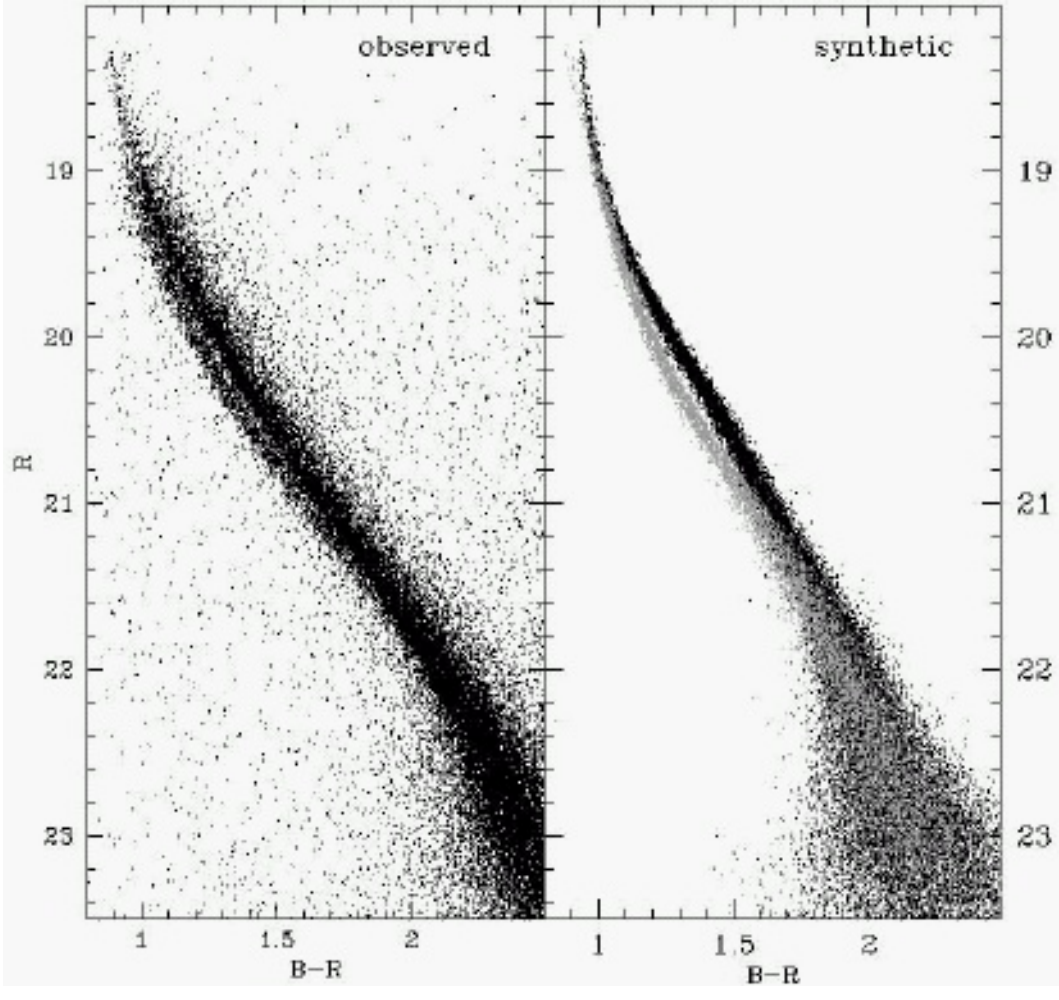

Comparison between the observed (R,$B-R$) CMD of ω Cen (left) with a synthetic CMD (right). Black points simulate stars with [Fe/H] $= -1.6$ and $Y = 0.246$, gray points simulate stars with [Fe/H] $= -1.3$ and $Y = 0.40$. Sollima et al. (2007, ApJ 654, 915)

Helium overabundance

- bMS has larger metallicity than rMS
- significant helium overabundance ($\Delta Y > 0.1$) can explain the observed bMS morphology
- no known chemical enrichment mechanism is able to produce the huge amount of helium required to reproduce the observed MS morphology without drastically increasing the metal abundance
- pure self-enrichment scenario may not be the best description of the evolution of ω Cen
- bMS population could have formed in a different environment, thus not partaking in the chemical enrichment process of ω Cen (external sources)
- part of the helium-enriched stars could form from gas ejected by field stellar populations surrounding ω Cen when it was the nucleus of an ancient dwarf galaxy and later fell into the central region of the system.
- EBHB

Stellar populations in the CMD: RR Lyrae stars

- metallicity spread among RR Lyrae stars
- two populations of RR Lyrae stars
  - Sollima et al. (2006, ApJ 640, L43)
  - MI RRLS, [Fe/H] ≈ -1.2
  - MP RRLS, [Fe/H] ≈ -1.7
- MI RRLS are fainter than the dominant MP population
  - this is in good agreement with the corresponding ZAHB models with cosmological He abundance $Y = 0.246$
- evidence for a non-He-enhanced MI population
- He-rich population is not expected to produce a sizable RR Lyrae component
- two populations with similar metallicities but very different helium abundances seem to coexist within the cluster

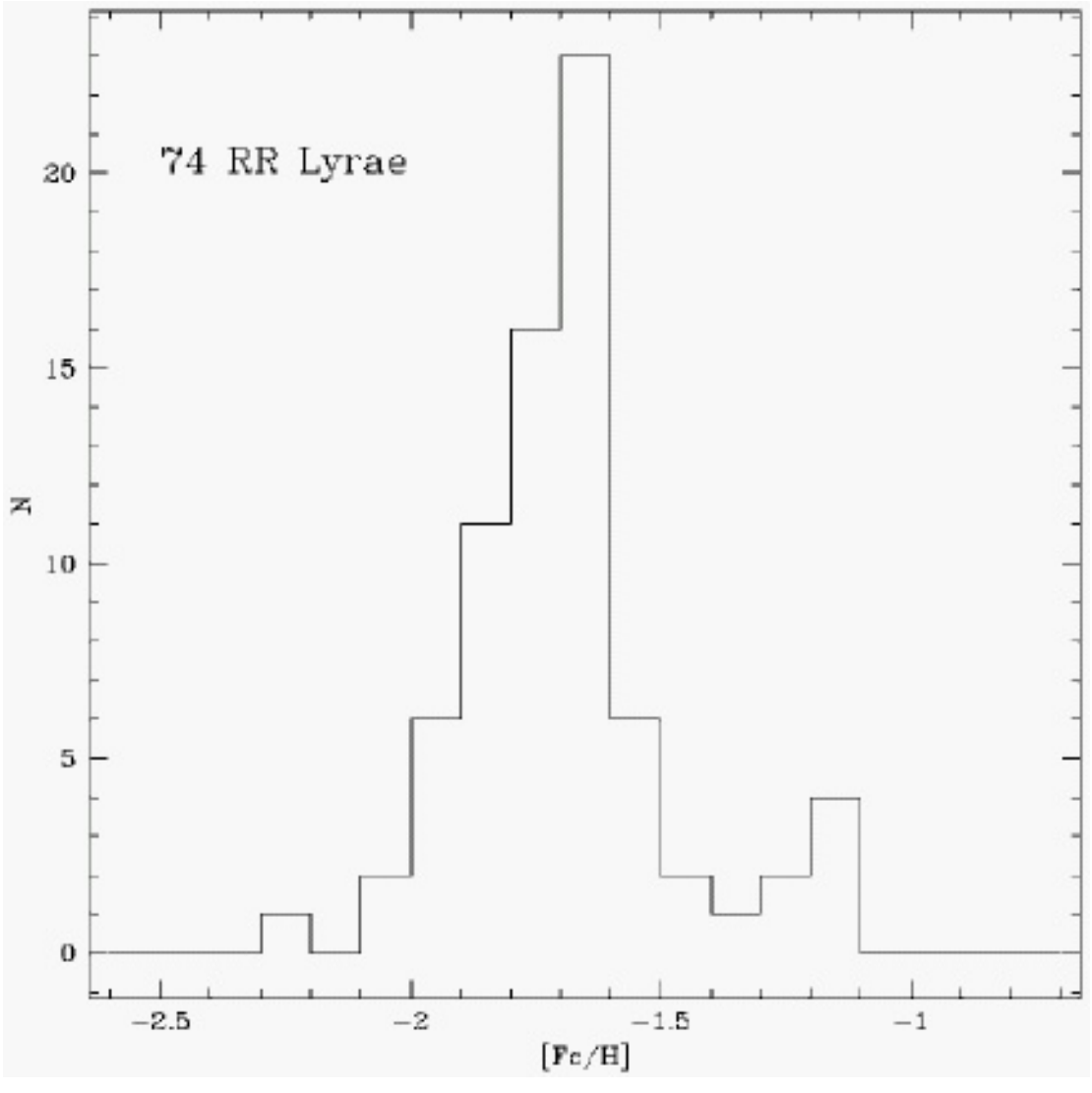

Metallicity distribution for the 74 observed RR Lyrae stars from ω Cen. Sollima et al. (2006, ApJ 640, 43)

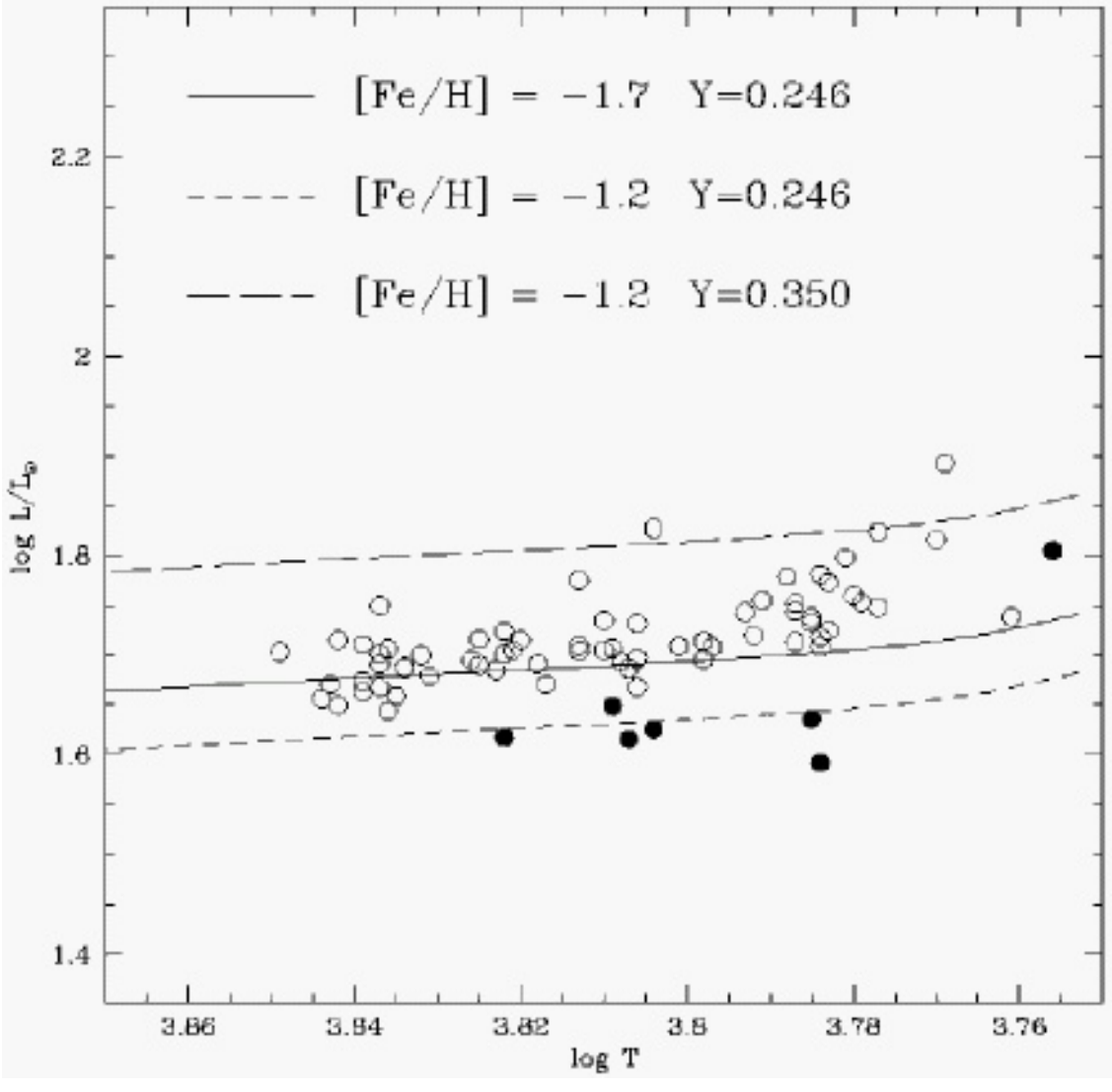

H-R diagram for the target RR Lyrae stars of ω Cen. Open circles mark stars with [Fe/H] < -1.35, and filled circles mark stars with [Fe/H] > -1.35. Different lines indicate the ZAHB luminosity for the indicated metallicity and helium abundance combinations. The ZAHB models with $Y = 0.246$ fit the lower envelopes of the respective MP and MI RR Lyrae stars nicely. Conversely, the He-enhanced ($Y = 0.35$) MI model is far too bright and does not match the observed MI RR Lyrae stars. Sollima et al. (2006, ApJ 640, 43)

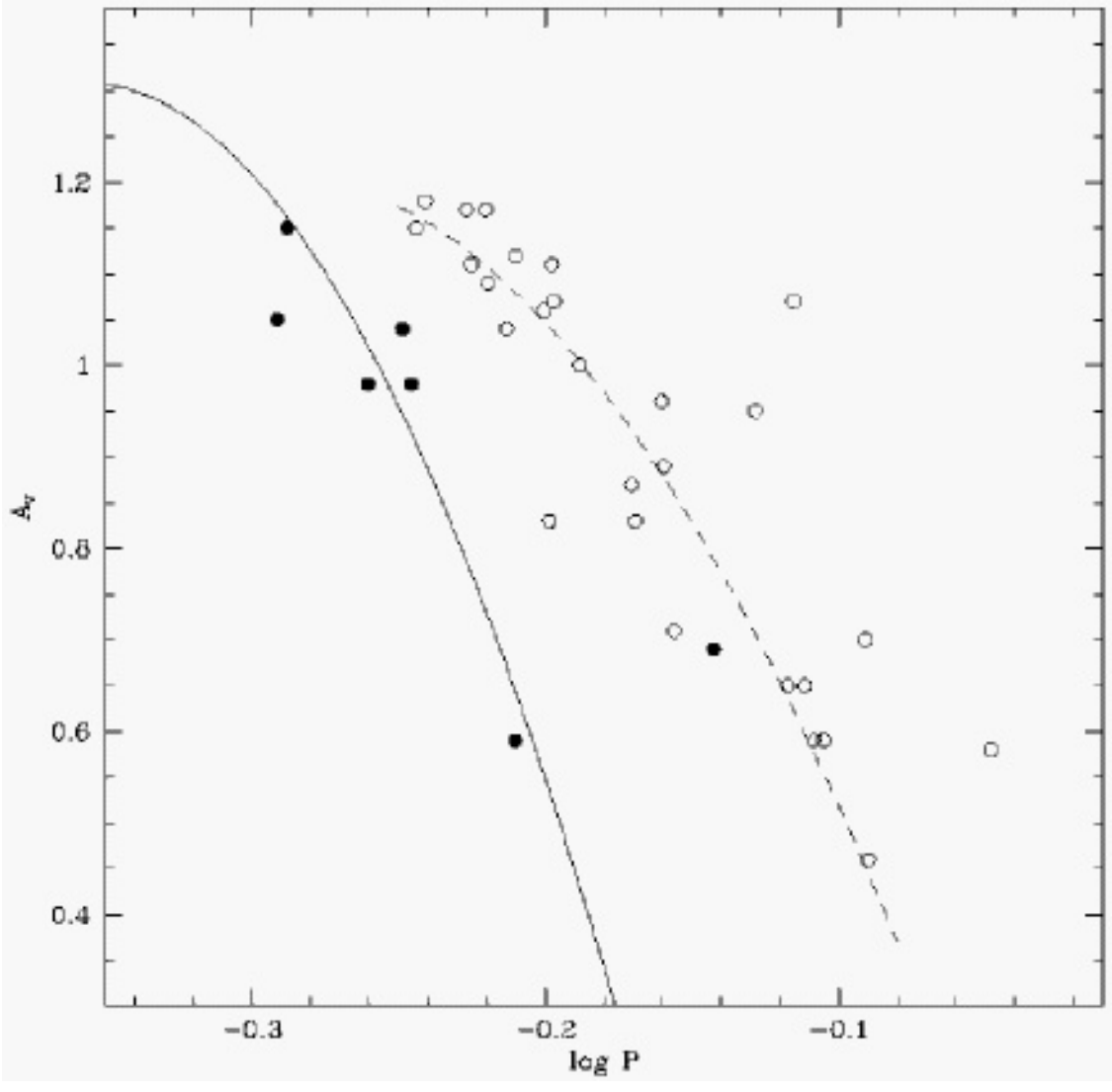

Period – V-amplitude relation for the two metallicity groups of RRab Lyrae stars in ω Cen. The solid line indicates the mean locus of the M3 variables (OoI), while the dashed line indicates the mean locus of the M92 variables (OoII). Sollima et al. (2006, ApJ 640, 43)

Multiple stellar populations in GGCs

Summary of Observational Facts

- GCs as SSP (the same age and initial chemical composition)
  - single isochrone in the CMD
- Spectroscopy:
  - metallicity spread (only in massive GC)
  - bimodality in CN strength
  - spread in abundance of light elements (Na, O, Al, Mg)
  - abundance patterns
  - Na-O and Mg-Al anticorrelations
- Photometry:
  - multiple sequences along RGB, SGB, MS
  - large width of MS
  - bimodal HB distribution (EBHB)
  - He overabundance ($\Delta Y \approx 0.15$)

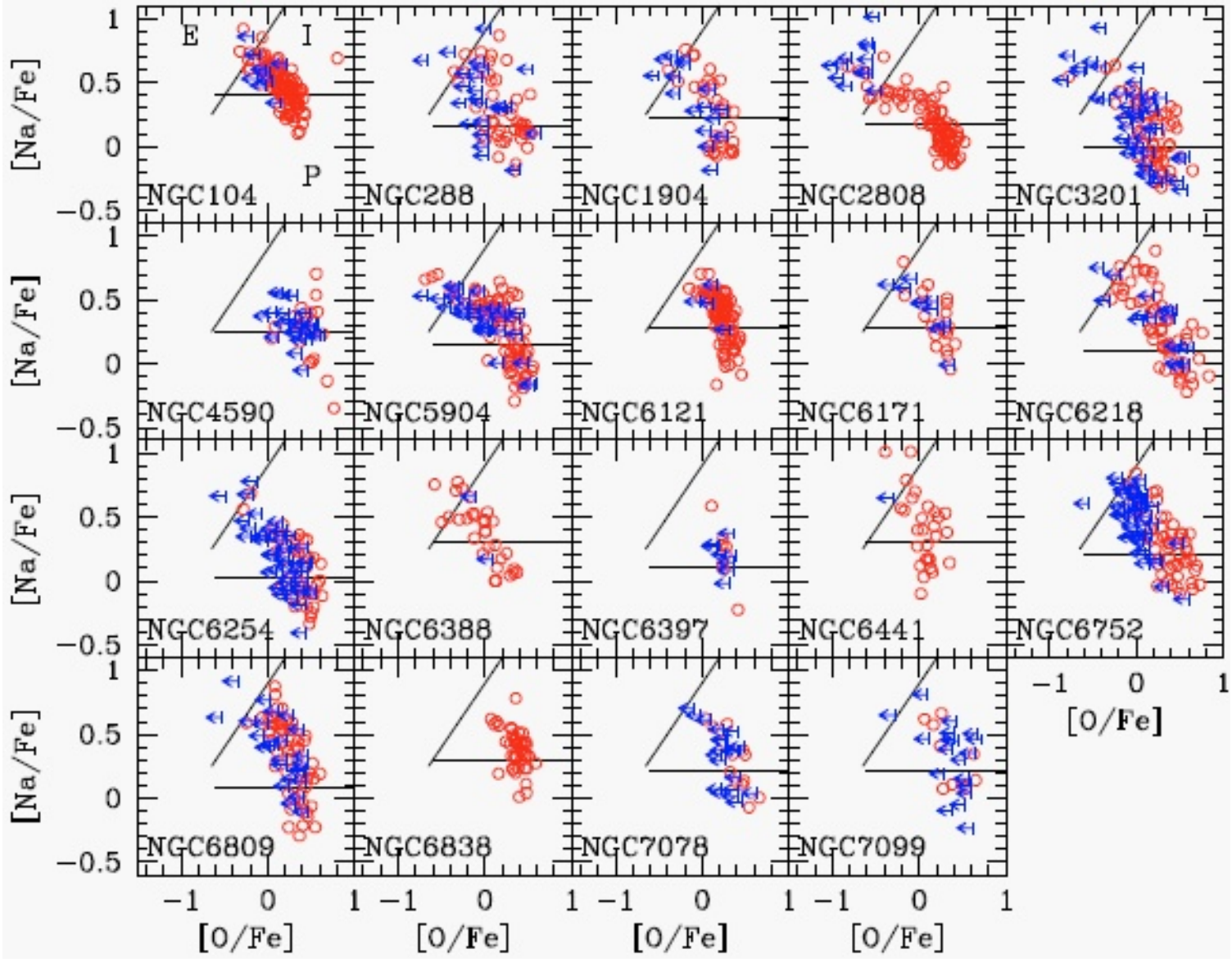

Summary of the Na-O anticorrelation observed in the 19 GCs. Arrows indicate upper limits in O abundances. The two lines in each panel separate the primordial component (located in the Na-poor/O-rich region), the Na-rich/O-poor extreme component, and the intermediate component in-between (called P, E, and I). Caretta et al. (2010, AAp 516, A55).

Multiple populations

- Dispersion in light elements among MS stars
  - no mechanism able to mix them to the surface in MS stars, at variance with RGB stars
  - abundance anomalies found in all evolutionary stages
  - primordial origin
- Multiple generations in GCs
- Several episodes/bursts of star formation
- Connection to
  - second-parameter problem
  - relation between GCs and halo of our Galaxy
  - relation between GCs and DG satellites of our Galaxy

Scenarios for GC formation

- Several generations of stars (Carretta et al. 2010, AAp 516, A55)
    - primordial, first-generation (FG) stars (similiar in abundance to halo stars)
    - second-generation (SG) stars (with peculiar composition not found among field stars)
        - elements involved in H-burning (C, N, O, F, Na, Mg, Al, Si)
- SG stars formed from material polluted by ejecta of a fraction of the FG stars
    - evidence in different evolutionary phases
- Most of the stars (70 %) in a GC belong to the SG
- GCs were created in massive episodes of SF and most of their original population has been lost

Massive GCs

- ω Cen (and M54, NGC2808, M22, 47 Tuc, NGC2419, NGC6388)
- spread in metallicity [Fe/H]
- three main sequences of RGB/SGB stars in ω Cen (Hilker et al., 2004, AAp 422, L9)
  - MPP, $-2.0 <$ [Fe/H] < -1.5, 70 %
  - IMP, $3 \times$ MINT, $-1.5 <$ [Fe/H] < -0.9, 25 %
  - MRP, RGB-a, $-0.9 <$ [Fe/H] < -0.6, 5 %
- two MS populations in ω Cen (Sollima et al., 2007, ApJ 654, 915)
  - rMS, [Fe/H]≈ -1.6, 75 %
  - bMS, [Fe/H]≈ -1.3, 25 %
  - redder weak MS found by Villanova et al. (2007), joining the RGB-a
- bluer sequence has $Y \approx 0.4$
- EBHB

Star Formation Histories of Massive GCs

- Joo and Lee (2013, ApJ 762, 36)
- ω Cen, M22, NGC1851
- Synthetic CMDs
    - Yonsei-Yale isochrones and HB evolutionary tracks including cases of He and CNO abundance enhancements
    - fiting synthetic models to the observed CMDs to find ages and He abundances

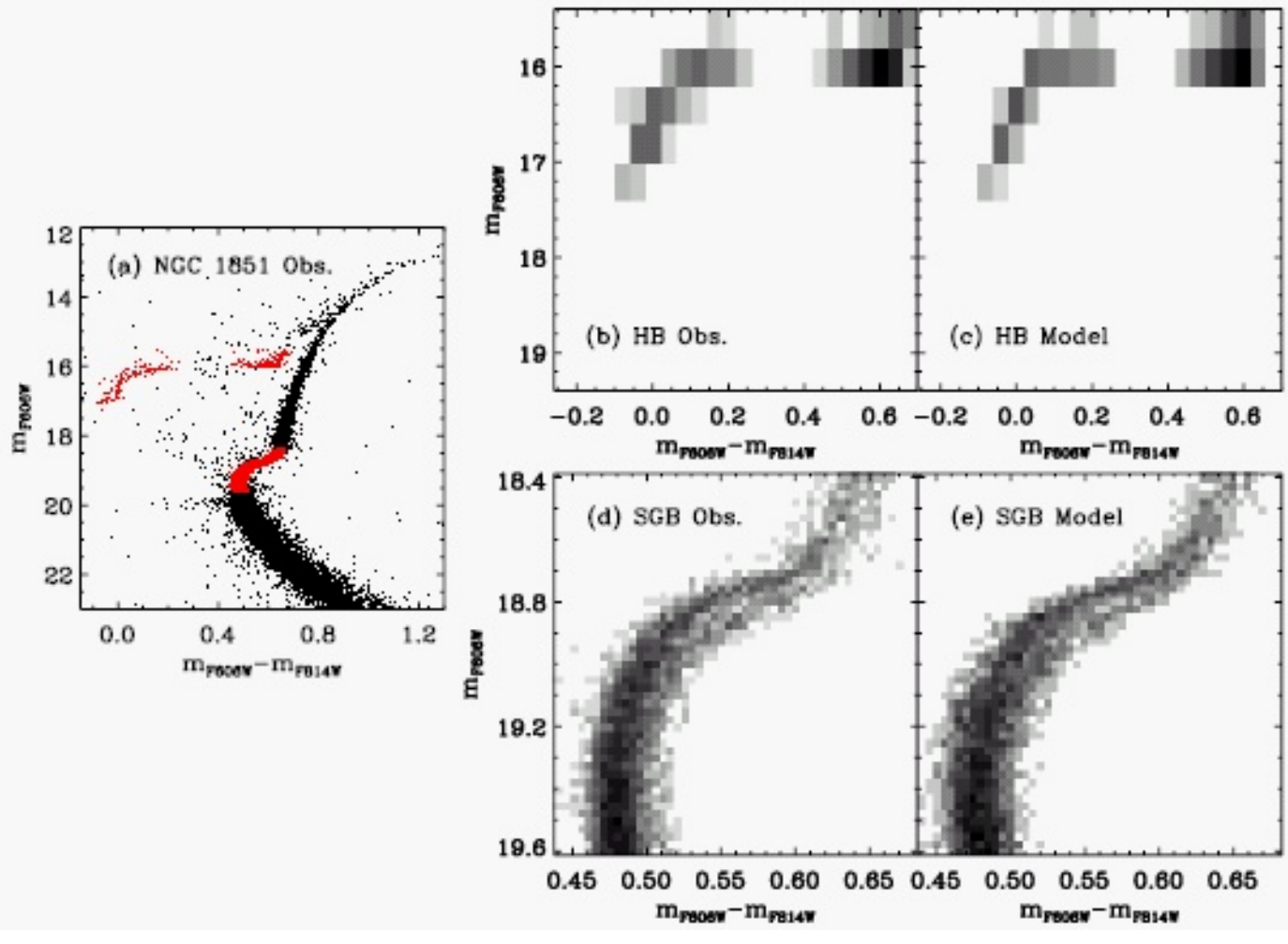

Example of the comparison between the observed and synthetic Hess diagrams used in our χ^2 minimization technique for NGC 1851. (a) Red points represent CMD regions used in our χ^2 minimization. (b)–(e) The observed and synthetic Hess diagrams for the HB and SGB regions, respectively. Joo and Lee (2013, ApJ 762, 36).

Parameters Suggested from Our Best Simulation of ω Cen

Population	Z	[Fe/H][a]	Δ[CNO/Fe][b]	Y	Age (Gyr)	Mass Loss[c] ($M_\odot$)	Fraction[d]	Other Name[d]
G1	0.0005	−1.81	0.0	0.231	13.1 ± 0.2	0.199	0.42	RGB-MP
G2	0.0009	−1.55	0.0	0.232	13.0 ± 0.3	0.217	0.28	RGB-MInt1
G3	0.0015	−1.31	0.14	0.41 ± 0.02	12.0 ± 0.4	0.171	0.17	RGB-MInt2
G4	0.0057	−1.01	0.47	0.38 ± 0.02	11.4 ± 0.4	0.220	0.08	RGB-MInt3
G5	0.0136	−0.62	0.47	0.39 ± 0.02	11.4 ± 0.5	0.251	0.05	RGB-a

Notes.

[a] $[\alpha/\mathrm{Fe}] = 0.3$.

[b] From Marino et al. (2012a).

[c] Mean mass loss on the RGB for $\eta = 0.53$.

[d] From Sollima et al. (2005a) and Pancino et al. (2000).

Joo and Lee (2013, ApJ 762, 36).

Star Formation Histories of Massive GCs

- Joo and Lee (2013, ApJ 762, 36)
- ω Cen, M22, NGC1851
- Metal-rich subpopulations in above GCs are also enhanced in helium abundance
- The age differences between the metal-rich and metal-poor subpopulations are fairly small ($0.3-1.7$ Gyr), even in the models with the observed variations in the total CNO content.
- These are required to simultaneously reproduce the observed EBHB and the splits on the MS, SGB, and RGB.

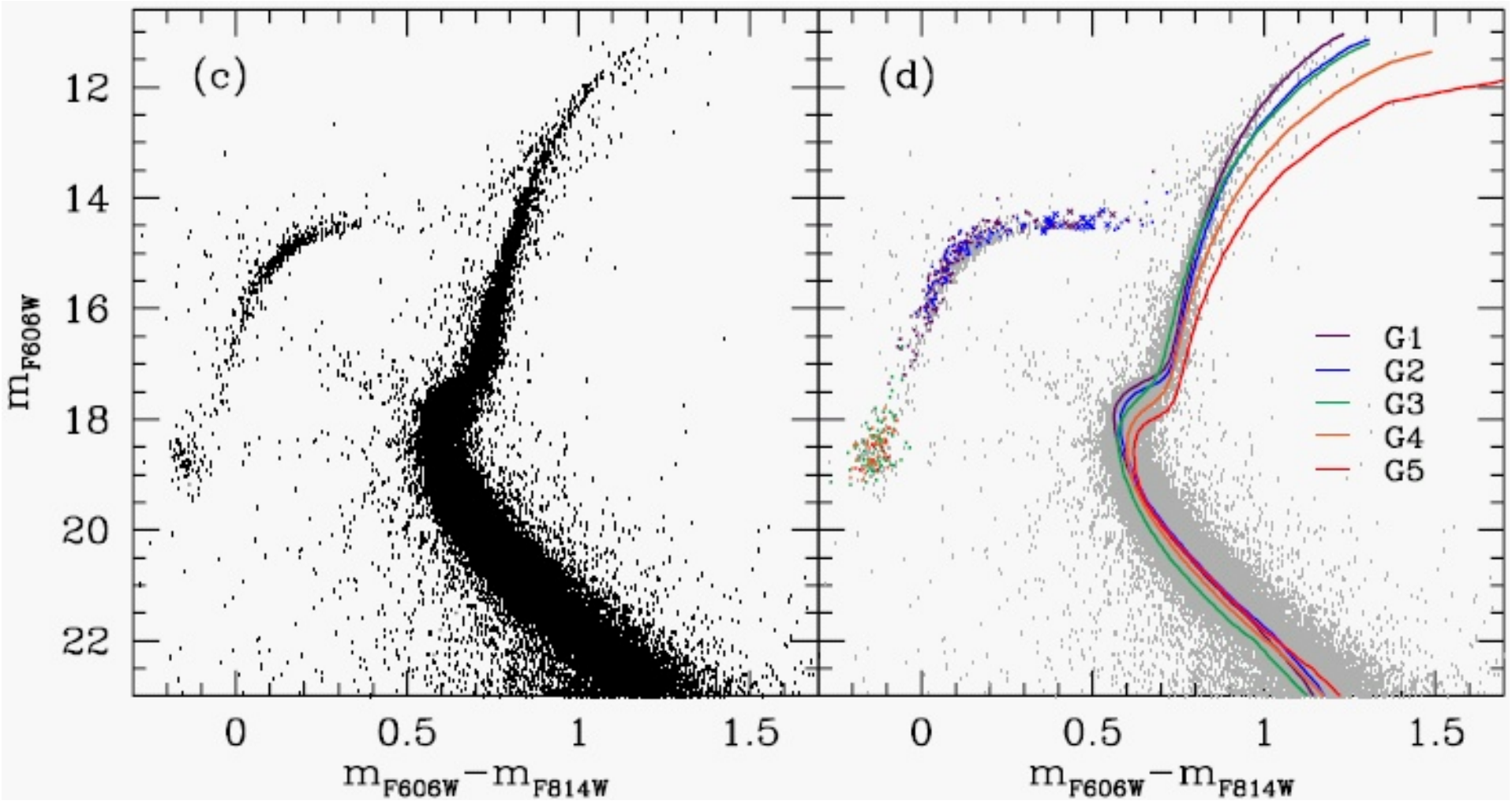

Comparison of models with the observations for ω Cen. (c) Observed CMDs by HST ACS/WFC for the F606W and F814W passbands (data from Bellini et al. 2010). (d) Our population models compared on the observed CMDs. Crosses denote the model RR Lyrae stars. Joo and Lee (2013, ApJ 762, 36).

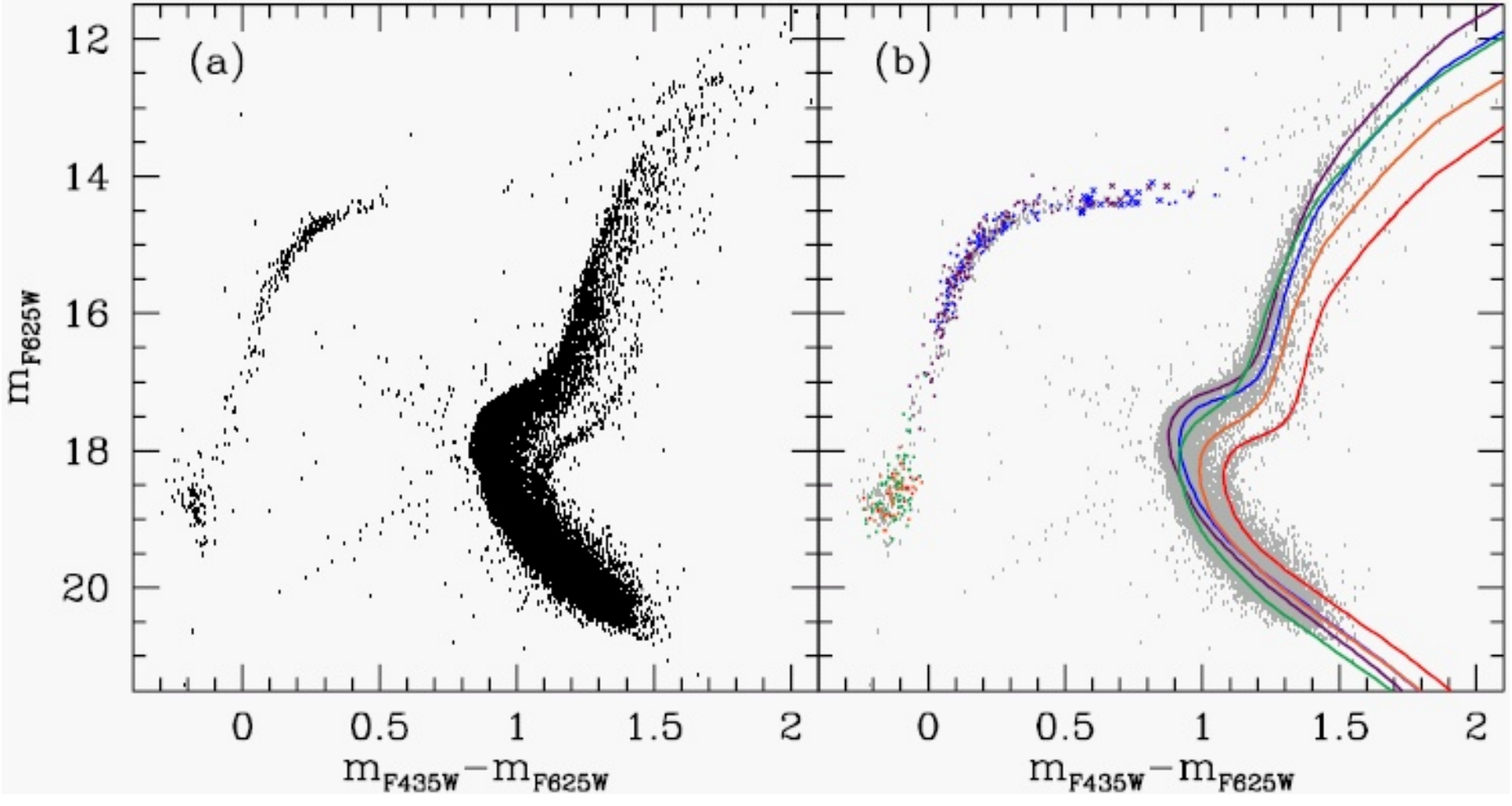

Comparison of models with the observations for ω Cen. (a) Observed CMDs by HST ACS/WFC for the F435W and F625W passbands (data from Bellini et al. 2010). (b) Our population models compared on the observed CMDs. Crosses denote the model RR Lyrae stars. Joo and Lee (2013, ApJ 762, 36).

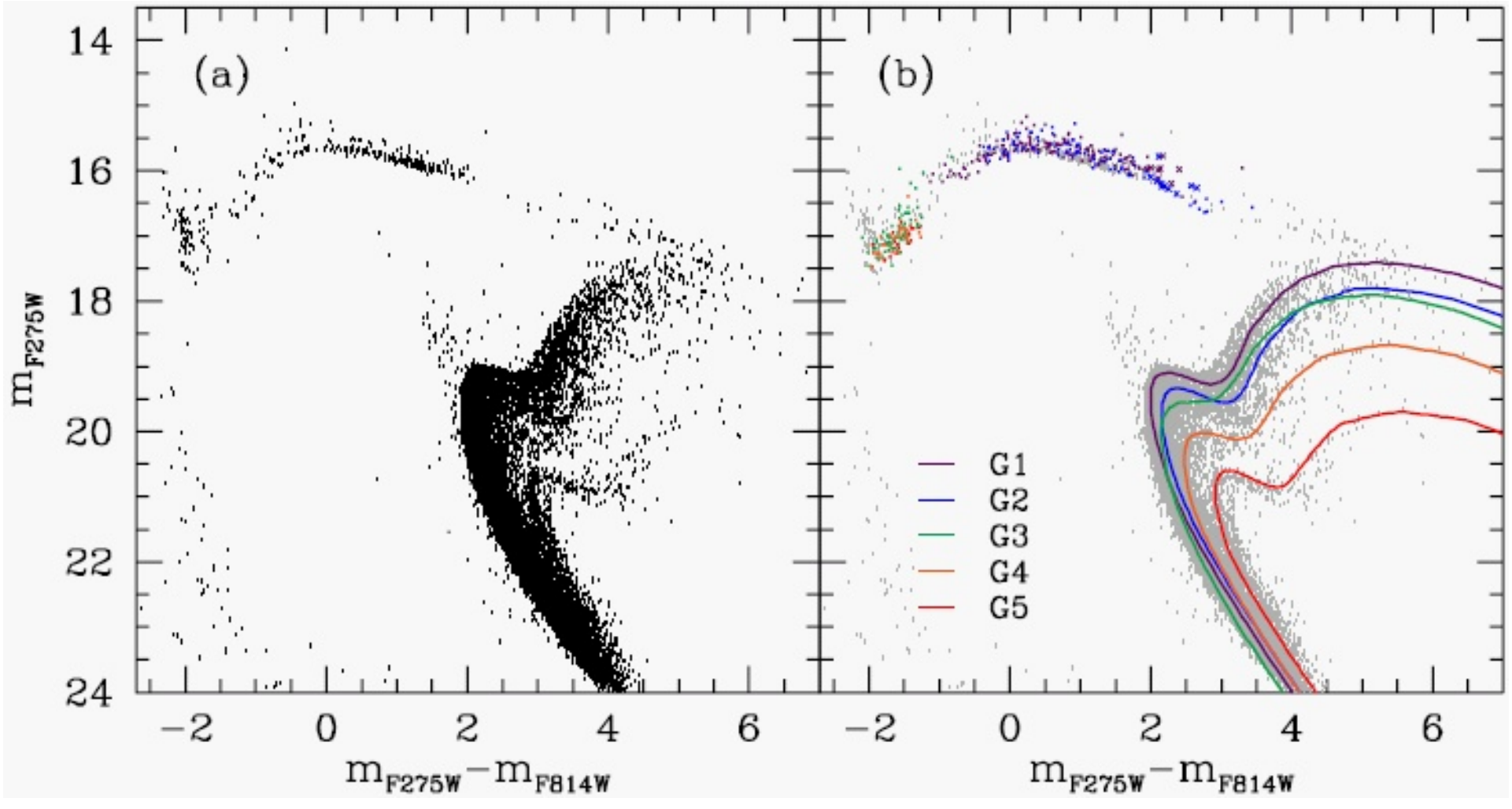

Comparison of models with the observations for ω Cen. (a) Observed CMDs by HST ACS/WFC for the F275W and F814W passbands (data from Bellini et al. 2010). Model parameters obtained from the optical (F435W, F625W) bands can also reproduce the observed features from the UV (F275W) and broad I (F814W) bands.(b) Our population models compared on the observed CMDs. Joo and Lee (2013, ApJ 762, 36).

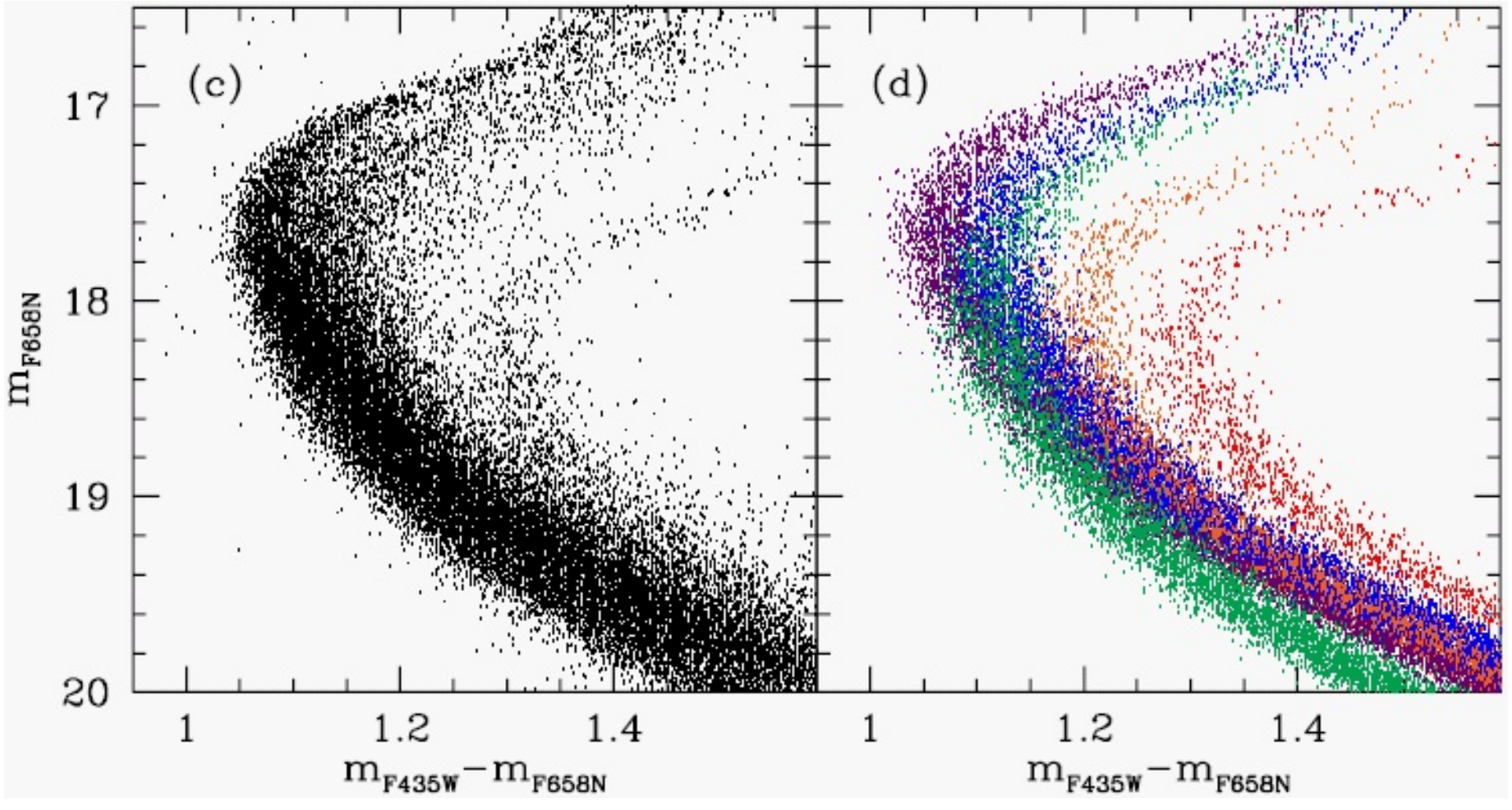

(c) CMD for the MS and SGB region in the F435W and F658N passbands. (d) Synthetic models constructed with the photometric errors and total number of stars comparable to the observed CMD in panel (c). Joo and Lee (2013, ApJ 762, 36).

- Variation in total CNO content between the subpopulations has the most significant impact on the age difference.

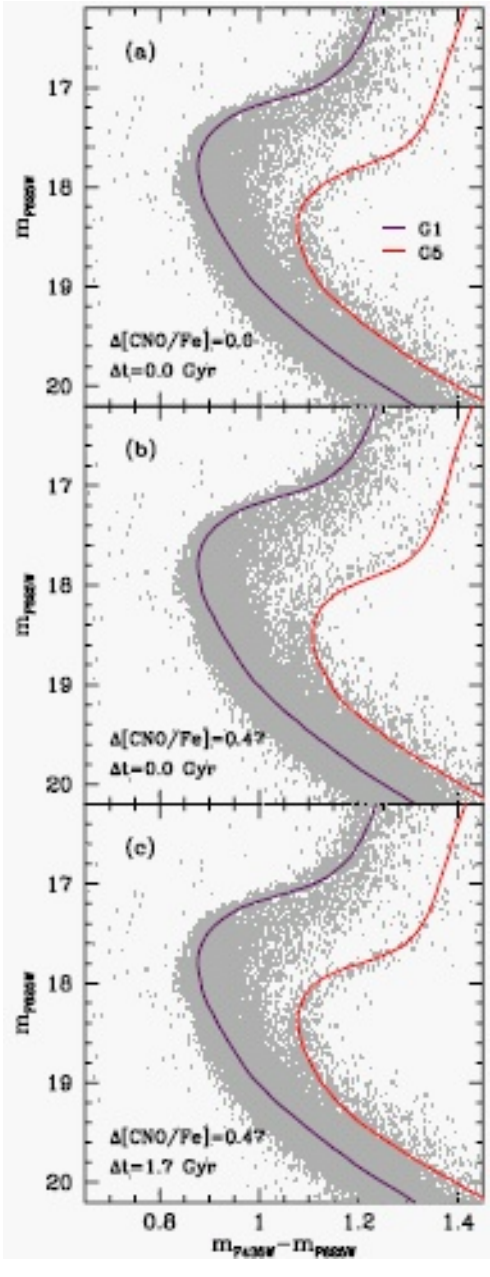

CMD for the MS and SGB. Synthetic models are constructed to illustrate the effects of Δ[CNO/Fe] on the age dating. (a) If Δ[CNO/Fe] = 0.0 between G1 and G5, no difference in age is obtained between them (they still differ in [Fe/H] and Y). (b) and (c) When the observed Δ[CNO/Fe] is included, $\Delta\tau = 1.7$ Gyr is required between G1 and G5, in the sense that G5 is younger, otherwise models would not match the observations.

- The fact that the bluer MS is more metal-rich than the redder MS strongly suggest that there is a large variation of He abundance.
- The presence of the unusually extended HB is also naturally explained by the sub-populations enhanced in He.

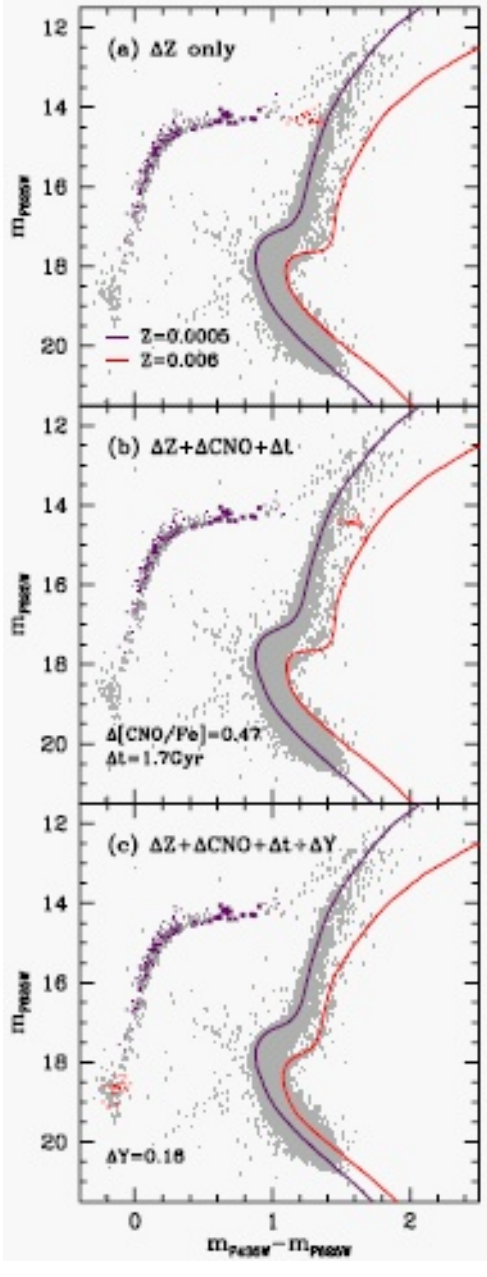

CMD for ω Cen. Synthetic models are constructed to illustrate, independently, the effects of metallicity, the total CNO content, age, and helium abundance on the overall morphology in the CMD.

NGC2419

- metal-poor GC, [Fe/H] = −2.1
- half-light radius significantly larger than that of other GGCs of the same luminosity (more akin to the nuclei of dSphG)
- EBHB (blue hook) in the CMD
- colour spread on the RGB significantly larger than that expected from observational errors
- Di Criscienzo et al. (2011) found that the observed RGB colour distribution can be consistently interpreted together with the peculiar HB morphology of the cluster by assuming that about 30 % of the cluster stars belong to a SG that is heavily enriched in He.
- Mucciarelli et al. (2012) found from 49 RGB stars
  - no intrinsic spread in Fe, Ti and Ca
  - huge spreads of Mg and K abundances ($-1.2 < [Mg/Fe] < +1.0$ and $-0.2 < [K/Fe] < +2.0$, and obvious bimodal distributions
- significant spread in Na abundance

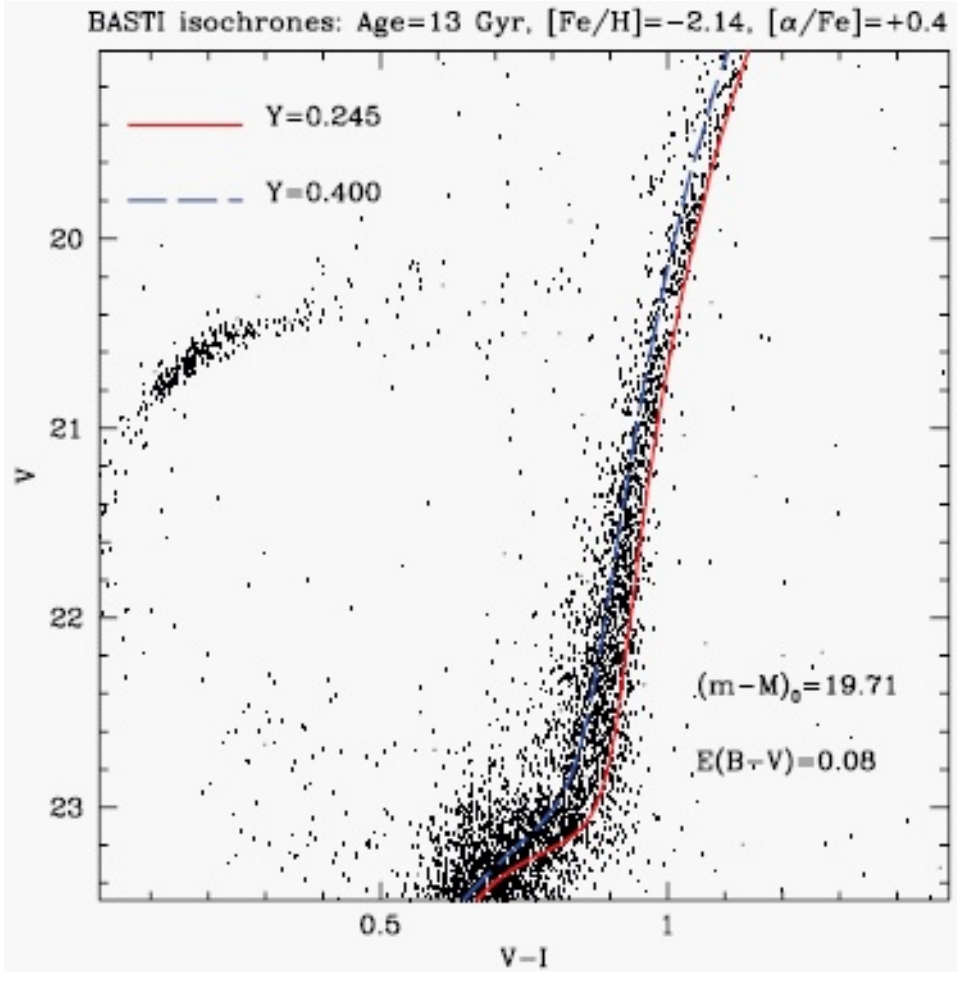

Theoretical isochrones from the BASTI data set (Pietrinferni et al. 2004) for two different He abundances are superimposed to the observed (V, $V-I$) CMD of NGC2419. The age, metallicity and [α/Fe] ratio have been adopted following Bellazzini et al. (2012); the adopted distance modulus and reddening are from Di Criscienzo et al. (2011). The He abundance of the two models is similar to that assumed by D11 for the first ($Y = 0.245$) and second generation ($Y = 0.400$) of stars they propose. Beccari et al. (2013, MNRAS 431, 1995).

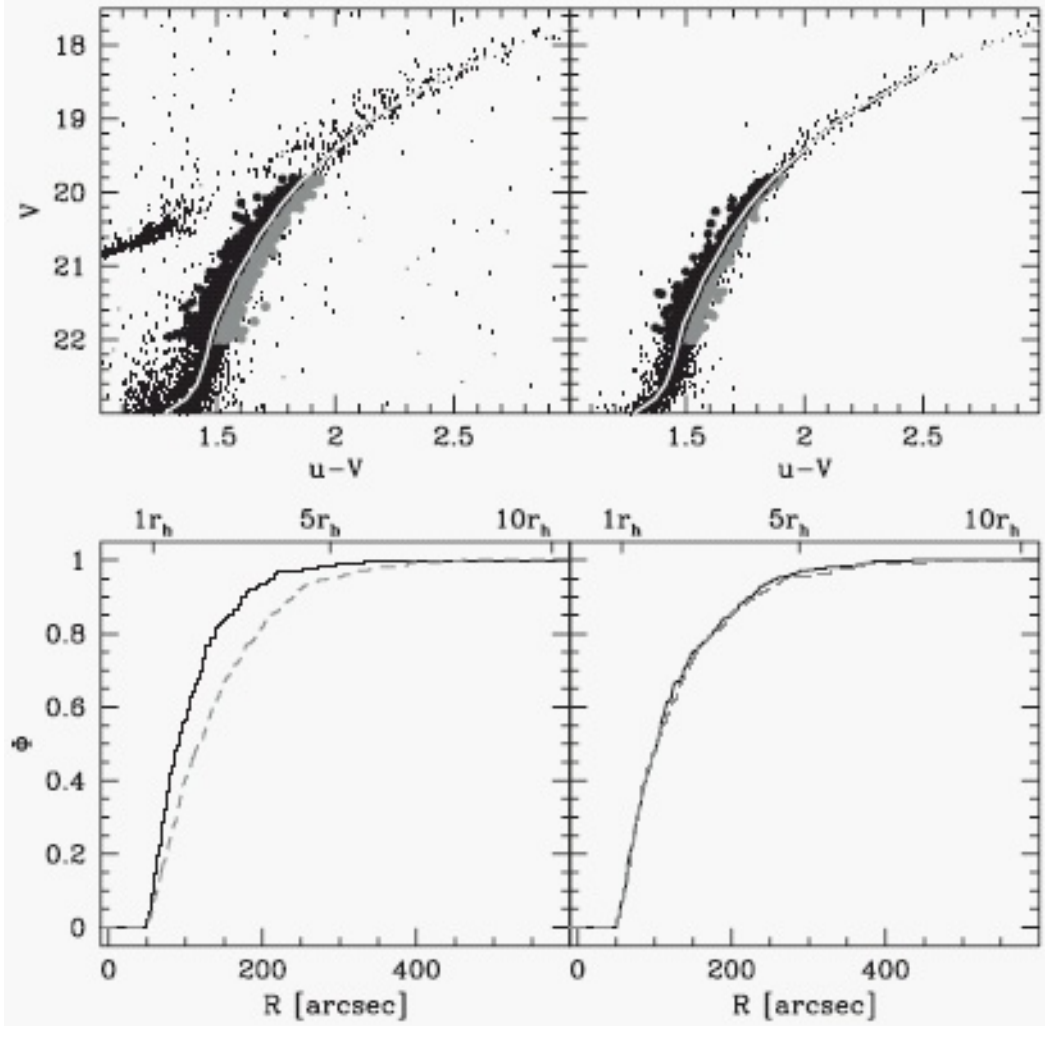

Upper panels: selection of RGB-Blue and RGB-Red stars in the $(V, u-V)$ CMDs: observed (left-hand panel) and constructed from artificial stars (righthand panel); the solid grey lines are the RGB ridge lines. Lower panels: comparisons between the radial distribution of blue (black solid line) and red (grey dashed line) RGB stars as selected in the corresponding CMDs. Beccari et al. (2013, MNRAS 431, 1995).

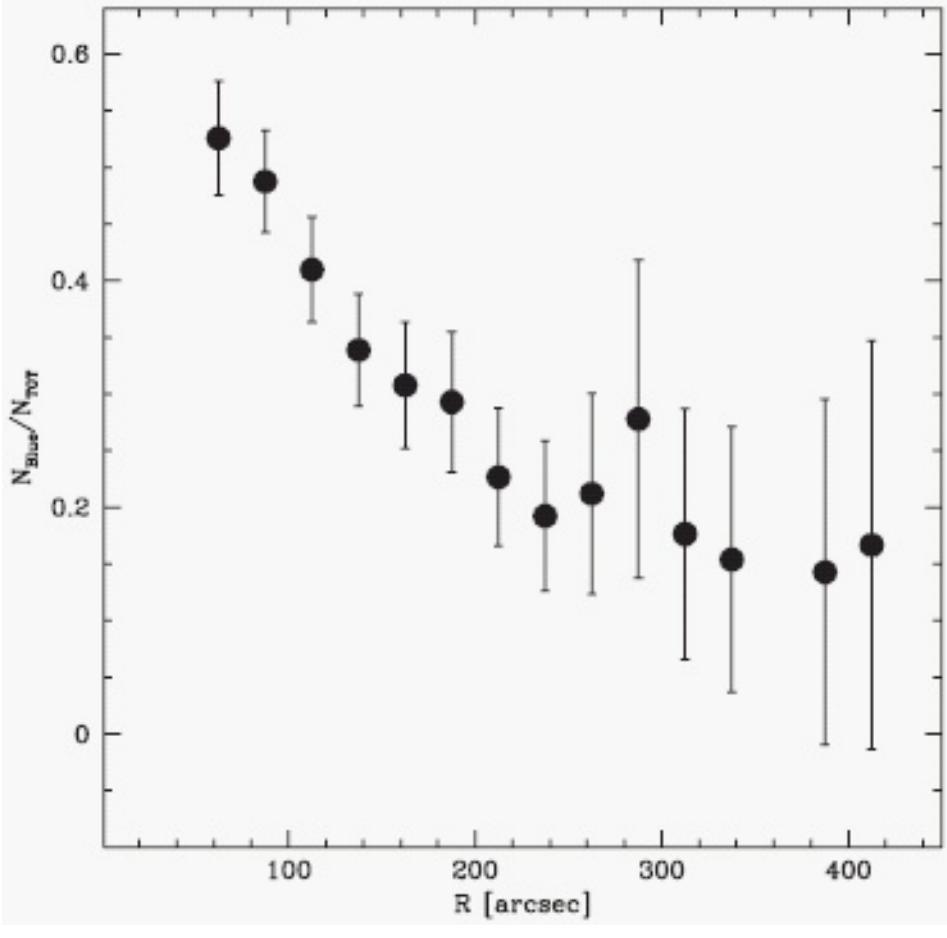

Fraction of blue RGB stars (selected in $(u-I)$) on the total number of RGB stars in the selected magnitude range as a function of distance from the cluster centre. The fraction is computed on running bins 50 arcsec wide with a step of 25 arcsec. The profile obtained from $(u-V)$ selected stars is indistinguishable. Beccari et al. (2013, MNRAS 431, 1995).

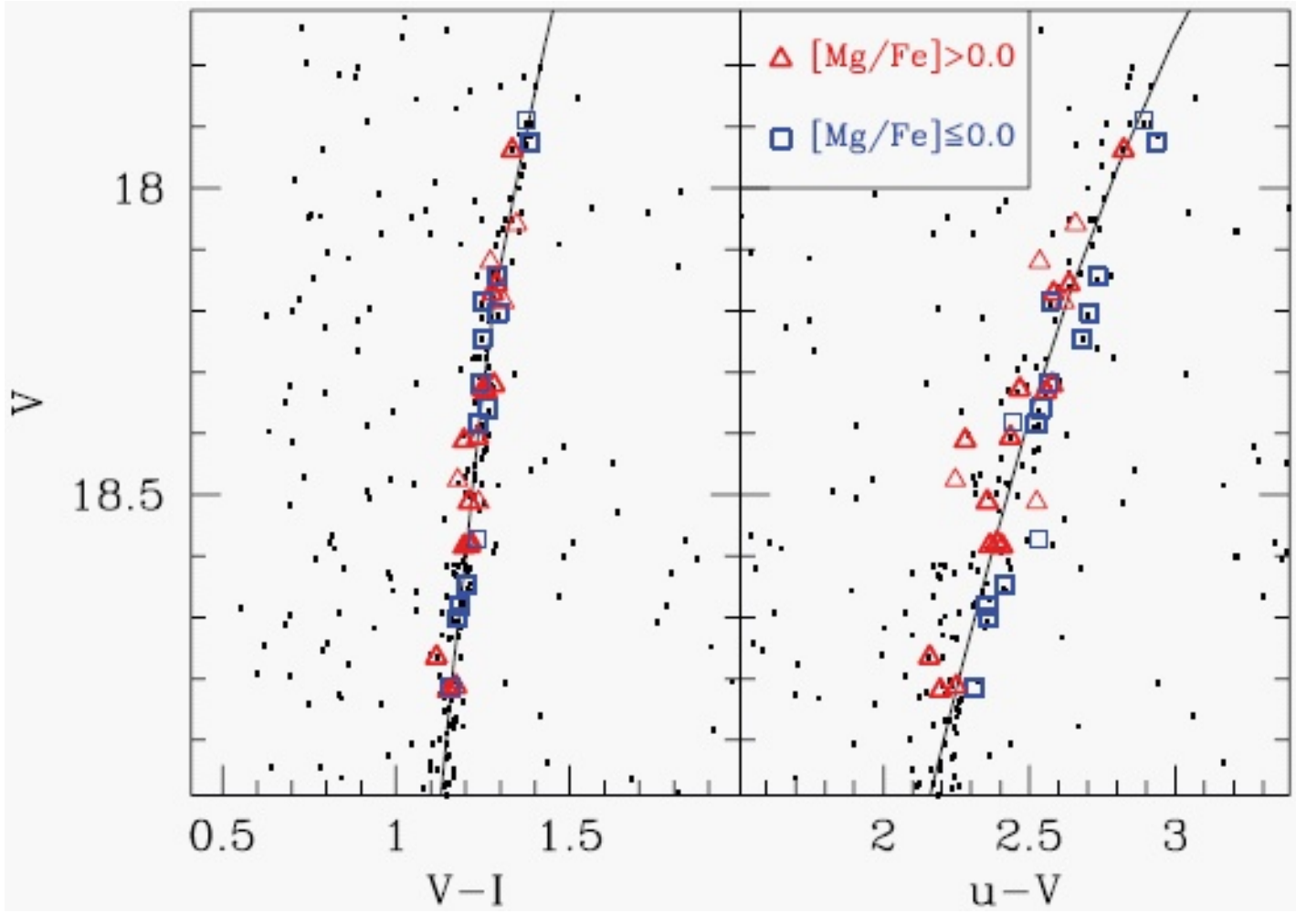

Location of Mg-deficient (blue squares) and Mg-rich (red triangles) stars from Mu12 in the $(V, V-I)$ (left-hand panel) and $(V, u-V)$ (right-hand panel) CMDs; the solid lines are the RGB ridge lines. Beccari et al. (2013, MNRAS 431, 1995).

Photometric signatures of multiple stellar populations

- Sbordone et al. (2011, AAp 534, A9)
- Theoretical predictions for the effect of abundance variations on the observed cluster CMDs
- Synthetic spectra for typical chemical mixtures found in various subpopulations of GCs
- CNO abundance variations affect mainly wavelengths shorter than 400 nm owing to the rise of molecular absorption bands in cooler atmospheres
- Mixtures:
  - reference (FG) : age 12 Gyr, $Y = 0.25$, $Z = 0.001$ ([Fe/H] $= -1.6$)
  - CNONa1/2 (SG) : coeval, CNONa (anti-)correlations
  - CNONa1 with $Y = 0.4$

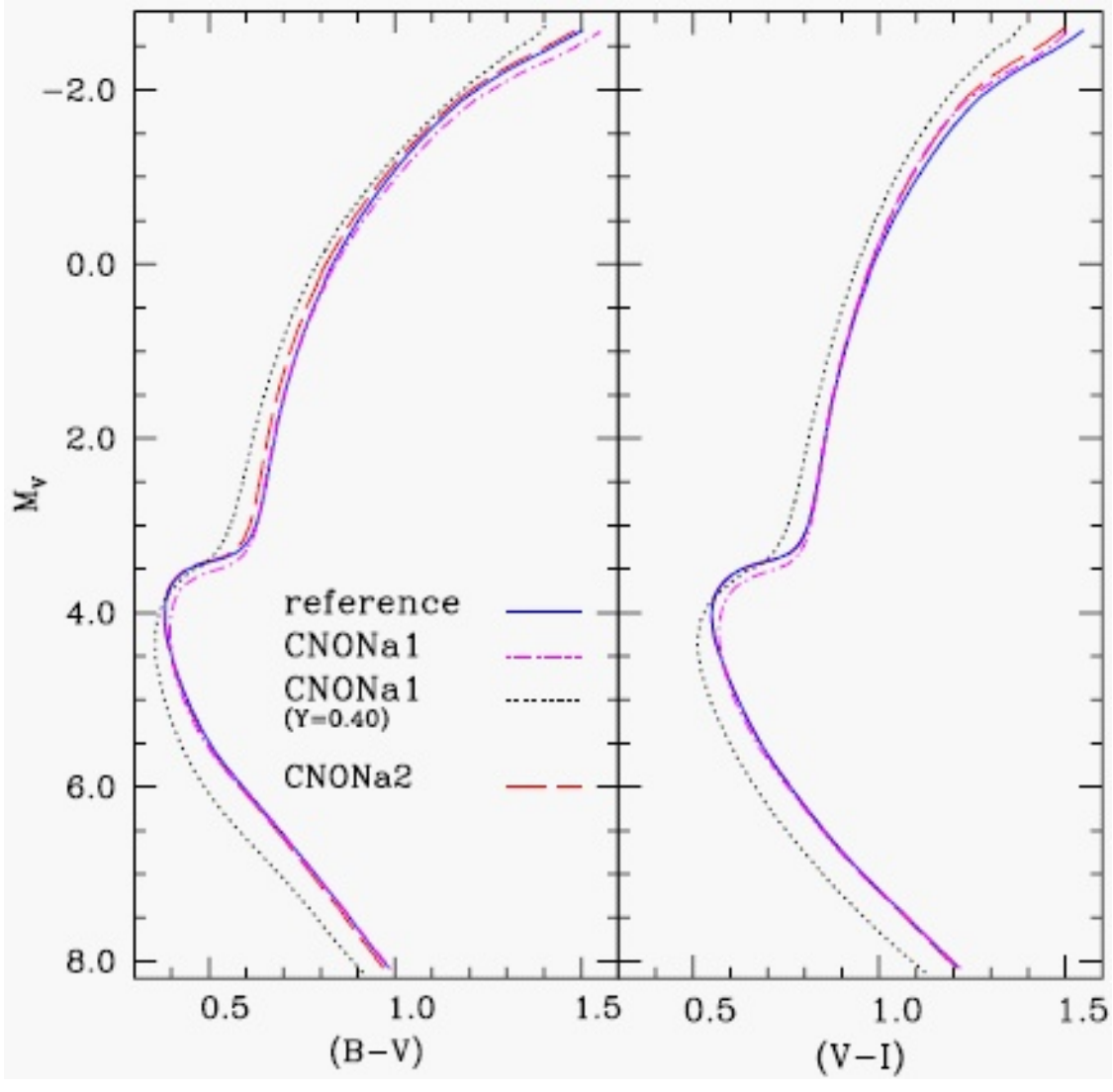

Left: the M_V vs. $(B-V)$ CMD for the same isochrones for different chemical compositions. Different line-styles correspond to different element mixtures. Right: as on the left, but for the M_V vs. $(V-I)$ CMD. Sbordone et al. (2011, AAp 534, A9).

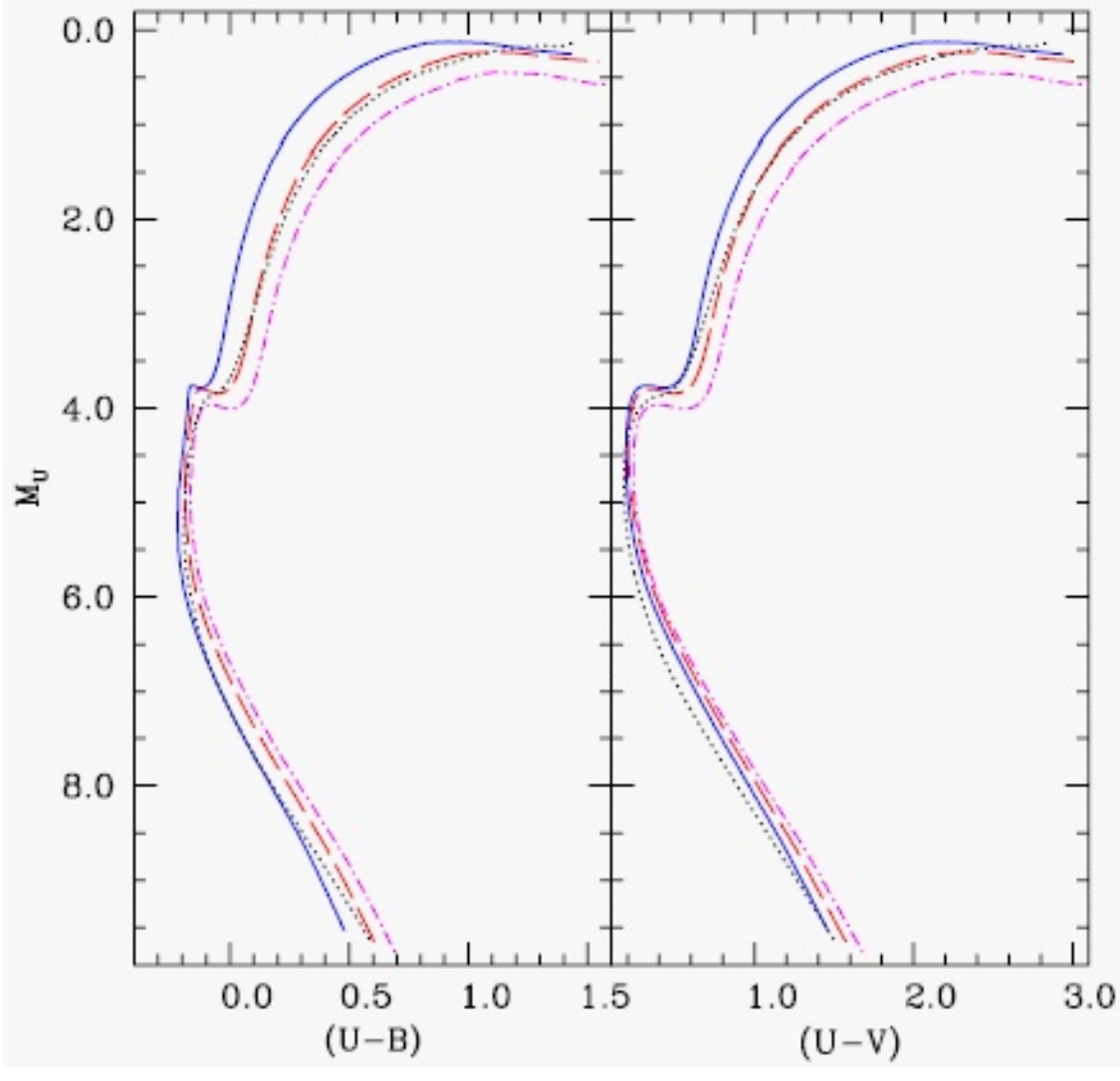

Left: the M_U vs. $(U-B)$ CMD for the same isochrones for different chemical compositions. Different line-styles correspond to different element mixtures. Right: as on the left, but for the M_U vs. $(U-V)$ CMD. Sbordone et al. (2011, AAp 534, A9).

SUMO project

- Monelli et al. (2013, MNRAS 431, 2126)
- 23 Galactic GCs
- $c_{UBI} = (U - B) - (B - I)$
  - colour index very effective for identifying multiple sequences along RGB (HB and AGB)
  - UV portion of the spectrum is strongly affected by the change in CN and CH abundances, owing to the light element anticorrelations observed in SG stars
- Broadened or multimodal RGBs
- Direct connection with chemical properties (abundances of O, Na, C, N, Al)
- FG : Na/N-poor and O/C rich stars (He-poor)
- SG : Na/N-rich and O/C poor stars (He-rich)

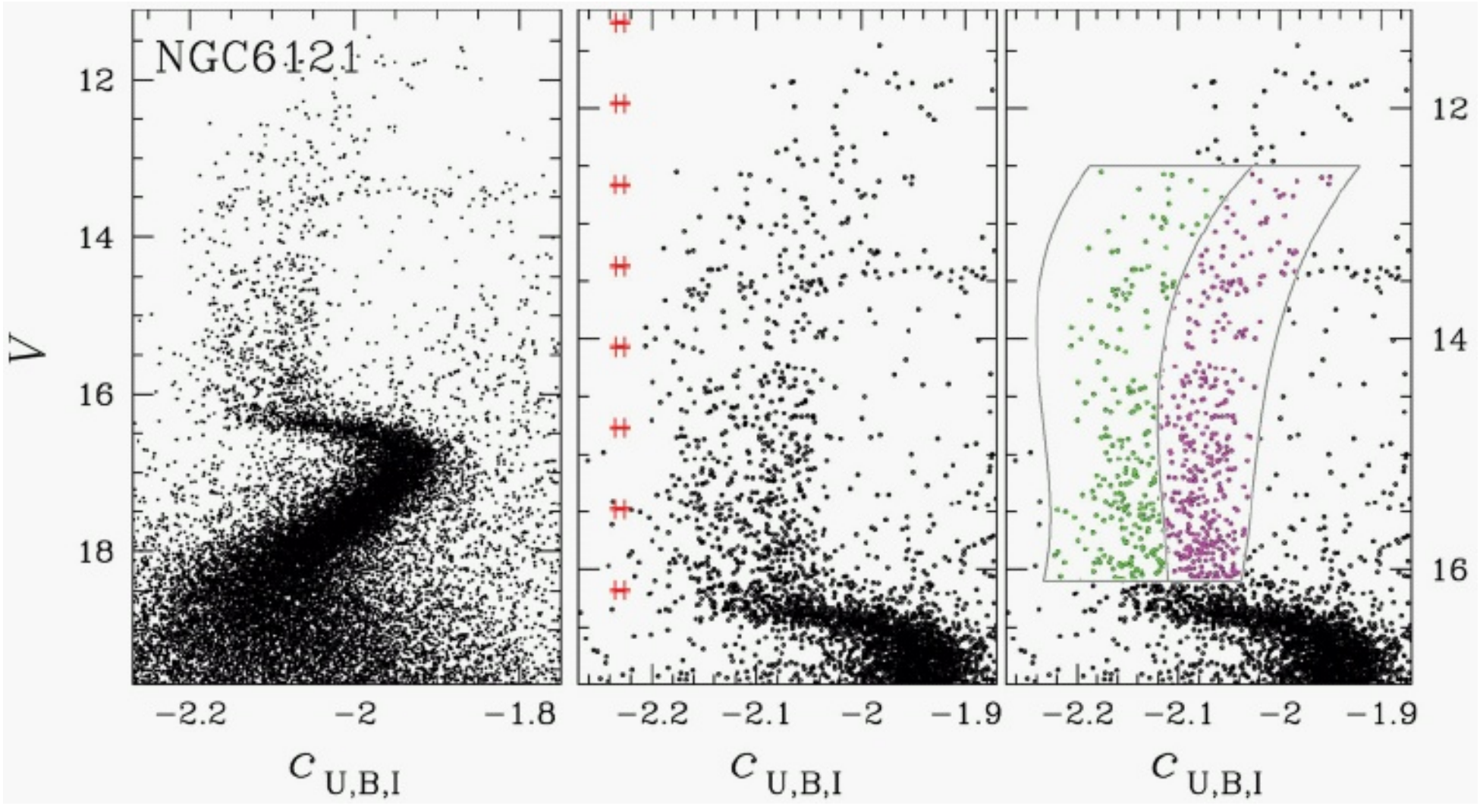

V vs. c_{UBI} pseudo-CMD for NGC6121 (= M4). The left and central panels show the entire diagram and a zoom in the RGB region, respectively. Using this diagram, two subpopulations are identified and are highlighted in the right panel. Monelli et al. (2013, MNRAS 431, 2126).

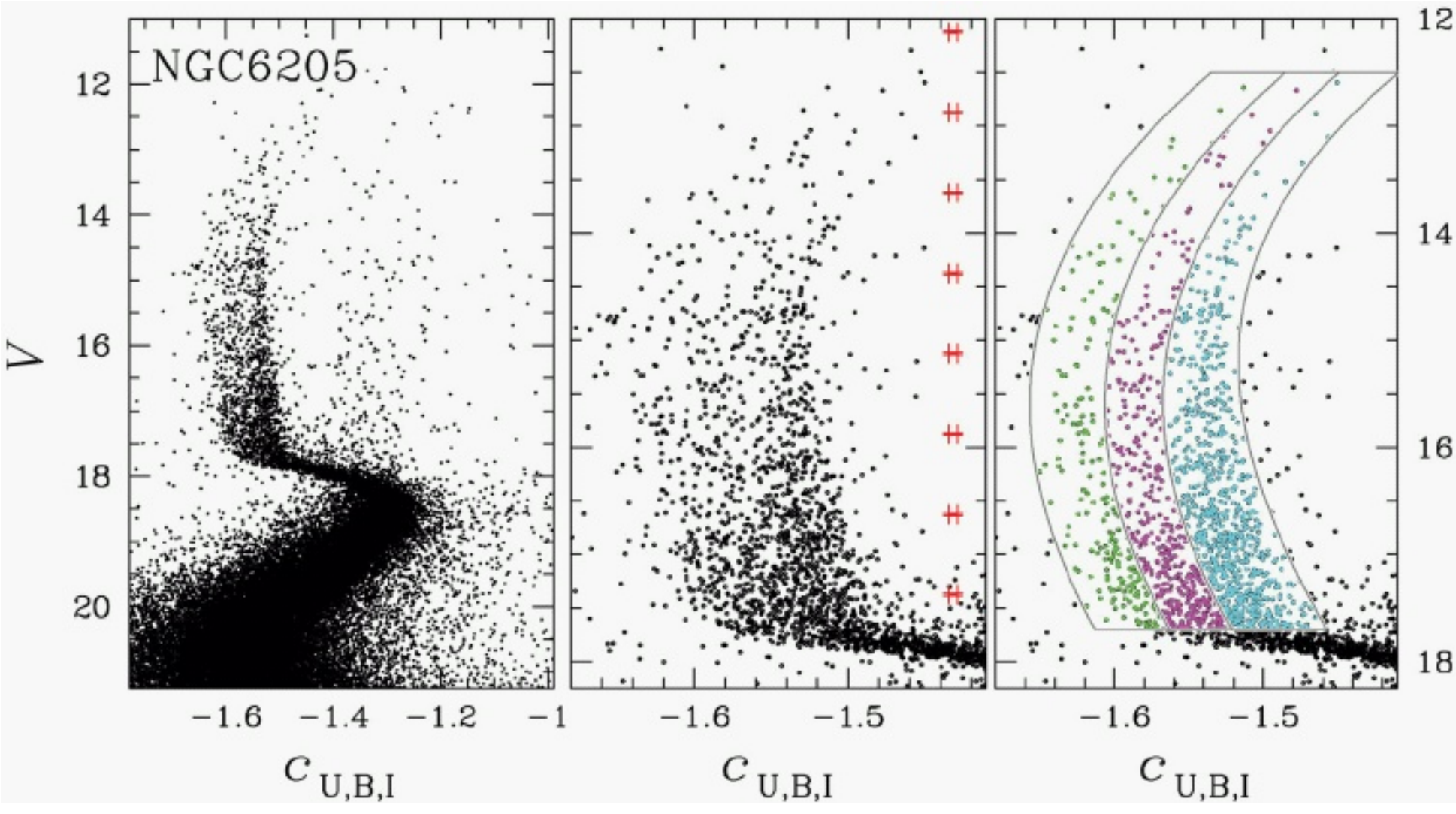

V vs. c_{UBI} pseudo-CMD for NGC6205 (= M13). The left and central panels show the entire diagram and a zoom in the RGB region, respectively. Using this diagram, two subpopulations are identified and are highlighted in the right panel. Monelli et al. (2013, MNRAS 431, 2126).

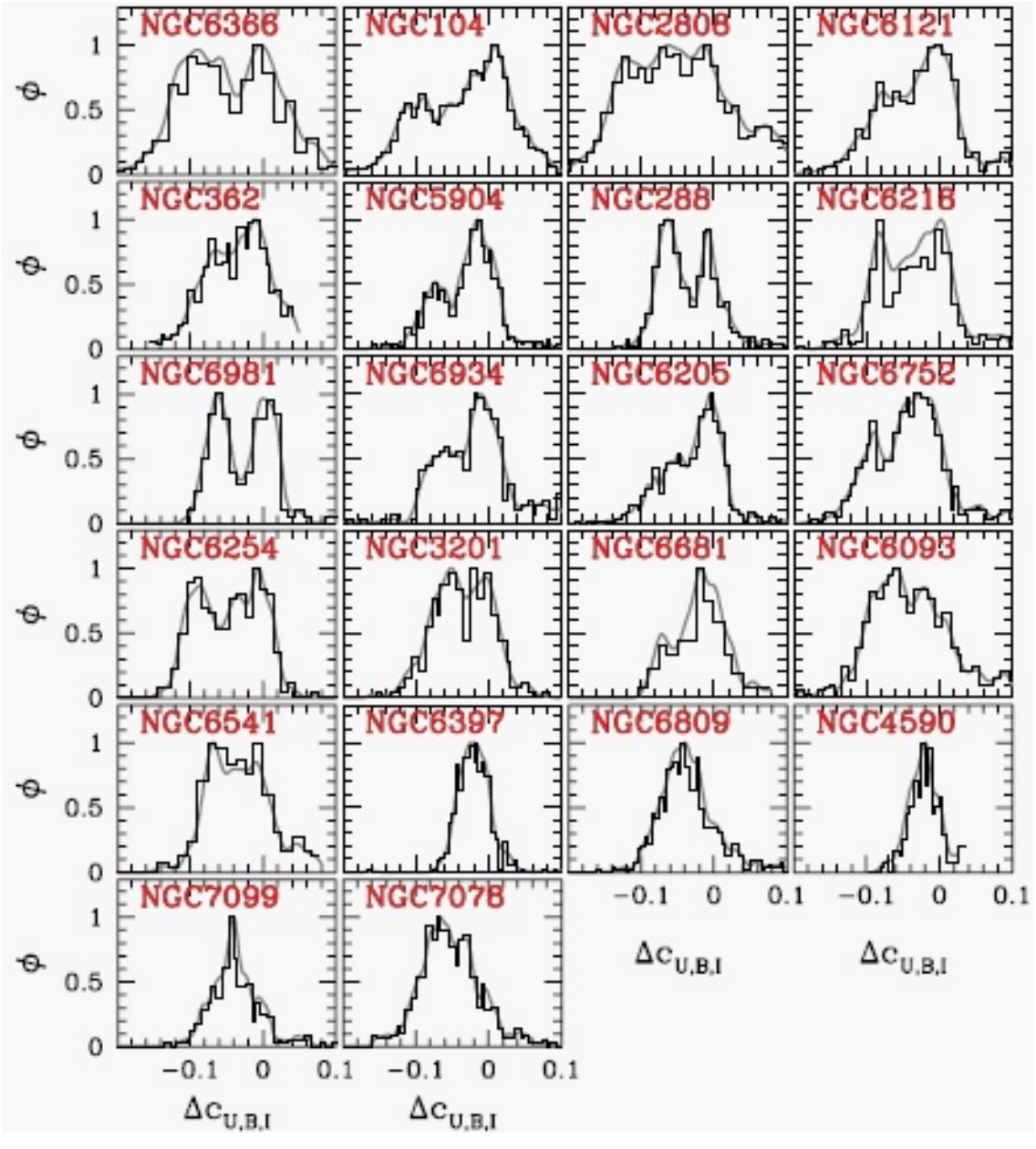

$\Delta c_{UBI} = c_{UBI} - c_{UBI,\mathrm{fiducial}}$ histograms for the 22 clusters analysed. The broad or complex morphology with multiple peaks is common to all globular clusters. Monelli et al. (2013, MNRAS 431, 2126).

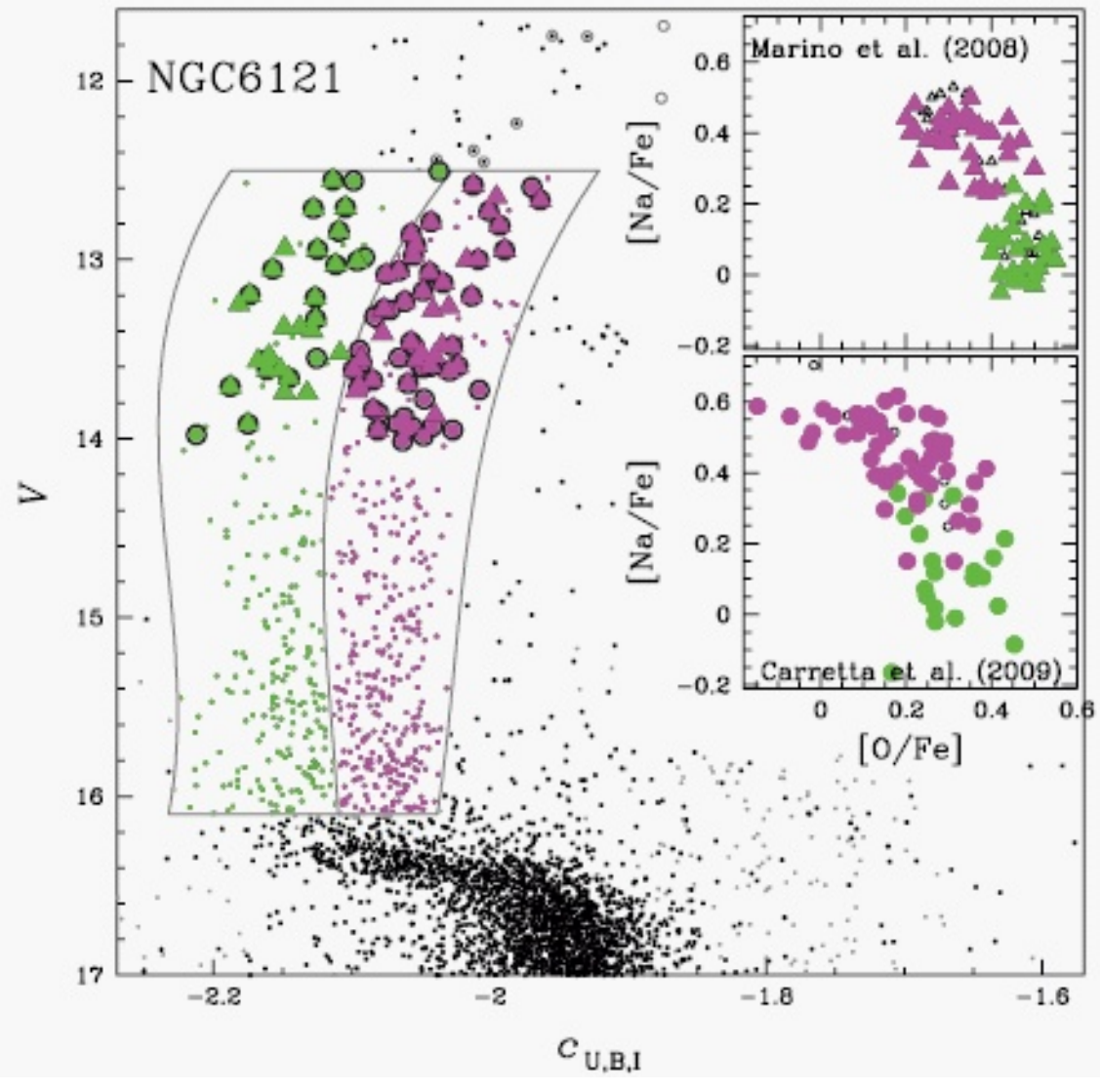

Correlation between the photometric and spectroscopic properties of RGB stars. The subpopulations selected in the V vs. c_{UBI} plane are found to have different chemical contents in terms of O and Na abundances. Monelli et al. (2013, MNRAS 431, 2126).

Polluters

- winds from FRMS stars ($12 - 50\ M_{\odot}$)
- mass loss from IM AGB stars ($4 - 8\ M_{\odot}$)
- timescale for the release of matter processed by H-burning at high temperature is few 10^7 yr

Possible scenario

- Formation of the FG stars from the gas having normal He and light element abundances.
- Pollution of the remaining gas by the winds from FRMSs and ejecta from IMAGB stars, which enhance He and change light element abundances.
- Formation of the SG stars from the gas now enriched in He and polluted in light element abundances.

Globular Cluster

- Massive GCs are showing spread in heavy element abundance.
- Evidence of SNe enrichment in addition to the spreads in light elements.
- Successive formation of stellar generations from the gas enriched by SNe.
- Relics of more massive primeval dwarf galaxies that were disrupted by and merged with the Galaxy.
- ***Normal*** GCs defined as those that have homogeneous abundance in heavy elements (Ca and Fe) but show variations in light elements such as an Na-O anticorrelation.

Summary

- Presence of several stellar populations is a common feature of GCs.
- Clear evidence for the existence of a correlation between splittings of evolutionary sequences in CMDs involving blue photometric bands and abundance anticorrelations.
- GCs are dominated by the SG stars (polluted; rich in Na, N, He, poor in O).
- SG stars are more centrally concentrated than the FG stars.
- During the early epochs of dynamical evolution, a proto-GC should have lost even 90 % of its primordial stellar population. A GC of a few 10^7 yrs old should have then appeared as a compact cluster immersed in a much larger loose association of stars and an even more extended expanding cloud of gas.